Design and Performance Assessments of Solar Driven Liquid Desiccant Air Conditioning System Components

A thesis submitted in fulfilment of the requirements for the degree of

Doctor of Philosophy

by

Bukke Kiran Naik

(Roll No. 146103001)

Department of Mechanical Engineering

Indian Institute of Technology Guwahati

Guwahati – 781039, India

January 2019

Department of Mechanical Engineering
Indian Institute of Technology Guwahati
Guwahati-781039
INDIA

THESIS CERTIFICATION

This is to certify that the work contained in this thesis entitled **Design and Performance Assessments of Solar Driven Liquid Desiccant Air Conditioning System Components** by **Bukke Kiran Naik,** a student of the Department of Mechanical Engineering, Indian Institute of Technology Guwahati, for the award of degree of **Doctor of Philosophy** has been carried out under my supervision and that this work has not been submitted elsewhere for any degree.

Prof. P. Muthukumar
Professor
Department of Mechanical Engineering
Indian Institute of Technology Guwahati
Guwahati-781039, Assam
INDIA

Dedicated To

My M-Tech and Ph.D. Thesis Supervisor

Prof. P. Muthukumar

ACKNOWLEDGEMENT

I would like to convey my profound sense of gratitude to my supervisor Prof. P. Muthukumar, Professor, Department of Mechanical Engineering, IIT Guwahati for his continuous guidance, support, motivation and constant encouragement helped me to complete this work successfully. Working under him has been a great experience for me and I am very much thankful to him for building up my confidence and for having faith in me during the project period, his suggestions broadened my views in engineering subjects as well as practical life.

I express my heartfelt thanks to Late Prof. S. C. Mishra, Professor, Department of Mechanical Engineering, IIT Guwahati for motivating me and for insisting me to pursue Ph.D. I will remember him throughout my career. I am grateful to Emeritus Prof. Manfred Groll, IKE, University of Stuttgart, Germany for providing valuable technical suggestions and ideas during the initial stage of my research work which forwarded my research progress to six months ahead.

I would like to thank Engineering Section, IIT Guwahati for proving financial support (Project No.: IITG/ENGG/15/NIQ/09). I thank DST for providing SERB–ITS travel grant (ITS/Off-529/2017-18) to attend the ISHPC 2017 international conference held at Waseda University, Tokyo, Japan. I also thank people of engineering and maintenance section especially, I thank Mr. A. Goswami, Mr. S. Senapati, Mr. Dasgupta, Mr. D. Bhagawathi, Mr. Indrajit Das, Mr. K. Barman and Mr. T. J. Singh for providing necessary support during the course of investigation. I am thankful to Mr. S. Ragahavan, Managing Director (MD), Best Systems and Services, Kodambakkam, Chennai for helping in fabricating the experimental setup. I also thank Mr. Nip Borah, Scientific officer for providing necessary equipment throughout the study. I also thank workers Mr. Dipankar, Mr. Atanu and Mr. Vimal of A/C plant and Cycle shop workers for their support and kind cooperation which helped me a lot, to work on my project successfully.

I am thankful to my doctoral committee members, Dr. Amaresh Dalal, Dr. Chandan Das and Prof. N. Sahoo for their valuable suggestions and encouragement during the period of my research work. I would like to express my sincere thanks to Prof. S. K. Dwivedy (HOD, Mechanical Engineering Department) for providing research facilities needed during my research work and financial support extended by Mechanical Engineering Department. I specially thank Mr. Amzad, Mr. Nip Borah and Mr. D. Chetri for their help during the course

of fabrication of the evacuated U – tube solar collector and also, for their assistance when needed during my experimental studies.

I am thankful to my seniors Dr. B. Satya Sekhar, Dr. S. Anbarasu, Dr. Hakeem Niyas, Mr. Chilaka Ravi Chandra Rao, Dr. Niraj Kumar Mishra, Ms. D. V. N Lakshmi, Dr. L. G. Kiran Kumar, Dr. Gyan Sagar Sinha and Dr. Debakanta Rabha for their career guidance and support whenever required. They also have motivated me in various aspects of my research work.

I am very much thankful to my project mates Mr. Ankit Soni, Mr. Ankit Varshney, Mr. Vikas Choudhary, Mr. Amit kumar, Mr. Chiraprabha Bhattacharya, Mr. P. Sunil Kumar, Mr. Mrinal Bhowmik, Mr. Mullapudi Joshi, Mr. Bhargava Sunkara, Mr. Lav Mittal, Mr. Balamurugan and Mr. Arvind for their assistance and support during my Ph.D.

I am also thankful to my lab colleagues, Mr. Vivek Selvan, Mr. Nithin Narmada, Mr. Lav Kumar Kaushik, Mr. Sunku Prasad, Mr. Vigneshwaran, Mr. Surendhar, Mr. Viswanth Ms. Jasinta Poonam Ekka, Ms. Sunita Deb, Mr. Malleswara Rao, Mr. Bharat kumar, Mr. Alok kumar, Mr. Sayanthan Jana, Mr. G. Sodhi, Mr. K. Durga Prasad, Mr. Jagath, Mr. R. Unnava, Mr. D. Pradeep, Mr. Narendra Naik, Mr. Mood Mohan, Mr. B. Ramesh Naik Mr. Yeswanth kumar, Mr. Mallikarjuna, Mr. Nagarjuna and other colleagues of IITG for their valuable friendship and making my stay at IIT Guwahati a memorable experience. I wish to express my deepest gratitude to all those who have helped me in various ways during the tenure of my PhD work at IIT Guwahati.

I am very much thankful to my parents Mr. B. Venkata Siddu and Mrs. B. Radhabai, my younger brother Mr. B. Suresh Naik, my wife Mrs. B. Lekhya, my Uncle Mr. B. Siva, my aunt Mrs. B. Kamala, my younger brother Mr. B. Hemanth Naik, my younger sister Ms. B. Kusuma and Father in law Mr. M. Bavasingh Naik and their family who's never ending support inspires me to do my best. Especially, I thank my parents who have encouraged me to pursue higher studies and their never ending sacrifices helped me to reach my career goals. I am thankful to my wonderful kid Master B. Rithik Naik for always making me smile. I also thank my B – Tech roommates, Mr. M. Krishna Sarath, Mr. Seelam Vishnu Vardhan Naidu and my B – tech friends, Mr. P. Venu, Mr. G. Pavan, Mr. P. V. R. Mohan, Mr. K. Dileep, Mr. Vamsi and Mr. T. Sudhakar for their support and motivation to pursue higher studies in premier institute IIT Guwahati.

Bukke Kiran Naik

ABSTRACT

In recent years, solar driven liquid desiccant based ACS has been projected as a promising alternative for handling large latent heat loads (> 50 TR or 176 kW) compared to solid desiccant, vapour compression and vapour absorption based ACSs. Dehumidifier, regenerator and solar collector are the key components of solar driven liquid desiccant based ACS. Dehumidifier works based on the principle of condensation whereas regenerator works based on the principle of evaporation. In the dehumidifier, desorption of water vapour takes place from ambient air to the liquid desiccant whereas in the regenerator, absorption of water vapour takes place from the liquid desiccant to the ambient air. During absorption and desorption processes, simultaneous heat and mass exchange occurs in between the air and the liquid desiccant. The driving force for heat exchange is the temperature difference whereas for the mass exchange, it is the vapour pressure difference between the air and the desiccant. These driving forces depend upon the changes in local temperature and vapour pressure at the air – desiccant interface.

Several thermodynamic models have been developed for predicting the simultaneous heat and mass exchange processes occur in the adiabatic dehumidification/regeneration system which includes finite difference model, ε – NTU model and simplified models. Considerable experimental studies have been also performed for analysing the performance of the adiabatic liquid desiccant dehumidification and regeneration systems by employing different liquid desiccant materials, packings in a packed tower and flow patterns. It is noted that very few researchers have carried out the exergy analyses of the liquid desiccant dehumidification/regeneration system.

Numerous studies reported on analysing the performance of the evacuated tube and flat plate type solar collectors showed that evacuated tube type solar collectors were more efficient compared to flat plate type solar collectors. Several types of evacuated tube solar collector configurations viz. U – type, H – type, T – type, heat pipe type, etc. have been reported for various solar thermal utilization applications. Among these, owing to simplicity in design and lower investment cost factors, evacuated U – tube solar collector is considered for present investigation. The solar radiation incident on the outer glass surface of the evacuated tube is transferred to the inner glass tube through radiative heat transfer and then the heat is absorbed

by the U – tube. From U – tube, the heat is exchanged to the working fluid. Research on evacuated tube type solar collectors have been initiated during 1970s. But the investigations on evacuated U – tube solar collector was started very recently. From the literature, it is observed that very few researchers have analysed the thermal performance of the evacuated U – tube solar collector by performing experimental studies and by employing numerical/mathematical models. The reported numerical/mathematical models are not suited for predicting the working fluid transition time and the variation of heat transfer characteristics along the length of the evacuated U – tube solar collector. Further, there is a lack of profound experimental studies on performance of the evacuated U – tube solar collector system (multiple evacuated U – tubes connected to a manifold). It is also observed from the literature that limited research works have been carried out on investigating energy and exergy efficiencies of the evacuated U – tube solar collector.

In view of the above, the following objectives are considered in the present work

- To develop thermal models for evaluating the performances of solar driven liquid desiccant ACS components such as liquid desiccant dehumidifier/regenerator and evacuated U – tube solar collector.
- To design and fabricate solar driven liquid desiccant ACS components for achieving dehumidified air of 18 kW capacity.
- To perform a detailed experimental study on solar driven liquid desiccant ACS components at different operating and ambient conditions.
- To carryout energy and exergy analyses on individual components of solar driven liquid desiccant ACS.

An experimental investigation for estimating the overall energy exchange between the liquid desiccant and the ambient air and the variation of ambient and operating parameters along the liquid desiccant dehumidification/regeneration system are presented in accordance with humid subtropical climate. An experimental correlation for specific humidity ratio difference in terms of known inlet parameters is developed for both the dehumidification and the regeneration systems. A thermodynamic model is developed for analyzing the heat and mass transfer interaction between air and desiccant solution along a counter-flow packed tower (liquid desiccant dehumidifier/regenerator). An algorithm using a backtracking approach is introduced for simulating the transfer processes in the packed tower. The predicted simulation results are in good agreement with the experimental data available in the literature for the counter-flow

packed tower. The contour plots are presented for analyzing the transfer processes along the height of the packed tower. The performances of the dehumidifier, the regenerator and the cooling tower are predicted at various operating conditions and tower specifications.

In addition, the coupled heat and mass transfer processes occurring in a cross-flow liquid desiccant dehumidifier and regenerator are analyzed. A novel finite difference based thermodynamic model is developed using the governing equations of mass, momentum and energy and a recursive algorithm is proposed for solving the developed model. The simulated results obtained from the developed model are validated with the experimental data reported in the literature and a good agreement is observed between them. The contour plots for the distribution of air and desiccant enthalpies, air specific humidity and solution concentration along the longitudinal and the transverse directions of the packed tower are represented. Also, the contour plots for the desiccant concentration at different Lewis numbers are presented. Further, the influence of Lewis number on operating and performance parameters are also discussed in detail.

Present investigation also focuses on deriving the expressions for energy, exergy and entransy (EEE) of the regenerator and quantifies them along the height of the liquid desiccant regenerator. By varying the operating parameters such as desiccant temperature and concentration, air temperature and humidity ratio and air and desiccant flow rates, the performance of the regenerator is investigated in terms of entransy, exergy and desorption efficiencies. From the EEE analyses, it is observed that by increasing the desiccant temperature from 60.3 °C to 65.2 °C and decreasing the air humidity ratio from 18.7 g_{wv}/kg_{da} to 14.3 g_{wv}/kg_{da} simultaneously, the overall energy exchange, exergy destruction and entransy dissipation are increased by 26%, 37% and 39%, respectively.

Further, an experimental setup of an evacuated U – tube solar collector system has been designed and fabricated for testing the performance of the system. Based on experimental analysis, three empirical correlations for predicting working fluid transition time, energy efficiency and exergy efficiency are developed as the function of operating parameters and ambient temperature. Data predicted from these correlations match with the experimental data with the maximum error of ±12.7 %, ±6.9 % and ±7.8 % for working fluid transition time, energy efficiency and exergy efficiency of an evacuated U – tube solar collector, respectively. A three dimensional numerical model is developed for predicting the working fluid outlet temperature of a single evacuated U – tube solar collector and for the whole solar collector

system. The model predictions are compared with the experimental data and a good agreement exists between them. The working fluid transition time in an evacuated U – tube solar collector is defined for analyzing the time taken by a working fluid to attain a steady state condition. The influence of average solar irradiance on efficiency and useful heat rate of the solar collector is studied theoretically for two different evacuated tube configurations. Further, performance of the evacuated tube solar collector is investigated theoretically by employing water and air as working fluid, copper, aluminium and brass as U–tube material, and graphite, magnesium oxide and aluminium oxide as filler material.

NOMENCLATURE

a_s	specific surface area per unit volume (m^2/m^3)
A_{n+1}	equally spaced node
A	area of the structure packing chamber (m^2)
AC	air conditioning
ACS	air conditioning system
A_c	area of the collector (m^2)
C_p	specific heat at constant pressure (kJ/kg – K)
G	mass flux or flow rate per unit cross sectional area (kg/m^2–s)
h	enthalpy (kJ/kg)
H	height of the packed tower (m)
Δh_{dil}	dilution enthalpy difference (kJ/kg)
I	solar intensity (kW/m^2)
k	integer denoting equally spaced 1 to ‘n’ no. of parts
k_m	thermal conductivity of the material (W/m – K)
L	length of the structured packing chamber (m)
L*	effective length of the packed tower (m)
Le	Lewis number
LDACS	liquid desiccant AC system
LHS	latent heat storage
L/G	liquid to gas ratio
$\dot{m}$	mass flow rate (kg/s)
N	no. of iterations

n	no. of parts
N_p	no. of packing materials
N	number of manifolds
P_s^{sat}	statured vapour pressure at air – desiccant interface (kPa)
P_{atm}	atmospheric pressure (kPa)
P	pressure (Pa)
Q_{ex}	exergy destruction (kW)
Q_{exs}	sensible exergy destruction (kW)
Q_{exl}	latent exergy destruction (kW)
Q_e	energy exchange (kW)
Q_{es}	sensible energy exchange (kW)
Q_{el}	latent energy exchange (kW)
Q_{en}	entransy dissipation (kW – K)
Q_{ens}	sensible entransy dissipation (kW – K)
Q_{enl}	latent entransy dissipation (kW – K)
Q_{useful}	useful heat gained by the working fluid (W)
R. H.	relative humidity (%)
T	temperature (^oC)
V	volume (m^3)
$\vec{v}$	velocity (m/s)
W	width of the structure packing chamber (m)
X	concentration of the desiccant solution (%)
Z	height (m)

Greek symbols

β	desiccant concentration ($kg_{des.}/kg_{sol.}$)
β_T	coefficient of thermal expansion (1/K)
α_m	mass transfer coefficient (kg/m^2s)
α_h	heat transfer coefficient (W/m^2K)
δ	latent heat of vaporization/condensation (kJ/kg)
φ	latent heat (kJ/kg)
ω	air humidity ratio (kg_v/kg_{da})
λ	evaporation/condensation rate (g/m^2s)
γ	ratio of mass flux of working fluid and air
ξ	effectiveness
τ_h	function of heat transfer coefficient and air mass flux
τ_m	function of mass transfer coefficient and air mass flux
ζ_T	logarithmic function of thermal effectiveness
ζ_m	logarithmic function of moisture effectiveness
ϕ_l	latent enthalpy (kJ/kg)
ϕ_s	sensible enthalpy (kJ/kg)
φ	no. of experimental runs
ω_s	saturated air humidity ratio (kg_v/kg_{da})
η	efficiency (%)
ρ	density (kg/m^3)
μ	dynamic viscosity of working fluid (N/m^2-s)
α	absorptivity of the U – tube material
α_c	absorptivity of the coating material

$\tau_{g,i}$	transmissivity of the inner glass tube
$\tau_{g,o}$	transmissivity of the outer glass tube
ζ	effective heat absorbed from the evacuated tube (kW/m^2)
τ	transmissivity of the glass tube
η_u	energy efficiency (%)
η_{ex}	exergy efficiency (%)
$\eta_{u,sc}$	energy efficiency of the evacuated U – tube solar collector system (%)
$\eta_{ex,sc}$	exergy efficiency of the evacuated U – tube solar collector system (%)

Subscripts

a	air
amb	ambient air
da	dry air
e	equilibrium
ex	exergy
en	entransy
h	heat transfer
ini	initial
l	working fluid
m	moisture/mass transfer
M	mean fluid temperature
o	overall
r	reference
s	liquid desiccant solution
sr	solar radiation

T	thermal
v	water vapour
wb	wet bulb temperature
wf	working fluid
w,o	working fluid outlet
w,i	working fluid inlet
wM1,i	working fluid inlet at manifold 1
wM1,o	working fluid outlet at manifold 1
wM2,i	working fluid inlet at manifold 2
wM2,o	working fluid outlet at manifold 2
wM3,i	working fluid inlet at manifold 3
wM3,o	working fluid outlet at manifold 3
wM1 – U,i	working fluid inlet at U – tube of manifold 1
wM1 – U,o	working fluid outlet at U – tube of manifold 1
wM2 – U,i	working fluid inlet at U – tube of manifold 2
wM2 – U,o	working fluid outlet at U – tube of manifold 2
wM3 – U,i	working fluid inlet at U – tube of manifold 3
wM3 – U,o	working fluid outlet at U – tube of manifold 3
wf,o	working fluid outlet
wf,i	working fluid inlet

Superscripts

avg	average
i	inlet
o	outlet

CONTENTS

LIST OF FIGURES

LIST OF TABLES

CHAPTER – 1

INTRODUCTION

During the 20th century, the HVAC industry brought AC out of the lab into millions of homes and commercial buildings. It was the period where the cooling and dehumidification swapped from being a luxury to a necessity. However, this success now presents new challenges in the field of ACS.

The source of major problems is due to heavy dependence on electricity. In HVAC systems, tremendous amount of fossil fuels (for generating electrical energy) are converted in to carbon dioxide each year. A rapidly growing demand for ACS accelerates the global climate change at a time when the world is struggling to reduce it. Air and water pollution could also increase as more power plants are built to meet the demand of additional electricity requirement. The reliability of electrical power transmission systems may be affected as AC creates high peak demands for power. Furthermore, rapid growth of HVAC industry also possesses many concerns on global warming, CO_2 emissions and ozone layer depletion.

Indoor air quality is another challenge to the HVAC industry, particularly in high humid climates. Sick Building Syndrome is a problem that can be corrected through better ventilation. However, in high humid climates, the increased ventilation can raise indoor humidity to a level that is uncomfortable and unhealthy.

Using traditional vapour compression or vapour absorption refrigeration systems, removal of latent load can be achieved by cooling of process air below its dew point temperature. Then the dehumidified air is reheated to meet the required indoor temperature conditions. If the latent load present in the process air is removed by other means than by cooling below dew point, then the energy required for cooling the supply air below its dew point temperature and the energy needed to reheat the air from dew point temperature to the supply air temperature will be avoided (Daou et al. 2006). Therefore, desiccant ACS is used as an alternative to conventional ACS for meeting the growing demand in air-conditioning fields.

1.1 Desiccant air-conditioning systems

Desiccant air-conditioning systems are used for cooling and dehumidification of ambient air.

1.1.1 Working procedure

Basically, desiccant systems transfer moisture from one airstream to another by using two processes.

- Sorption process
- Desorption process

a) Sorption process

The desiccant system transfers moisture from the ambient air (humid/moist air) to the desiccant material due to vapour pressure difference between the humid air and the desiccant material. If the desiccant material is dry and cold, then its surface vapour pressure is lower than that of the moist air, and therefore, moisture in the air is absorbed by the desiccant material. During this process, the latent heat of the water vapour is released, and the air temperature increases and the desiccant material becomes wet.

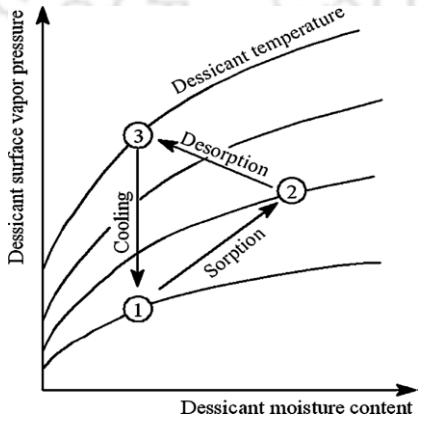

Fig. 1.1, Process of moisture transfer by desiccant (Sarbu et al. 2013)

b) Desorption process

In this process, the captured moisture is released to the airstream by increasing the temperature of the desiccant. This process is also called as regeneration process. During this process thermal energy is needed because the desiccant has to be heated to release the moisture. This is an opportunity to use low grade energy such as solar energy, biogas, waste heat and geothermal power to transfer moisture.

After regeneration, the desiccant material is cooled down by the cold airstream. Then, it is ready to absorb the moisture again. When these processes are cycled, the desiccant system can transfer the moisture continuously by changing the desiccant surface vapour pressures, as illustrated in Fig. 1.1.

1.1.2 Benefits

Desiccant materials are used in the air-conditioning applications with advantages in the following conditions (ASHRAE fundamentals, 1989).

a) The latent load is large in comparison to the sensible load.
b) The cost of energy to regenerate the desiccant is low when compared with the cost of energy to dehumidify the air by chilling it below its dew point.

1.1.3 Types of desiccant materials

Fig. 1.2 illustrates the classification of desiccant materials.

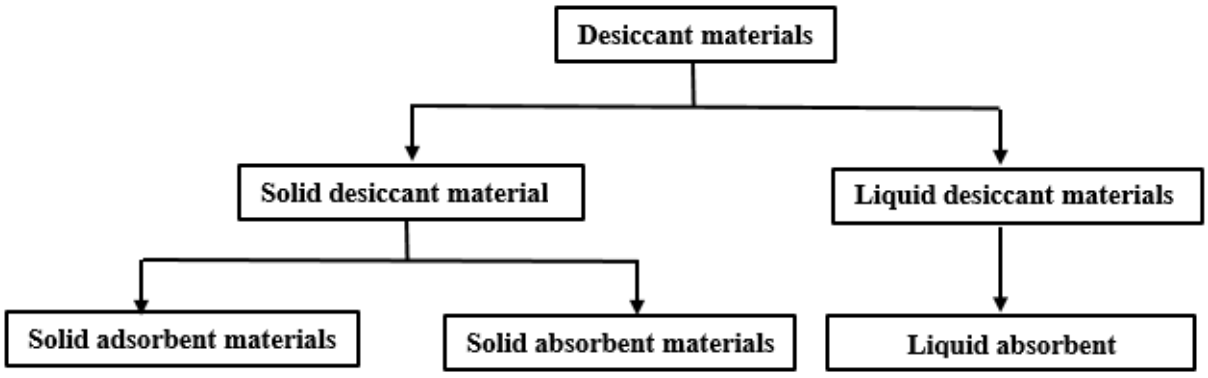

Fig. 1.2, Classification of desiccant materials

a) Solid desiccant materials

Solid desiccant materials are of two types

- Solid adsorbent materials
- Solid absorbent materials

i) Solid adsorbent materials

The solid material which has an affinity to adsorb moisture content present in the process air is said to be solid adsorbent material. Adsorption capacities and other parameters of solid adsorbent materials are listed in Table 1.1.

Table 1.1, Adsorption capacities and other parameters of solid adsorbent materials

Adsorbent	Adsorbent temperature (°C), RH (%)	Adsorption capacity ($g\text{-}H_2O/g\text{-}sorb$)	Textural properties*	Regeneration temperature (°C)	References
Silica				70-150	(Ha et al. 2006)
Silica gel (Type A)	27, 60	0.08-0.36	2-10 nm	70	(Ha et al. 2006)
Silica gel (Type B)	30-40, 60	0.34	349-690 m^2/g	70-80	(Li et al. 2007)
MCM-41	27,60	0.46	3.5 nm	70	(Ha et al. 2006)
Zeolite Y	27, 60	0.02-0.30	Nil	250-350	(Ha et al. 2006)
Activated carbon	27, 60	0.18-0.29	2 nm	70	(Ha et al. 2006)
Composites					
$CaCl_2$/Silica gel	35, 40	0.19	Nil	60-80	(Ha et al. 2006)
$CaCl_2$/MCM-41	25, 70	0.75	2-10 nm	70-120	(Tokarev et al. 2002)
Metal organic framework					
MOF-MIL-101 (Cr)	30–40, 60	1.5–1.7	4,150 m^2/g	70–80	(Seo et al. 2012)
MOF-MIL-100 (Fe)	30–40, 60	>0.84	2,300 m^2/g	70–80	(Seo et al. 2012)
MOF-MIL-100 (Cr)	30–40, 60	0.84	1,980 m^2/g	70–80	(Seo et al. 2012)
MOF-MIL-100 (Al)	30–40, 60	0.84	1,970 m^2/g	70-80	(Seo et al. 2012)
Others					
Dry coconut coir	32, 75	0.3	Nil	Nil	(Fang et al. 2011)
Dry durian peel	32, 75	0.17	Nil	Nil	(Fang et al. 2011)

Molecular sieve	Nil	Nil	Nil	130	(Gershon et al. 1981)

*Textural properties – surface area (m^2/g) and average pore diameter (nm).

ii) Characteristics of solid adsorbent materials

- No loss of desiccant through deliquescence.
- Very good dehumidification.
- Cost is moderate.

iii) Solid absorbent materials

Table 1.2, characteristics of solid absorbent materials (Ameel et al. 1995)

Absorbent	Regeneration temperature (°C)	Dehumidification	cost	Deliquescent property
LiCl	>130	Very good	High	High
$CaCl_2$	70	Good	low	High

The solid material which has an affinity to absorb moisture content present in the process air is said to be solid absorbent material. Examples of solid absorbent materials are lithium chloride (LiCl) and calcium chloride ($CaCl_2$). The characteristics of solid absorbent materials is listed in Table 1.2.

iv) Merits of solid desiccant materials

- No leakage problem
- Little or no corrosion and environmental hazards
- Little maintenance

v) Demerits of solid desiccant materials

- High air pressure drop through desiccant beds

b) Liquid desiccant materials

i) Liquid absorbent material

The liquid material which has an affinity to absorb moisture content present in the process air is said to be liquid absorbent material.

ii) Comparison of liquid absorbent materials

A comparison of thermo-physical properties for TEG, MEG, LiCl, LiBr, $CaCl_2$ and KCOOH is presented in Table 1.3. In order to assess the liquid desiccants characteristics, vapour pressure is chosen as key parameter which decides the dehumidification and regeneration capabilities of the liquid desiccant. In this aspect, it is observed that compared to other liquid desiccants LiCl exhibits lowest vapour pressure in both dehumidification and regeneration processes (G. Fekadu and S. Subudhi, 2018). Further, it is also found that LiCl is the most stable liquid desiccant. But LiCl is costlier, corrosive in nature and forms crystallization compared to other liquid desiccants. Corrosiveness can be eradicated using plastics as a packing material and crystallization can be avoided using less concentration of LiCl.

iii) Merits of liquid desiccant materials

- Low air pressure drop.
- Ease of isothermal dehumidification.
- Ease of heat recovery.
- High storage capability.
- Operational flexibility.
- Less maintenance.
- Flexibility in design.
- Utilization of low – grade thermal energy source for regeneration of liquid desiccant.

iv) Demerits of liquid desiccant materials

- Possibility of leaks.
- Corrosion hazard.
- Possibility of crystallization or evaporation.

Table 1.3, Characteristics of liquid desiccant materials (Gershon et al. 1981, A. Gasperalla, 2005 & Sanjeev et al. 2007)

Characteristic	Triethylene glycol (TEG)	Monoethylene Glycol (MEG)	LiCl	LiBr	$CaCl_2$	KCOOH
Regeneration temperature	65-80 °C	65-80 °C	80 °C	80 °C	60 °C	50 °C
Dehumidification	Moderate	Moderate	Good	Good	Poor	Moderate
Cost	High	Moderate	High	High	Low	High
Toxicity	Nontoxic	Small	Nontoxic	Nontoxic	Nontoxic	Nontoxic
Crystallization	No	No	Present	Present	Present	Present
Corrosion hazard	Moderate	Moderate	High	High	Moderate	less
Desiccant evaporation	High (regeneration)	High	No loss	No loss	No loss	No loss

1.2 Solar driven desiccant ACS

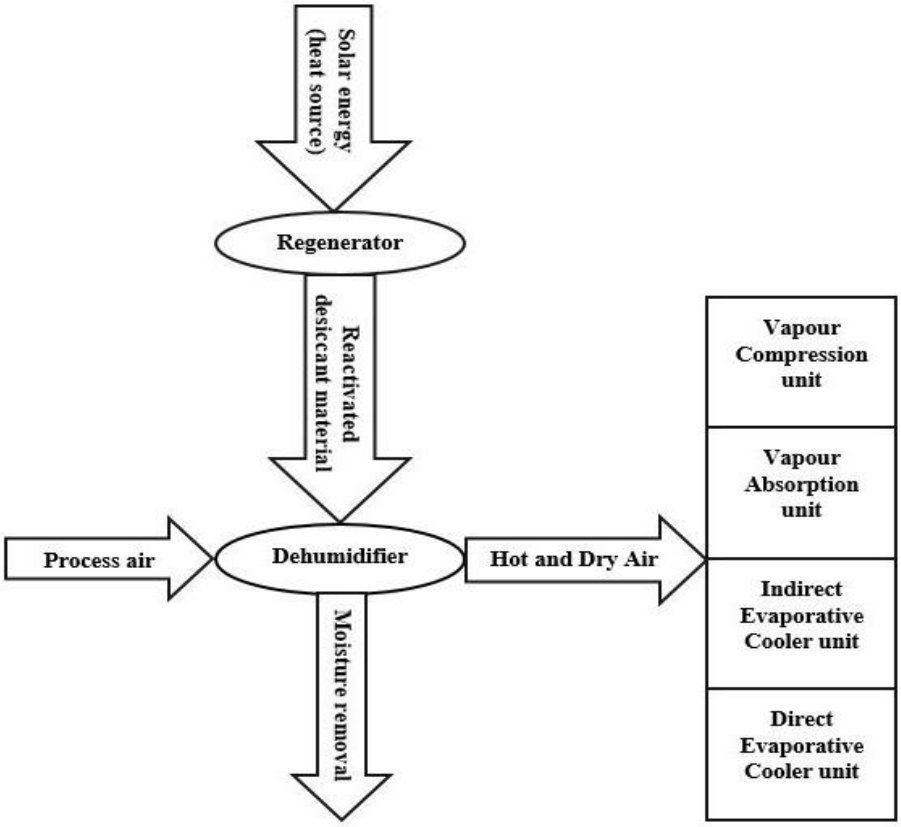

Fig. 1.3, Working principle of solar driven desiccant ACSs

In the present investigation, the possibilities of solar driven desiccant ACSs are explored. These ACS are classified as

- Solar driven solid desiccant ACSs
- Solar driven liquid desiccant ACSs

a) Solar driven solid desiccant ACSs

Ambient air is dehumidified when it comes in contact with desiccant wheel (coated with solid desiccant material) which rotates slowly between the process and the regeneration air streams; then, to provide sensible cooling to the dehumidified air, traditional vapour compression, vapour absorption, and direct or indirect evaporative cooler units are used, and the dehumidified air is sent to the conditioned space. As shown in Fig. 1.4, to regenerate the desiccant, the wheel passes through a hot reactivation air (ambient air heated using solar energy) and the process begins again.

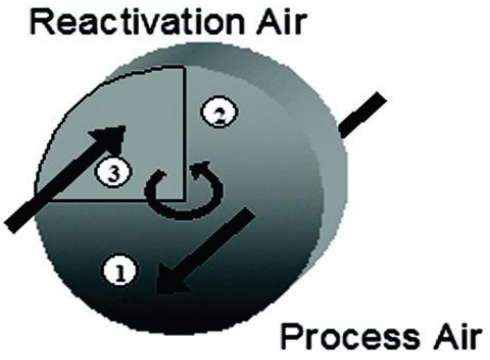

Fig. 1.4, Schematic of solid desiccant wheel (Ameel et al. 1995)

b) Solar driven liquid desiccant ACSs

Ambient air is dehumidified when it comes in contact with the strong liquid desiccant; then, to provide sensible cooling to the dehumidified air, traditional vapour compression, vapour absorption, and direct or indirect evaporative cooler units are used, and the dehumidified air is sent to the conditioned space (Fig. 1.5). When the solution is weakened by absorption of moisture, it is sent directly to the regeneration process to release the moisture using external heat sources like solar energy. This process is called "reactivating" of desiccant (Mei et al. 1992).

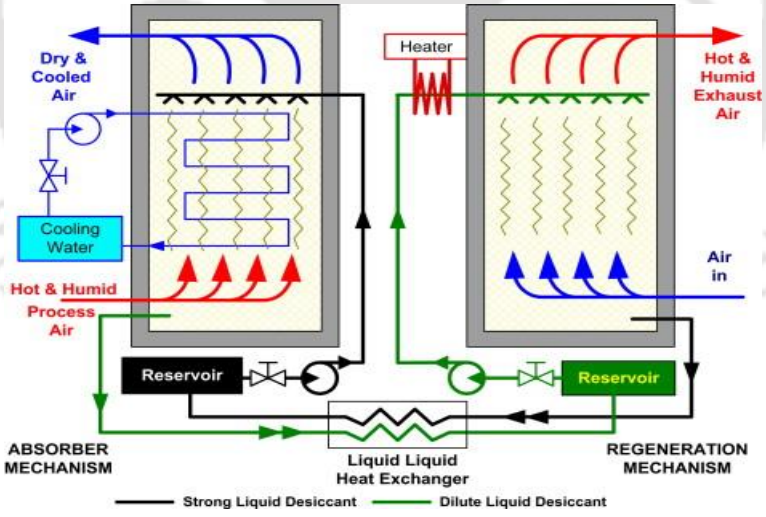

Fig. 1.5, Liquid desiccant dehumidification system (*Jain and Bansal, 2007*)

1.3 Comparison of solar driven liquid and solid desiccant based ACSs

From Table 1.4 and sections 1.1.4 and 1.1.5, it is observed that liquid desiccant based ACS has been proven as a promising alternative for handling high latent loads compared to solid desiccant based ACS. Their capacity to absorb moisture is generally greater than that of solid

desiccants. Liquid desiccants require lower regenerating temperature, mostly in the range of 40–70 °C while, solid desiccant system requires in the range of 60–115 °C (Kassem et al. 2013). Besides, liquid desiccants can be stored in the form of concentrated solution for use during periods when solar energy is absent and thus, offer more flexible operational characteristics. These systems are attractive because of their operational flexibility and their capability of absorbing air borne pollutants and bacteria (Oberg et al. 1998).

Compared to the solid desiccants, they are generally regenerated at relatively lower temperature and equally cause lower airside pressure drops (Daou et al. 2006). Moreover, the latest developments are focused on liquid sorption applications since the liquid sorption materials have advantages of higher air dehumidification at the same driving temperature, as well as the possibility of high energy storage by means of hygroscopic solutions (Yunho et al. 2007). The liquid desiccant assisted ACS can achieve up to 40% of energy savings with regard to traditional ACS and those savings become even greater when the required energy needed for regeneration is drawn from solar energy (Vafai et al. 2004). During dull sunlight, the weak liquid desiccant can be stored until required regeneration heat is not available. These systems are capable of handling large heat loads (> 50 TR or 176 kW) and minimizes the overall energy demand. Further, they can be employed in large capacity industrial deep drying applications.

Table 1.4, Comparison between solar driven liquid and solid desiccant ACSs (Ghafoor et al. 2015, Deng et al. 2011)

Characteristics	**Liquid desiccant ACSs**	**Solid desiccant ACSs**
Materials	Liquid desiccant material	Solid desiccant material
Regeneration temperature	60-90 °C hot water or 80-110 °C hot air	60-150 °C hot water or 50-80 °C composite desiccant
Capacity range	50-500 kW, 3000-140,000 $m^3 h^{-1}$	5-350kW, 500-50,000 $m^3 h^{-1}$
Cooling method	Cooling water or air-cooled	Cooling water
COP	0.5-1.3	0.3-1.0+
Deep dehumidification	Not suitable	Suitable
Power consumption	2.7 kW/TR	3.5 kW/TR

Applications	1) Large capacity industrial deep drying dehumidification applications. 2) Building comfort and indoor air quality control. 3) Especially the site for removing airborne contaminants.	1) Industrial process or storage. 2) Cold foot print buildings, building comfort and indoor air quality control. 3) Power augmentation of gas turbine.

1.4 Motivation of present work

In hot and humid climates, to maintain comfort conditions, remove air borne contaminants and protect sophisticated equipment, dehumidification of ambient air is crucial. Before 20th century, for dehumidifying the ambient air, traditional vapour compression and vapour absorption based ACSs were widely used. These types of dehumidification processes consume more power and possess high energy demand. To overcome this issue, in recent years, desiccant based ACS has been introduced.

Desiccant based ACS is classified as solid desiccant based ACS and liquid desiccant based ACS. As discussed earlier, compared to solid desiccant based ACS, liquid desiccant based ACS is advantageous due to less air side pressure drop, less maintenance, operational flexibility and utilization of low- grade thermal energy sources such as solar or waste heat for the regeneration of liquid desiccant. Therefore, solar driven liquid desiccant based ACS is chosen for the present investigation.

Key components of solar driven liquid desiccant ACS are dehumidifier, regenerator and solar collector. In this thesis, numerical, experimental and thermodynamic analyses of the dehumidifier, regenerator and evacuated U–tube solar collector are presented. Further, the exergy destruction and entransy dissipation of the liquid desiccant regenerator are investigated. A major importance is given for analysing the heat and mass transfer characteristics along the structured packing chamber of a liquid desiccant dehumidifier/regenerator and the heat transfer characteristics across the evacuated U–tube solar collector.

1.5 Structure of the thesis

The performance of the solar driven liquid desiccant ACS mainly depends upon the heat and mass transfer aspects of the dehumidifier/regenerator and the heat transfer aspects of the evacuated U–tube solar collector. Therefore, aforementioned system components such as liquid desiccant dehumidifier/regenerator and evacuated U–tube solar collector are fabricated as individual systems and the performance is investigated of each system (liquid desiccant dehumidification/regeneration system and evacuated U–tube solar collector system) at different operating and ambient conditions.

This thesis is organized in seven chapters. A brief description of the content of each of the chapters is discussed below:

Chapter 1 starts with a brief introduction of various methods and concepts of dehumidification systems. The advantages of solar driven liquid desiccant based ACS is elucidated. Importance of liquid desiccant ACS components, various applications and motivation of the present work are presented.

In Chapter 2, the state-of-art on various aspects of the liquid desiccant dehumidification system, the liquid desiccant regeneration system and the evacuated U – tube solar collector system are described briefly. Literatures published on developed numerical models and experimental investigations are reviewed. On the basis of literature survey, objectives of the present thesis work are framed.

Chapter 3 presents thermal models developed for simultaneous heat and mass exchange between the ambient air and the desiccant solution in counter-flow direction of the liquid desiccant dehumidification/regeneration system. Also, the numerical model developed for evacuated U – tube solar collector system for assessing the heat gained by the working fluid from the solar radiation is discussed. Further, the theoretical model for analyzing the variation of heat and mass transfer characteristics along the structured packing chamber and the variation of heat transfer characteristics along the evacuated U – tube solar collector is discussed.

Chapter 4 presents the design details and test procedure of liquid desiccant dehumidification/regeneration and evacuated U – tube solar collector systems. In accordance with humid sub – tropical climate, several experiments are conducted at different operating conditions and the outcome of the study is presented. In addition, a procedure for developing

experimental correlations and the variation of developed correlations with the operating and ambient parameters are also discussed in detail.

Chapter 5 covers the energy exchange between the ambient air and the desiccant solution during regeneration processes and exergy destruction with respect to reference environment along the liquid desiccant regeneration system. Further, energy and exergy analyses of the individual evacuated U – tube solar collector as well as whole solar collector system are presented.

Chapter 6 depicts a finite difference based thermal model for analyzing the heat and mass transfer processes across the cross-flow liquid desiccant dehumidifier/regenerator. Effect of Lewis number on operating and performance parameters of the dehumidifier and regenerator and the effect of inlet parameters on the performance of the packed tower are described in detail.

Chapter 7 introduces the concept of entransy dissipation along the liquid desiccant regenerator. Further, the effect of air and desiccant inlet parameters on entransy efficiency of the liquid desiccant regenerator is presented.

Chapter 8 outlines the major conclusions arrived from numerical, experimental, energy and exergy analyses of the liquid desiccant dehumidification/regeneration systems and evacuated U – tube solar collector system. Further, key observations made from the entransy dissipation theory of the liquid desiccant regeneration system are also presented in detail.

CHAPTER – 2

STATE OF ART

The concept of liquid desiccant ACS was initially explored in 1955, when Loef indicated the concept for the first time of using a tri ethylene glycol open-cycle ACS (Gommed et al. 2004). In 1970's the technique was further developed by many investigators to save energy consumption in conventional ACSs by shifting the major part of the cooling load to the more energy-efficient desiccant systems (Oberg et al. 1998). During mid-1970's, desiccant dehumidifiers were primarily used for dehumidification in the field of industrial applications such as the manufacture of moisture-sensitive products and the prevention of corrosion or other moisture damage during storage. In the late 1970s, public concern on energy issues led investigators to focus new attention on desiccant dehumidification for commercial and residential AC applications.

2.1 Design of Liquid Desiccant Dehumidification/Regeneration System

Liquid desiccant A/C systems usually require two desiccant air contact devices, namely dehumidifier and regenerator. They are basically three types of configurations for liquid desiccant dehumidifiers or regenerators, namely spray chamber, packed tower and spray coil arrangement. Packed tower configuration has received more attention because of a high heat and mass transfer rate per unit volume (Dai et al. 2004).

Gandhidasan and co-workers in Saudi Arabia have made extensive studies on liquid desiccant systems with packing configurations (Farayedhi et al. 2002). In the design of liquid desiccant systems, the desiccant was sprayed into the air stream to absorb the moisture. During this process, some liquid desiccant carry-over was experienced. Since the lithium solutions (usually lithium chloride or lithium bromide) are corrosive, they may be harmful to people's health due to inhalation of the droplets.

The carry-over of the working solution in a traditional stripping tower is of serious concern in real applications. Some research groups employed two methods to overcome the carry-over problem in liquid desiccant systems in their recent research.

a) Low flow liquid desiccant system
b) U-shaped spray tower

2.1.1 Low Flow liquid desiccant systems

Falling film liquid desiccant dehumidification systems can be internally heated or cooled while conditioning the air or regenerating the desiccant. This has significant potential performance benefits. The low-flow liquid-desiccant technology is used to achieve high energy efficiency and eliminate carry-over of desiccant droplets.

Mesquita and Harrison (2005) conducted a 2-dimensional numerical analysis on an internally cooled or heated flat plate liquid desiccant system. Mesquita (2007) conducted further experimental analysis on a single channel low flow flat plate liquid desiccant system. The system was operated under both isothermal and non-isothermal conditions. It was concluded that water temperature and mass flow rate of desiccant have a strong effect on the performance of the flat plate dehumidifier and regenerator. Lowenstein et al. (2007) build and tested a pre-commercial prototype low flow liquid desiccant system. The benefit of zero desiccant process air carryover was emphasized. Miller and Lowenstein (2008) investigated an important benefit of a liquid desiccant system coupled to a solar thermal array. A preliminary cost benefit analysis of a 6000 CFM (cubic feet per minute) unit charged with $CaCl_2$ showed a payback of 10 years with a 30% investment tax credit.

2.1.2 U-shaped spray tower

The other method uses a U-shaped spray tower to prevent the carry-over problem. A U-shaped spray tower for preventing carry-over has been designed to study the stripping of water vapour from aqueous desiccant solutions of 91.8 to 95.8 wt. % triethylene glycol (Chung et al. 1999).

2.2 Thermal Models Reported on Liquid Desiccant Dehumidification/Regeneration System

Treybal (1969) was the first person to describe the complex heat and mass transfer process which occurs during air dehumidification by proposing a simple mathematical model. Merkel (1925) came up with an analytical model to describe the heat and mass interactions between air and the working fluid for evaporative cooling purposes, but his model does not consider the evaporation loss. Nottage (1941) and Yadigaroghu and Pastor (1974) modified the Merkel model by considering evaporation loss and achieved higher accuracy compared to Merkel's model. Zhang et al. (2012) proposed an analytical model for analyzing the simultaneous heat and mass transfer processes involved in a counter – flow cooling tower and validated with the experimental data available in the literature. Peng and Howell (1981) developed mathematical models for two liquid desiccant systems powered by solar or geothermal energy and using triethylene glycol as the desiccant solution. Their parametric analysis showed that the optimum absorber height for the process recirculation mode is 1.2 m, while for the exhaust recirculation mode it is 0.9 m. The exhaust recirculation mode has better thermal performance and lower fan power requirements at full capacity, but the process recirculation mode produces cooler and drier air. Factor et al. (1980), Fumo and Goswami (2002) and Khan et al. (1992) developed finite difference based thermodynamic models to evaluate the liquid desiccant dehumidifier and regenerator, whereas Stevens et al. (1989) provided analytical expressions of the air and desiccant parameters in the counter-flow dehumidifier. Jain et al. (1994) attempted to evaluate seven liquid desiccant cycles for hot and humid climates. A computer simulation model was developed based on the constant effectiveness of heat exchangers and evaporative coolers. The effect of various outdoor conditions and the effectiveness of heat exchangers on the cooling capacity have been investigated. It was found that a combination of dehumidifier and wet surface heat exchanger shows better performance, for a wide range of outdoor conditions. Oberg et al. (1998) introduced NTU method to analyze the performance of the aforementioned systems.

Babakhani et al. (2010) and Liu et al. (2010) compared their mathematical models based on finite difference/NTU method with the experimental findings and concluded that their models were in good agreement with the experimental data. Chengquin et al. (2006) developed a model for heat and mass transfer interactions in a liquid desiccant dehumidifier/regenerator. Patil et al. (2016) developed an empirical correlation for estimating the actual gas – liquid contact area and found more accurate than other correlations with a maximum deviation of ±15%. Zalewski et al. (1997) developed a mathematical model by introducing a correction factor for mass transfer coefficient. Gandhidasan (2004, 2005) presented a simplified model using dimensionless parameters such as moisture and thermal effectiveness and formulated the correlations for predicting the evaporation and condensation rates in terms of heat and mass exchange effectiveness. The proposed model has been compared with the experimental data of Fumo and Goswami (2002), and the error has been found to be within ±13%. Peng et al. (2017) studied the heat and mass transfer characteristics of a packed tower by proposing a thermodynamic model. They compared the developed model with the experimental data of Fumo and Goswami (2002) and observed a maximum error of ±18%. Lu et al. (2001) & Ren et al. (2006) reported a method for finding the analytical solution of the coupled heat and mass transfer performance for the dehumidifier and regenerator. Analytical solutions of the air enthalpy and desiccant equivalent enthalpy field within the cross-flow dehumidifier/regenerator were given by Liu et al. (2006, 2007), where the air and desiccant are not mixed breadthwise (which means the transfer processes of the air and desiccant are both two dimensional). The enthalpy field gained from the analytical solutions compares well with numerical solutions, and the analytical enthalpy efficiency compares well with experimental results of the cross-flow dehumidifier. Researchers (Dai et al. 2004; Khan et al. 1998; Liu et al. 2007) have developed mathematical models of the coupled heat and mass transfer processes in the dehumidifier or regenerator, and most of the models were solved numerically. Davoud and Meysam (2009) presented a new analytical solution of heat and mass transfer processes in a packed bed liquid desiccant dehumidifier. Their results revealed that design variables such as desiccant concentration, desiccant temperature, air flow rate, and air humidity ratio have the greatest impact on the performance of the dehumidifier. The liquid flow rate and the air temperature did not have a significant effect. Furthermore, the effects of air and liquid desiccant flow rate have been reported on the humidity effectiveness of the column. Langroudi et al. (2014) statistically evaluated the performance of the liquid desiccant dehumidification system using response surface methodology (RSM) and studied the heat and mass transfer processes occurring in the liquid desiccant dehumidification system. They compared the proposed model

with the NTU model available in the literature and found good agreement with an accuracy of ±13%. Chung and Gosh (1996) developed heat and mass transfer correlations and studied performance of the liquid desiccant dehumidifier using lithium chloride as a desiccant solution. Yin et al. (2009) investigated the heat and mass transfer interactions along the liquid desiccant dehumidifier and regenerator using a mathematical model validated by the experimental data.

In the aspect of theoretical studies, several thermodynamic models have been developed for predicting the heat and mass exchange processes in the adiabatic dehumidification/regeneration system which includes finite difference model (Factor and Grossman, 1980; Oberg and Goswami, 1998; Liu et al. 2007), ε – NTU model (Babakhani and Soleymani, 2009, 2010; Peng and Zhang, 2011; Stevens and Braun, 1989) and simplified models (Gandhidasan 2004, 2005; Liu et al. 2006). In the present study, a two dimensional finite difference based thermodynamic models are developed for counter-flow adiabatic liquid desiccant dehumidification/regeneration system. On the basis of present investigation, a comparison is made with the notable contributions presented in the literature for highlighting the importance of the proposed thermodynamic model as listed in Table 2.1.

Table 2.1, Comparison of present model with the two dimensional models available in the literature for the liquid desiccant dehumidification/regeneration system.

Authors (year)	Flow pattern	Type of system	Notable contribution
Liu et al. (2007)	Cross	Dehumidifier/regenerator	Developed a finite difference model by assuming Le = 1 and NTU as an input parameter.
G. Diaz (2010)	Parallel	Dehumidifier	Developed a transient model for analysing the flow dynamics along the parallel flow liquid desiccant dehumidifier.
Luo et al. (2014)	Counter	Dehumidifier	Developed a CFD model for predicting the local film thickness, local water vapour concentration and working fluid temperature along the dehumidifier.
Luo et al. (2014)	Counter	Dehumidifier	Developed a CFD model for predicting the flow situations in the dehumidifier.
Huang et al. (2017)	Cross	Dehumidifier	Developed a coupled heat and mass transfer model for analysing the

			simultaneous heat and mass transfer processes across the liquid desiccant dehumidifier.
Das and Jain (2015)	Cross	Dehumidifier	Influence of different types of flat plate membrane contactors on performance characteristics of dehumidifier are analyzed.
Liu et al. (2007)	Cross	Dehumidifier and regenerator	Studied the air and desiccant parameters numerically by taking constant Lewis number (Le = 1).
Khin et al. (2013)	Cross	Dehumidifier	Performance characteristics of the dehumidifier is analyzed using air to air heat and mass transfer processes.

2.3 Experimental Studies for Liquid Desiccant Dehumidification/Regeneration System

Chen et al. (1989), Patnaik et al. (1990), McDonald et al. (1992), Chung et al. (1993), and Pontis and Lenz (1996) reported experimental results of packed bed dehumidifiers using salt solutions as desiccant. Chung et al. (1995) reported experimental findings and developed correlations for heat and mass transfer coefficient of a structured packed column using structured packing and tri ethylene glycol (TEG) as the desiccant. Oberg and Goswami (1998) developed a model for simultaneous heat and mass transfer between air and TEG desiccant in a packed bed absorption tower. A comparison between the experimental and the theoretical results showed that the model gave good predictions of the heat and mass transfer between desiccant and air. Bravo et al. (1985) studied the structured packing and found excellent performance characteristics with a relatively low ratio of pressure drop to heat and mass transfer coefficient per unit volume. Lazzarin et al. (1999) developed a numerical model of a packed tower and carried out a parametrical study using LiBr and $CaCl_2$ to obtain the optimum operative conditions. The experimental results matched closely with values predicted by the numerical model. Sanjev et al. (2000) studied theoretically and experimentally a liquid desiccant cooling system made of a falling film tubular absorber and a falling film regenerator. For the purpose of performance evaluation, the authors defined wetness factors to characterise the uniformity of wetting of the surface of the contactors (dehumidifier and regenerator) by the desiccant solution. Their study is of great interest from designing viewpoint, as it can help

calculate more accurately the size of the contactors. Hamed (2003) investigated the desorption characteristics of a packed porous bed. The measurements were compared with the analytical solution. Zurigat et al. (2003) investigated the performance of an air dehumidifier employing TEG under hot and humid conditions using two different structured packing's, wood and aluminium. The performance of the dehumidifier was evaluated and expressed in terms of moisture removal rate and dehumidifier effectiveness.

Gommed et al. (2004) experimentally studied the performance of packed-bed heat and mass exchangers flooded with lithium chloride solutions. The researchers first implemented their conditioner and regenerator as internally cooled units using either copper tubes or polypropylene tubes as the contact surface. Liu et al. (2006) experimentally invetigated the performance of a cross-flow liquid-desiccant conditioner that used structured packing flooded with a solution of lithium bromide. Performance was reported in terms of the moisture removal rate for the conditioner and its dehumidification effectiveness (i.e., the change in the humidity ratio of the air expressed as a percentage of the theoretical maximum change) at different desiccant flow rates, airflow rates, desiccant inlet temperature, desiccant inlet concentration, air inlet temperature, and air inlet humidity ratio. Chen et al. (2005) reported the regenerator's average COP was 0.82 and the average COP for the overall cooling process was 1.50. Mohan et al. (2008, 2015) studied the performance of dehumidifier and regenerator for a liquid desiccant –vapour compression system and found that higher room temperature lowers air dehumidification and desiccant regeneration.

In the present study, using LiCl as liquid desiccant, an experimental investigation is carried out in accordance with humid subtropical climate for counter-flow adiabatic liquid desiccant dehumidification/regeneration system. Based on present investigation, a comparison of the present investigation is made with respective investigations in the literature (Table 2.2).

Table 2.2, Notable contributions of experimental investigations in the literature using LiCl as liquid desiccant for the counter-flow liquid desiccant dehumidification/regeneration system.

Authors (year)	Type of system	Notable contribution
Chung and Gosh (1996)	Dehumidifier	Compared the performance of the random and structured packing dehumidifier and developed empirical correlations for heat and mass transfer coefficients of the

		random and structured packing liquid desiccant dehumidifier.
Fumo and Goswami (2002)	Dehumidifier/regenerator	Studied the influence of ambient and operating parameters on evaporation and condensation rates. Further, analysed the performance of the liquid desiccant dehumidifier and regenerator in accordance with hot and humid climate.
Longo and Gasparella (2005)	Dehumidifier/regenerator	Studied the mass transfer characteristics of the randomly packed column dehumidifier and regenerator. Also, investigated the performance of the dehumidifier and the regenerator using LiCl, LiBr and KCOOH as a liquid desiccant materials.
Zhang et al. (2010)	Dehumidifier/regenerator	Developed dimensionless correlations for mass transfer coefficient of the liquid desiccant dehumidifier and regenerator. Further, investigated the performance of the structured packing dehumidifier/regenerator for summer and winter climatic conditions.
Wang et al. (2016)	Dehumidifier	Developed empirical correlations for enthalpy and moisture effectiveness. Further, experimentally investigated the influence of packing height for different desiccant flow fluctuations and consequently, optimized the packing height of the liquid desiccant dehumidifier.
Xian Li et al. (2016)	Dehumidifier	Studied the heat and mass transfer characteristics of the liquid desiccant dehumidifier and compared the developed dynamic model with the results obtained from the experimental analysis.
Qiong Wu et al. (2017)	Dehumidifier	Developed a desiccant solution regulation strategy for the liquid desiccant dehumidifier and studied the effectiveness of this strategy in different working conditions.

2.4 Exergy and Entransy Analyses of a Liquid Desiccant Regenerator

Many researchers have analysed the coupled heat and mass transfer processes in the liquid desiccant regeneration system by conducting experimental studies (Martin and Goswami, 2000; Jain et al. 2000; Fumo and Goswami, 2002) and also employing numerical schemes (Gandhidasan, 2005; Ren et al, 2006; Liu et al. 2010; Babakhani and solymeni, 2010). Jain et al. (2000) experimentally studied the simultaneous heat and mass transfer characteristics of the falling film plate type liquid desiccant regenerator. Longo and Gasparella (2005) experimentally studied the performance of the liquid desiccant dehumidification/regeneration system based on random packing configuration. Liu et al. (2013) developed a finite difference model for studying the effect of performance parameters on the liquid desiccant regenerator. Some researchers have focused on optimization of operating parameters for improving the heat and mass transfer characteristics of the regeneration system (Sultan et al. 2002; Yin et al. 2009). Sultan et al. (2002) investigated the influence of inlet parameters on coupled heat and mass transfer processes and provided an optimal solution for increasing the contact time between the air and the desiccant solution. Yin et al. (2009) studied the heat and mass transfer behaviour of an internally – cooled regenerator and also discussed the effect of heat and mass transfer coefficients on performance of the regenerator.

Very few researchers have carried out exergy and entransy analyses of the liquid desiccant dehumidification system (Wang et al. 2010; Xiang et al. 2010; Zhang et al. 2012; Zhang et al. 2014; Zhang et al. 2017; L. Zhang et al. 2017). Xiang et al. (2010) and Zhang et al. (2014) studied the exergy performance of the liquid desiccant dehumidification system and identified the sources of exergy destruction. Wang et al. (2010) investigated the exergy transfer rates of the ideal liquid desiccant dehumidification system. Zhang et al. (2012) carried out preliminary investigations on liquid desiccant ACS (LDACS) based on entransy theory. Zhang et al. (2017) studied the exergy and entransy analyses of the humid air handling process between air and the desiccant solution. Zhang et al. (2017) analysed the heat and mass transfer characteristics of a counter – flow packer tower and LDACS based on entransy theory.

2.5 Application of Solar Energy as Low-Grade Energy

For liquid desiccant ACSs, energy is required to regenerate the liquid desiccant for dehumidification purpose, which may come from clean energy sources such as natural gas or low grade heat sources such as solar energy and geothermal energy.

The most popular type of energy source used in the commercial market is solar energy. There have been numerous attempts in capturing the benefits of desiccants in a solar driven ACSs. Löf proposed a solar air conditioner that used triethylene glycol (Lof, 1955). In the early 1980s, American Solar King manufactured and sold a residential solar cooling system that used a lithium-chloride solid-desiccant rotor (Coellner, 1986). When energy prices declined in the late 1980s, American Solar King converted their product to a gas-fired unit. Robison conducted a 2-year field test on a solar cooling system that used a calcium-chloride liquid-desiccant conditioner (Robison, 1983). The test demonstrated the technical feasibility of this solar cooling system, but there was no attempt to commercialize the technology. Schlepp and Schultz (1984) have summarized the experiences of many solar desiccant cooling activities that followed the energy crisis of the 1970s. Most of the research on solar driven liquid desiccant based ACS began in the early 1990s.

In solar driven liquid desiccant based ACS, solar collector is one of the important component because as discussed earlier, solar heat is required to regenerate the liquid desiccant for reuse in dehumidification process. Numerous studies were carried out for analysing the performance of the evacuated tube and flat plate type solar collectors. These studies concluded that evacuated tube type solar collectors were more efficient compared to flat plate type solar collectors (Gautam and Chamoli, 2017).

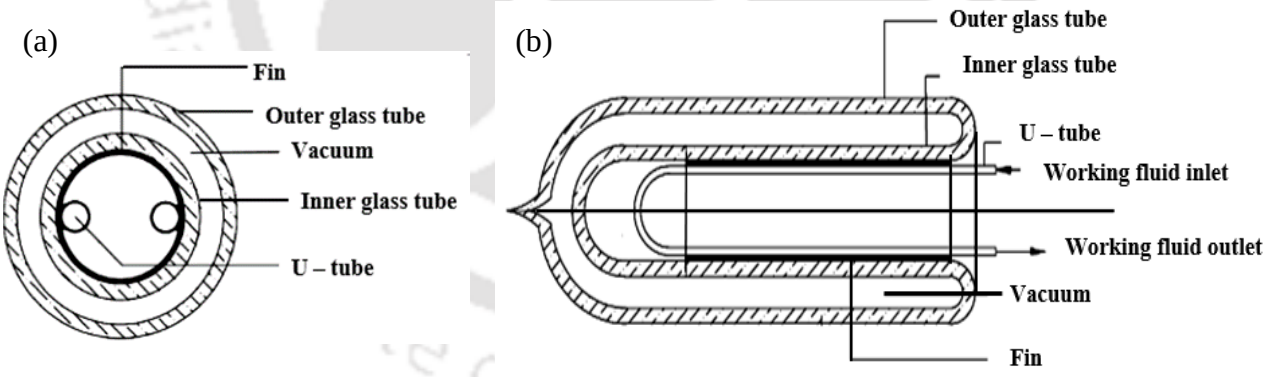

Fig. 2.1, Schematic of evacuated U–tube solar collector a) Cross section and b) Longitudinal section.

Several types evacuated tube solar collector's viz. U – type, H – type, T – type, heat pipe type, etc. for various solar thermal utilization applications have been reported in the literature (Shah and Furbo, 2004; Ataee and Ameri, 2015; Nkwetta and Smyth, 2012). Among these, owing to practical applicability, simplicity in design and lower investment cost, evacuated U – tube solar collector is chosen for the present investigation. Evacuated U – tube solar collector is basically a heat exchanger which transfers the energy from solar radiation from sun to the working fluid. The solar radiation incident on the outer glass surface of the evacuated tube is transferred to

the inner glass tube through radiative heat transfer process and then the heat is absorbed by the U – tube. From U – tube, the heat is exchanged to the working fluid (Fig. 2.1).

2.5.1 Numerical studies on evacuated U – tube solar collector

The study on heat transfer occurring in an evacuated tube solar collector was initiated during 1970s. The first mathematical model for heat transfer analysis and performance predictions of the aforementioned collector was reported by Eberlein (1976) using air as working fluid. The author found that the overall heat loss was very small in the collector due to the evacuated annular space between the glass tubes. Zhiqiang et al. (1984) and Morrision et al. (2004, 2005) investigated the natural circulation flow in the collector tube using water as working fluid. They concluded that buoyancy effect and mass flow rate inside the tube played a significant role in heat transfer process. Hazami et al. (2013) and Nkwetta and Smyth (2013) studied the thermal performance of water in an evacuated tube solar collector with different inner glass surface coating. Shah and Furbo (2004) investigated the theoretical flow of an all-glass evacuated tube collector and mentioned that collector tube with shorter length achieved the highest efficiency. Kim et al. (2016) compared the numerically investigated model with Eberlein's model and suggested that one-dimensional numerical model could be used in designing the all-glass solar collector tube very efficiently for different geometrical parameters. Badar et al. (2011) evaluated the overall heat transfer coefficient of an evacuated U–tube collector both theoretically and experimentally and reported that the numerically predicted overall heat transfer coefficient has good agreement with the experimental data. Gao et al. (2014) proposed a new mathematical model for predicting the thermal performance of an evacuated U–tube solar collector by taking into account the temperature distribution along the tube radius and axis, and validated their model with experimental data obtained using aluminum as a fin. They investigated the dependence of thermal efficiency on ambient condition and tube design parameters. Kiran et al. (2015) developed an analytical solution for predicting the thermal performance of an evacuated tube solar collector by employing three different working fluids. Ayala et al. (2015) numerically studied the evacuated U–tube solar collector for a special case where the working fluid inlet temperature was less than the ambient temperature. They also predicted the outlet temperature of the heat transfer fluid using two different models, viz. the Boussinesq approximation (BA) model and the variation of thermophysical properties with temperature (VPT) model. They concluded that the BA model has a closer match for both thermal efficiency and outlet temperature compared to the VPT model. Vishal and Avadesh (2017) theoretically

studied the effect of pressure drop and mass flow rate of working fluid on the performance of evacuated tube solar collector using air as a working fluid. Liangdong et al. (2010) developed a thermal model for analysing the effect of absorber coating on the thermal performance of the evacuated U – tube. Farjallah et al. (2016) numerically investigated the thermal performance of the evacuated U – tube solar collector with and without using filler material inside the evacuated tube. From their analysis, it was concluded that performance of the evacuated U – tube solar collector was better when the filler material was used.

2.5.2 Experimental studies on evacuated U – tube solar collector

The studies on evacuated tube type solar collectors have been initiated during 1970s. But the investigations on evacuated U – tube solar collector were started very recently. Badar et al. (2011) experimentally studied the effect of overall heat transfer coefficient on working fluid temperature of the evacuated U – tube solar collector. Later, Gao et al. (2014) carried out experimental studies for analysing the dependency of thermal efficiency on ambient temperature and tube design parameters. Further, they also investigated the temperature distribution across the evacuated U – tube solar collector. Neeraj and Avdhesh (2015) experimentally investigated the performance of two types of evacuated tube solar collectors, viz. first like the above described one and second with a LHS integrated to the collector tube of the working fluid. From the experimental studies, they have observed that the outlet temperature of the working fluid was higher with LHS than without LHS. Kaya et al. (2018) investigated the influence of nanofluid on the thermal performance of evacuated U – tube solar collector and concluded that ZnO/ethylene glycol – water nanofluid provides the better performance than water or air. Rodriguez et al. (2018) developed a methodology for determining the working fluid outlet temperature of an evacuated U – tube solar collector arranged in series. Chen et al. (2017) studied the heat absorbing and vapour generating characteristics of LiBr – H_2O mixture in an evacuated tube solar collector. Lamnatou et al. (2012) investigated the thermodynamic performance of the evacuated tube solar collector for solar dryer application. Liang et al. (2011) validated the theoretical and experimental investigations of U tube evacuated tube collector with filled type and concluded that this collector has a better thermal performance than normal U-tube evacuated type solar collector without filler material.

In the present study, numerical and experimental studies on evacuated U – tube solar collector as well as for the whole system are carried out using water as working fluid and for low solar

intensity regions. Further, for optimizing the performance of the evacuated U – tube solar collector as well as for the system, exergy analysis of the aforementioned system is carried out. On the basis of present study, some of the notable contributions presented in the literature for both the experimental and numerical studies as well as exergy performance of the individual evacuated U – tube solar collector and whole system (array of solar collectors) are listed in Table 2.3.

Table 2.3, Notable contributions available in the literature for evacuated U – tube solar collector.

Authors (year)	Experimental/ theoretical model	Energy/exergy efficiency analysis	Notable Contribution
Liangdong et al. (2010)	Theoretical	Energy efficiency	Studied the thermal performance of evacuated U – tube solar collector by developing a mathematical model.
Liang et al. (2011)	Experimental and theoretical	Energy efficiency	Investigated the thermal performance of the solar collector using a filler material (graphite) in – between the absorber tube and the U – tube.
Gao et al. (2014)	Experimental and theoretical	Energy efficiency	Developed a mathematical model for analysing the temperature distribution across the solar collector and for optimizing the evacuated tube solar collector design. Further, experimentally analysed the working fluid heat transfer characteristics.
Ataee and Ameri (2015)	Theoretical	Energy and exergy efficiency	Theoretically studied the exergy and energy efficiencies of the evacuated U – tube solar collector using CO_2 and air as working fluid.
Liangdong et al. (2016)	Theoretical	Energy efficiency	Developed a heat transfer model for analysing the thermal performance of the filler type evacuated U – tube solar collector.
Farjallah et al. (2016)	Theoretical	Energy efficiency	Developed a numerical model for investigating the evacuated U – tube solar collector

			performance with and without using a filler material.
Kim et al. (2016)	Theoretical	Energy efficiency	Theoretically investigated the efficiency of the evacuated U – tube solar collector using Al_2O_3, CuO, SiO_2 and TiO_2 nanofluids as working fluid.
Xianhua et al. (2017)	Experimental	Energy efficiency	Tested the thermal performance of the evacuated U – tube solar collector at low solar intensities and working fluid inlet temperatures.
Kim et al. (2017)	Experimental	Energy efficiency	Experimentally investigated the performance of the evacuated U – tube solar collector using Al_2O_3 nanofluid as a working fluid.
Kaya et al. (2018)	Experimental	Energy efficiency	Using ZnO/Ethylene glycol – pure water nanofluids, the experimental investigations were carried out on evacuated U – tube solar collector.

2.6 Literature closure

From the literature survey, the following conclusions are made.

2.6.1 Liquid desiccant dehumidification/regeneration system

- From the literature, it is observed that the reported mathematical/thermodynamic models were used for predicting the performance of the liquid desiccant dehumidification/regeneration system by employing complicated numerical procedure.
- There is a lack of profound numerical analysis for analysing the heat and mass transfer behaviour at the air – working fluid interface and also for predicting the variation of evaporation/condensation rates along the tower height.
- Several researchers faced challenges in the estimation of heat and mass transfer coefficients or Lewis number theoretically.
- Several researchers experimentally analysed the performance of the liquid desiccant dehumidification/regeneration system using LiCl as liquid desiccant. But these experimental studies lack the field analysis in accordance with humid subtropical climate.

- Further, there is a lack of profound experimental investigations on sensible and latent energy exchange processes occurring between the liquid desiccant and the ambient air for both liquid desiccant dehumidification and regeneration systems.
- It is also observed that there is a lack of profound exergy analysis which accounts for the irreversibility of heat and mass transfer processes on the liquid desiccant regenerator.
- There is also a lack of profound theoretical studies on analysing the influences of operating parameters on the performance of regenerator based on entransy dissipation theory.

2.6.2 Evacuated U – tube solar collector system

- The energy needed for regeneration of liquid desiccant can be obtained from low grade energy like solar energy. Using solar energy, the performance of liquid desiccant AC is found to be much better.
- Most of the reported studies were focused on analysing the performance of the solar collector using different tube designs and absorber coating materials and very few studies have investigated the effect of filler material (filled inside the absorber/inner tube) on collector efficiency of the evacuated tube.
- Very few researchers have analysed the thermal performance of the evacuated U – tube solar collector by performing experimental studies and by employing numerical/mathematical models.
- The reported numerical/mathematical models are not suited for predicting the working fluid transition time and the heat transfer characteristics along the length of the evacuated U – tube solar collector.
- Further, there is a lack of profound experimental investigation on the performance of the evacuated U – tube solar collector system (multiple evacuated U – tubes connected to a manifold).
- Also, very limited research works has been carried out on investigating energy and exergy efficiencies of the evacuated U – tube solar collector.

2.6.3 Objectives of the present work

Based on the literature closure, the following core objectives are chosen for this thesis:

- To develop a thermal model for analyzing the simultaneous heat and mass transfer processes occurring in a counter-flow packed chamber and to predict the performance of the structured packing chamber.

- To develop a 3D numerical model for evaluating the performance of the individual evacuated U – tube solar collector as well as for the whole solar collector system.
- To design and fabricate a liquid desiccant dehumidification/regeneration system of 18 kW capacity.
- To design and fabricate evacuated U – tube solar collector system for achieving the working fluid temperature difference of 35 ^{o}C.
- To perform a detailed experimental study on liquid desiccant dehumidification/regeneration system and evacuated U – tube solar collector system at different operating and ambient conditions.
- To validate the developed thermal models with the experimental data for both the dehumidification/regeneration system and also for the evacuated U – tube solar collector system.
- To carryout energy and exergy analyses of the liquid desiccant dehumidification/regeneration system and the evacuated U – tube solar collector system.
- To analyze the entransy dissipation due to heat and mass transfer processes between the ambient air and the liquid desiccant.
- To propose a simplified thermodynamic model for predicting the heat and mass transfer coefficients along the cross-flow packed chamber by considering the effect of Lewis number.

CHAPTER – 3

NUMERICAL STUDIES

In this chapter, thermal models developed for theoretically assessing the heat and mass transfer characteristics along the liquid desiccant dehumidifier/regenerator and the heat transfer characteristics across the evacuated U – tube solar collector are presented. This chapter mainly focuses on the following;

- To develop a thermal model for assessing the performance of dehumidifier/regenerator.
- To solve developed model for dehumidifier/regenerator using backtracking algorithm.
- To propose a numerical model for predicting the performance of the solar collector.
- To theoretically investigate the performance of the solar collector using filler material.

3.1 Liquid desiccant dehumidification/regeneration system

Packed tower is an important component in the liquid desiccant dehumidification/regeneration system. This tower is generally used for exchanging heat and mass between gas – liquid or liquid –liquid interfaces. Other than packed tower, falling film type and spray type towers are also used for heat and mass transfer interactions. But the packed type is more preferable. This is because, it can handle strong flow fluctuations, has relatively low pressure drop and is compact in nature. Also, it is capable of achieving relatively high mass transfer efficiency (Perry et al, 2007). Further, it is economically feasible and can be easily scaled up to any

capacity. In this study, heat and mass interactions between the air and the desiccant solution of a packed tower is analysed.

In the packed tower, ambient air enters into a column where it exchanges heat and mass with a desiccant solution that enters the column in counter-flow direction. The operating conditions of the packed tower are chosen depending upon the type of component (dehumidifier/regenerator). If it is a dehumidifier, the heat and mass transfer processes take place from air to desiccant solution (dehumidification process), whereas in a regenerator, the transfer processes occur from desiccant solution to air (humidification process), as shown in Fig. 3.1.

From the literature, it is observed that the reported mathematical/thermodynamic models were used only for predicting the performance of the liquid desiccant dehumidifier/regenerator employing complicated numerical procedure. Further, major challenges faced by several researchers are the estimation of heat and mass transfer coefficients (Zhang et al. 2012; Yimo et al. 2014; Patil et al. 2016). It is observed from the reported works that there is a lack of profound numerical analysis for analyzing the heat and mass transfer behaviour at the air – desiccant desiccant solution interface and also predicting the variations of evaporation/condensation rates along the tower height. Therefore, the present study focuses on developing a simplified thermodynamic model based on finite difference method for analyzing the heat and mass transfer interactions that take at the air – desiccant desiccant solution interface. In addition, the proposed model also aims at developing simplified expressions for predicting the heat and mass transfer coefficients compared to previous models reported in the literature. A backtracking and recursive algorithm are proposed for computing the developed thermodynamic model in Matlab R2013a. The simulation results are validated with the experimental data of the liquid desiccant dehumidifier/regenerator. On the basis of simulated results, contour plots are developed for analyzing the heat and mass transfer interactions take place along the height of the packed tower in a counter-flow direction. Also, the evaporation/condensation rate variation is reported along the height of the counter-flow packed tower.

3.1.1 Thermodynamic model for counter-flow packed tower

The schematic representation for heat and mass transfer processes occurring between the desiccant solution and the ambient air in a counter-flow packed tower is shown in Fig. 3.1. Following assumptions are considered to simplify the analysis,

- Adiabatic evaporation or condensation process.
- Mass flux along the packed tower for desiccant solution and air are constant (Naik and Muthukumar, 2017).
- Thermo – physical properties of air and desiccant solution do not vary with temperature.
- Variation of air and desiccant properties along the width of the packed tower is negligible (Changquin et al. 2006; Koronaki et al. 2013).
- Pressure drop across the tower height is neglected (Elsarrag et al., 2005).

a) Air side

Heat and mass balance across the interface for air side is formulated as

$$G_a dh_a = G_a \left(C_{p,v} T_a + \delta\right) d\omega_a + \alpha_h a_s \left(T_l - T_a\right) dZ \tag{3.1}$$

where G_a is air mass flux (kg/m^2–s), ω_a is air humidity ratio (kg$_v$/kg$_{da}$), T_a and T_l are the air and desiccant desiccant solution temperature (^{o}C), α_h is heat transfer coefficient (W/m^2–K), a_s is specific surface area per unit volume (m^2/m^3), h_a is air enthalpy (kJ/kg), δ is latent heat of vaporization (kJ/kg) and Z is tower height (m).

The enthalpy on the air side is given by

$$h_a = (C_{p,a} + \omega_a C_{p,v}) T_a + \omega_a \delta \tag{3.2}$$

Eq. (3.2) can be differentiated as

$$dh_a = C_{p,a} dT_a + \delta d\omega_a + C_{p,v} \left(T_a d\omega_a + \omega_a dT_a\right)$$

(3.3)

Combining Eqs. (3.1) & (3.3), the change in air temperature along the height of the packed tower is obtained as

$$\frac{dT_a}{dZ} = \frac{\tau_h \left(T_l - T_a\right)}{C_{p,a} + \omega_a C_{p,v}} \tag{3.4}$$

where $\tau_h = \frac{\alpha_h a_s}{G_a}$; τ_h is the function of heat transfer coefficient and air mass flux.

On integration, Eq. (3.4) can be represented as

$$\int_{T_a^i}^{T_a^o} \frac{dT_a}{(T_a - T_l)} = \int_0^z \frac{-\tau_h}{C_{p,a} + \omega_a C_{p,v}} dZ \tag{3.5}$$

After integrating Eq. (3.5), the air outlet temperature can be expressed as,

$$\frac{T_a^o - T_a^i}{T_l^{avg} - T_a^i} = 1 - \exp\left(\frac{-\tau_h z}{C_{p,a} + \omega_a^{avg} C_{p,v}}\right) \tag{3.6}$$

where $\omega_a \sim \omega_a^{avg}$ and $T_l \sim T_l^{avg}$.

Here, air specific humidity ratio in the packed tower (ω_a) might be equal to the inlet air specific humidity ratio ($\omega_{a,i}$) or equal to the outlet air specific humidity ratio ($\omega_{a,o}$). Therefore ω_a is assumed as ω_a^{avg} and the average of the specific humidity is calculated along the height of the packed tower using Eq. 3.28 presented in Section 3.1.2b. Similarly, T_a is assumed as T_a^{avg} and the average temperature of air is calculated using Eq. 3.31 presented in Section 3.1.2c.

Eq. 3.6 can be written as

$$\frac{(T_a^o - T_a^i)(T_l^i - T_a^i)}{(T_l^i - T_a^i)(T_l^{avg} - T_a^i)} = 1 - \exp\left(\frac{-\tau_h z}{C_{p,a} + \omega_a^{avg} C_{p,v}}\right) \tag{3.6a}$$

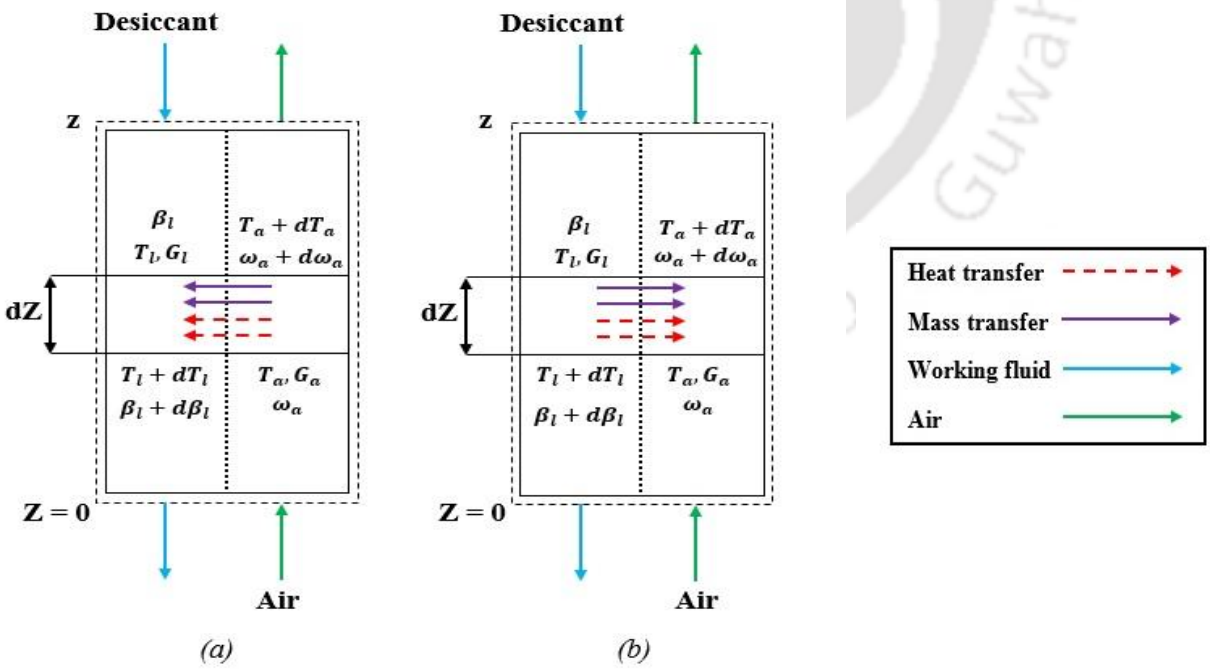

Fig. 3.1, Energy and mass balance across a packed tower (a) counter-flow dehumidifier and (b) counter – flow regenerator.

The major performance characteristics for heat and mass transfer are the heat transfer coefficient and the mass transfer coefficient. To calculate them, thermal effectiveness and moisture effectiveness are used (sections 3.1.1c and 3.1.1f).

b) Thermal effectiveness

The thermal effectiveness is given as (Gandhidasan, 2004, 2005; Naik and Muthukumar 2017)

$$\xi_T = \frac{(T_a^o - T_a^i)}{(T_l^i - T_a^i)} = \frac{(T_a^i - T_a^o)}{(T_a^i - T_l^i)} \tag{3.7}$$

The thermal effectiveness (ξ_T) in terms of heat transfer coefficient (α_h), height of the packed tower (z) and air mass flux is derived from Eqs. (3.6a) & (3.7) as,

$$\xi_T = \left(\frac{T_l^{avg} - T_a^i}{T_l^i - T_a^i}\right)\left[1 - \exp\left(\frac{-\tau_h z}{C_{p,a} + \omega_a^{avg} C_{p,v}}\right)\right] \tag{3.8}$$

As $\frac{T_l^{avg} - T_a^i}{T_l^i - T_a^i} \approx 1$, the final expression is written as,

$$\xi_T = 1 - \exp\left(\frac{-\tau_h z}{C_{p,a} + \omega_a^{avg} C_{p,v}}\right) \tag{3.8a}$$

From Eqs. (3.7) & (3.8a), the expression for air outlet temperature can be derived as,

$$T_a^o = T_a^i + \left(T_l^i - T_a^i\right)\left[1 - \exp\left(\frac{-\tau_h z}{C_{p,a} + \omega_a^{avg} C_{p,v}}\right)\right] \tag{3.9}$$

c) Heat transfer coefficient

Since $\tau_h = \frac{\alpha_h a_s}{G_a}$, the heat transfer coefficient (α_h) in terms of height of the packed tower (z) and air mass flux (G_a) is represented from Eq. (3.8a) as,

$$\alpha_h = \frac{G_a \zeta_T \left(C_{p,a} + \omega_a^{avg} C_{p,v}\right)}{a_s z} \tag{3.10}$$

where $\zeta_T = \ln\left(\frac{1}{1 - \xi_T}\right)$; ζ_T is the logarithmic function of thermal effectiveness.

d) Air outlet humidity ratio

The change in air humidity ratio along the height of the packed tower is written as (Yimo et al. 2014),

$$\frac{d\omega_a}{dZ} = \tau_m\left(\omega_e - \omega_a\right) \tag{3.11}$$

where $\tau_m = \frac{\alpha_m a_s}{G_a}$; τ_m is the function of mass transfer coefficient and air mass flux.

On integration, Eq. (3.11) is represented as,

$$\int_{\omega_a^i}^{\omega_a^o} \frac{d\omega_a}{\left(\omega_e - \omega_a\right)} = \tau_m \int_0^z dZ \tag{3.12}$$

After integrating Eq. (3.12), the air outlet specific humidity is expressed as,

$$\frac{\omega_a^o - \omega_a^i}{\omega_e - \omega_a^i} = 1 - e^{-\tau_m z} \tag{3.13}$$

$$or:\ \omega_a^o = \omega_a^i + \left(\omega_e - \omega_a^i\right)\left(1 - e^{-\tau_m z}\right) \tag{3.14}$$

e) Moisture effectiveness

The moisture effectiveness (ξ_m) is given as (Gandhidasan, 2004, 2005; Naik and Muthukumar 2017)

$$\xi_m = \frac{\omega_a^o - \omega_a^i}{\omega_e - \omega_a^i} = \frac{\omega_a^i - \omega_a^o}{\omega_a^i - \omega_e} \tag{3.15}$$

The moisture effectiveness in terms of height of the packed tower (z), mass transfer coefficient (α_m), air mass flux (G_a) and specific surface area of packing (a) is formulated using Eqs. (3.13) & (3.15) as,

$$\xi_m = 1 - e^{-\tau_m z} \tag{3.16}$$

f) Mass transfer coefficient

Since $\tau_m = \frac{\alpha_m a_s}{G_a}$, the mass transfer coefficient in terms of height of the packed tower (z) and air mass flux (G_a) is represented from Eq. (3.16) as,

$$\alpha_m = \frac{G_a \zeta_m}{a_s z} \tag{3.17}$$

where $\zeta_m = \ln\left(\frac{1}{1-\xi_m}\right)$; ζ_m is the logarithmic function of moisture effectiveness.

g) Desiccant solution side

Heat and mass balance across the interface for the desiccant solution side is written as,

$$G_l dh_l = G_a \tau_h \left(T_a - T_l\right) dZ - G_a \left(C_{p,v} T_a + \delta\right) d\omega_a \tag{3.18}$$

The desiccant solution enthalpy is given as,

$$dh_l = C_{p,l} dT_l \tag{3.19}$$

By combining Eqs. (3.11), (3.18) & (3.19), the desiccant solution temperature change along the height of the packed tower is obtained as,

$$\frac{dT_l}{dZ} = \frac{\gamma}{C_{p,l}}\left[\tau_h \left(T_a - T_l\right) - \left\{\tau_m \left(\omega_e - \omega_a\right)\left(C_{p,v} T_a + \delta\right)\right\}\right] \tag{3.20}$$

where $\gamma = \frac{G_a}{G_l}$; γ is the ratio of mass flux of desiccant solution and air.

After integrating Eq. (3.20), the desiccant solution outlet temperature for a counter-flow packed tower is written as (Fig. 3.1),

$$T_l^o = T_a^{avg} + \left(T_l^i - T_a^{avg}\right)\exp\left(\frac{\gamma z}{C_{p,l}}\left[\left\{\tau_m \frac{\left(\omega_e - \omega_a^{avg}\right)}{\left(T_a^{avg} - T_l^{avg}\right)}\left(C_{p,v} T_a^{avg} + \delta\right)\right\} - \tau_h\right]\right) \tag{3.21}$$

where $\omega_a \sim \omega_a^{avg}$, $T_l \sim T_l^{avg}$ and $T_a \sim T_a^{avg}$.

h) Outlet desiccant concentration for the dehumidifier and the regenerator

The amount of water vapour desorbed from the air across the dehumidifier is equal to the change in concentration of the liquid desiccant, therefore the change in desiccant concentration is expressed as (Koronaki et al. 2013),

$$d\beta = -\gamma \beta d\omega_a \tag{3.22}$$

After integrating Eq. (3.22), the outlet desiccant concentration for the packed tower is expressed as,

$$\beta_l^o = \beta_l^i \exp(\gamma(\omega_a^i - \omega_a^o)) \tag{3.23}$$

i) Condensation rate for the dehumidifier

The rate of water vapour condensed (absorbed) from the air side to the desiccant solution side is defined as condensation rate for the dehumidifier and is given as,

$$d\lambda = -G_a d\omega_a \tag{3.24}$$

$$or:\ \lambda = -G_a(\omega_a^o - \omega_a^i) \tag{3.25}$$

j) Evaporation rate for the regenerator

The rate of water vapour evaporated from the desiccant solution side to the air side is defined as evaporation rate for the regenerator and is given as,

$$d\lambda = G_a d\omega_a \tag{3.26}$$

$$or:\ \lambda = G_a(\omega_a^o - \omega_a^i) \tag{3.27}$$

3.1.2 Numerical simulation

In order to analyze the heat and mass transfer distributions along the packed tower and to predict the outlet and performance parameters of the packed tower (dehumidifier/regenerator), thermodynamic model derived in the aforementioned section needs to be solved numerically using an algorithm. Therefore, a backtracking algorithm is introduced to solve the developed model and Matlab R2013a is used as a simulation software for numerical simulation purposes. The developed thermodynamic model can be alternatively solved by a number of semi – analytical and semi-numerical methods such as the Adomian decomposition method (ADM), the differential transform method (DTM) and the variational iteration method (VIM) (Bizar et al. 2004; Fatoorehchi and Abolghasemi, 2014). But in the present study, the backtracking algorithm is chosen for simplification purpose.

a) Backtracking algorithm

Backtracking algorithm is basically an iterative method in which the generated desiccant solution is compared with a set of conditions at each step. If the conditions are not satisfied, backtracking is done using slightly different set of input data. This process continues till the given set of conditions is satisfied. Then the iteration is terminated. This approach is

advantageous because the number of iterations required during the simulation is much less as compared to other types of algorithms. Hence, the desired output can be attained quickly (Yuan et al. 2015; Turgut, 2017). In the present study, it is necessary to take assumptions for some unknown parameters and check which set of assumed parameters; this provides more accurate results. Further, to validate the present model for multiple parameters, a large number of possible desiccant solutions needs to be tested. Therefore, it is desirable to implement a backtracking algorithm which eliminates the numerous unnecessary test runs by preventing further iterations and advancing to the next set of conditions/instructions whenever it finds the optimal desiccant solution.

The backtracking algorithm used for developing the numerical simulation is shown in Fig. 3.2. The simulation procedure involves a nested loop and three iterative loops. The input parameters that are used for obtaining the outlet and performance parameters (T_a^o, T_l^o, ω_a^o, β_l^o and λ) of the packed tower are air and desiccant desiccant solution inlet temperatures (T_a^i & T_l^i), air inlet humidity ratio (ω_a^i), air and desiccant desiccant solution mass flux (G_a & G_l), specific humidity at equilibrium (ω_e), desiccant desiccant solution inlet concentration in case of the dehumidifier and the regenerator (β_l^i), air and desiccant desiccant solution thermo – physical properties and the packed tower specifications.

Initially in the nested loop, equally spaced moisture and thermal effectiveness (ξ_m & ξ_T) values are generated in between 0 and 1 for predicting the outlet air temperature and specific humidity values (T_a^o & ω_a^o) using Eqs. (3.7) & (3.15). These values are compared with the experimental results reported in the literature. The combination of $\xi_m$and ξ_T is chosen depending upon the accuracy of T_a^o and ω_a^o. Using the predicted ω_a^o value, β_l^o and λ values are calculated using Eqs. (3.23) & Eq. (3.25) or (3.26).

The average values of air temperature and specific humidity (T_a^{avg} & ω_a^{avg}) are calculated for predicting T_l^o. Two iterative loops are performed to estimate these average values. In these loops, the height of the packed tower is divided into 'n' equal parts using 'n+1' equally spaced nodes namely A_1, A_2, A_3, ……., A_{n+1} (Fig. 3.3).

b) Calculation procedure for ω_a^{avg}

The expression for outlet air specific humidity developed in the present model (Eq. (3.14)) will be used for predicting the specific humidity at each node, i.e.

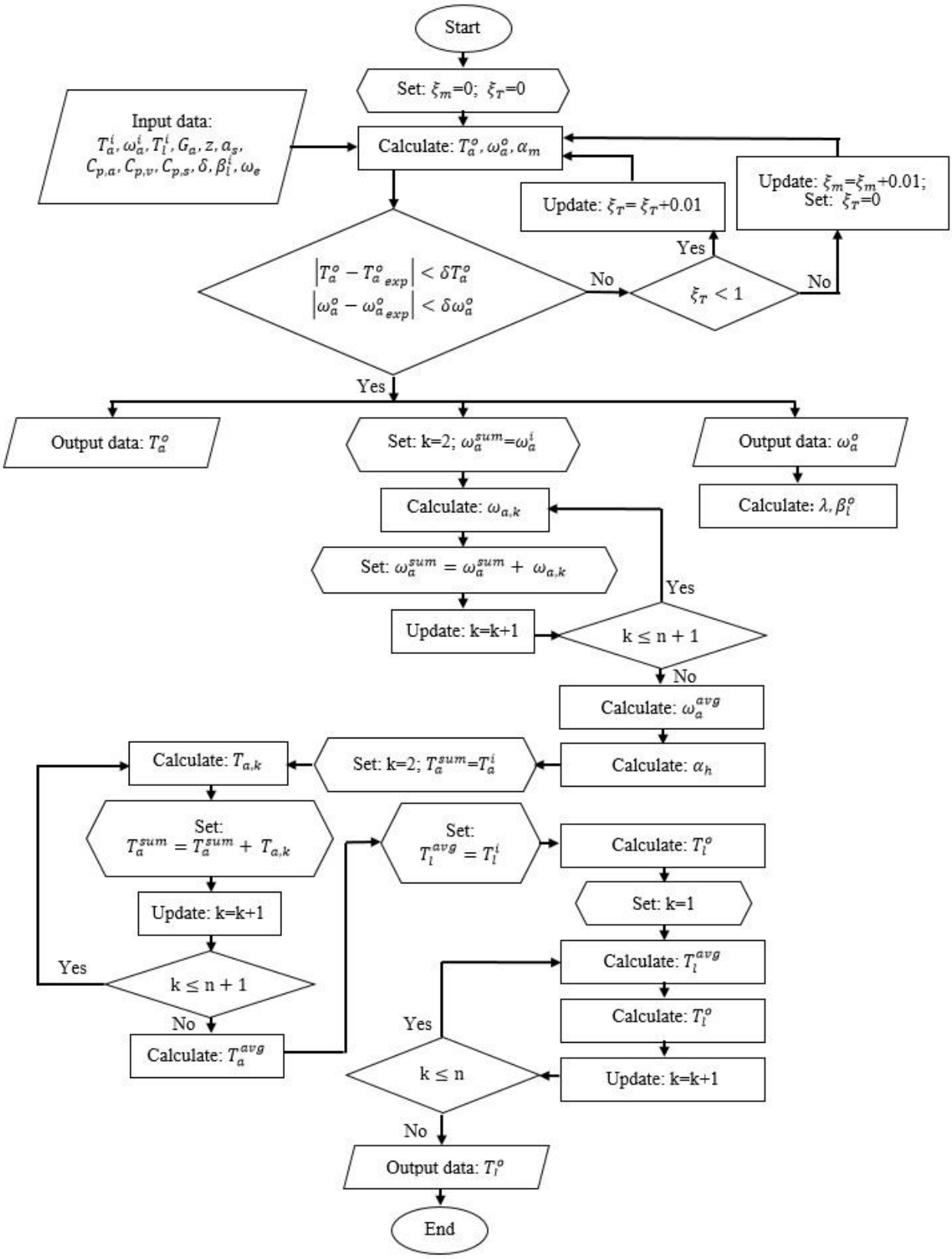

Fig. 3.2, Flowchart for numerical simulation of the developed model.

$$\omega_{a,k} = \omega_a^i + \left(\omega_e - \omega_a^i\right)\left(1 - exp\left(-\tau_m\left(\frac{(k-1)z}{n}\right)\right)\right) \tag{3.28}$$

where k = 2, 3, 4, ……., n+1.

At node A_1, the air specific humidity is defined as

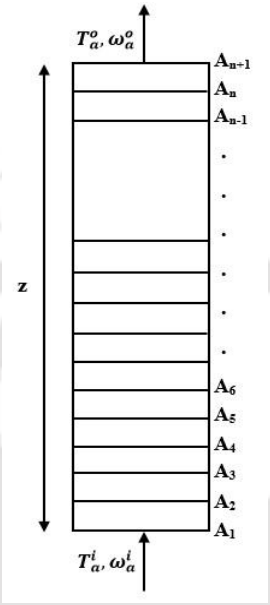

Fig. 3.3, Height of the column divided into 'n' equal parts.

$$\omega_{a,1} = \omega_a^i \tag{3.29}$$

These values from node A_1 to A_{n+1} are added and then, the sum is divided by 'n+1' to obtain ω_a^{avg},

$$\omega_a^{avg} = \frac{\omega_{a,1} + \omega_{a,2} + \omega_{a,3} + ... + \omega_{a,n} + \omega_{a,n+1}}{n+1} \tag{3.30}$$

c) Calculation procedure for T_a^{avg}

The air temperature in each node is predicted using the expression for air outlet temperature developed in the present model (Eq. (3.9)),

$$T_{a,k} = T_a^i + \left(T_l^i - T_a^i\right)\left[1 - \exp\left(\frac{-\tau_h\left(\frac{(k-1)z}{n}\right)}{\left(C_{p,a} + \omega_a^{avg} C_{p,v}\right)}\right)\right] \tag{3.31}$$

where k = 2, 3, 4, ……., n+1.

In the Eq. (3.31), the ω_a^{avg} value is taken from Eq. (3.30).

At node A_1, the air temperature is defined as

$$T_{a,1} = T_a^i \tag{3.33}$$

These values from A_1 to A_{n+1} are added and then, the sum is divided by 'n+1' to obtain T_a^{avg},

$$T_a^{avg} = \frac{T_{a,1} + T_{a,2} + T_{a,3} + \ldots\ldots\ldots + T_{a,n} + T_{a,n+1}}{n+1} \tag{3.34}$$

For obtaining desiccant solution outlet temperature (T_l^o), average desiccant solution temperature (T_l^{avg}) has to be calculated in addition to T_a^{avg} and ω_a^{avg}. Therefore, an iterative loop is performed for calculating T_l^{avg}. In this loop for the first iteration, T_l^o is calculated by assuming $T_l^{avg} = T_l^i$ using the appropriate equation (Eq. 3.21). Then, T_l^{avg} is updated by taking the average of T_l^i and T_l^o obtained in the first iteration. The updated value of T_l^{avg} is then used to calculate T_l^o again. This process is repeated n times to attain accurate T_l^o (Fig. 3.2).

3.1.3 Validation of developed thermodynamic model

a) Comparison of predicted results with experimental data

To use the aforementioned model for predicting the performance parameters of the packed tower with reasonable accuracy, proper validation is needed. Therefore, a comparison is made between the experimental data available in the literature (Fumo and Goswami, 2002; Langroudi et al. 2014; Chung and Ghosh, 1996) and the results predicted from the developed model.

Initially, the validation is carried out for the counter – flow dehumidifier for fifteen cases of experimental data reported by Langroudi et al. (2014) and nine cases of experimental data reported by Chung and Ghosh (1996). Then, the counter – flow regenerator is validated for thirteen cases of experimental data of Fumo and Goswami (2002). Table 3.1 shows the operating conditions used for validating the developed model.

Table 3.1, Operating conditions for the packed tower

Parameter	Langroudi et al. (2014)	Chung and Ghosh (1996)	Fumo and Goswami (2002)
Height of column (m)	0.5	0.4	0.6
Desiccant desiccant solution	LiBr	LiCl	LiCl
Air inlet temperature (°C)	27.7-37.3	21-24.1	29.4-40

Air inlet humidity ratio (g_v/kg_{da})	13.3-20	11.1-16.8	17.7-21
Air mass flux (kg/m^2s)	3.3-5.1	1.3-1.7	0.83-1.44
Desiccant desiccant solution inlet temperature (^oC)	21.8-28.2	16.4-18.9	65-65.8
Desiccant desiccant solution mass flux (kg/m^2s)	3.4-7	10.5-16.8	5.19-7.54
Desiccant inlet concentration (%)	38-48	31-37	32.8-34.9
Type of component	Dehumidifier	Dehumidifier	Regenerator
Type of flow	Counter-flow	Counter-flow	Counter-flow

b) Dehumidifier

Figs. 3.4 and 3.5 show the comparison of predicted values obtained from the developed model with the experimental data available in the literature (Langroudi et al. 2014; Chung and Ghosh, 1996) for the packed tower. Fig. 3.4a – 3.4e and Table 3.2 show the comparison of predicted values with the experimental data (Langroudi et al. 2014; Chung and Ghosh, 1996) of the counter-flow dehumidifier. It is observed that the predicted condensation rate, air and desiccant solution outlet temperatures and air humidity ratio have the maximum deviations of ±8.0%, ±0.6 °C, ±0.9 °C and ±6.1% and the mean deviations of ±4.5%, ±0.2 °C, ±0.3 °C and ±2.7%, respectively with the respective experimental values reported by Langroudi et al. (2014) and Chung and Ghosh (1996) whereas the mean and maximum deviations of desiccant solution concentration is almost negligible.

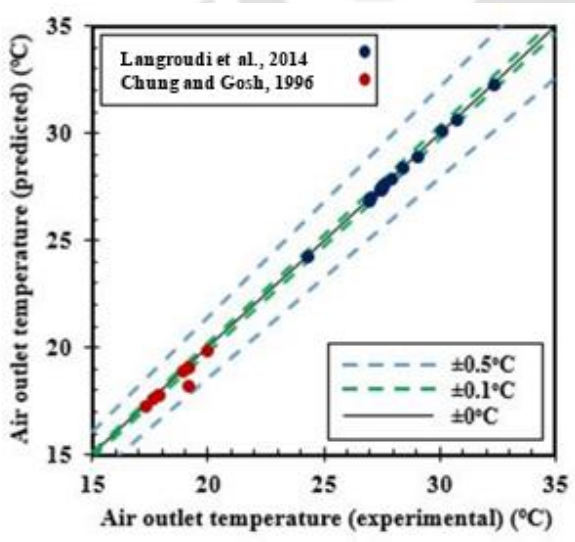

(a)

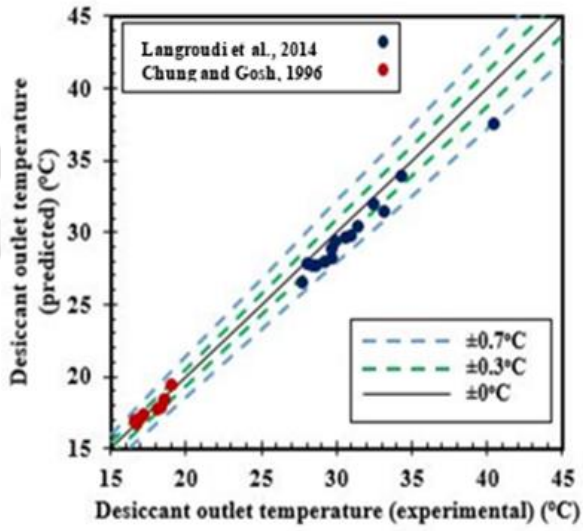

(b)

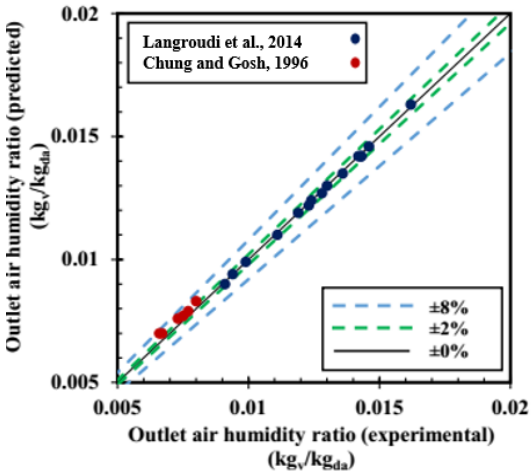

(c)

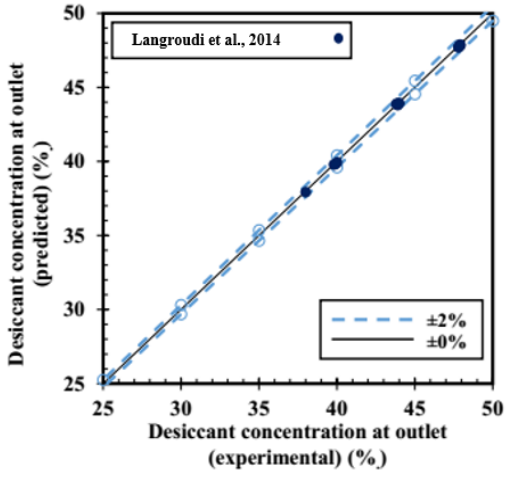

(d)

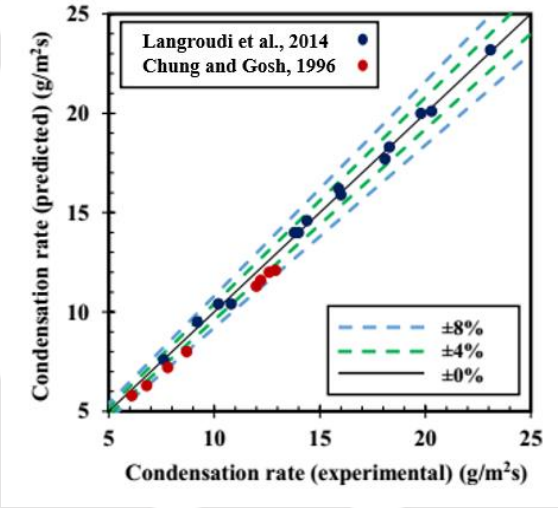

(e)

Fig. 3.4, Comparison of model predictions with the experimental results reported by Langroudi et al. (2014) and Chung and Ghosh (1996) for the counter-flow dehumidification systems: (a) air outlet temperature, (b) desiccant outlet temperature, (c) outlet air humidity ratio, (d) desiccant concentration at outlet and (e) condensation rate.

d) Regenerator

The comparison of predicted data with the experimental data (Fumo and Goswami, 2002) of counter-flow regenerator are shown in Fig. 3.5a – 3.5e and Table 3.2. It is found that the predicted values of evaporation rate, air and desiccant solution outlet temperatures, air humidity ratio and desiccant solution concentration showed the maximum deviations of ± 0.2 ^{o}C, ± 0.3 ^{o}C, $\pm 2.2\%$, $\pm 1.8\%$ and $\pm 1.5\%$, respectively with the experimental values reported by Fumo and Goswami (2002) for the counter-flow regenerator.

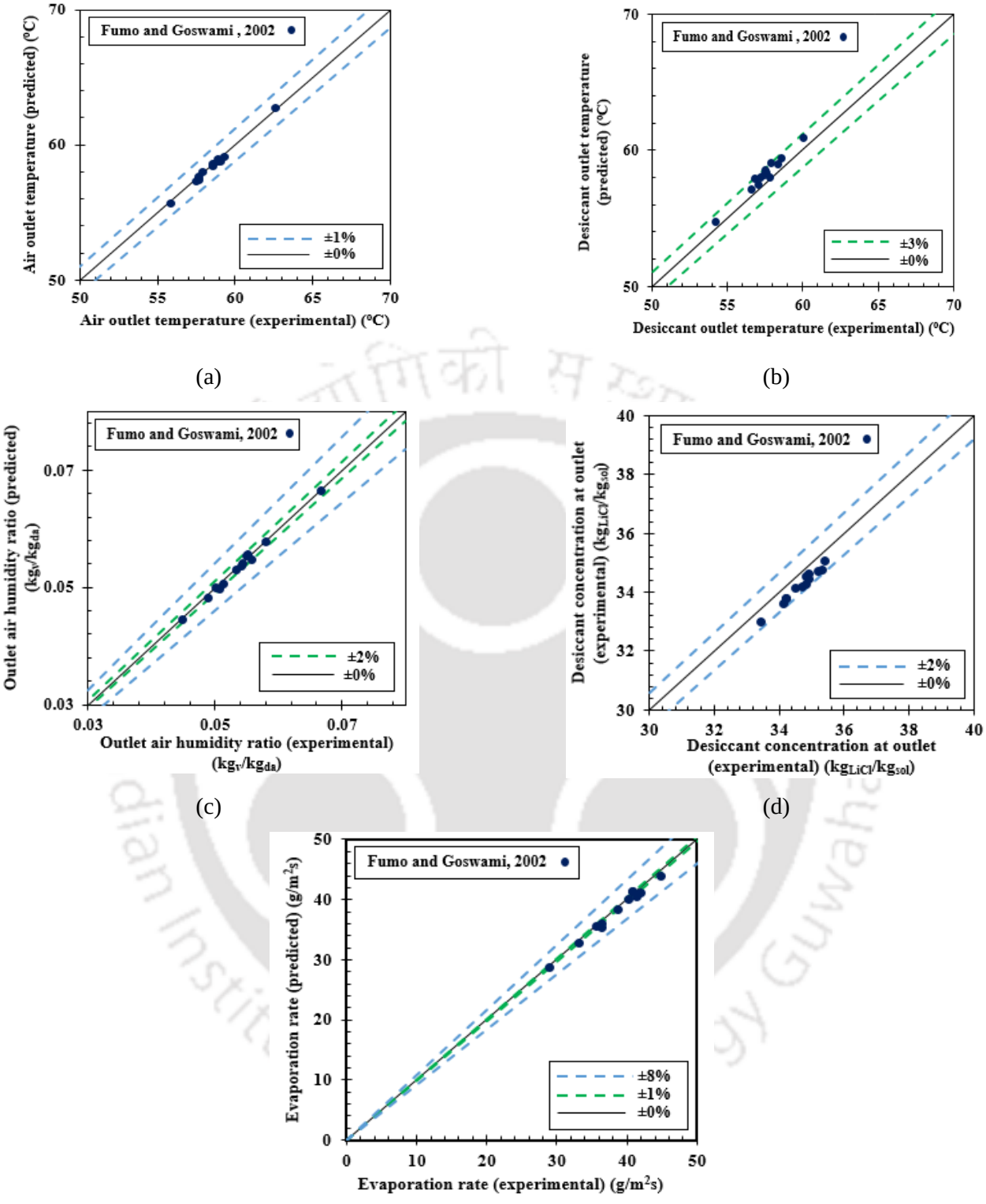

Fig. 3.5, Comparison of model predictions with the experimental results reported by Fumo and Goswami, (2002) for the counter-flow regeneration systems: (a) air outlet temperature, (b) desiccant outlet temperature, (c) outlet air humidity ratio, (d) desiccant concentration at outlet and (e) evaporation rate.

From Figs. 3.4 and 3.5 and Table 3.2, it is observed that the maximum deviation for the performance parameters rarely crosses beyond ±8% and in most of the cases, it is within ±5%. It is also observed that the desiccant solution outlet temperature has a slightly higher discrepancy when compared with other performance parameters. This discrepancy is due to the assumptions made in the analysis and also, due to the fixed number of iterations carried out during the simulation process. It is found that for most of the cases, a closer agreement is achieved at 5000 iterations (N = 5000). By considering the maximum and mean deviations presented in Table 3.2, it is concluded that the developed thermodynamic model is well suited for analyzing the heat and mass transfer processes occurring across the packed tower with better accuracy than the models reported in the literature (Langroudi et al. 2014; Chung and Ghosh, 1996; Fumo and Goswami, 2002).

Table 3.2, Maximum and mean deviations of predicted values with the experimental data reported in the literature for the dehumidifier and regenerator systems

Parameters	Dehumidifier				Regenerator	
	Langroudi et al. (2014)		Chung and Ghosh (1996)		Fumo and Goswami (2002)	
	Max.	Mean	Max.	Mean	Max.	Mean
Outlet air temperature (°C)	±0.2	±0.1	±0.6	±0.2	±0.2	±0.1
Outlet air humidity ratio	1.2%	0.7%	6.1%	-2.7%	1.8%	0.7%
Outlet desiccant solution temperature (°C)	±0.9	±0.3	±0.3	±0.2	±0.2	±0.2
Concentration of desiccant solution	±1.3%	±0.6%	-	-	±1.5%	±1.1%
Evaporation/ Condensation rate	±3.7%	±1.3%	±8.0%	±4.5%	±1.3%	±0.4%

3.1.4 Contour plots for air and desiccant solution operating and performance parameters

Using the developed numerical model, it is also possible to analyze the heat and mass transfer processes occurring along the height of the counter-flow packed tower. The operating (air and desiccant inlet parameters) and performance parameters (condensation/evaporation rate) chosen for analyzing the transfer processes of a counter-flow packed tower are given in Table 3.3. Figs. 3.6 and 3.7 show the air and desiccant solution temperature, air humidity ratio,

desiccant concentration and evaporation/condensation rate distribution plots along the height of the counter-flow dehumidifier and regenerator (using the inlet parameters represented in Table 3.3).

Table 3.3, Inlet and outlet parameters used for analyzing the performance characteristics of the counter-flow packed tower

Dehumidifier (Langroudi et al. (1996)); (Desiccant solution – LiBr)							
	G_a (kg/m^{2}s)	T_a (^{o}C)	ω_a (kg$_v$/kg$_{da}$)	G_l (kg/m^{2}s)	T_l (^{o}C)	β_l (%)	λ (g/m^{2}s)
Inlet parameters	3.3	37.3	0.0185	7	28.2	48	-
Outlet Parameters (experimental)	-	30.1	0.013	-	32.4	47.9	18.3
Outlet parameters (predicted)	-	30.2	0.013	-	32.09	47.87	18.3
Percentage difference (%)	-	-0.1	0.00	-	0.96	0.05	0.00
Regenerator (Fumo and Goswami (2002)); (Desiccant desiccant solution – LiCl)							
Inlet parameters	1.10	30.1	0.0180	6.21	65.1	34.1	-
Outlet Parameters (experimental)	-	59.3	0.0532	-	57.8	34.8	38.6
Outlet parameters (predicted)	-	59.15	0.053	-	58.05	34.31	38.52
Percentage difference (%)	-	0.25	0.9	-	0.4	1.4	0.25

In the counter-flow dehumidifier, the air is cooled and dehumidified simultaneously along its flow direction (Fig. 3.6a, 3.6c), whereas the desiccant solution is heated and diluted along its flow direction (Fig. 3.6b, 3.6d). The condensation rate decreases along the air flow direction (Fig. 3.6e), because the potential for moisture transfer from air to desiccant solution decreases due to decrease in vapour pressure difference.

In the counter-flow regenerator, the air is heated and humidified simultaneously along its flow direction (Fig. 3.7a, 3.7c), whereas the desiccant solution is cooled and concentrated along its flow direction (Fig. 3.7b, 3.7d). The evaporation rate decreases along the air flow direction (Fig. 3.7e). It happens due to the decrease in vapour pressure difference between the air and the desiccant solution.

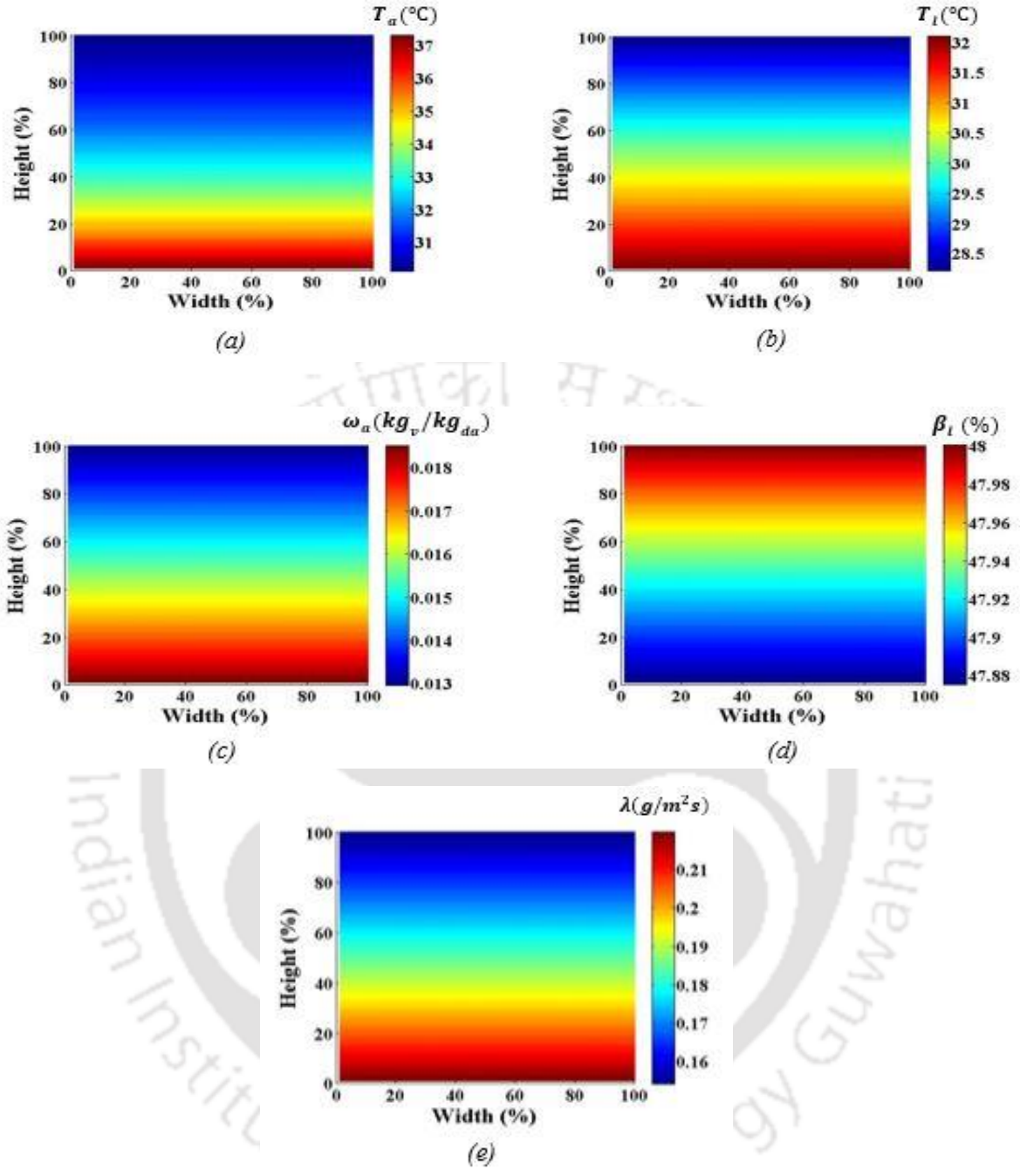

Fig. 3.6, Contour plots for the counter – flow dehumidifier using the inlet parameters given in Table 3: (a) Air temperature, (b) Desiccant solution temperature, (c) Air humidity ratio, (d) Desiccant concentration and (e) Condensation rate.

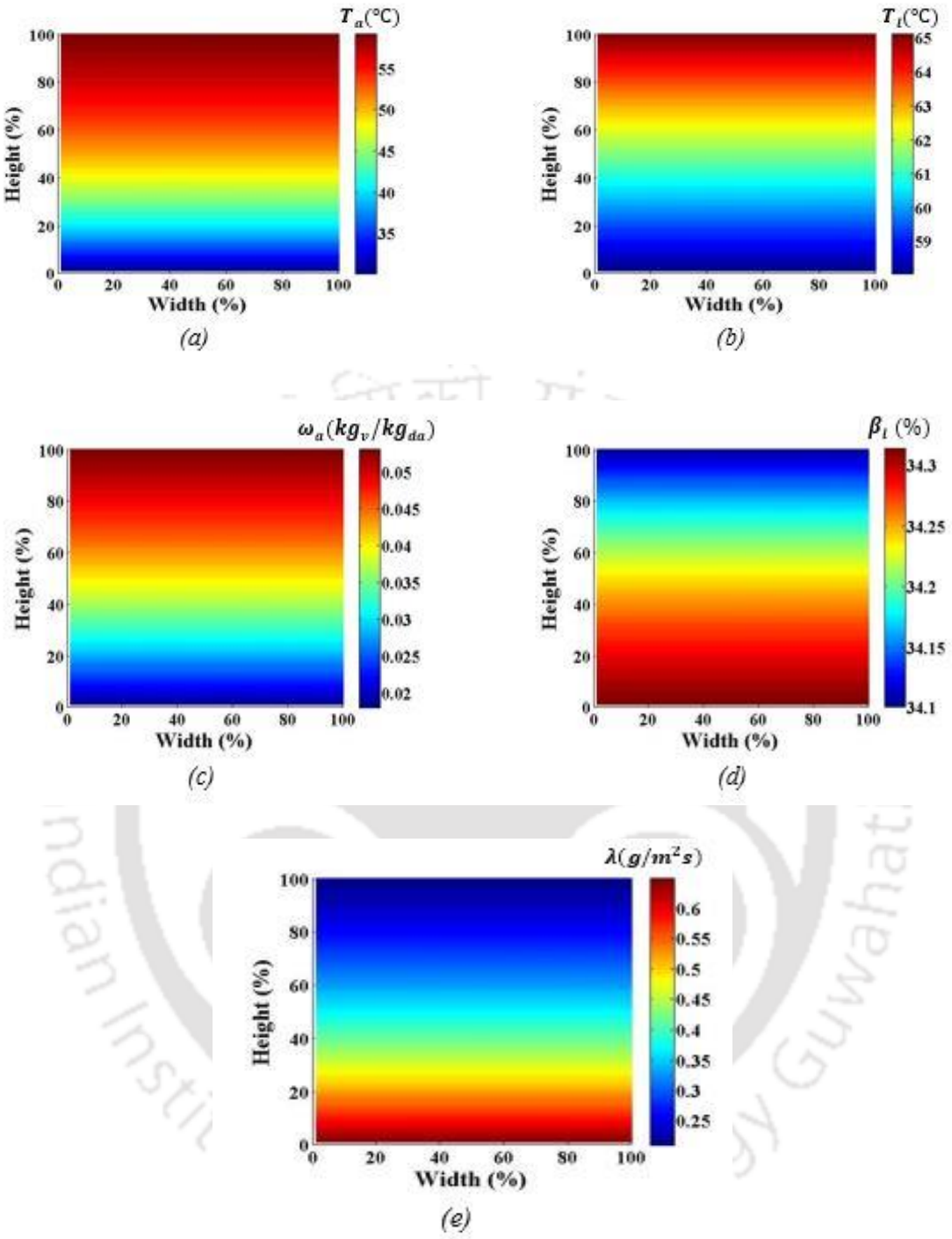

Fig. 3.7, Contour plots for the counter-flow regenerator using the inlet parameters given in Table 3: (a) Air temperature, (b) Desiccant solution temperature, (c) Air humidity ratio, (d) Desiccant concentration and (e) Evaporation rate.

In Figs. 3.6 and 3.7, the value of condensation/evaporation rate (λ) obtained from the simulation process for a particular point is much smaller when compared with the experimental value. This is because the experimental results indicate the total evaporation/condensation rate

for the entire height of the packed tower, whereas the simulated results presented in Figs. 3.6 and 3.7, depict the individual values of λ for a specific partition of height i.e., all the values of λ obtained in the simulated plots would add up to attain the total λ given in the experimental data.

It should be noted that most of the thermodynamic models reported in the literature (Gandhidasan, 2004, 2005; Yimo et al. 2014) have been employed for predicting the outlet and performance parameters ($T_a^o, T_l^o,\ \omega_a^o,\ \beta_l^o$ and λ) of the packed tower. But, this work emphasizes on the coupled heat and mass interactions across the counter-flow packed tower using the distribution plots for air and desiccant temperatures, air humidity ratio, desiccant concentration and evaporation/condensation rate (Figs. 3.6 – 3.7). It is observed from these plots that variation of air and desiccant solution temperatures, air humidity ratio and evaporation rate are significant along the height of the regenerator whereas in the dehumidifier, the variation of desiccant temperature, air humidity ratio and condensation rate are significant. Further, from Figs. 3.6 and 3.7, it is also observed that the evaporation/condensation rate always decreases along the air flow direction.

3.2 Evacuated U – tube solar collector system

The evacuated tube solar collector is similar to a heat exchanger which absorbs solar energy and transfers it to the working fluid (Fig. 2.1). In the present investigation, a finite element method based three dimensional evacuated U–tube solar collector model for both filled and unfilled type is chosen because to compare the accuracy of two dimensional and one dimensional numerical models. 3-D model is expected to provide accurate outlet parameters of the evacuated U-tube solar collector and also useful to visualize the thermal behaviour across and along the evacuated U-tube solar collector. The developed three dimensional numerical model is based on following assumptions,

- Solid materials (glass, aluminium or copper) and the working fluid are isotropic,
- Steady state fluid flow condition along the U–tube, flow is laminar,
- Only radiative heat transfer takes place across the annular–space between the inner and outer glass tube,
- Air gap between the inner glass surface and fin material (aluminium or copper) is negligible
- Conductive heat transfer between the fin material and air is negligible, due to low thermal conductivity of air medium.

The continuity and momentum equations (Eqs. 3.35 and 3.36) are solved simultaneously for predicting the behaviour of the working fluid flowing inside the U–tube. The energy equation (Eq. 3.41) is solved using the velocity field obtained from the solution of Eqs. 3.35 and 3.36. In order to find the temperature distribution of the working fluid, solar irradiation on the surface coating of the inner glass tube and the heat transfers from inner glass tube surface to the solid fin (copper or aluminium), from solid fin to U–tube and from U–tube to the working fluid are considered. The continuity, momentum and energy equations for both the filled and unfilled type U–tube solar collectors are solved with an accuracy of 10^{-3} using the GRMS solver. In this model, variation of working fluid thermo – physical properties on the temperature are considered (See Fig. 2.1).

Continuity equation:

$$\nabla.\vec{V} = 0 \tag{3.35}$$

Momentum equation:

$$\rho_{wf}\vec{V}\left(\nabla\cdot\vec{V}\right) = -\nabla P + \mu\nabla^2\vec{V} \tag{3.36}$$

Energy equation:

Radiation equation: solid – vacuum interface region

Outer glass: $\nabla.\left(k_g\nabla T\right) = \frac{\sigma\varepsilon\Delta T^4}{V}$ (3.37)

Inner glass: $\frac{\sigma\varepsilon\Delta T^4}{V} = \nabla.\left(k_a\nabla T\right)$ (3.38)

Conduction equation: solid – solid interface region

Fin: $\nabla.\left(k_a\nabla T\right) = \nabla.\left(k_f\nabla T\right)$ (without filler material) (3.39)

Fin: $\nabla.\left(k_a\nabla T\right) = \nabla.\left(k_f\nabla T\right) + \nabla.\left(k_{fr}\nabla T\right)$ (with filler material) (3.39a)

U–tube: $\nabla.\left(k_f\nabla T\right) = \nabla.\left(k_u\nabla T\right)$ (without filler material) (3.40)

U–tube: $\nabla.\left(k_f\nabla T\right) + \nabla.\left(k_{fr}\nabla T\right) = \nabla.\left(k_u\nabla T\right)$ (with filler material) (3.40a)

Convection equation: solid – liquid interface region

$$\nabla.\left(k_u\nabla T\right) = \vec{V}.\rho_{wf}c_{p,wf}\nabla T \tag{3.41}$$

3.2.1 Boundary conditions

- The front, back and bottom sides of the evacuated U–tube solar collector are adiabatic (see Fig. 2.1 and 3.8).

$$n.\left(k_m \nabla T\right)=0; \qquad (3.42)$$

where 'n' is the normal vector.

- At upper glass tube surface there is a constant heat input (ζ).
- The outer surface of the glass tube and the inlet of the U–tube are at ambient temperature (T_{amb}) and the working fluid inlet temperature ($T_{w,i}$), respectively.

3.2.2 Mesh generation

Free unstructured triangular mesh has been adapted to ensure that relatively small geometries (U–tube) are discretized with a sufficient number of elements. The grid size for the working fluid is smaller than that for the evacuated tube as it represents a smaller volume. The distribution of elements depending upon the mesh generation is given in Table 3.4a and 3.4b.

Table 3.4a, Grid size and number of mesh elements for evacuated U–tube models.

Sl. No.	Evacuated tube solar collector model	Grid size (mm) Evacuated tube Min	Max	U–tube material Min	Max	Type of mesh element	No. of mesh elements
1	Copper as U–tube material and air as working fluid (Model A)	1.26	6.66	0.50	4.65	Tetrahedral Prism Triangular Quadrilateral Edge Vertex	736472 87788 161465 128 10921 72
		Total no. of mesh elements (radial × axial)				996846 (2716 × 367)	
2	Aluminium as U–tube material and	1.35	7.51	0.63	5.62	Tetrahedral Prism Triangular Quadrilateral Edge Vertex	814873 90744 171465 128 10991 72

Water as working fluid (Model B)		
	Total no. of mesh elements (radial × axial)	1088273 (2857 × 381)

Table 3.4b, Total number of grid elements.

Grid name	Number of elements Evacuated U–tube collector model	
	A (material – copper)	B (material – aluminium)
G_1	7, 68, 437	8, 47,052
G_2	9, 96,846	10, 88,273
G_3	11, 55,344	12, 09,828

3.2.3 Performance parameters

a) Useful heat rate

The amount of heat absorbed by the working fluid from the evacuated tube solar collector is given as

$$Q_{useful} = \dot{m} c_{p,wf} (T_{w,o} - T_{w,i}) \tag{3.43}$$

b) Collector Efficiency

The thermal performance of an evacuated tube solar collector is represented by the collector efficiency (η). It is defined as the ratio of useful heat gained by the working fluid to the product of effective solar radiation incident on the collector (I) and area of the collector (A_c).

$$\eta = \frac{\dot{m} c_{p,wf} (T_{w,o} - T_{w,i})}{\zeta A_c} \tag{3.44}$$

3.2.4 Validation of developed numerical model

Table 3.5, Evacuated tube collector dimensions and surface properties.

Parameters	Evacuated tube collector model - A (Gao et al. 2014)	Evacuated tube collector model - B (Neeraj and Avadesh, 2015)
Outer glass tube diameter (m)	0.047	0.058
Outer glass tube thickness (m)	0.0012	0.002
Outer glass tube transmittance (τ)	0.8	0.8
Thermal conductivity of glass (W/m–K)	1.2	0.74
Inner glass tube outer diameter (m)	0.037	0.047
Inner glass tube thickness (m)	0.0012	0.002
Absorptivity of inner tube (α)	0.92	0.92
Inner glass tube inner surface, emissivity (ε)	0.8	0.8
Air gap (m)	0.001	0.001
Air thermal conductivity (W/m–K)	0.03	0.03
Type of fin	Copper	Aluminium
Fin thickness (mm)	0.6	0.25
Thermal Conductivity of fin (W/m–K)	368	202
U tube outer diameter (m)	0.008	0.01
U tube inner diameter (m)	0.0074	0.0095
Collector tube length (m)	1.5	1.8
Working fluid	Air	Water
Specific heat at constant pressure (C_p) (kJ/kg–K)	1.005	4.2
Heat transfer coefficient between U–tube and working fluid $h_{c(1-c)}$ (W/m^2–K)	250	700
Reynolds number (Re)	Re < 4000	Re < 4000

In order to validate the numerical model, the results obtained for the outlet temperatures of the working fluid from evacuated tube collector are compared with the data reported by Gao et al, (2014) and Neeraj and Avadhesh (2015). The surface properties and specifications of the models are given in Table 3.5. The boundary conditions (section 2.2) are applied to the investigated models for numerical validation. The inlet parameters presented in Table 3.6 are taken as initial and boundary conditions. The numerically predicted working fluid outlet

temperature shows good agreement with the experimental data reported in the literature (Gao et al, 2014 and Neeraj and Avadhesh, 2015) (Table 3.6). The maximum and mean deviations of the predicted data from experimental values are 2.2 °C and -0.03 °C, respectively. In all the 10 cases, the predicted values for working fluid temperature are slightly higher or lower (±2.5 °C) than the experimental values. This small deviation could be due to the variation in thermo–physical properties of the working fluid and experimental uncertainties and due to the assumptions made in the developed model.

Table 3.6, Comparison of experimental results with the present model.

Working fluid – Air (Gao et al, 2014) for evacuated tube collector, Model A							
Inlet parameters					Outlet parameters		
Case	T_{amb} (°C)	$T_{w,i}$ (°C)	$\dot{m}$ (kg/s)	ζ (W/m^2)	$T_{w,o}$ (°C)		
					Exp.	Numerical	difference
1	32	32	0.035	495	39.8	37.9	1.9
2	34.5	34.5	0.035	662	44.5	42.3	2.2
3	35.5	35.5	0.035	748	46.4	44.8	1.6
4	36	36	0.035	836	48	45.9	2.1
5	34	34	0.018	469	39.4	40.5	-1.1
6	35	35	0.018	621	42.3	44.1	-1.8
7	36.5	36.5	0.018	758	44.3	46.4	-2.1
8	37	37	0.018	813	46.4	47.5	-1.1
Working fluid – Water (Neeraj and Avadhesh, 2015) for evacuated tube collector, Model B							
Inlet parameters					Outlet parameters		
	T_{amb} (°C)	$T_{w,i}$ (°C)	$\dot{m}$ (kg/s)	S_{eff} (W/m^2)	$T_{w,o}$ (°C)		
					Exp.	Numerical	difference
9	23.7	22.9	0.027	926	29	30.2	-1.2
10	23.9	56.6	0.030	860	61	61.8	-0.8

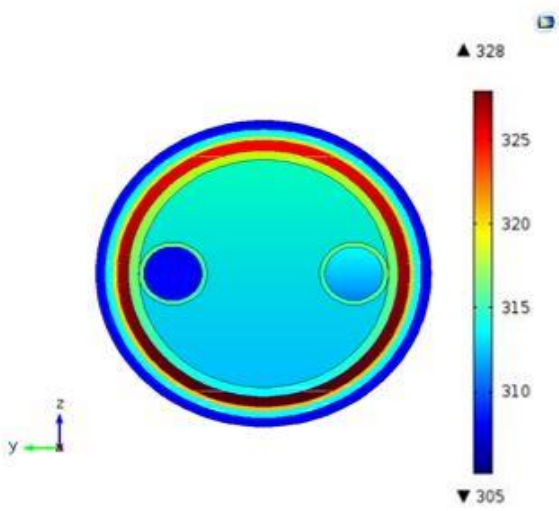

Fig. 3.8, Temperature variation across the evacuated tube solar collector (Front view).

Fig. 3.9, Temperature variation of working fluid along the collector length.

Fig. 3.8 shows the temperature distribution across the front side of evacuated tube solar collector for case 1. As expected, maximum temperature is observed at the inner glass surface due to high radiative heat transfer. After attaining theoretical temperature contour variation plot for whole evacuated U–tube solar collector, individual partwise temperature variation is analyzed along the longitudinal direction. It is observed that there is a significant variation in temperature along the U–tube compared to other parts (aluminium fin and evacuated tube). Therefore, only the contour plot for temperature variation along the length of the U–tube is presented in fig. 3.9.

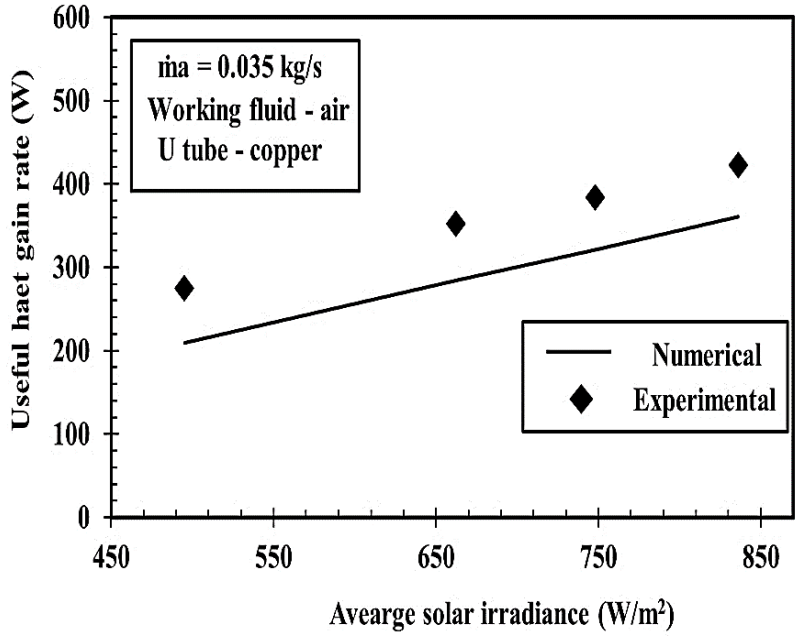

(a)

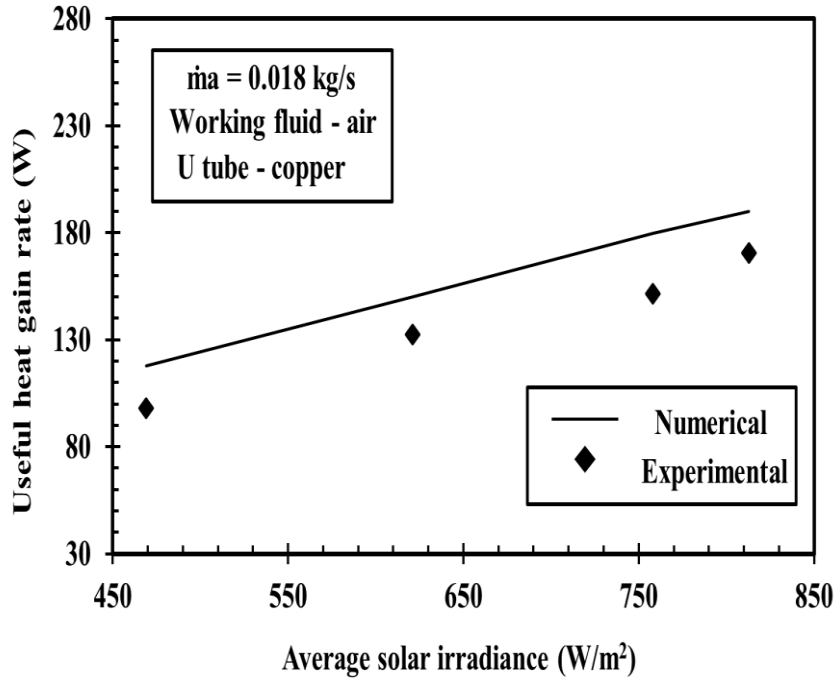

(b)

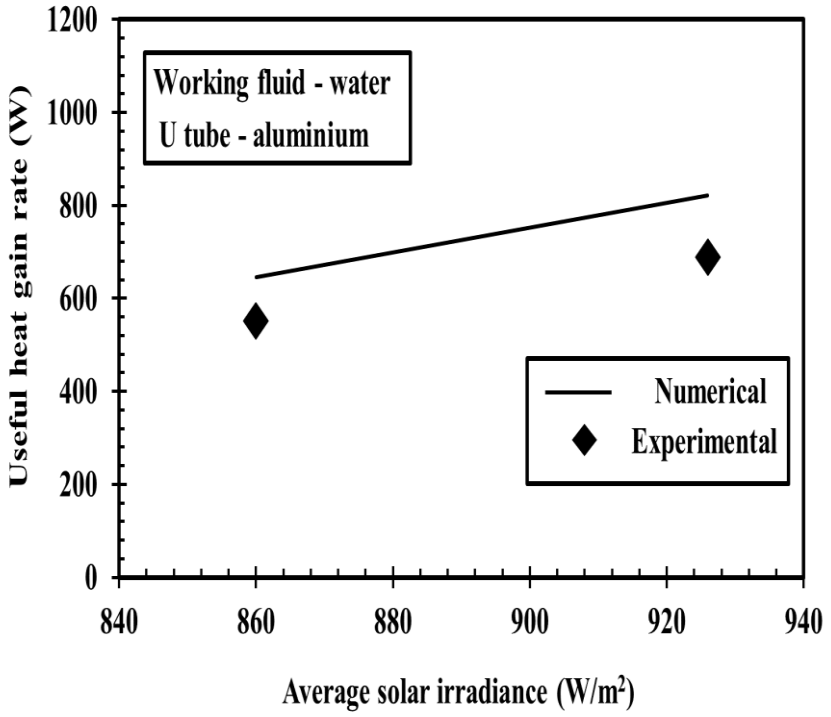

(c)

Fig. 3.10, Comparison of numerically predicted heat gain with experimental data (Gao et al, 2014 and Neeraj and Avadhesh, 2015): Influence of average solar irradiance on heat gain for working fluid air (a and b) and water (c).

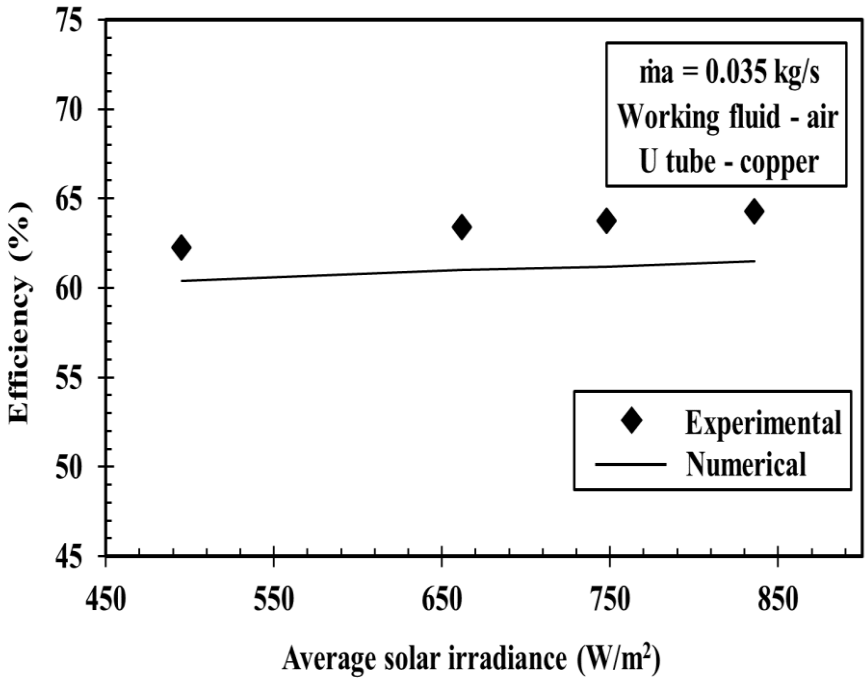

(a)

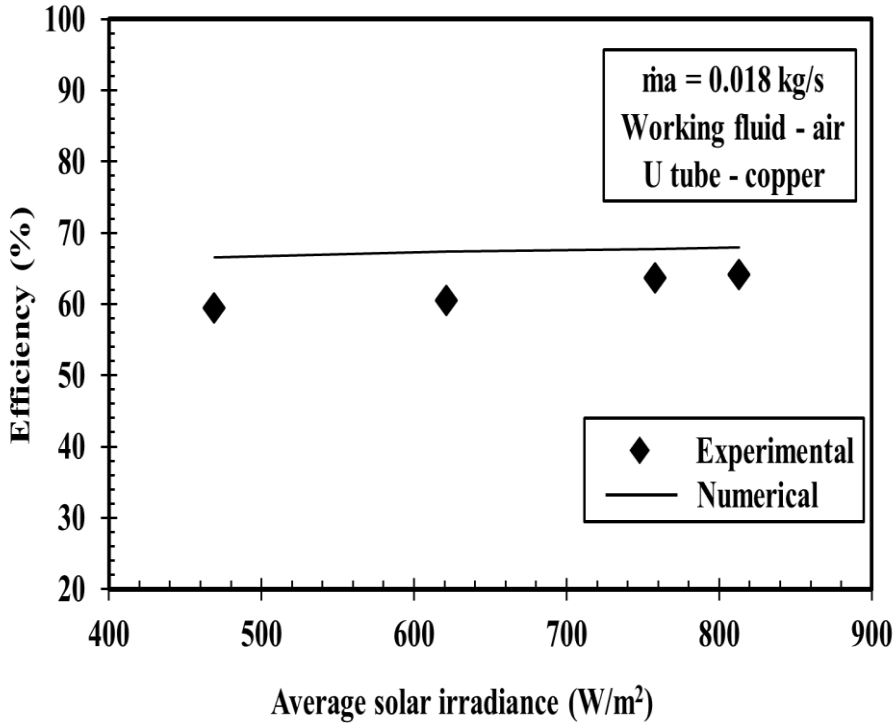

(b)

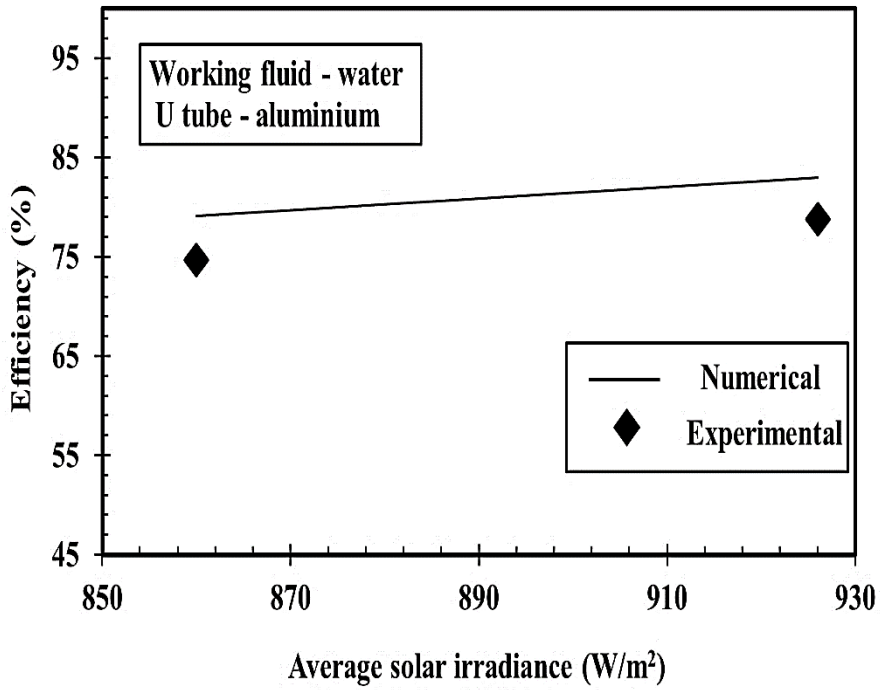

(c)

Fig. 3.11, Comparison of experimental results (Gao et al, 2014 and Neeraj and Avadhesh, 2015) with the numerical results: Influence of average solar irradiance on efficiency of the evacuated tube solar collector (air (a and b) and water (c)).

Figs. 3.10 and 3.11 show the comparison of experimental results for heat absorption and efficiency with the numerical predicted results. The heat gained by the working fluid increases with increase in average solar irradiance (fig. 3.10a – 3.11c). At higher average solar irradiance, there will be a higher heat transfer from the outer glass to the U–tube (copper or aluminum) and subsequently, a higher potential for convective heat transfer between the U–tube and the working fluid. It is observed from Fig. 3.11a – 3.11c that there is only a minimal increase in efficiency with an increase in average solar irradiance. For a given average solar irradiance, the maximum deviation of predicted data from experimental values for useful heat gained by the working fluid and efficiency of the solar collector are found to be $\pm$ 7.7 % and $\pm$ 8.3 % (fig. 3.10a – 3.10c & 3.11a – 3.11c), respectively.

Based on this preliminary investigation, it is concluded that the proposed numerical model is well suited for predicting the various performance parameters such as outlet temperature of the working fluid, useful heat rate and collector efficiency of the evacuated tube collector.

3.2.5 Grid independence test

As shown in Fig. 3.12a and 3.12b, a grid independence test is carried out by analysing the effect of different element sizes on the variation of useful heat rate along the collector length for both evacuated U–tube solar collector models. The details of grid elements used in both the evacuated U–tube solar collector models (model A and B) are presented in Table 3.4a.

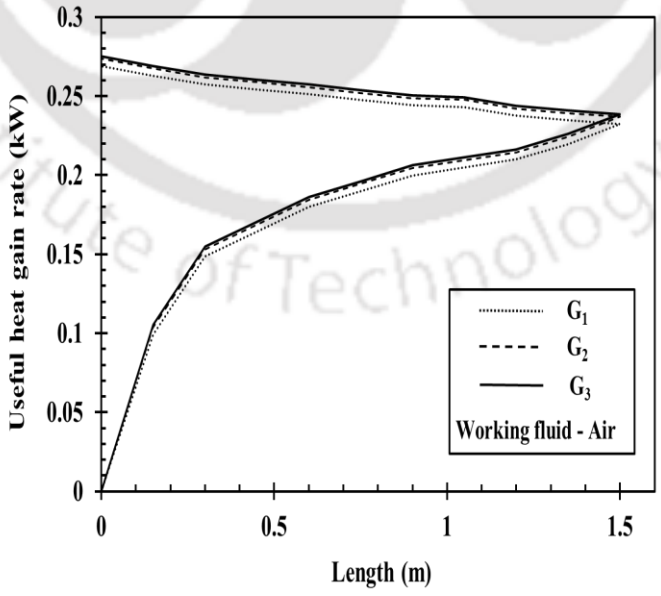

(b) Evacuated tube model – A.

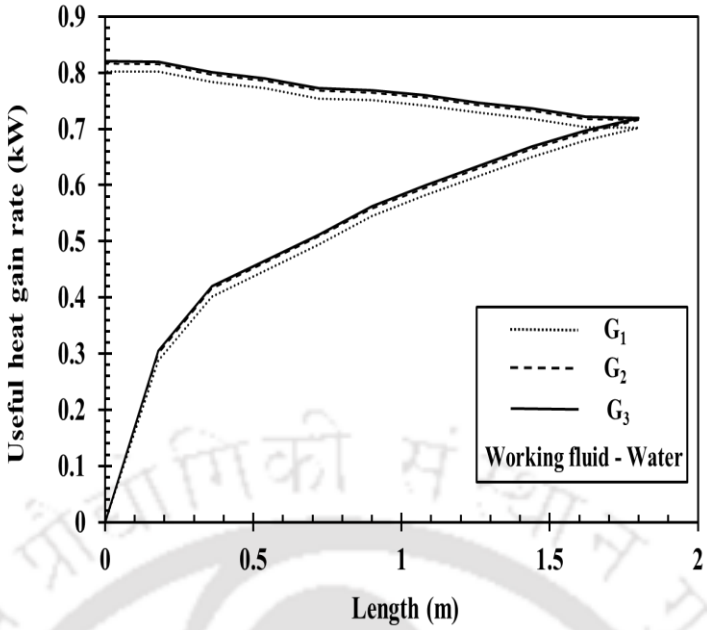

(b) Evacuated tube model – B.

Fig. 3.12, Grid independent test.

From Fig. 3.12a and 3.12b and Table 3.4a, it is observed that for a given length, there is a small difference in working fluid useful heat rate with increase in total grid elements from 7, 68, 437 to 11, 55,344 for the evacuated tube collector model – A (tube material – copper) and 8, 47,052 to 12, 09,828 for the evacuated tube collector model – B (tube material – Aluminium), respectively. By varying the total grid elements from 9, 96,846 to 11, 55,344 for model A and from 10, 88,273 to 12, 09,828 for model B, the variation in useful heat rate along the collector length is negligible. Therefore, for saving the computational time, 9, 96,846 and 10, 88,273 elements are selected for further investigation of evacuated U–tube models A and B. The maximum and minimum grid sizes and type of mesh element for the aforementioned grid elements of both the evacuated U–tube collector models (model A and B) are presented in Table 3.4b.

3.2.6 Results and discussion

Table 3.7, Operating parameters for parametric investigation.

Sl. No.	Operating parameters	Operating values
1	Ambient air temperature (°C)	32
2	Working fluid inlet temperature (°C)	36
3	Mass flow rate of working fluid (kg/s)	0.030
4	Average solar irradiance (W/m^2)	836

5	Dimensions of evacuated tube collector	Evacuated tube Collector – Model B (Table 3.5)
6	Working fluid	Water and air
7	U–tube material	Brass, copper, aluminium
8	Thermal conductivity (Young, 1992) (W/m–K)	Copper – 368 Brass – 109 Aluminium – 202
9	Fin material	Aluminium/copper
10	Density (Young, 1992) (kg/m^3)	Copper – 8978 Brass – 7400 Aluminium – 2712

With the developed thermal model, the variation in working fluid outlet temperature and useful heat rate along the collector length, the influence of mass flow rate on useful heat rate along the collector length and the effect of useful heat rate on collector efficiency are investigated using two different working fluids (water and air) and three different collector materials (brass, copper and aluminum). Further, the performance comparison of evacuated U–tube solar collector with filled absorber tube and unfilled absorber tube are also investigated. The list of parameters considered for the present analysis are given in Table 3.7.

a) Variation of temperature along the collector length

Fig. 3.13a and 3.13b shows the predicted working fluid temperature variation along the U–tube collector length. For a particular working fluid (air or water), the outlet temperature for copper is higher in comparison with brass and aluminium (Fig. 3.13a and 3.13b). This is due to the difference in thermal conductivity of the U–tube material. As the copper (k_{cu} = 401 W/m–K) has higher thermal conductivity than brass (k_{br} = 205 W/m–K) and aluminium (k_{al} = 109 W/m–K), employing copper as a U–tube material will achieve higher heat transfer than aluminium and brass as U–tube materials. Therefore, copper as a U–tube material will have less uniformity in temperature along the length compared to aluminium and brass as the U–tube materials. It is observed from Fig. 3.13a and 3.13b that for a given U–tube material, there is a significant increase in working fluid temperature up to certain collector length (0 m to approximately 1.6 m) and after that there is only a marginal increase in working fluid temperature along the remaining collector length (approximately 1.6 m to 0 m). This happens because from 0 to approximately 1.6 m, the difference in working fluid and the U–tube inner wall surface

temperature is high. As the working fluid temperature increases, the temperature difference between the working fluid and the U–tube inner wall surface decreases and hence there is only a marginal increase in working fluid temperature.

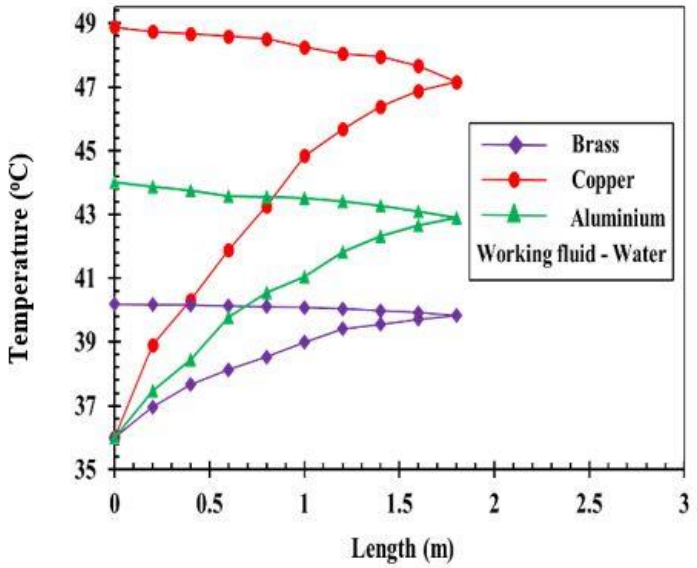

(a)

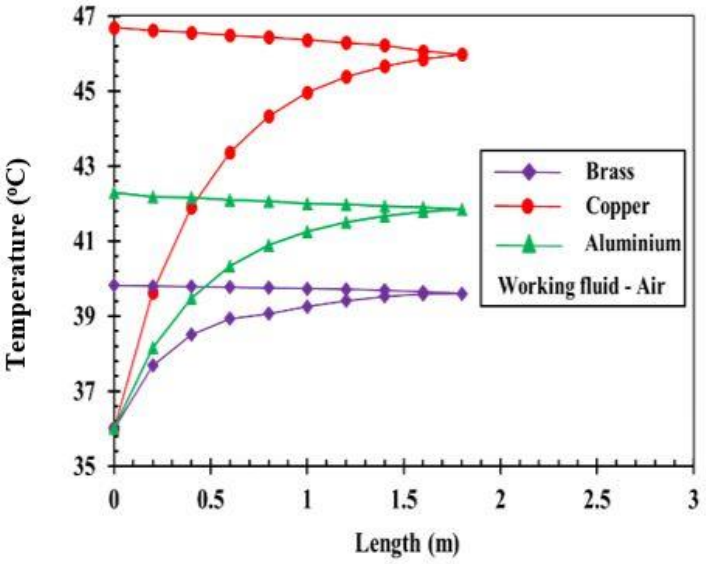

(b)

Fig. 3.13, Comparison of working fluid temperature variation along the U–tube collector length for different U–tube materials: (a) working fluid – water and U–tube material – Brass, Copper and aluminium; (b) working fluid – air and U–tube material – Brass, Copper and aluminium.

It is also observed from Fig. 3.13a and 3.13b that the difference in outlet temperature between the brass and the copper material based U–type evacuated tube collector are 8.6 °C with water

as working fluid and 7.0 °C with air as working fluid. The difference in outlet temperature between the brass and aluminium based U–tube evacuated tube collector are 4.0 °C with water working fluid and 2.3 °C with air as working fluid. This indicates that for either water or air as a working fluid, the copper U–tube is a good choice. However, if cost and density of the fin material is an issue then aluminium may be chosen instead of copper and reducing the aluminium fin thickness because with decrease in thickness of aluminium fin, the same heat transfer can be obtained (equivalent to the heat transfer from the absorber tube to the copper fin material) from the absorber tube to the aluminium fin. From Fig. 3.13a and 3.13b, it is also found that for a particular U–tube material, the outlet temperature of water is higher compared to air.

b) Variation of useful heat rate along the collector length

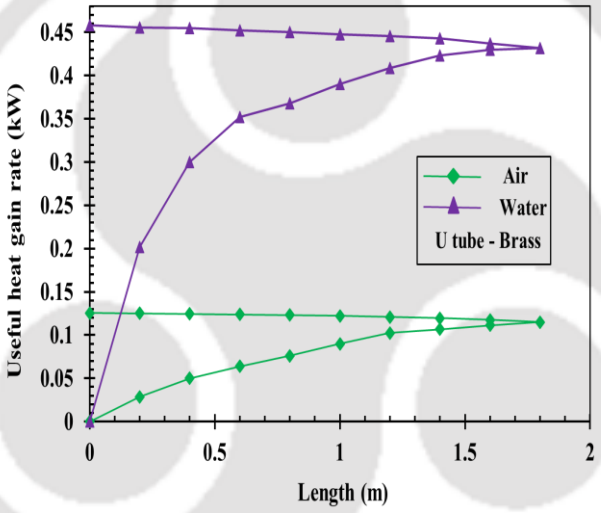

(a)

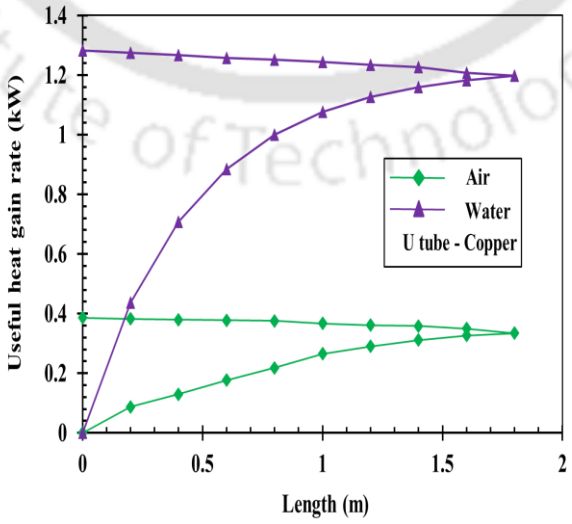

(b)

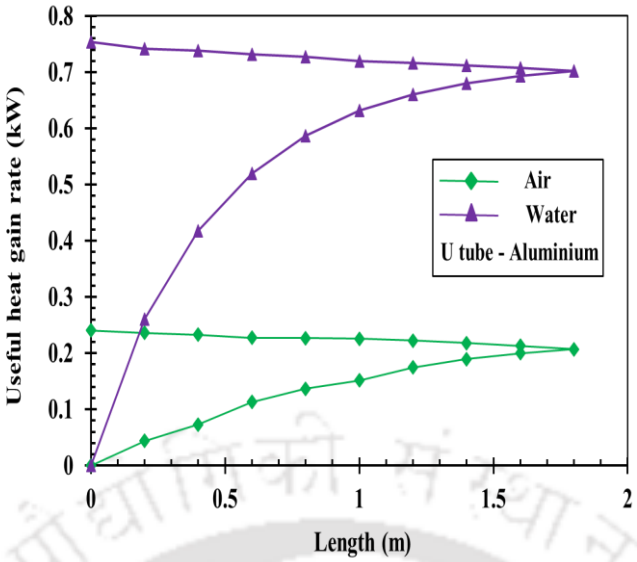

(c)

Fig. 3.14, Comparison of working fluid heat gain variation along the collector length for different U–tube materials: (a) U–tube material – Brass and working fluid – air and water; (b) U–tube material – Copper and working fluid – air and water and (c) U–tube material – Aluminium and working fluid – air and water.

The variation of the numerically predicted useful heat rate of the working fluid along the U–tube collector length is shown in Fig. 3.14a – 3.14c. It is observed that water gains more heat in comparison with air. This happens because of the difference in specific heat of the working fluid as well as heat transfer coefficient between the U–tube inner surface and the working fluid. It is observed from Fig. 3.14a – 3.14c that for a given U–tube material, there is a significant increase in the amount of heat absorbed by the working fluid up to certain collector length (0 m to approximately 1.6 m) and after that there is only a marginal increase in working fluid heat gain along the U–tube collector length (approximately 1.6 m to 0 m). This is due to the fact that, from 0 m to 1.6 m collector length, the difference in heat transferred by the U–tube inner wall surface to the working fluid is high. As the heat absorbed by the working fluid increases, aforementioned difference will decrease. Subsequently, the convective heat transfer between the U–tube inner wall surface and the working fluid decreases. Hence, there is only a marginal increase in heat gained by the working fluid. From Fig. 3.14a – 3.14c, it is observed that the difference in useful heat rate between air and water for brass, copper and aluminium U–tube materials is found to be 71 %, 68 % and 66 %, respectively. This indicates that for all the U–tube materials investigated, water is a better working fluid than air.

c) Effect of mass flow rate for different U–tube material/working fluid combinations

Fig. 3.15a – 3.15f illustrates the numerical results obtained for the useful heat absorbed by the water and air at different mass flow rates varying from 0.01 kg/s to 0.05 kg/s and for different U–tube materials. For a given flow rate, the useful heat absorption rate increases logarithmically from 0 m to 1.6 m collector length and then there is a marginal increase (from approximately 1.6 m to 0 m) in heat gain. For a particular collector length, as the flow rate increases, the amount of heat absorbed by the water also increases. This indicates that higher flow rates will absorb more heat from the inner surface of the U–tube, thereby reducing the temperature gradient between U–tube and bulk working fluid, and maintaining constant heat transfer along the collector length. It is observed from Fig. 3.15a, 3.15c & 3.15e that for a particular working fluid (water), in order to achieve the high heat gain of about 0.8 kW, the flow rate should be 0.052 kg/s, 0.02 kg/s and 0.031 kg/s, respectively, for brass, copper and aluminium. This implies that for a low thermal conductivity material, with an increase in working fluid flow rate higher heat gain will be attained. From Fig. 3.15a – 3.15b, it is found that for a particular U–tube material (brass), to achieve heat gain of 0.2 kW, air and water should operate at a flow rate of 0.011 kg/s and 0.048 kg/s, respectively. This indicates that a higher specific heat of the fluid, attains the same heat gain at lower fluid flow rate. For a given collector length, increasing the mass flow from 0.01 kg/s to 0.05 kg/s, improve the useful heat absorption rate by 81 %, 84 % & 76 % for water and 81 %, 82.5 % & 80 % for air, respectively, for brass, copper and aluminium as U–tube materials.

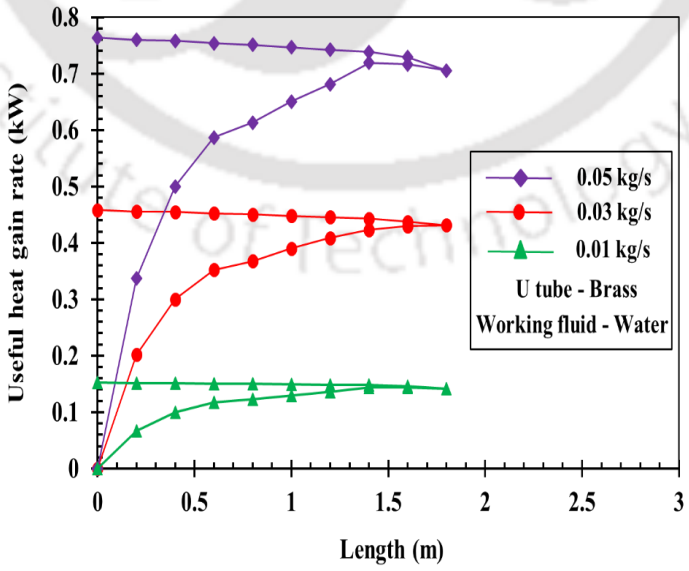

(a)

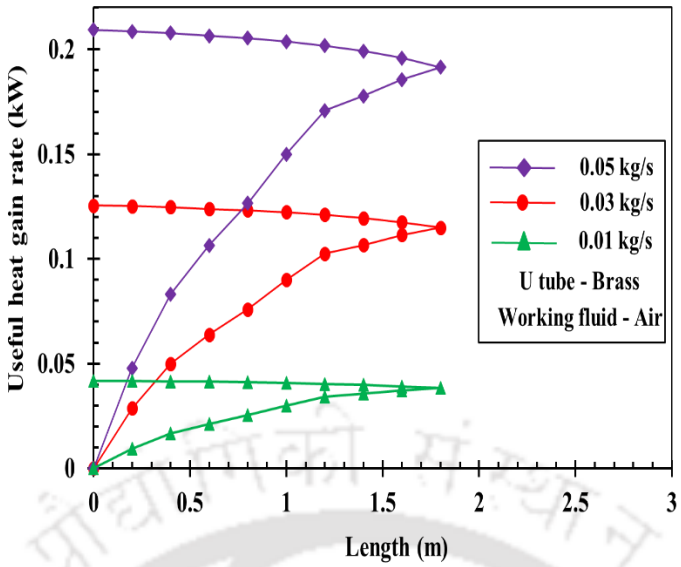

(b)

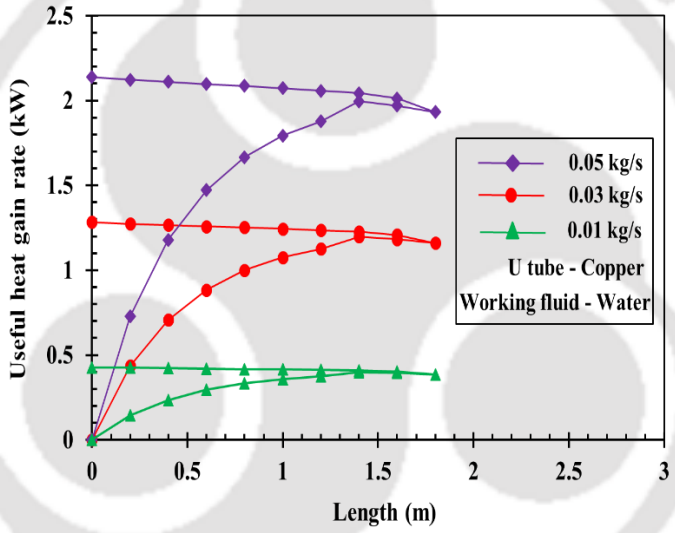

(c)

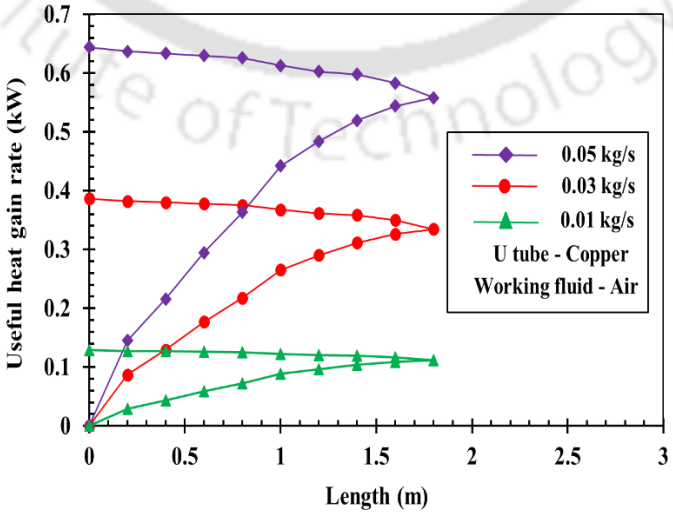

(d)

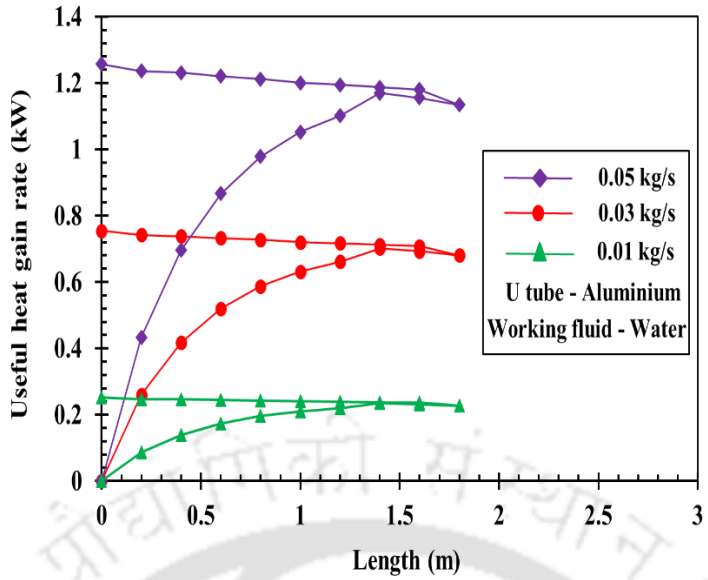

(e)

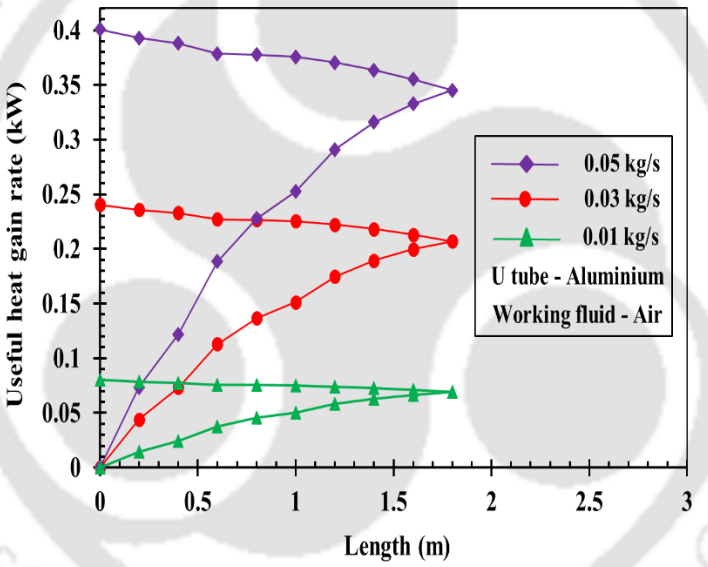

(f)

Fig. 3.15, Comparison of working fluid heat gain variation along the U–tube collector length for different mass flow rates: (a) U–tube material – brass and working fluid – water; (b) U–tube material – brass and working fluid – air; (c) U–tube material – copper and working fluid – water; (d) U–tube material – copper and working fluid – air; (e) U–tube material – aluminium and working fluid – water and (f) U–tube material – aluminium and working fluid – air.

d) Effect of working fluid/U–tube material combinations on collector efficiency

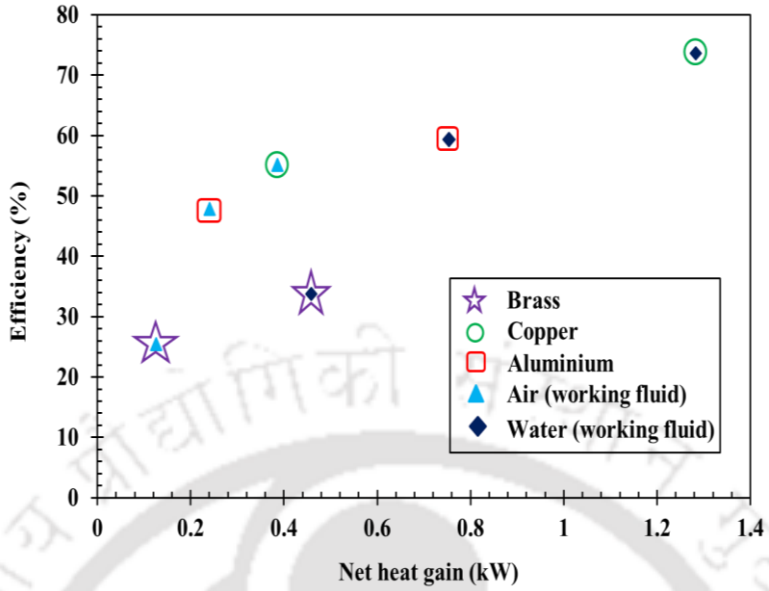

Fig. 3.16, Influence of useful heat gained on efficiency of the evacuated tube solar collector.

The influence of working fluid useful/net heat gain (water, air) on the efficiency of the evacuated tube solar collector for three different U–tube materials (brass, copper and aluminium) is illustrated in Fig. 3.16. From Fig 3.16, it is observed that for a given working fluid, the collector efficiency is found to be higher with copper as U–tube material than brass and aluminium, and water gives better results than air for a particular U–tube material.

e) Influence of filler material on performance of the solar collector

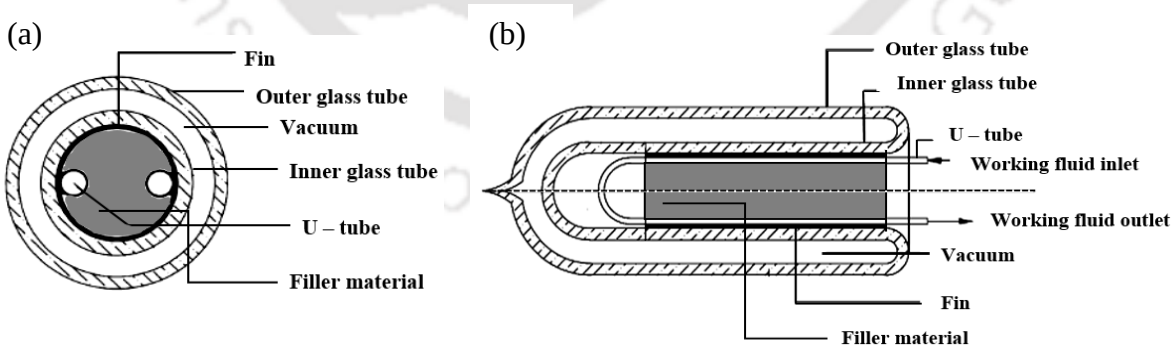

Fig. 3.17, Schematic of evacuated U–tube solar collector with filler material, a) Cross section and b) Longitudinal section.

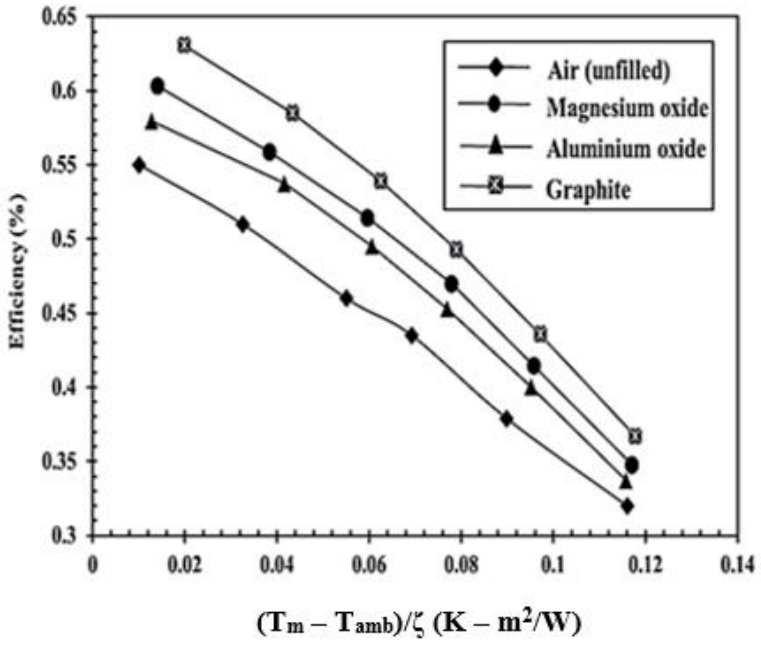

Fig. 3.18, Influence of filler material on evacuated tube solar collector efficiency.

The numerical model developed in Section 2 is used for analysing the performance of the filled type U–tube solar collector. Only difference between the filled and unfilled type U–tube solar collector is filling of filler material (graphite/aluminium oxide/magnesium oxide) instead of air (unfilled) between the U–tube (Fig. 3.17). Using the surface properties and dimensions of evacuated collector model – A (Gao et al. 2014) listed in table 3.5, a parametric investigation on the influence of a filler material between the U–tube and the absorber surface (copper fin surface) has been carried out (Fig. 3.17). Filler materials used for performance improvement are magnesium oxide, aluminium oxide and graphite. As the thermal conductivity of air filled space is very low (0.03 W/m-K), the performance of evacuated tube collector filled with high thermal conductivity powders such as aluminium oxide, magnesium oxide and graphite (30 W/m-K, 60 W/m-K and 168 W/m-K) is expected to be better (Young, 1992). Predicted results are presented in Fig. 3.18. It is observed that the efficiency with graphite filler material is higher compared to magnesium oxide, aluminium oxide and no filler material. This happens because by employing filler material, the heat transfer due to conduction from inner glass surface to the U–tube increases because of high thermal conductivity of the filler material compared to air (unfilled). As a consequence, the thermal resistance between the inner glass tube and the fin decreases and the useful heat gained by the working fluid due to convective heat transfer from the filled – type U–tube to the working fluid increases. Thus, employing filler material will enhance the heat transfer from inner glass tube surface to the U–tube and improves the

performance of the evacuated U–tube solar collector. It is also observed that at normalized heat gain [$(T_m - T_{amb})/\zeta$], the graphite filler yields 7.8 %, 12.3 % and 15.3 % higher efficiency than the magnesium oxide filler, the aluminium oxide filler and the case of no filler (air filled space).

From Fig. 3.18, it is concluded that employing filler material will enhance the heat transfer from inner glass tube surface to the U–tube and improve the performance of the evacuated U–tube solar collector.

3.3 Summary

3.3.1 Liquid desiccant dehumidifier/regenerator

A numerical model is developed for analyzing the heat and mass transfer processes occurring along the counter-flow packed tower. For investigating the performances of dehumidifier and regenerator, expressions for outlet parameters are derived in terms of known inlet and thermo – physical parameters. A backtracking algorithm is proposed for simulating the developed model. The predicted data for the outlet and performance parameters showed good agreement with the experimental data reported in the literature. With the proposed model, variation of operating parameters and evaporation/condensation rate along the height of the counter-flow packed tower (dehumidifier/regenerator) are studied in detail. Distribution contour are predicted for analyzing the heat and mass transfer processes along the height of the packed tower and found that evaporation/condensation rate decreases along the air flow direction.

3.3.2 Evacuated U – tube solar collector

A profound numerical analysis on thermal processes occurring in an evacuated U–tube solar collector is carried out using a 3D numerical model based on finite element method. The performance characteristics of the solar collector, viz. outlet temperature of the working fluid, efficiency and useful heat rate of the collector, predicted from the numerical model showed good agreement with the experimental data available in the literature. It is found that the average solar irradiance has a significant effect on the useful heat gained by the working fluid and an insignificant effect on the efficiency of the solar collector. By employing three different U–tube materials (aluminium, copper and brass), two different working fluids (air and water) and three different filler materials (graphite, magnesium oxide and aluminium oxide), the thermal performance of the evacuated tube solar collector is investigated theoretically.

CHAPTER 4

EXPERIMENTAL STUDIES

In this chapter, the experimental studies on fabricated liquid desiccant dehumidification/regeneration system and evacuated U – tube solar collector system are presented. The major objectives of this chapter are,

- Experimentally studying the performance of dehumidification/regeneration system.
- Developing correlations for analysing vapour transfer along the packed chamber.
- Experimentally investigating the performance of evacuated U – tube solar collector system.
- Defining working fluid transition time for an evacuated U – tube solar collector.

4.1 Experimental studies on liquid desiccant dehumidification/regeneration system

4.1.1 Details of experimental setup and test procedure

The schematic and pictorial views of the fabricated experimental setup of the counter – flow adiabatic liquid desiccant dehumidification/regeneration system is shown in Fig. 4.1a, 4.1b and 4.1c. The major components of these systems are packed tower, solution tank, collection tank, centrifugal pump and centrifugal blower (Figs. 4.1a – 4.1c). The ambient air is supplied into the packed tower using a centrifugal air blower of capacity 0.75 kW (Static pressure of the blower: 0.73 kPa). In the counter-flow adiabatic packed tower (dehumidifier/regenerator), Celdek structured packing made up of perforated polypropylene plastic sheets, having a specific surface area of 179 m^2/m^3 is used. The flute height of the packing material is 1 ± 0.05

cm (Fig. 4.1d). The overall length, width and height of the structured packing are about 0.6 m, 0.6 m and 0.75 m, respectively (Table 4.1). The packed tower consists of four chambers such as solution spray chamber, structured packing chamber, air blown chamber and solution collection chamber (shown in Fig. 4.1f) and the whole packed tower is made up of stainless steel.

In the current experimental study, LiCl is used as a desiccant material. The fresh unused desiccant solution is stored in a tank and the temperature of the solution is either heated to a required temperature using a submerged stainless steel coil (during regeneration experiments (Fig. 4.1b)) or cooled below ambient temperature by using external cooling bath (during dehumidification experiments (Fig. 4.1a)). Distilled water is used for preparing the solution. An anti – corrosive centrifugal pump of capacity 0.75 kW is used for pumping the desiccant solution into the packed tower (Fig. 4.1a and 4.1b). From the liquid desiccant storage tank to the packed tower, the solution flows through a 2.54 cm diameter stainless steel pipe. The incoming desiccant solution from the storage tank is sprayed across the structured packing chamber through three evenly distributed stainless steel pipes of diameter 1.27 cm and each pipe consists of five spray nozzles of 0.4mm dia. (Fig. 4.1e). The diluted/concentrated desiccant solution that comes out from the packed tower is collected in a collection tank during dehumidification/regeneration experiments. Various components, dimensions and specifications of the liquid desiccant dehumidification/regeneration system are given in Table 4.1.

Table 4.1, Components, dimensions and specifications of the liquid desiccant dehumidification/regeneration system.

Liquid desiccant	Lithium chloride solution
Packing length (m)	0.6
Packing width (m)	0.6
Packing height (m)	0.75
Specific surface area (m^2/m^3)	179
Type of packing material	Polypropylene plastic sheets
Anti-corrosive pump capacity (kW)	0.75 (nos. 1)
Blower capacity (kW)	0.75 (nos. 1)
Immersion heater capacity (kW)	10 (nos. 5)

When the air and desiccant solution interacts in the structured packing chamber in counter-flow direction, the heat and mass exchange takes place between the ambient air and the desiccant solution. During this exchange process, in the dehumidifier, the ambient air desorbs moisture to the desiccant solution due to vapour pressure difference and releases the sensible heat due to temperature difference between the process air and the highly concentrated desiccant solution, chemical heat due to mixing of water vapour and desiccant solution and latent heat due to condensation of water vapour at the air – desiccant interface. As a result, the ambient air and the solution are heated up. Whereas, in the regenerator, the ambient air absorbs water vapour from the desiccant solution due to vapour pressure difference by taking latent heat due to evaporation of water vapour and chemical heat due to desorption of water vapour from the desiccant solution. As a result, the solution is cooled and concentrated. Due to sensible heat exchange between the air and the solution, air is further heated up.

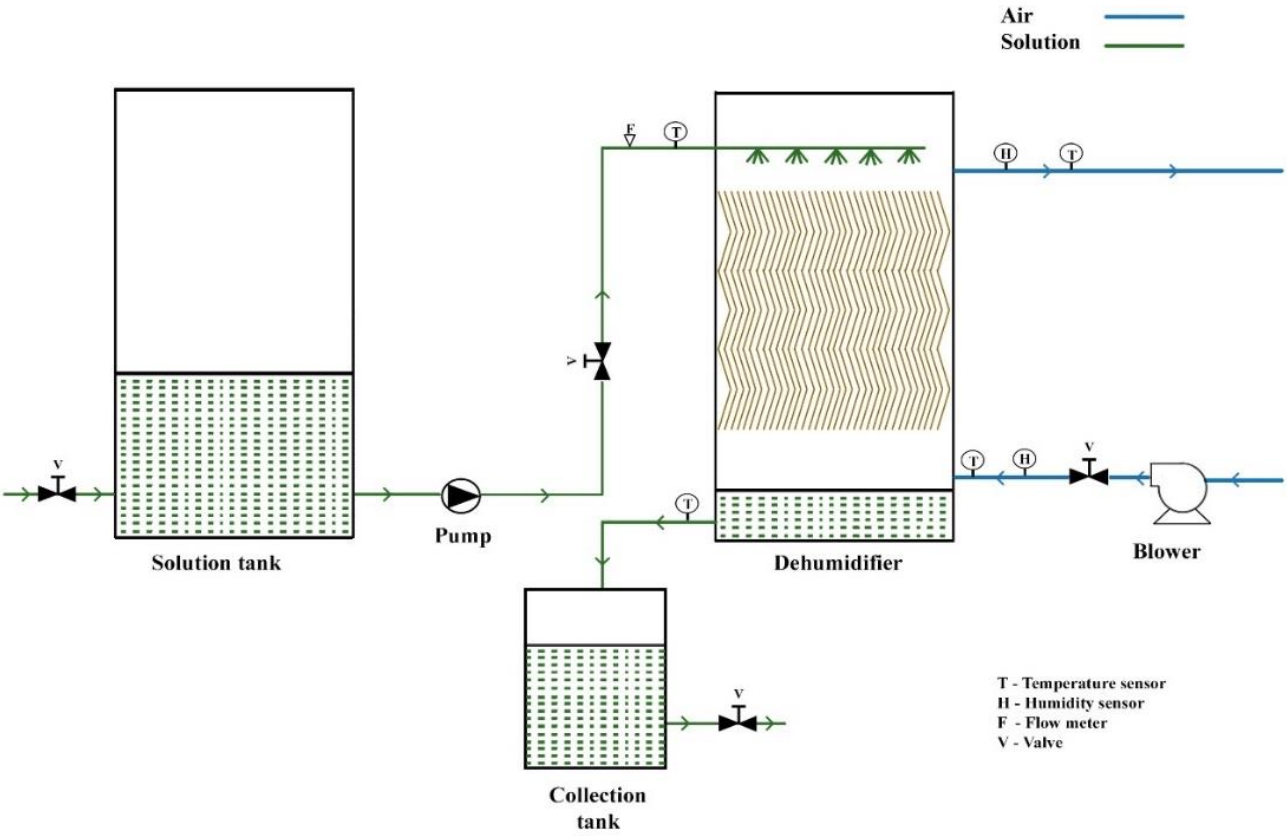

(a) Schematic of liquid desiccant dehumidification system.

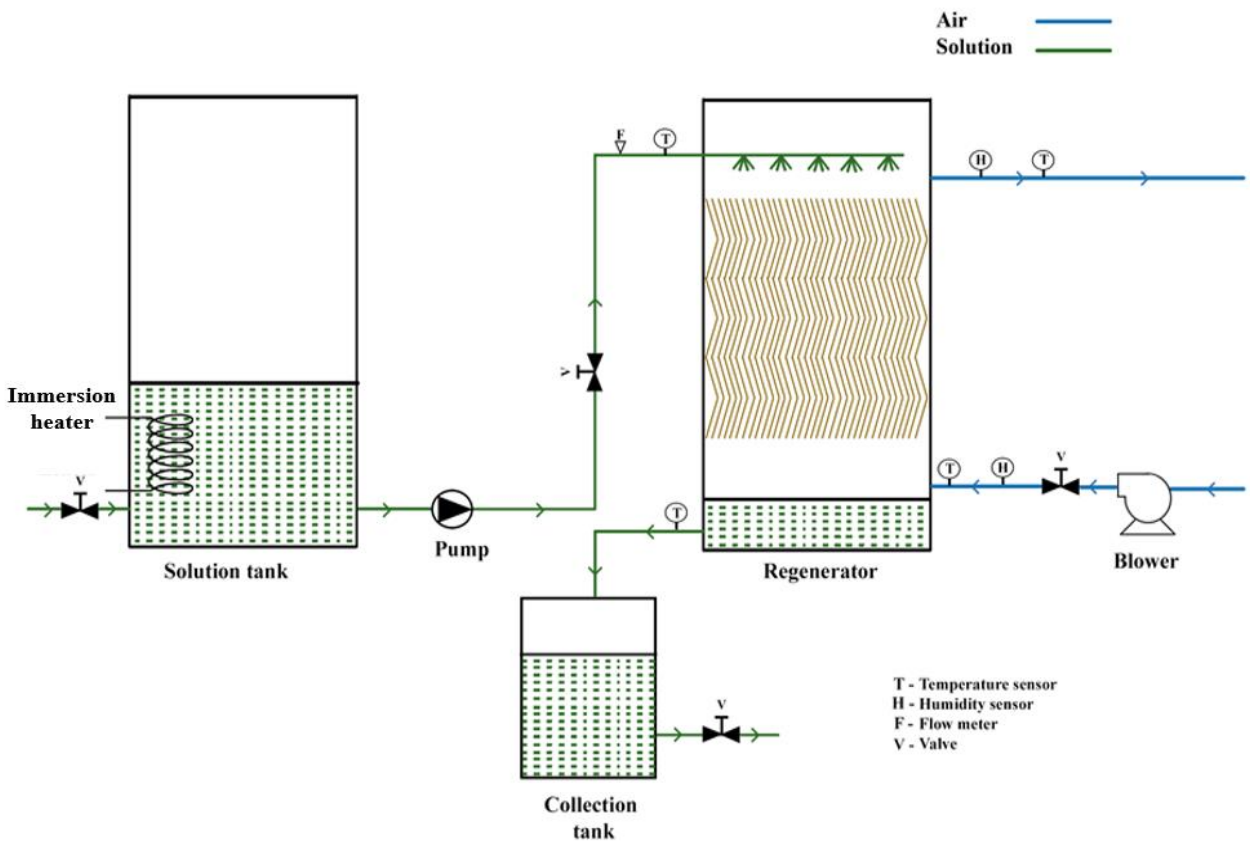

(b) Schematic of liquid desiccant regeneration system.

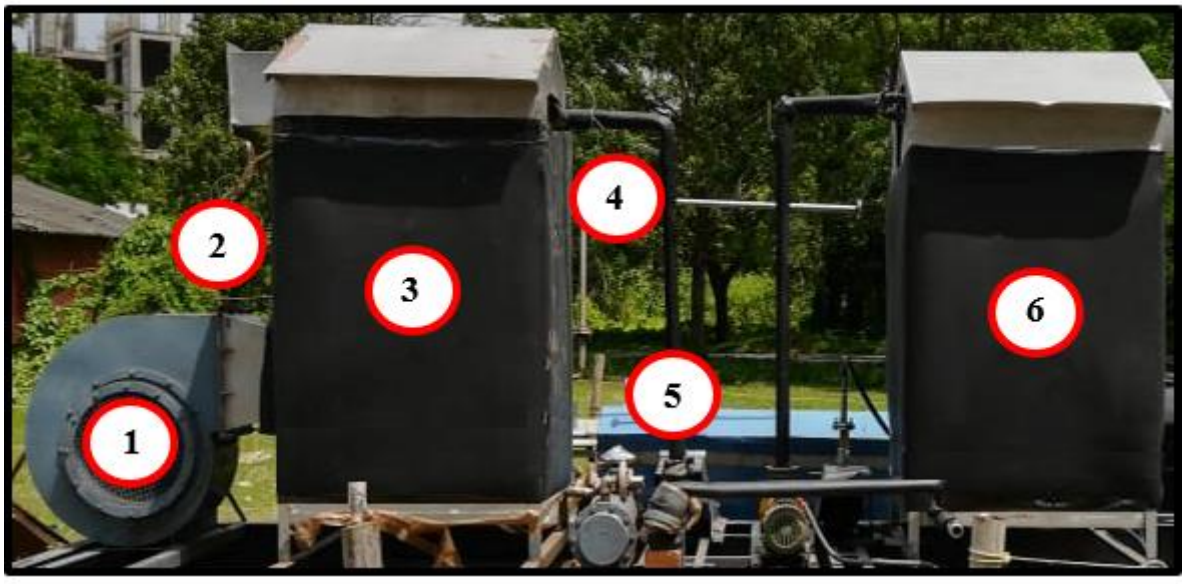

(c) Pictorial view of the fabricated liquid desiccant dehumidification/regeneration system – (1) Blower, (2) Air flow regulating valve, (3) Packed tower (dehumidifier/regenerator), (4) Solution flow regulating valve, (5) Non – corrosive pump and (6) Solution tank.

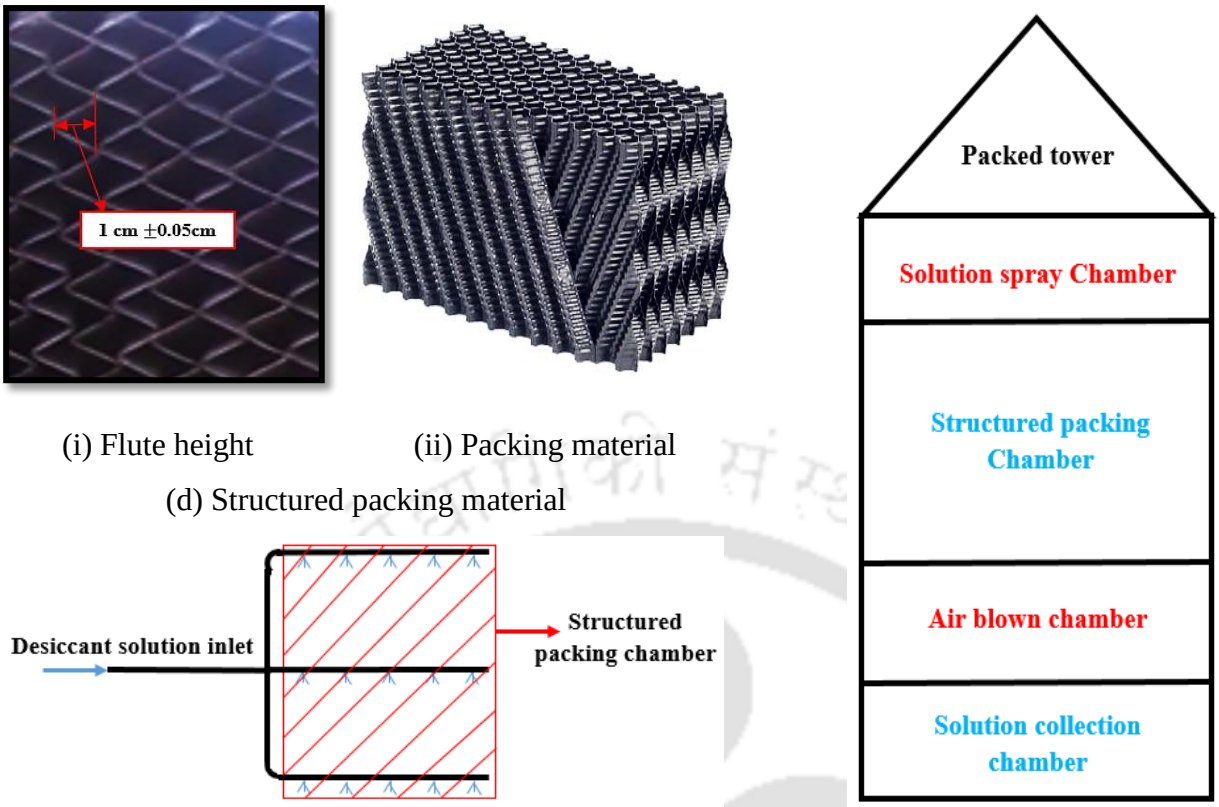

(i) Flute height (ii) Packing material

(d) Structured packing material

(e) Direction of solution spray in solution spray chamber. (f) Chambers in packed tower.

Fig. 4.1, Details of liquid desiccant dehumidification/regeneration system.

For determining dimensions of the structured packing chamber (Fig. 2), the design guidelines provided by the Elsarrag et al. (2005) was implemented. Initially, the dehumidification system capacity is decided as 18 kW (5 TR). Based on the system capacity, the air flow rate is estimated as 2,000 CFM (since, 1 TR = 400 CFM). From the literature, the minimum L/G ratio required for dehumidification of ambient air/regeneration of liquid desiccant is observed to be 0.8 [47, 49]. Accordingly, the minimum solution flow rate is predicted. On the basis of air and solution flow rates, the cross sectional area of the structured packing chamber is determined. Using the heat and mass transfer coefficient correlations from Eqs. 3.10 and 3.17, the optimum height of the structured packing is obtained as 0.75 m by assuming the moisture and the thermal effectiveness as 0.65.

The air temperature and relative humidity are measured at the inlet and outlet of the packed tower using temperature and humidity sensors (accuracy: 0.1 ^{o}C, 2% R.H.). The solution temperatures at the entrance and exit of the packed tower are measured using T – type thermocouples (accuracy: ±0.1 ^{o}C). Data acquisition system (Agilent – 34972A) is used for

acquiring the outputs from thermocouples. Samples of the desiccant solution at the entrance and exit of the packed tower are collected during the experiments and analysed for estimating the desiccant concentration using flame photometer (Model: Systronics – 128; ±1% accuracy). Flow control valves are placed in appropriate places for regulating the desiccant solution and the ambient air flow (Fig. 4.1a and 4.1b). A portable ultrasonic flow meter (Model: UFM6730; ±1% accuracy) and rotating vane anemometer (Model: TESTO – 490; accuracy: ± 0.1 m/s) are used for measuring the desiccant solution and the ambient air flow rates, respectively. K – Flex thermocol sheets are used as an insulation material for insulating the components such as packed tower, storage tank and stainless steel pipes (connected in between the storage tank and the packed tower).

4.1.2 Uncertainty in measurement

For evaluating the consistency/accuracy of the dependent parameters, uncertainty analysis is carried out. The uncertainties involved in the estimation of dependent parameters such as air/solution enthalpy, evaporation/condensation rate and energy exchange are calculated using Eq. 4.1 (Kline and Mc – Clintok, 1953). The respective estimated values are ± 4.3 %, ± 3.2 %, and ± 4.3 %.

$$\Delta\Omega = \sqrt{\left(\frac{\partial\Omega}{\partial k_1}\Delta k_1\right)^2 + \left(\frac{\partial\Omega}{\partial k_2}\Delta k_2\right)^2 + \left(\frac{\partial\Omega}{\partial k_3}\Delta k_3\right)^2 + \ldots\ldots\ldots\ldots\ldots + \left(\frac{\partial\Omega}{\partial k_n}\Delta k_n\right)^2} \qquad (4.1)$$

where 'Ω' is the dependent parameter and k_1, k_2, k_3 …… k_n are different independent parameters (measured quantities). The calculation procedure for uncertainties in the dependent parameters such as air/solution enthalpy, evaporation/condensation rate and energy exchange are presented in Appendix B.

4.1.3 Performance characteristics

In the present study, for analysing the performance of the liquid desiccant dehumidification/regeneration system, the following three performance characteristics are used,

(a) Overall energy exchange (Q_e)

The overall energy exchange between the air and the desiccant solution along the liquid desiccant dehumidification/regeneration system is estimated as

$$Q_e = -\dot{m}_s dh_s = \dot{m}_a dh_a \tag{4.2}$$

Change in air enthalpy: $dh_a = C_{p,m} dT_a + \delta d\omega$ (4.2a)

Change in solution enthalpy: $dh_s = C_{p,s} dT_s + \delta d\omega_{sat}$ (4.2b)

where 'ω_{sat}' is the specific humidity of saturated air which is in thermal equilibrium with the desiccant solution at the local desiccant temperature and concentration i.e. ω_{sat} (T_s, β) and this saturated air specific humidity is calculated using desiccant concentration versus temperature graph available in the literature (Koronaki et al. 2013).

(b) Condensation rate (λ_c)

The rate of water vapour condensed from the air to the desiccant solution (absorbed by the desiccant solution from the air) is defined as condensation rate and is given as,

$$d\lambda_c = -G_a d\omega \tag{4.3}$$

$$or:\ \lambda_c = G_a(\omega_i - \omega_o) \tag{4.3a}$$

(c) Evaporation rate (λ_e)

The rate of water vapour evaporated from the desiccant solution to the ambient air is defined as evaporation rate and is given as,

$$d\lambda_e = G_a d\omega \tag{4.4}$$

$$or:\ \lambda_e = G_a(\omega_o - \omega_i) \tag{4.4a}$$

4.1.4 Experimental results and discussion

For a given range of operating parameters (Table 4.2), the influence of relative humidity on ambient air enthalpy, solution enthalpy, solution concentration and air specific humidity is investigated experimentally for both dehumidification and regeneration systems and the results are plotted in Figs. 4.2 and 4.3. In order to analyse the variation of aforementioned parameters

with relative humidity, the ambient condition has been monitored throughout the year in accordance with humid subtropical climate. Further, percentages of increment/decrement of aforementioned parameters from the entrance to the exit of the packed tower (dehumidifier/regenerator) are also shown in Figs. 4.2 and 4.3. In this experimental study, the air and desiccant solution enthalpies are calculated using Eq. 4.2a and 4.2b. The air inlet specific humidity is obtained from the psychrometric chart using the air temperature and relative humidity data measured during the experimental field analysis.

Table 4.2, Operating range and reference values.

	Liquid desiccant dehumidification system		Liquid desiccant regeneration system	
Parameters	Range	Reference value	Range	Reference value
Air temperature (^oC)	25 – 36	30	25 – 36	30
Air specific humidity (g_{wv}/kg_{da})	12.7 – 27.4	19.23	12.7 – 27.4	19.23
Ambient air flow rate ($kg/m^2 – s$)	1.32 – 4.51	3.67	1.32 – 4.51	3.67
Solution flow rate ($kg/m^2 – s$)	3.43 – 6.89	3.67	3.43 – 6.89	3.67
Solution temperature (^oC)	23 – 31	28	61 – 73	67
Solution concentration ($kg_{LiCl}/kg_{sol.}$)	31.8 – 38.2	34	31.8 – 38.2	34
L/G ratio	0.76 – 5.22	1	0.76 – 5.22	1

From Figs. 4.2a and 4.3a, it is observed that for a given set of inlet conditions (Table 4.2), with increase in relative humidity, the outlet ambient air enthalpy decreases during dehumidification and regeneration processes. This is due to the fact that with increase in relative humidity, the vapour pressure present in the ambient air increases. This results in high vapour pressure air and leading to more dissipation of latent heat of condensation into the ambient air. Whereas in the regeneration system, as the vapour pressure of air is a function of relative humidity, a higher relative humidity results in lesser amount of moisture absorption from the desiccant solution. As a consequence, lesser amount of heat interaction occurs at the interface. With increase in relative humidity from 63% to 87%, the outlet air enthalpy decreases by 3% and 8% in the dehumidification and regeneration systems, respectively (Figs. 4.2a and 4.3a and Table 4.3). The reason for higher change in enthalpy of air during the regeneration process is due to higher temperature difference between the air and the desiccant solution.

Further, from Figs. 4.2a and 4.3a and Table 4.3, it is also observed that with increase in relative humidity from 63% to 87%, the air enthalpy difference between inlet and exit increases from 1% to 5% along the dehumidifier and decreases from 64.5% to 44.3% along the regenerator. This happens because with increase in relative humidity, the vapour pressure difference between the air and the desiccant solution increases in the dehumidifier and decreases in the regenerator. By which the potential for latent heat exchange increases along the dehumidifier and decreases along the regenerator.

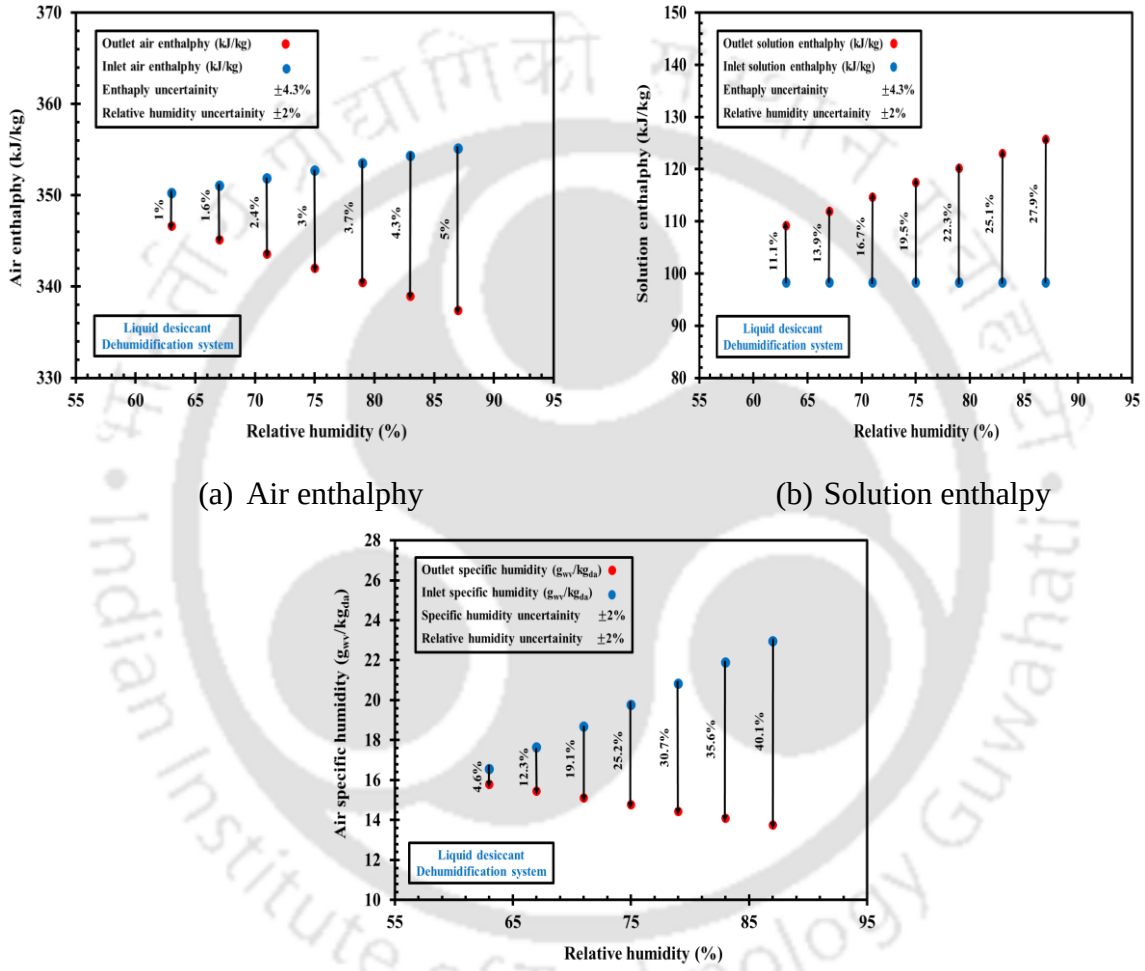

(a) Air enthalpy (b) Solution enthalpy

(c) Air specific humidity

Fig. 4.2, Influence of relative humidity on operating parameters of liquid desiccant dehumdifcation system.

For a given relative humidity, the solution enthalpy at the outlet of the dehumidifier increases and decreases at the outlet of the regenerator (Figs. 4.2b and 4.3b). From Figs. 4.2b and 4.3b, it is also observed that for a given set of inlet conditions (Table 4.2), as the relative humidity increases, the relative outlet solution enthalpy increases during dehumidification and regeneration processes. It is due to the fact that increase with relative humidity, there is a high

potential for moisture desorption from ambient air to desiccant solution whereas in the regenerator there is a low potential for moisture absorption from desiccant solution to the ambient air. As a consequence, latent heat transfer at the air–desiccant interface increases in the dehumidifier and decreases in the regenerator. Thus, with increase in relative humidity from 63% to 87%, the outlet solution enthalpy increases by 15% and 4% in the dehumidification and regeneration systems, respectively. Further, from Figs. 4.2b and 4.3b and Table 4.3, it is found that as the relative humidity increases from 63% to 87%, the solution enthalpy difference increases from 11.1% to 27.9% along the dehumidifier and decreases from 13% to 9.2% along the regenerator. From this analysis, it is observed that with increase in relative humidity, the solution enthalpy difference between the inlet and the exit of the packed tower increases during dehumidification process and decreases during regeneration processes.

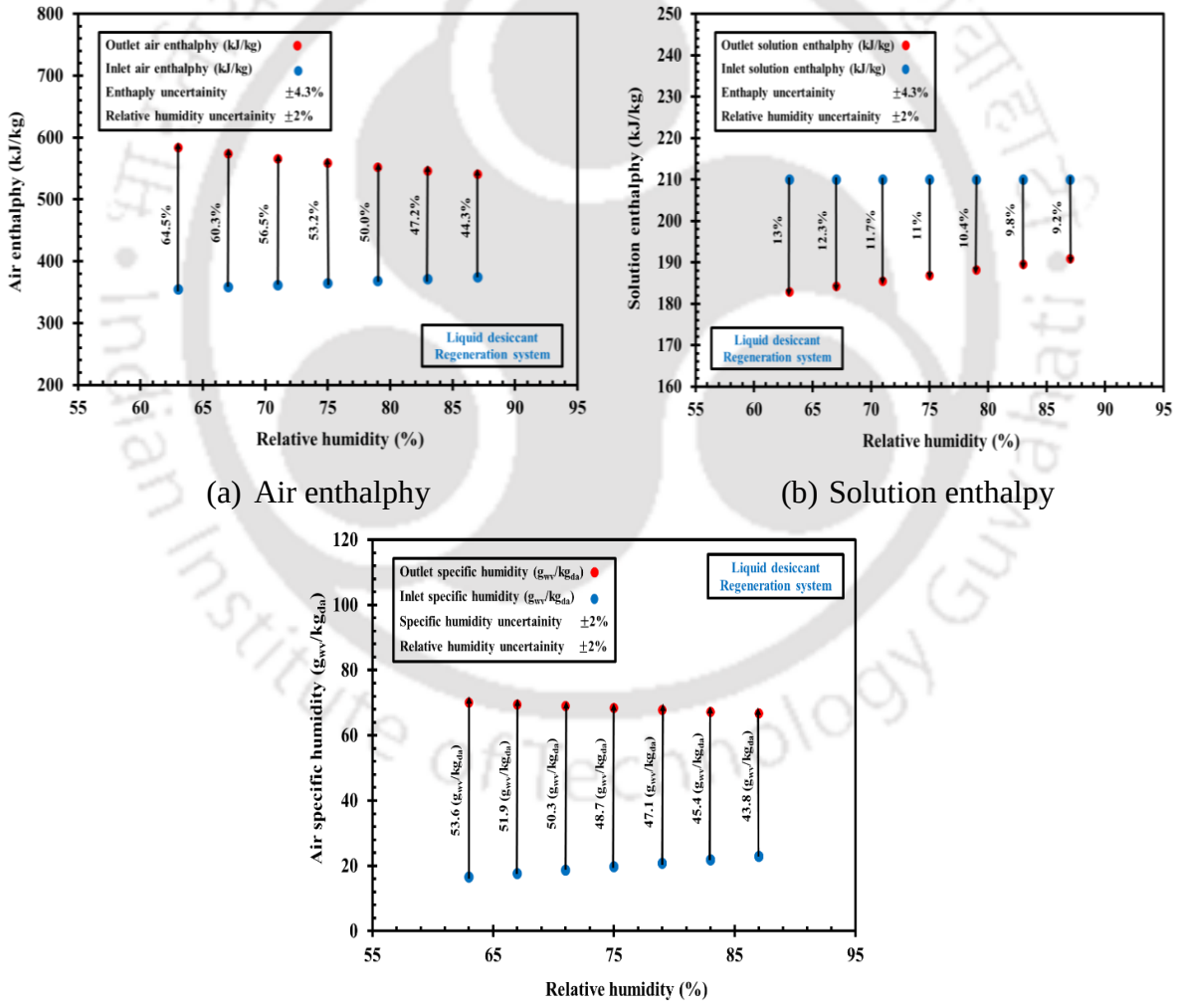

(a) Air enthalphy (b) Solution enthalphy

(C) Air specific humidity

Fig. 4.3, Influence of relative humidity on operating parameters of liquid desiccant regneration system.

For a given relative humidity, the air specific humidity at the outlet of the dehumidifier decreases whereas at the outlet of the regenerator it increases (Fig. 4.2c and 4.3c). From Figs. 4.2c and 4.3c, it also found that for a given set of inlet conditions (Table 4.2), with increase in relative humidity, the outlet air specific humidity decreases significantly in the dehumidification and the regeneration systems as shown in Figs. 4.2c and 4.3c. This happens because with increase in relative humidity, water vapour present in the ambient air increases. As a result, desiccant solution absorbs more amount of water vapour from the ambient air in the dehumidification system, whereas in the regeneration system, the ambient air doesn't absorb a higher amount of water vapour from the desiccant solution due to low vapour pressure difference. From Figs. 4.2c and 4.3c and Table 4.3, it is observed that as the relative humidity increases from 63% to 87%, the ambient air specific humidity at the outlet decreases by 13% and 6% in the dehumidification and regeneration systems, respectively.

From Figs. 4.2c and 4.3c and Table 4.3, it is also found that at relative humidity's of 63%, 67%, 71%, 75%, 79%, 83% and 87%, the percentage decrement in ambient air specific humidity from the entrance to the exit of the packed tower are 4.6%, 12.3%, 19.1%, 25.2%, 30.7%, 35.6% and 40.1% during dehumidification process whereas during regeneration process, they are 53.6%, 51.9%, 50.3%, 48.7%, 47.1%, 45.4% and 43.8%, respectively. From this analysis, it is understood that with increase in relative humidity, the difference in air specific humidity between the entrance and the exit of the packed tower increases during dehumidification process and decreases during regeneration process. This is due to the occurrence of high mass transfer in the dehumidification system and low mass transfer in the regeneration system.

Table 4.3, Influence of relative humidity on operating parameters.

Parameter	Liquid desiccant dehumidification system		Liquid desiccant regeneration system	
	ϕ = 63% – 87% (↑)		ϕ = 63% – 87% (↑)	
	Outlet	Difference	Outlet	Difference
Air enthalpy (kJ/kg)	3% (↓)	1% – 5% (↑)	8% (↓)	64.5% – 44.3% (↓)
Solution enthalpy (kJ/kg)	15% (↑)	11.1% – 27.9% (↑)	4% (↑)	13% – 9.2% (↑)
Specific humidity ratio (g_{wv}/kg_{da})	13% (↓)	4.6% – 40.1% (↑)	6% (↓)	53.6% – 43.8% (↓)
Solution concentration ($kg_{LiCl}/kg_{sol.}$)	2% (↓)	0.3% – 2.1% (↓)	1% (↓)	1.8% – 0.9% (↓)

For a given set of inlet conditions (Table 4.2), as the relative humidity increases, there is a significant decrease in outlet desiccant concentration (increase in conversion of concentrated

to diluted desiccant solution) in the dehumidification system whereas in the regeneration system, outlet desiccant concentration decreases (decrease in conversion of diluted to concentrated desiccant solution) with increase in relative humidity (Table 4.3). This is due to increase in vapour absorption from ambient air to the desiccant solution in the dehumidification system and due to decrease in vapour absorption from desiccant solution to the ambient air in the regeneration system. Further, from Table 4.3, it is observed that as the relative humidity increases, the desiccant concentration difference decreases during dehumidification and regeneration processes.

4.1.5 Energy exchange

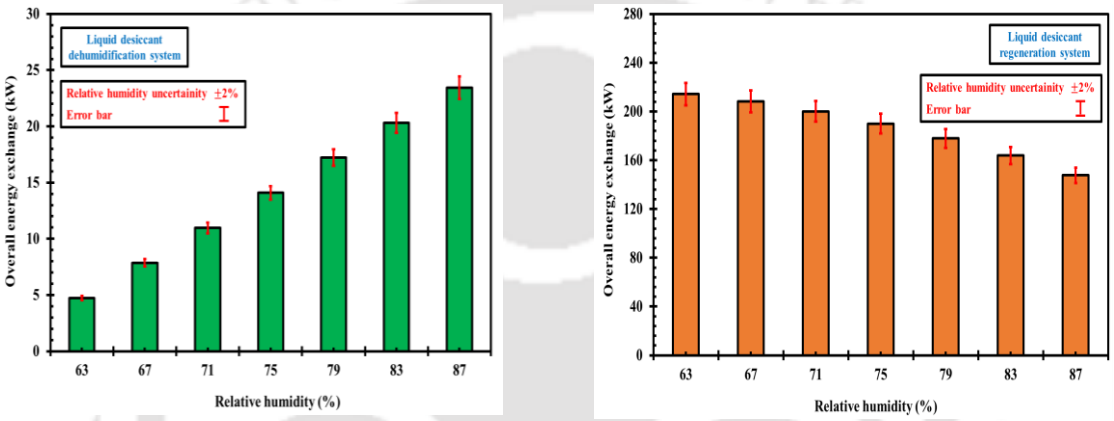

(a) Energy exchange – dehumidification system.

(b) Energy exchange – regeneration system.

Fig. 4.4, Influence of relative humidity on energy exchange.

Fig. 4.4 shows the influence of relative humidity on overall energy exchange for the liquid desiccant dehumidification and regeneration systems. From Fig. 4.4, it is observed that with increase in relative humidity, the overall energy exchange increases for the dehumidification and decreases for the regeneration systems. This happens because as the relative humidity increases, the moisture content present in the ambient air increases and this increase leads to increase in air vapour pressure. Therefore, there is a high potential for latent heat of condensation into the ambient air for the dehumidification system whereas in the regeneration system, there is a low potential for latent heat of evaporation from the desiccant solution to the ambient air. From Fig. 4, it is also observed that for a given set of inlet conditions (Table 4.2), with increase in relative humidity from 63% to 87%, the overall energy exchange for the dehumidification system increases by 80% and for the regeneration system, this energy exchange decreases by 31%, respectively. From this analysis, it is found that the percentage

contribution in overall energy exchange is high for the latent energy exchange compared to sensible energy exchange in the dehumidification and regeneration systems.

4.1.6 Experimental Correlation

In the present investigation, experimental correlations are developed for the specific humidity difference as the function of operating parameters (air and solution inlet temperatures, L/G ratio, air inlet specific humidity and desiccant inlet concentration) for both liquid desiccant dehumidification and regeneration systems. In order to develop the experimental correlations, Design Expert Software (Version 10.0.1) is used. The response surface methodology – central composite design (RSM – CCD) design matrix is implemented for developing the experimental correlations. This RSM – CCD technique is chosen because it optimizes the number of experiments to be carried out.

The operating parameters such as air inlet temperature and specific humidity, L/G ratio and desiccant inlet temperature and concertation are denoted as X_1, X_2, X_3 and X_4 for liquid desiccant dehumidification system and Y_1, Y_2, Y_3 and Y_4 for the liquid desiccant regeneration system, respectively. The response, specific humidity difference is designated as $\Delta\omega_d$ (g_{wv}/kg_{da}) for liquid desiccant dehumidification system and as $\Delta\omega_r$ (g_{wv}/kg_{da}) for liquid desiccant regeneration system. After selecting the operating parameters and their ranges (Table 4.2), based on RSM – CCD technique, the number of runs is designed and corresponding responses are attained from the series of experiments. The number of runs required (φ) is obtained using Eq. 4.6.

$$\varphi = 2^n + 2k + k_c \quad \text{(G. Mehrorang and N. K. Syamak, 2015)} \tag{4.6}$$

where 'k' is number of variables and k_c is number of centre points

A correlation is formulated by relating the response with the independent parameters using linear and quadratic terms as follows

$$\text{Dehumidification system: } \Delta\omega_d = \tau_o + \sum_{i=1}^{4}\tau_i X_i + \sum_{i=1}^{4}\tau_{ii} X^2{}_i + \sum_{i=1}^{3}\sum_{j=i+1}^{4}\tau_{ij} X_i X_j \tag{4.7}$$

$$\text{Regeneration system: } \Delta\omega_r = \tau_o + \sum_{i=1}^{4}\tau_i Y_i + \sum_{i=1}^{4}\tau_{ii} Y^2{}_i + \sum_{i=1}^{3}\sum_{j=i+1}^{4}\tau_{ij} Y_i Y_j \tag{4.7a}$$

where X_i and X_j and Y_i and Y_j are the coded values of the parameters for dehumidification and regeneration systems, respectively and τ_o, τ_i, τ_{ii} and τ_{ij} are the constant, linear, quadratic and interaction coefficients, respectively.

In order to establish a correlation between the specific humidity difference and known inlet parameters for the liquid desiccant dehumidification/regeneration systems, number of experimental runs needs to be designed. From Eq. 4.6, within the given range of operating parameters, the number of experimental runs for the liquid desiccant dehumidification and regeneration systems were estimated as 29 and 35, respectively. Using Eq. 4.7 and 4.7a, experimental correlations of specific humidity difference for both the dehumidification and the regeneration systems are formulated. For identifying the significance of the direct and interactive effects of the operating parameters on the air specific humidity difference, analysis of variance (ANOVA) is performed for each parameter and a P – value (level of marginal significance) of less than 0.05 is chosen (B. K. Naik and P. Muthukumar, 2017; G. Mehrorang and N. K. Syamak, 2015). During this analysis, it is observed that the relationship between the specific humidity difference and the five operating parameters (air and solution inlet temperatures, L/G ratio, air inlet specific humidity and desiccant inlet concentration) for liquid desiccant dehumidification and regeneration systems are best fitted to a linear equation. The best fit equation and the statistical parameters obtained from the analysis of variance are given in Tab. 4.4 for both the dehumidification and regeneration systems.

Table 4.4, Coefficients of the specific humidity difference correlation.

System	Correlation					
Dehumidifier	$\Delta\omega_d\ (g_{wv}/kg_{da}) = \tau_0 + \tau_1 X_1 + \tau_2 X_2 + \tau_3 X_3 + \tau_4 X_4 + \tau_5 X_5$					
Regenerator	$\Delta\omega_r\ (g_{wv}/kg_{da}) = \tau_0 + \tau_1 Y_1 + \tau_2 Y_2 + \tau_3 Y_3 + \tau_4 Y_4 + \tau_5 Y_5$					
	τ_0	τ_1	τ_2	τ_3	τ_4	τ_5
$\Delta\omega_d$	-0.18	-8.98×10^{-17}	1.86×10^{-17}	-0.59	0.74	0.16
$\Delta\omega_r$	-101.72	-6.35×10^{-16}	-1.5×10^{-16}	2.85	-0.47	-0.89
Statistical parameters						
Regression Statistics	Dehumidifier			Regenerator		
R^2	0.96			0.98		
Adjusted R^2	0.93			0.94		

F significance		1.1×10^{-38}			7.7×10^{-37}	
P – value	τ_0	τ_1	τ_2	τ_3	τ_4	τ_5
Dehumidifier	0.65	0.0093	0.018	2.7×10^{-31}	5.7×10^{-41}	4.9×10^{-17}
Regenerator	1.1×10^{-21}	0.041	0.038	5.1×10^{-39}	1.4×10^{-13}	3.7×10^{-11}

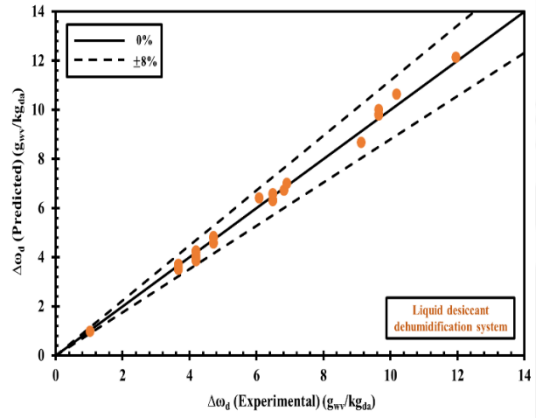

(a) Correlation validation – dehumidification system

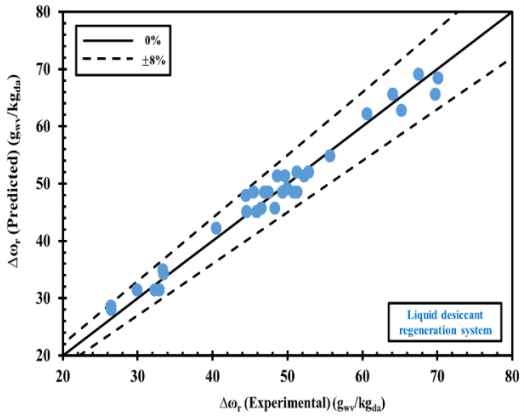

(b) Correlation validation – regeneration system

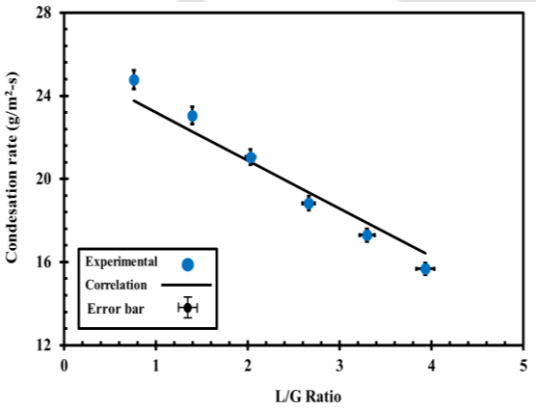

(c) Variation of condensation rate with L/G ratio – dehumidification system

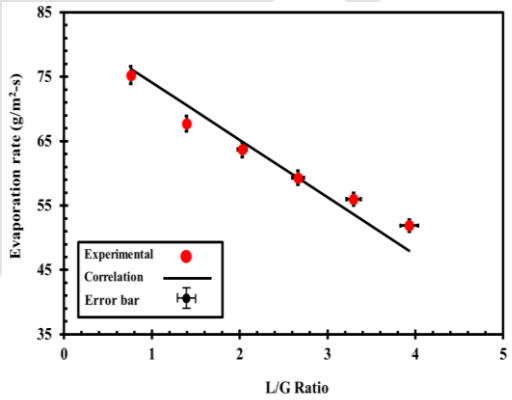

(d) Variation of evaporation rate with L/G ratio – regeneration system.

Fig. 4.5 – Validation of developed experimental correlation with the experimental results and the influence of L/G ratio on the variation of condensation and evaporation rates.

It is observed from Tab. 4.4 that the R^2 values are 96% and 98% for the dehumidification and regeneration systems whereas the adjusted R^2 values are obtained as 93% and 94%, respectively. The adjusted R^2 value describes the variation obtained by the experimental correlation after adjusting the number of variables present in it. Further, the value of adjusted

R^2 indicates the perfectness of the developed correlation and higher the value of adjusted R^2 signifies higher reliability of the developed correlation (B. K. Naik and P. Muthukumar, 2017; G. Mehrorang and N. K. Syamak, 2015). From Tab. 4.4, by analysing R^2, adjusted R^2, F – significance and P – value, it is concluded that the developed correlations of specific humidity difference for both the liquid desiccant dehumidification and regeneration systems match well with the experimental data.

For the given range of operating conditions (Tab. 4.2), Fig. 4.5 presents the comparison of predicted condensation and evaporation rates from the developed correlations with the experimental data obtained from the field analysis of liquid desiccant dehumidification and regeneration systems. It is found that the condensation and evaporation rates obtained from the developed correlation match well with the experimental data with a maximum error of $\pm$ 8%. Fig. 4.5c and 4.5d shows the variation of condensation and evaporation rates with the L/G ratio for dehumidification and regeneration systems, respectively. It is found that, for a given set of inlet conditions (Tab. 4.2), with increase in L/G ratio, the condensation and evaporation rates decrease. This can be explained by the fact that as the L/G ratio increases, the flow rate of the desiccant solution increases or the flow rate of the ambient air decreases. Therefore, the potential for mass exchange between the desiccant solution and the ambient air decreases and as a result, the moisture desorption/absorption rate (evaporation/condensation rate) between the ambient air and the desiccant solution decreases. From Fig. 4.5c and 4.5d, it is also observed that with increase in L/G ratio from 0.8 to 3.9, the condensation rate and the evaporation rate decrease by 51% and 58%, respectively.

4.2 Evacuated U – tube solar collector system

4.2.1 Details of experimental Setup and test procedure

The schematic and pictorial views of the fabricated evacuated U – tube solar collector system and the details of the experimental setup are presented in Fig. 4.6a and 4.6b. The flow arrangement between the manifold and the evacuated U – tube solar collector and the cross – sectional and longitudinal views of the evacuated U – tube are shown in Fig. 4.6c, 4.6d and 4.6e.

The major components of this system are a centrifugal pump of capacity 0.4 kW, thirty evacuated tubes made up of borosilicate glass, thirty copper U – tubes, three manifolds (M_1, M_2 and M_3), a storage tank and a collection tank. The manifolds are connected in series and

each manifold is connected with ten evacuated U – tube solar collectors in parallel (copper U – tube integrated with evacuated tube is connected to a cold and hot header in parallel (Fig. 4.6c)). Each manifold is connected to 10 copper pipes, which are insulated with the K – flex thermocol for reducing the heat loss to the surroundings.

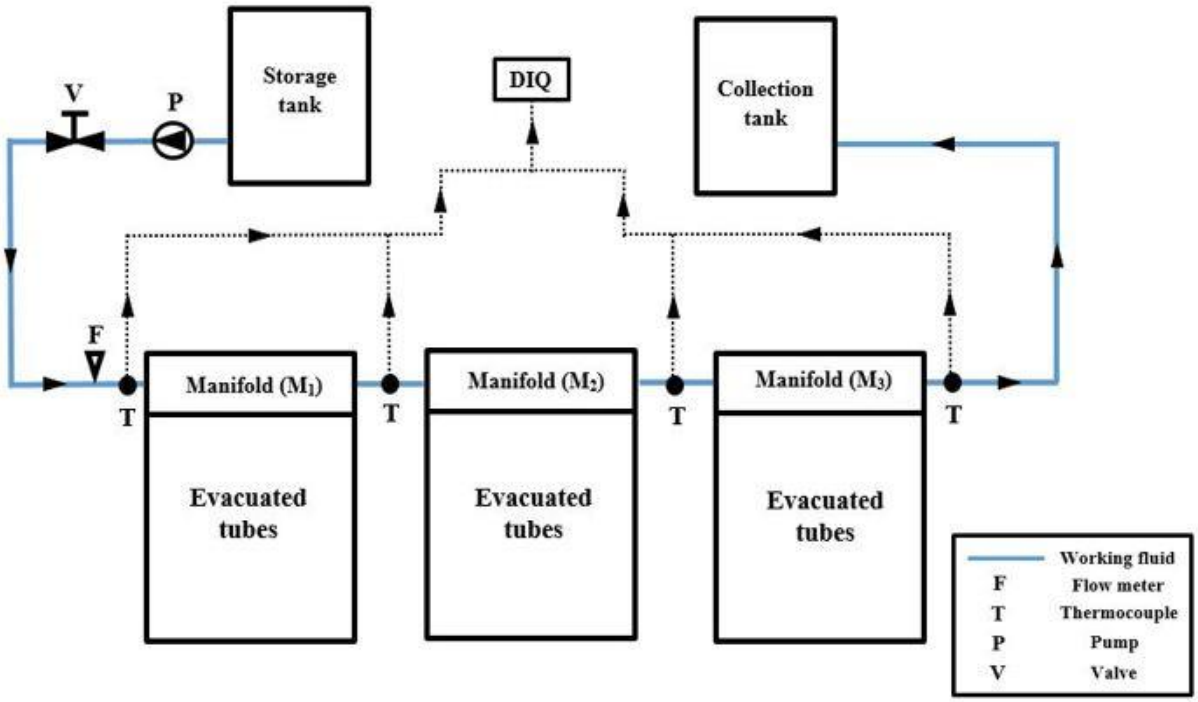

(a) Evacuated U – tube solar collector system schematic

(b) Evacuated U – tube solar collector system – pictorial view.

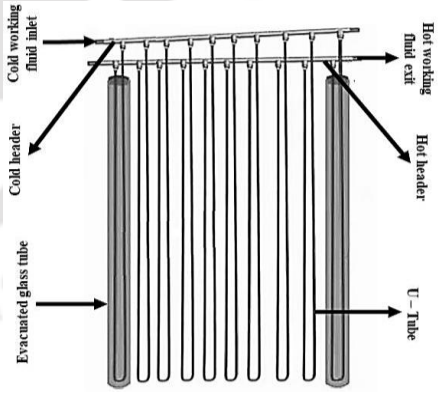

(c) Evacuated U – tube configuration inside the manifolds – M_1, M_2 and M_3.

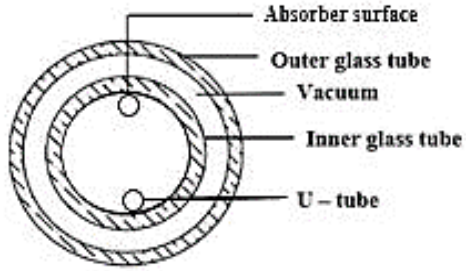

(d) Cross–sectional view of evacuated U – tube.

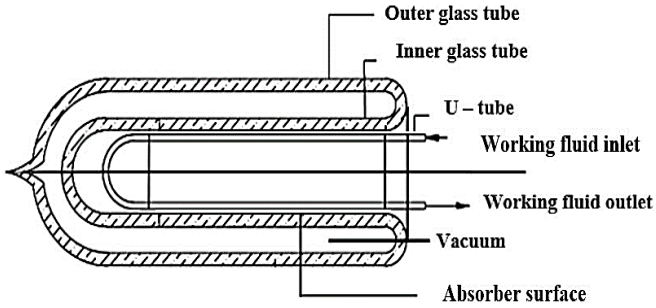

(e) Longitudinal view of evacuated U – tube.

Fig. 4.6, Evacuated U – tube solar collector system.

As shown in Fig. 4.6a, the cold working fluid is supplied from the working fluid storage tank to the manifold – M_1 through a 0.5 HP motor pump. In manifold – M_1, the cold working fluid is circulated from the cold header (Copper tube – 1.27 cm dia.) to the evenly distributed evacuated copper U – tube solar collectors (Fig. 4.6c). The working fluid flowing inside the copper U – tube of 0.95 cm dia. absorbs the heat gained by the evacuated tube due to the solar radiation incident on the upper surface of the evacuated tube (Fig. 4.6d and 4.6e). Thus, the heated working fluid enters into the hot header (Copper tube – 1.27 cm dia.) located inside the manifold – M_1. For gaining additional heat, the heated working fluid is passed into the manifolds – M_2 and M_3 which are connected in series with manifold – M_1 (Fig. 4.6a). The hot working fluid coming out from manifold – M_3 is supplied to the collection tank.

The atmospheric temperature and the inlet and outlet temperatures of the working fluid (water) flowing across each manifold are measured using the T – type thermocouples (accuracy of ±0.2 ^oC). The solar radiation incident on the evacuated tube solar collector is measured using a pyranometer (Apogee: Model SP – 110; accuracy of ±5 W/m^2). Data acquisition system (Agilent – 34972A) is used for acquiring the outputs of thermocouples and pyranometer. A control valve and a turbine type flow meter (Aqua RE: Model H1305726; ±0.2% accuracy) are fitted before the manifold – M_1, for regulating the flow and for monitoring the flow rate. The solar collector inclination angle is chosen based on maximum solar radiation that can be incident on the evacuated U – tube solar collector system. According to humid subtropical climate solar irradiance data, this inclination angle has been fixed at 60^o from the horizontal plane. The dimensions, thermo – physical properties and the operating range of the evacuated U – tube solar collector system are listed in Table 4.5.

Table 4.5, Dimensions, surface properties and operating parameters chosen for experimental and numerical analyses of the evacuated U – tube solar collector.

Table 4.5a, Dimensions

Outer glass tube outer diameter (cm)	5.8
Outer glass tube thickness (cm)	0.2
Inner glass tube outer diameter (cm)	4.7
Inner glass tube thickness (cm)	0.2
Air gap (cm)	0.1
U – tube outer diameter (cm)	0.1
U – tube inner diameter (cm)	0.95
Collector tube length (m)	1.8
Header diameter (cm)	1.27
Header thickness (cm)	0.1
Working fluid	Water
Type of U – tube material	Copper
Coating material	AI-N*
Hot and cold header's material	Copper

Table 4.5b, Thermo – physical properties

Glass tube transmittance (τ)	0.91
Absorptivity of coating material (α)	0.92
Reflectivity of parabolic reflector (ρ)	0.89
Water density (g/cm^3)	1
C_p of water (kJ/kg – K)	4.2
Copper conductivity (W/m – K)	307

Table 4.5c, Operating range and reference values

Ambient temperature (^{o}C)	26 – 34	31
Solar intensity (kW/m^2)	0.52 – 1.08	0.8
Working fluid inlet temperature (^{o}C)	23 – 38	30
Working fluid flow rate (U – tube) (ml/s)	6 – 24	15
Working fluid flow rate (header) (l/s)	0.06 – 0.24	0.15
Reynolds number (Re)	Re < 4000	

*AI-N: Aluminium Nitrate (coating material)

4.2.2 Uncertainty in measurement

For evaluating the reliability and accuracy of dependent parameters, uncertainty analysis is carried out. The uncertainties involved in the estimation of dependent parameters such as useful heat gained per unit area is calculated using Eq. 4.1 (Kline and Mc – Clintok, 1953) and it is estimated as ± 3.2 %. The calculation procedure for uncertainty in the dependent parameter, useful heat gained per unit area is presented in Appendix B.

4.2.3. Thermal modelling

a) Model description

For predicting the variation in U – tube surface temperature and working fluid heat gain rate along the length of the U – tube, an experimental approach is complicated. Therefore, a numerical approach is chosen. In this work, a three dimensional numerical model is developed using COMSOL 5.3a simulation software. Fig. 4.7a shows the cross sectional view of the three dimensional U – tube solar collector model containing working fluid inside the U – tube. In

this model, copper and water are chosen as the U – tube material and the working fluid, respectively. The surface properties and dimensions taken for designing the U – tube model are specified in Table 4.5a and 4.5b. As the proposed U – tube collector operates below 200 °C, the material properties are assumed to be constant. The following assumptions are made to simplify the current numerical analysis.

- Working fluid is incompressible and Newtonian.
- Initially, U – tube collector surface is at uniform temperature throughout its length.
- Buoyancy effect is quantified using the Boussinesq approximation.
- In between the evacuated tube and the U – tube, heat transferred by the process air is negligible.

b) Governing equations

The continuity and Naiver – Stokes momentum equations are solved simultaneously for simulating the behaviour of working fluid flowing inside the U – tube (Eqs. 4.9 and 4.10). The velocity field obtained from Eqs. 4.9 and 4.10 is used for solving the convective heat transfer taking place from U – tube wall surface to the working fluid (Eq. 4.11). The continuity, momentum and energy equations are solved using GRMS solver. The simulations are carried out with a time step of 0.1 s.

Continuity equation:

$$\rho \nabla \overrightarrow{V_{wf}} = 0 \tag{4.9}$$

Momentum equation:

$$\frac{\partial \overrightarrow{V_{wf}}}{\partial t} + \left(\overrightarrow{V_{wf}}.\nabla\right)\overrightarrow{V_{wf}} = \frac{\mu}{\rho}\nabla^2 \overrightarrow{V_{wf}} - \frac{1}{\rho}\nabla P - \vec{g}\beta_T \left(T_{amb} - T\right) \tag{4.10}$$

Energy equation:

$$\rho C_{p,wf} \frac{\partial T}{\partial t} + \rho C_{p,wf} \left(\overrightarrow{V_{wf}}.\nabla T\right) = k\nabla^2 T \tag{4.11}$$

where ρ, V_{wf}, and $C_{p,wf}$ are the density (kg/m^3), velocity (m/s) and specific heat (kJ/kg – K) of the working fluid and k is the thermal conductivity (kW/m – K) of the U – tube material. The elaborative derivation of the developed model is presented in Appendix A.

a) Boussinesq approximation

In buoyancy – driven flows, Boussinesq approximation model is used instead of variation of properties with temperature model (VPT) because it converges faster. Density term is treated as constant in all the governing equations expect for buoyancy term in momentum equation (Eq. 4.10). Also, this approximation couples the temperature and flow fields in the momentum equation (Ayyala et al. 2015). Boussinesq approximation considered in this model is given by

$$\rho_{\infty} - \rho = -\rho\beta_T (T_{\infty} - T) \tag{4.12}$$

where 'ρ' is the density of the flow, T is the operating temperature and β_T is the thermal expansion coefficient (0.000206 (1/K)) (Ayyala et al. 2015).

c) Initial and Boundary conditions

- Initially there is no flow of working fluid inside the U – tube and all the domains (U – tube and working fluid) are specified at a constant temperature of T_{intial}. At any time t > 0, the inlet of the fluid flow is specified as $T_{wf,i}$ ($T_{intial} = T_{wf,i}$) and fluid flow velocity is maintained constant.
- The working fluid flow rate (ṁ) and the atmospheric pressure ($P = P_{atm}$ =101.3 kPa) are imposed as the boundary conditions at the entrance and exit of the U – tube, respectively.
- No slip boundary condition between the U – tube material and the working fluid.
- Constant heat flux along the upper surface of the U – tube i.e. $\zeta = \tau_{g,o}\tau_{g,i}\alpha_c I$.

  where ζ is the effective heat absorbed from the evacuated tube (kW/m^2), $\tau_{g,o}$ and $\tau_{g,i}$ are the transmissivity of the outer and inner glass surface, respectively, I is the solar intensity and α_c is the absorptivity of the coating material.

4.2.4 Mesh generation and Grid independence test

a) Mesh generation

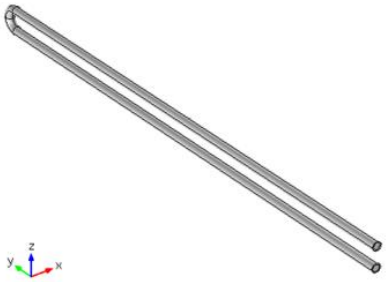

(a) U – tube solar collector model.

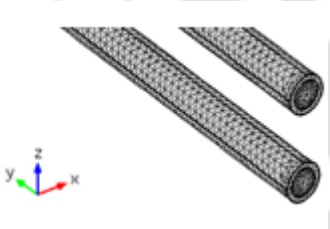

(b) Mesh generated at the inlet and outlet of the U – tube.

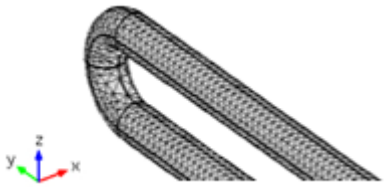

(c) Mesh generated at the U – bend.

Fig. 4.7, Details of U – tube solar collector module.

The domains and boundaries of the U – tube are meshed using free unstructured tetragonal and triangular meshes. These type of meshes are chosen to ensure the discretization of relatively smaller sections of the U – tube i.e. the entrance and the exit of the U – tube (Fig. 4.7b).

Table 4.6, Grid size and number of mesh elements for evacuated U – tube models.

Sl. No.	Component	Grid size (mm)				Number of mesh elements
		U – tube material (copper)		Working fluid (water)		
		Min	Max	Min	Max	
1	U – tube solar collector	1.31	5.63	0.50	2.65	623,127

Finer mesh sizes are applied at working fluid inlet/outlet, along the working fluid boundary layer and across the 'U' bend (Fig. 4.7c). The distribution of elements depending upon the mesh generation is given in Table 4.6.

b) Grid independence test

Simulations with different mesh element sizes were performed for testing the dependency of numerical results on the mesh element size. Fig. 4.8, shows the surface temperature variation of U – tube solar collector module with different no. of mesh elements viz. 867,891, 623,127 and 440,634 elements. Convergence issues were found for the developed model with mesh elements less than 440,634. It can be observed from Fig. 4.8 that the numerical simulation demands more number of mesh elements, due to the free convective movement of the working fluid. For all the cases of grid independence test, initially all the domains are specified at T_{intial} of 316 K and at any time t > 0, the working fluid flows at 15 ml/s with an inlet temperature of 31 °C. Also, a constant heat flux of 0.8 kW/m^2 has been imposed at the upper surface of the U – tube. From Fig. 4.8, it is noticed that the model with 623,127 elements is found to be grid independent for the U – tube solar collector module.

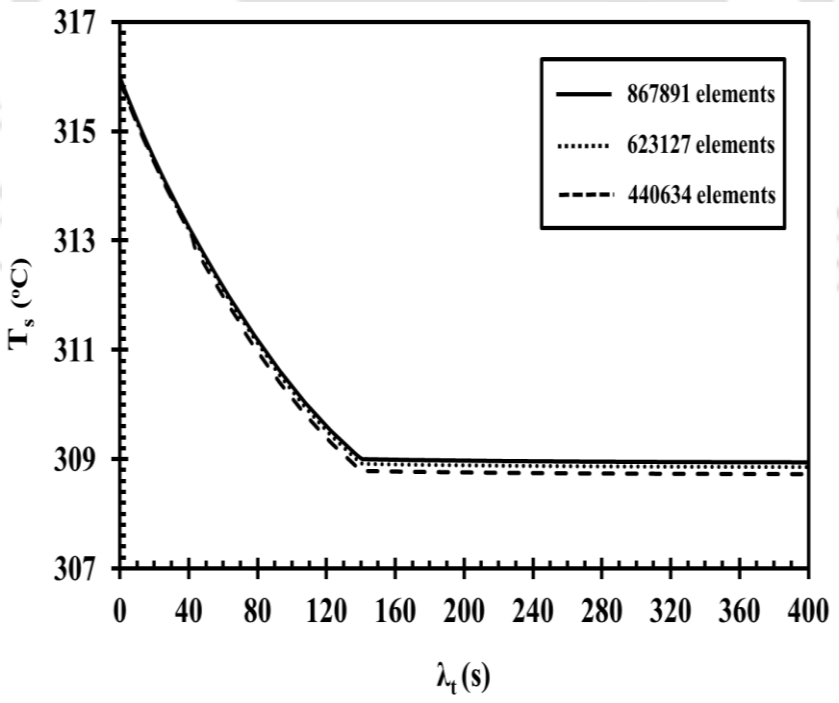

Fig. 4.8, Grid independence test for U – tube solar collector module.

(Note: λ_t = working fluid transition time)

4.2.5 Performance characteristics

a) Instantaneous heat gain (Q_i)

For a particular operating and ambient conditions, the instantaneous heat gained by the working fluid along the length of the U – tube from the U – tube wall surface is indicated as instantaneous heat gain and is formulated as

$$Q_i = \dot{m}_{wf} c_{p,wf} (T_{wf,l}(l) - T_{wf,i}) \tag{4.13}$$

b) Useful heat flux (Q_{uh})

For a given ambient and operating conditions, the useful heat absorbed by the working fluid per unit area from a U – tube wall surface is indicated as useful heat flux and it is expressed as

$$Q_{uh} = \rho_{wf} v_{wf} c_{p,wf} (T_{wf,o} - T_{wf,i}) \tag{4.14}$$

4.2.6 Model validation

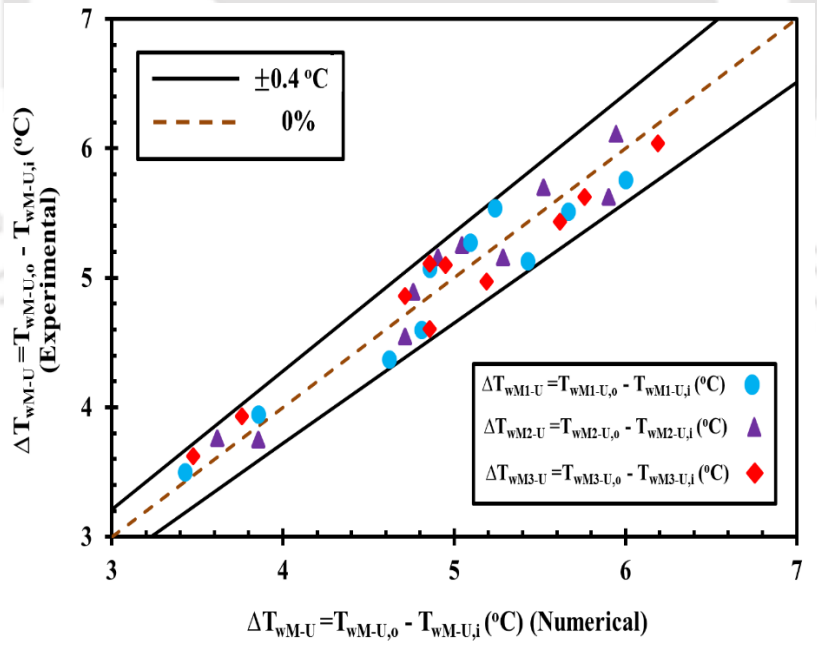

Fig. 4.9a, Comparison of model predictions with the experimental data for working fluid inlet and outlet temperature difference along the manifolds M_1, M_2 and M_3.

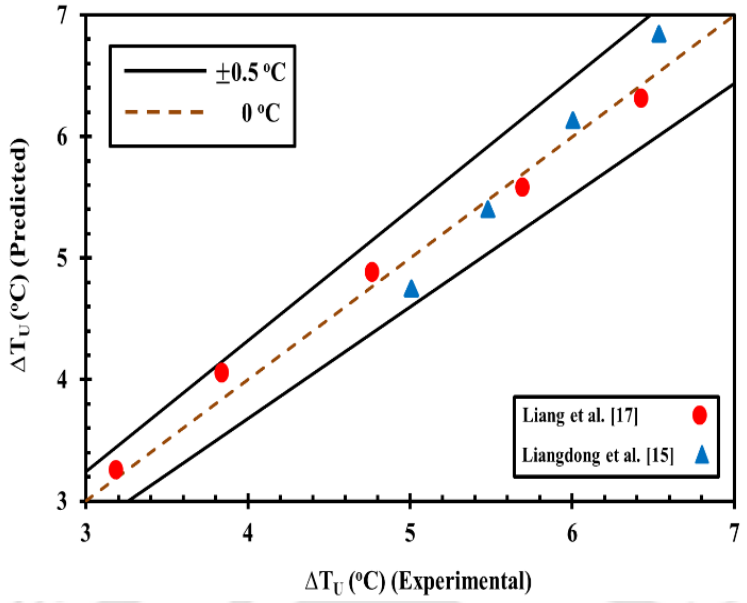

Fig. 4.9b, Comparison of model predictions with the experimental data reported in the literature (Liangdong et al. 2010; Liang et al. 2011) for the working fluid temperature difference along the U – tube.

In order to ensure the consistency of the developed numerical model, validation with the real – time experimental data is essential. Therefore, the experimental results obtained for the working fluid inlet and outlet temperature difference along the manifolds M_1, M_2 and M_3 of the evacuated U – tube solar collector system and the useful heat gained by the working fluid along the evacuated U – tube solar collector are compared with the numerical predictions obtained from the developed model (Figs. 4.9 – 4.11). While predicting the working fluid outlet temperature across each manifold, it is assumed that the working fluid inlet and exit temperatures in each manifold ($M_1/M_2/M_3$) is equal to the inlet and exit temperatures of the U – tube (since manifolds are connected in series and each manifold is integrated with ten evacuated U – tubes in parallel). Further, to predict the working fluid outlet temperatures at the manifolds – M_2 and M_3, the predicted outlet temperatures attained at the manifolds – M_1 and M_2 are taken as the inlet temperatures, respectively. From Fig. 4.9, it is observed that for a given range of operating conditions (Table 4.5c), the experimental values of working fluid temperature difference between the inlet and exit of each manifold (M_1, M_2 and M_3) are in good agreement with the numerical values obtained from the simulated results and they match within ±0.4 ^{o}C. Further, the numerical results obtained from the developed model for the working fluid temperature difference between the inlet and the exit of the U – tube (ΔT_u) are validated with the experimental data reported in the literature (Liangdong et al. 2010; Liang et

al. 2011) as shown in Fig. 4.9b. From this figure, it is found that the developed model is in good agreement with the experimental data available in the literature and they match within ±0.5 ^{o}C. During this validation analysis, the dimensions, surface properties and inlet parameters of the U – tube solar collector are taken from Liangdong et al. (2010) and Liang et al. (2011), respectively.

a) Useful heat flux for an evacuated U – tube solar collector

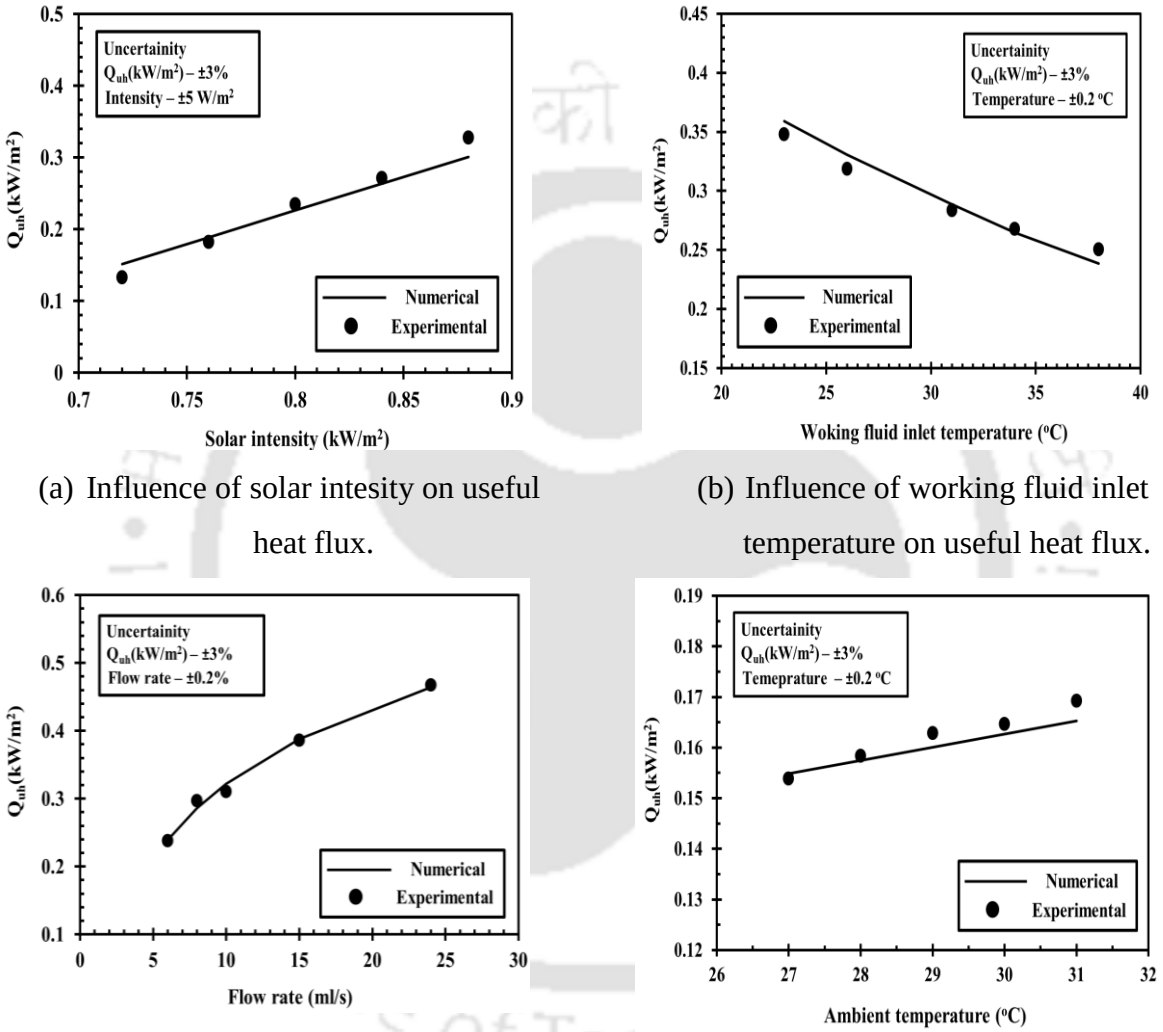

(a) Influence of solar intesity on useful heat flux.

(b) Influence of working fluid inlet temperature on useful heat flux.

(c) Influence of working fluid flow rate on useful heat flux.

(d) Influence of ambient temperature on useful heat flux.

Fig. 4.10, Comparison of experimental data with the developed numerical model predictions and influences of operating parameters on useful heat flux.

In Fig. 4.10a – 4.10d, the experimental results of useful heat flux (useful heat per unit area) attained by the working fluid from an evacuated U – tube solar collector are compared with the results obtained from the numerical model. From Fig. 4.10a, it is observed that the useful heat gained by the working fluid per unit area increases with increasing solar intensity incident on

the evacuated U – tube solar collector. This is due to the fact that increase in solar intensities, the potential for heat exchange from the evacuated U – tube to the working fluid is high, resulting in higher working fluid heat gain. Increasing in solar intensity from 0.72 kW/m^2 to 0.88 kW/m^2 increases the useful heat flux by 66%.

As illustrated in Fig. 4.10b, the useful heat gained by the working fluid per unit area decreases with increase in working fluid inlet temperature. This can be explained by the fact that the heat transfer from the evacuated U – tube to the working fluid depends upon the temperature difference between the absorber tube and the working fluid and higher the temperature difference, higher will be the useful heat gained by the working fluid. Increasing the working fluid inlet temperature from 23 ^{o}C to 38 ^{o}C, the useful heat flux gets decreased by 33%. In Fig. 4.10c, it is observed that the working fluid heat gain per unit area increases significantly with increase in working fluid flow rate from 6 ml/s to 24 ml/s. It happens because with increase in flow rate, the heat transfer rate from the absorber tube to the working fluid increases and the temperature difference between the absorber tube and the working fluid decreases. Thus, the useful heat gained by the working fluid per unit area increases significantly. From Fig. 4.10d, it is observed that with increase in ambient temperature from 27 ^{o}C to 31 ^{o}C, the useful heat flux hardly increases only by 4%. From this analysis, it is realized that the influence of ambient temperature doesn't have significant effect on useful energy gained by the working fluid per unit area.

It is concluded from Fig. 4.10 that for a given range of operating parameters and ambient temperatures (Table 4.5c), solar intensity and working fluid inlet temperature and flow rate have significant effect on useful heat gained by the working fluid. Further, it is also concluded that proposed numerical model is well tested and also reliable for predicting the performance of an evacuated U – tube solar collector.

b) Working fluid temperature difference along the manifolds – M_1, M_2 and M_3

With reference to the results presented in Fig. 4.11a – 4.11c, it is observed that for a given range of operating parameters (Table 4.5c), measured working fluid inlet and outlet temperature difference along the manifolds M_1, M_2 and M_3 match well with the numerically predicted values. Fig. 4.11a – 4.11c also shows the variations of working fluid temperature difference between the inlet temperature at manifold M_1 and exit temperatures at manifolds M_1, M_2 and M_3 for different working fluid flow rates, solar intensities and working fluid inlet

temperatures. From Fig. 4.11a, it is seen that for a given set of inlet condition, with increase in working fluid flow rate, the temperature difference between the inlet temperature at manifold M_1 and exit temperatures at manifolds M_1, M_2 and M_3 decreases significantly. This is due to fact that with increase in working fluid flow rate improves the heat transfer rate from the U – tube surface to the working fluid and subsequently decrease U – tube surface temperature and inner glass absorber surface temperature. As a result, the working fluid outlet temperature decreases with increase in flow rate. It is also observed that with increase in flow rate from 0.06 l/s to 0.24 l/s, the temperature difference between the working fluid inlet temperature at manifold M_1 and exit temperatures at manifolds M_1, M_2 and M_3 reduces by 3.2 ^oC, 6.7 ^oC and 11.5 ^oC, respectively.

In Fig. 4.11b, it is seen that for a given set of inlet condition, higher solar intensities result in higher temperature differences along the manifolds M_1, M_2 and M_3. This happens because as the solar intensity increases, the heat transfer rate increases from outer glass surface to the U – tube. As a consequence, there will be higher rate of convective heat transfer between the U – tube and the working fluid. It is also found that as the solar intensity increases from 0.74 kW/m^2 to 0.82 kW/m^2, the temperature difference between the working fluid inlet temperature at manifold M_1 and exit temperatures at manifolds M_1, M_2 and M_3 is raised by 2.8 ^oC, 4.2 ^oC and 7.6 ^oC, respectively. This indicates that with increase in manifolds connected in series will enhance the working fluid exit temperature at higher solar intensities than at lower solar intensities.

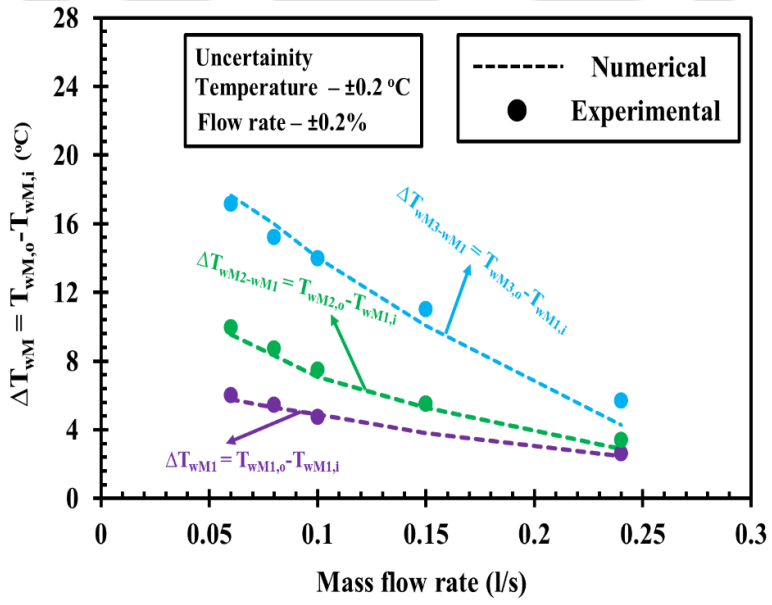

(a) Variation of temperature difference with working fluid flow rate.

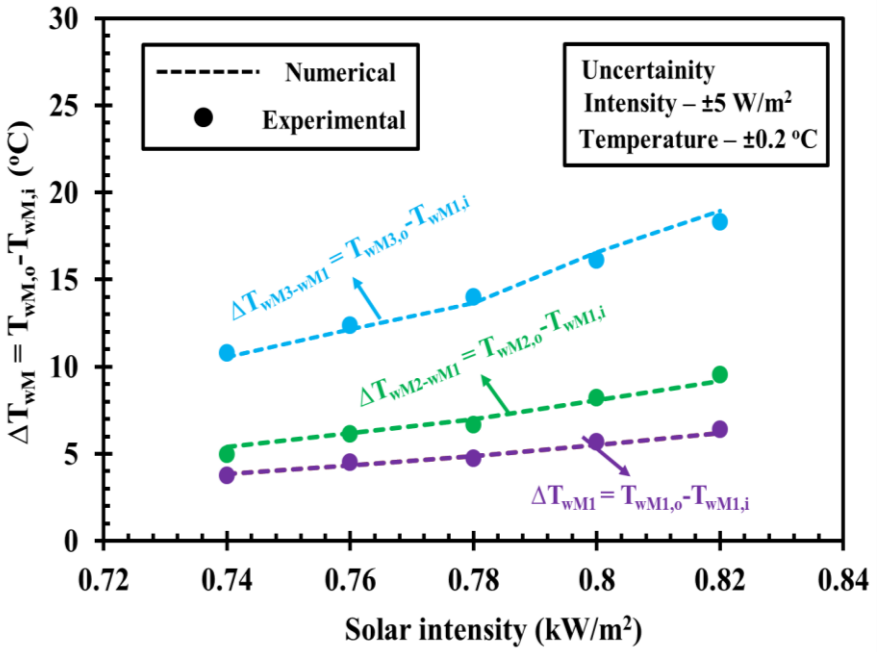

(b) Variation of temperature difference with solar intensity.

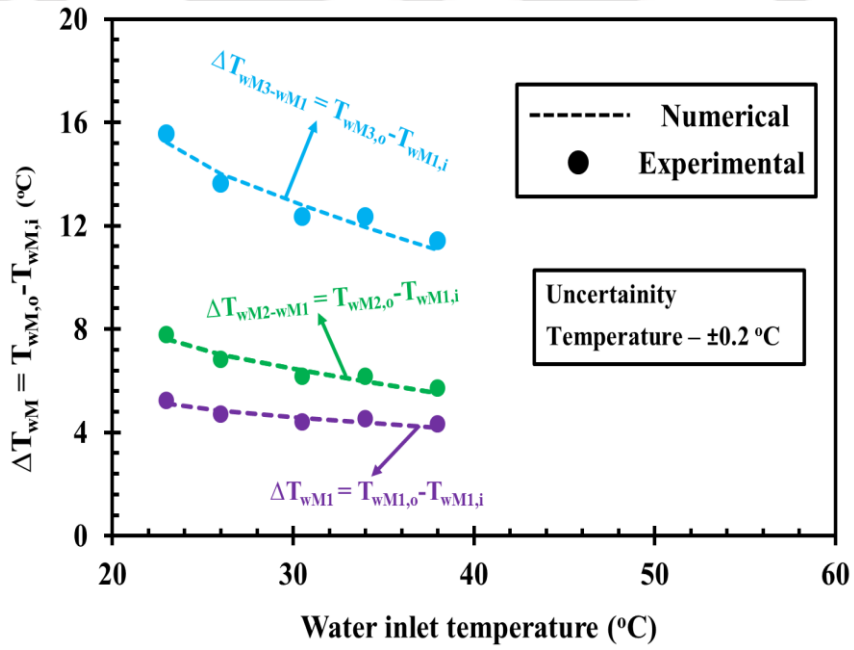

(c) Variation of temperature difference with working fluid inlet temperature.

Fig. 4.11, Numerical model validation and the variation of working fluid temperature difference along the manifolds M_1, M_2 and M_3 for a given range of operating parameters (Table 4.5c).

For a given set of inlet conditions, the variation in temperature difference along the manifolds M_1, M_2 and M_3 decrease with increase in working fluid inlet temperature as shown in Fig. 4.11c. This is due to decrease in overall heat transfer rate between the absorber surface and the working fluid with raise in working fluid inlet temperature. From Fig. 4.11c, it is also observed that an increase in working fluid inlet temperature from 23 ^oC to 38 ^oC, the temperature differences between the working fluid inlet temperature at manifold M_1 and exit temperatures at manifolds M_1, M_2 and M_3 reduces by 1 ^oC, 2.1 ^oC and 4.2 ^oC, respectively. This analysis illustrates that an increase in manifolds connected in series improves the heat transfer rate at lower working fluid inlet temperature more than at higher working fluid inlet temperature.

From Fig. 4.11, it is concluded that the manifolds connected in series give better performance at higher solar intensities and lower working fluid flow rates and inlet temperatures. Further, it is also observed that the developed numerical model is well suited for analysing the performance of any evacuated U – tube solar collector systems (manifolds connected in series and a manifold consisting of ten evacuated U – tubes integrated in parallel).

4.2.7 Working fluid transition time for an evacuated U – tube solar collector

The working fluid transition time (λ_t) is defined as the time taken by a working fluid to attain a steady state condition when it is passed through an evacuated U – tube. It is measured when the change in working fluid inlet temperature and flow rate, change in solar intensity and ambient temperature occurs. It can be expressed as

$$\lambda_t = f\left(T_{amb}, I, T_{wf,i}, \dot{m}_{wf}\right) \tag{4.15}$$

Working fluid temperature takes some time to reach steady state value due to throttling of a valve for attaining a required flow rate, sudden loss of power in the pump, variation in speed of an operating pump and sudden change in ambient temperature. Here, rather than measuring the working fluid transition time of whole solar collector system, individual evacuated U – tube solar collector is measured i.e. the transition time for an evacuated U – tube solar collector is measured/predicted instead of working fluid transition time at the exit of the manifold – M_3.

a) Empirical correlation for working fluid transition time

For deriving an empirical correlation for working fluid transition time in terms ambient temperature, solar intensity and working fluid inlet temperature and flow rate, Design Expert software (version 10.0.1) is used. The response surface methodology – Box Behnken Design

technique (RSM – BBD) is implemented for developing the correlation. The advantage of this technique lies in its practical application.

The four selected operating parameters/independent parameters such as ambient temperature, solar intensity and working fluid inlet temperature and flow rate are defined as X_1, X_2, X_3 and X_4, respectively. The response, working fluid transition time is denoted as λ_t. After the selection of operating parameters and their ranges (Table 4.5c), based on BBD technique, the number of runs is designed and the corresponding response is obtained from experiments. The number of runs (ψ) is calculated using Eq. 4.16 (Mehrorang and Syamak, 2015).

$$\psi = 2^n + 2n + n_c \tag{4.16}$$

where n is number of variables and n_c is the number of center points

To formulate a correlation, the response is related to the independent parameters by linear and quadratic terms as follows (Mehrorang and Syamak, 2015);

$$\lambda_t = \delta_o + \sum_{i=1}^{4} \delta_i X_i + \sum_{i=1}^{4} \delta_{ii} X^2{}_i + \sum_{i=1}^{3} \sum_{j=i+1}^{4} \delta_{ij} X_i X_j \tag{4.17}$$

where X_i and X_j are the coded values of the parameters and δ_o, δ_i, δ_{ii} and δ_{ij} are the constants, linear, quadratic and interaction coefficients, respectively.

Using Eq. 4.16, thirty-one experimental runs were performed to predict the working fluid transition time (λ_t) in an evacuated U – tube solar collector (Table 4.5c). Using Eq. 4.17, correlation is formulated between the working fluid transition time and the independent parameters. In order to identify the significance of direct and interactive effects of the independent parameters on working fluid transition time, analysis of variance (ANOVA) was implemented for each parameter (P – value less than 0.05 is considered). During this analysis, it is observed that the relationship between the working fluid transition time and the independent parameters is best fitted to a first order polynomial equation. The best fit equation and the statistical information about ANOVA are given in Table 4.7.

Table 4.7, Coefficients of the working fluid transition time correlation.

		Correlation			
Evacuated U – tube solar collector	$\lambda_t = \delta_o + \delta_1 X_1 + \delta_2 X_2 + \delta_3 X_3 + \delta_4 X_4$				
	δ_o	δ_1	δ_2	δ_3	δ_4

λ_t (s)	-172.8	-3.24×10^{-15}	535.02	-3.82	-1.11×10^{-16}

Statistical information					
Regression Statistics					
R^2	0.93				
Adjusted R^2	0.89				
F – value	161.47				
F – significance	2.2×10^{-14}				
P – value	δ_o	δ_1	δ_2	δ_3	δ_4
	0.00077	0.013	5×10^{-16}	1.3×10^{-5}	2.5×10^{-7}

It is observed from Tab. 4 that the R^2 and the adjusted R^2 values are 93 % and 89 % for the developed correlation. The adjusted R^2 value determines the variation obtained by the correlation after adjusting number of variables present in it. High value of adjusted R^2 indicates the goodness of the developed correlation (Mehrorang and Syamak, 2015). From the P – value listed in Table 4.7 for each independent parameter, it is observed that the ambient temperature has insignificant effect on the working fluid transition time. This is because the P – value close to 0.05 is the ambient temperature i.e. the independent parameter which is close to the P – value = 0.05 will have most insignificant effect on the dependent parameter (working fluid transition time) (Mehrorang and Syamak, 2015). Therefore, the ambient temperature has very less influence on the working fluid transition time.

For a given range of operating and ambient conditions, the working fluid transition time predicted from the developed empirical correlation and those obtained from the experiments are compared in Fig. 4.12. It is found that the developed empirical correlation has a good agreement with the experimental data with a maximum error of $\pm$12.7 %. Here, the experimental working fluid transition time was measured till the outlet temperature of the evacuated U – tube reached the steady state. As the evacuated U – tube is connected in parallel to a manifold – M_1, the working fluid inlet and outlet temperatures measured at the entrance and exit of the manifold – M_1 is considered as the inlet and outlet temperatures of the evacuated U – tube (Fig. 4.6a).

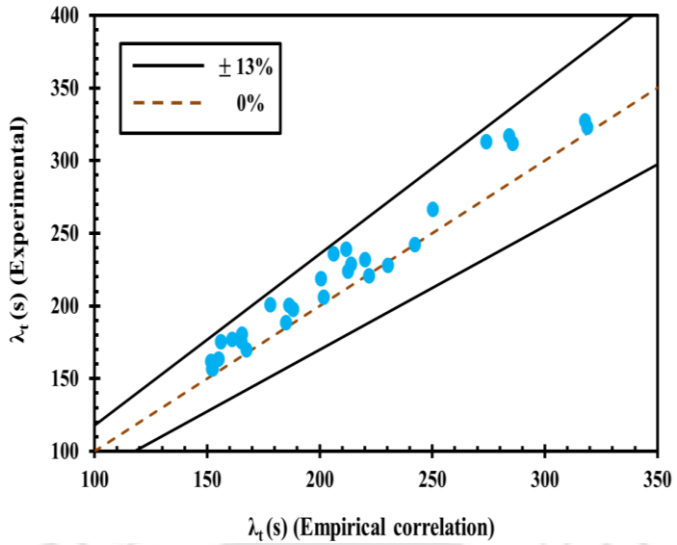

Fig. 4.12, Comparison of empirical correlation with the experimental data for the working fluid transition time (λ_t) in an evacuated U – tube solar collector.

b) Case study

An experimental case study is chosen for validating the developed numerical model for analysing the working fluid transition time condition. The inlet condition of the operating parameters listed in Table 4.8 remains unchanged during the test period. From Fig. 4.13a, it is observed that the time taken for a working fluid to attain steady state condition is about 144 s and the change in the working fluid outlet temperature reduces significantly from 315.8 K (λ_t = 1 s) to 309 K (λ_t = 144 s) and attains a steady state condition at 309 K (λ_t = 144 s). Further, it is also observed from Fig. 4.13a that for a given inlet condition, the temperature difference between the working fluid inlet and outlet temperatures after reaching steady state condition is about 4.9 K. From Fig. 4.13a and Tab. 4.8, it is found that the numerically predicted working fluid outlet temperature variation attains a closer agreement with the experimental result.

Table 4.8, Case study chosen for analysing the working fluid transition time

Inlet parameters				Outlet parameter (at steady state condition)	Working fluid transition state temperature difference (unsteady state to steady state)	Working fluid transition time
T_{amb} (°C)	$T_{wf,i}$ (°C)	$\dot{m}_{wf}$ (ml/s)	I (kW/m^2)	$T_{wf,o}$ (°C)	$T_{wf,o}$ (°C)	λ_t (s)

				Exp.	Num.	Diff.	Exp.	Num.	Exp.	Num.
30	31	15	0.8	35.5	35.9	0.4	42.8 ± 0.2 °C – 35.5 ± 0.2 °C (ΔT = 7.3)	43 – 35.9 (ΔT = 7.1)	147	144

Fig. 4.13b shows the contours of U – tube surface temperature for the inlet condition presented in Table 4.8. This U – tube surface temperature plot variation is difficult to obtain in a practical situation. Therefore, a numerical simulation is carried out using COMSOL 5.3a as a simulation software for analysing the surface temperature variation from initial condition to the steady state condition (working fluid transition time). From Fig. 4.13b, it is observed that initially there is no fluid flow along the U – tube (λ_t = 0 s). At time λ_t = 1 s, the working fluid starts flowing through the U – tube and the decrement in surface temperature of the U – tube is faster till the transition time (λ_t) reaches 27 s and then, the time taken to reach steady state condition increases significantly. This happens because the temperature difference between the working fluid and the U – tube surface is high initially (λ_t = 0 s) but as the time progresses, the temperature difference between them reduces. Therefore, the time taken to reach steady state condition increases with decrease in surface temperature and attains steady state condition at λ_t = 144 s.

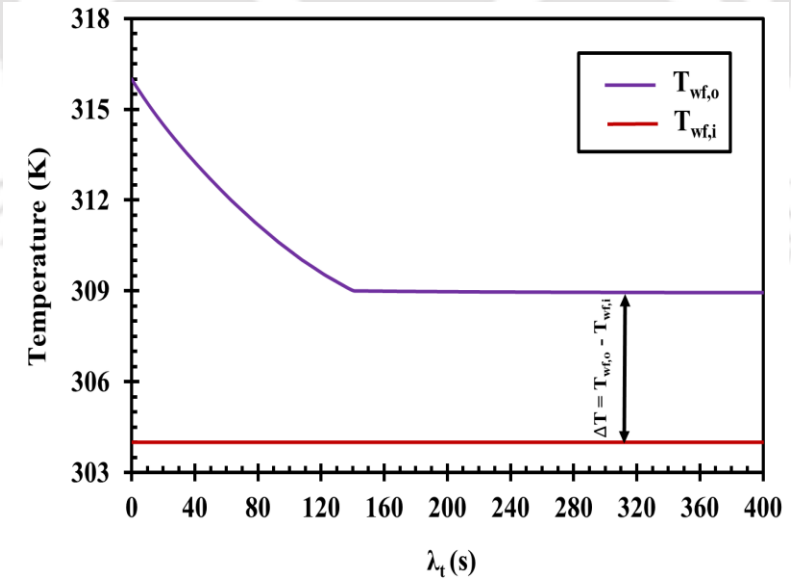

(a) Varition of working fluid temperature during transition time.

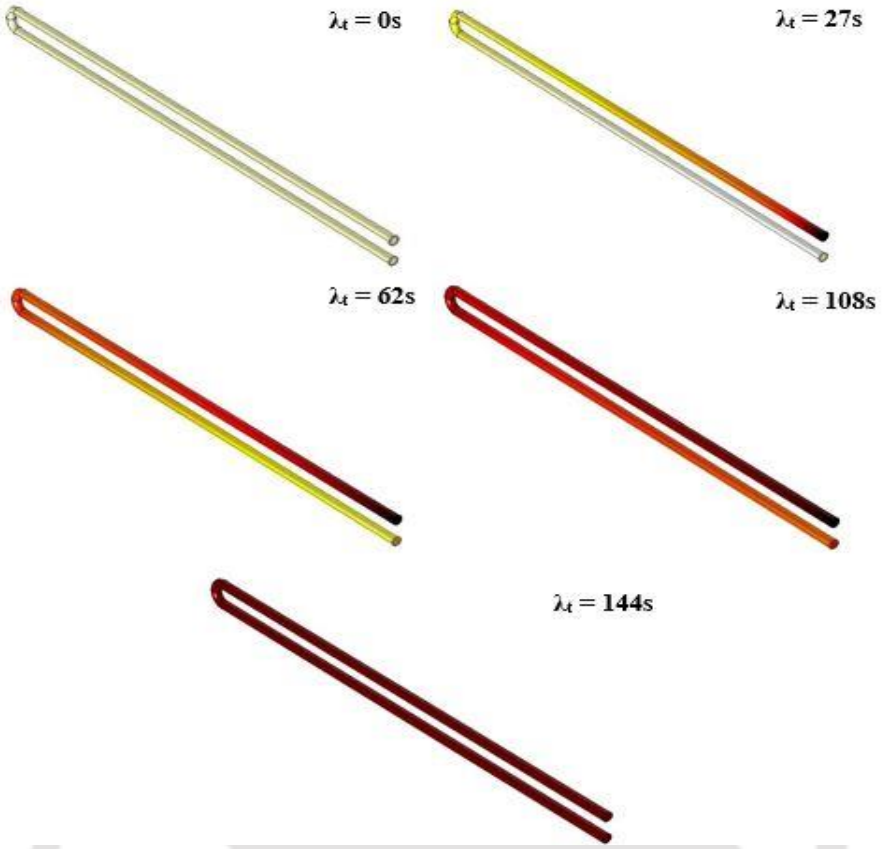

(b) U – tube surface temperature variation countours during working fluid transition time.

Fig. 4.13, Numerical analysis for the case study.

c) Heat transfer and fluid flow characteristics after attaining steady state condition

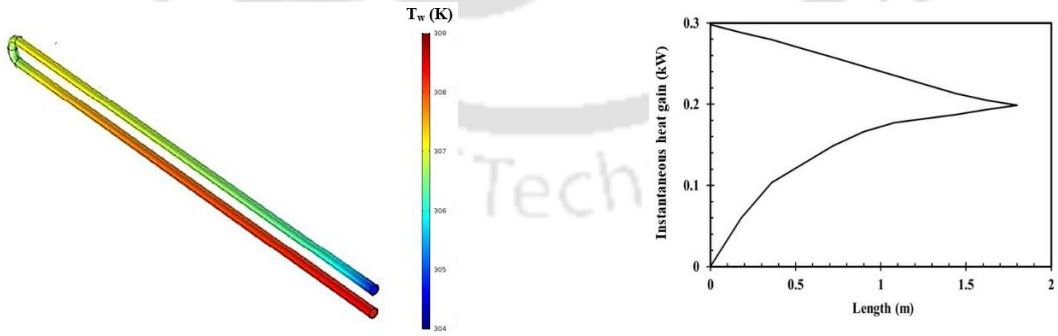

(a) Temperature variation contour plot.

(b) Variation of instantaneous heat gain along the length of the collector.

Fig. 4.14, Working fluid heat transfer characteristic variation along the length of the U – tube after attaining the steady state condition.

For the given inlet condition (Table 4.8), Fig. 4.14 shows the variation of working fluid temperature and instantaneous heat gain along the length of the U – tube after attaining steady state condition. During the real time experimental study, the working fluid temperature variation and the instantaneous heat gain along the length of the U – tube solar collector are difficult to measure. Therefore, a numerical analysis is carried out for predicting the instantaneous heat gain along the length of the U – tube. It is observed from Fig. 4.14 that there is a significant increase in working fluid temperature and heat gain up to certain collector length (0 m to approximately 1.8 m). After that there is only a marginal increase in working fluid temperature and instantaneous heat gain along the U – tube collector length (approximately 1.8 m to 0 m). This happens because from 0 m to 1.8 m collector length, the difference in temperature and heat transferred from the U – tube inner surface to the working fluid is high. As the heat absorbed by the working fluid increases, the temperature difference and convective heat transfer between the U – tube inner surface and the working fluid decrease. Therefore, there is only a marginal increase in heat gained by the working fluid.

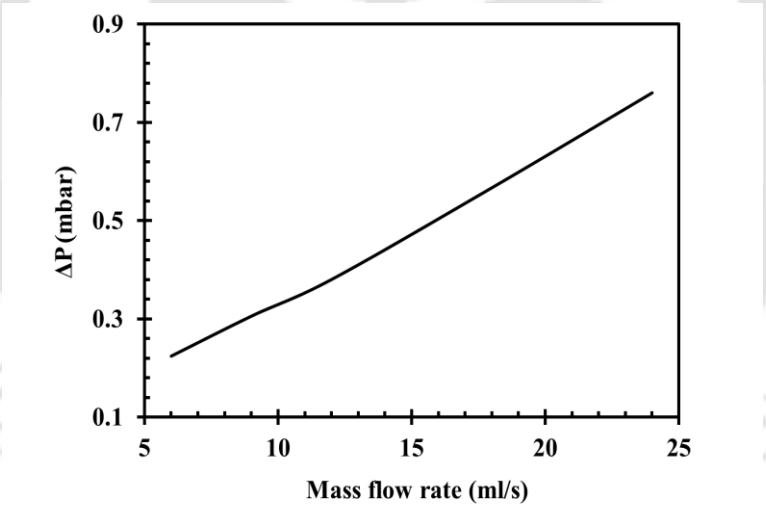

Fig. 4.15, Influence of mass flow rate on the pressure drop in the U – tube.

Since, the flow rate is increased from 6 ml/s to 24 ml/s (Table 4.5c) which is considered to be forced convection flow through the U – tube, it is important to predict the influence of mass flow rate on pressure drop by keeping rest of the operating parameters as constant (Fig. 4.15). It is observed from Fig. 4.15 that with increase in flow rate, pressure drop increases. This happens because as the flow rate increases, dynamic pressure loss due to change in flow direction along the 'U' bend and frictional loss due to increase in fluid velocity increase. As a consequence, the pressure drop along the U – tube increases. It is also observed that for a given range of flow rate variation, the pressure drop variation is negligible because with increase in

flow rate from 6 ml/s to 24 ml/s, the pressure drop hardly increases from 0.26 mbar to 0.74 mbar.

d) Variation of working fluid transition time with operating parameters

Fig. 4.16a-c compares the transition time obtained from developed numerical model with the developed empirical correlation at different solar intensities, working fluid inlet temperatures and flow rates. It is observed from Fig. 4.16 that for a given range of operating parameters (Table 4.5c), the values predicted from the developed empirical correlation match well with the numerical model and also follows the similar trend. From Fig. 4.16a, it is found that with increase in solar intensity, the working fluid transition time increases. This happens because as the solar intensity increases, the convective heat transfer rate between the U – tube surface and the incoming working fluid increases. Therefore, the time taken for the working fluid to attain a steady state condition increases and hence, the working fluid transition time increases. From Fig. 4.16a, it is also found that with increase in solar intensity from 0.85 kW/m^2 to 1.05 kW/m^2, the percentage of increment in working fluid transition time is about 82%.

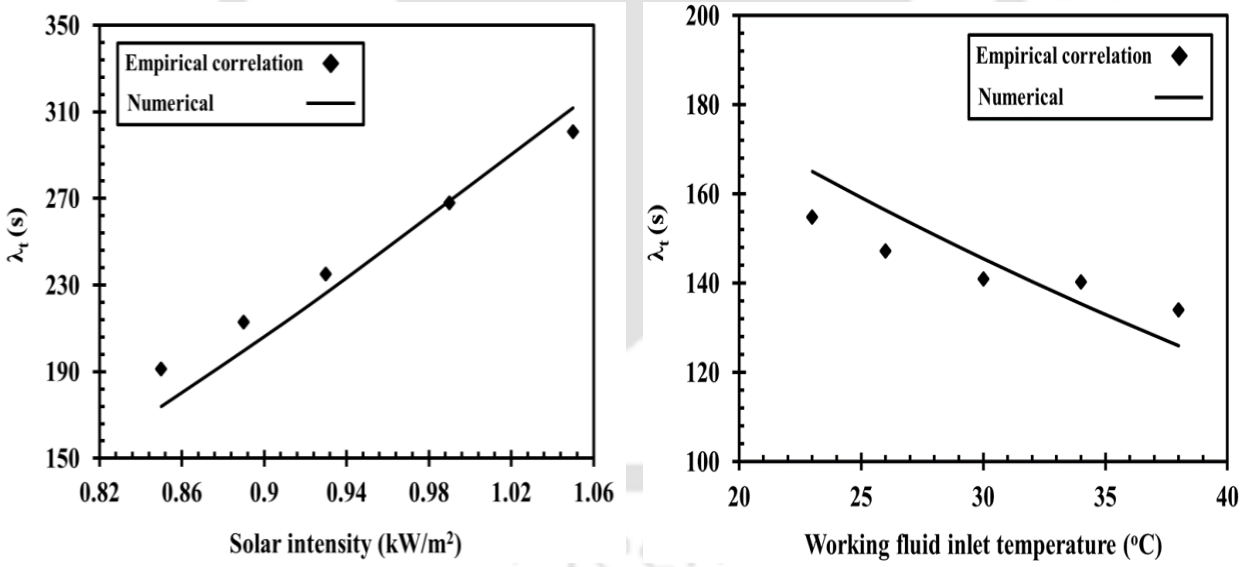

(a) Variation of working fluid transition time with solar intensity.

(b) Variation of working fluid transition time with working fluid inlet temperature.

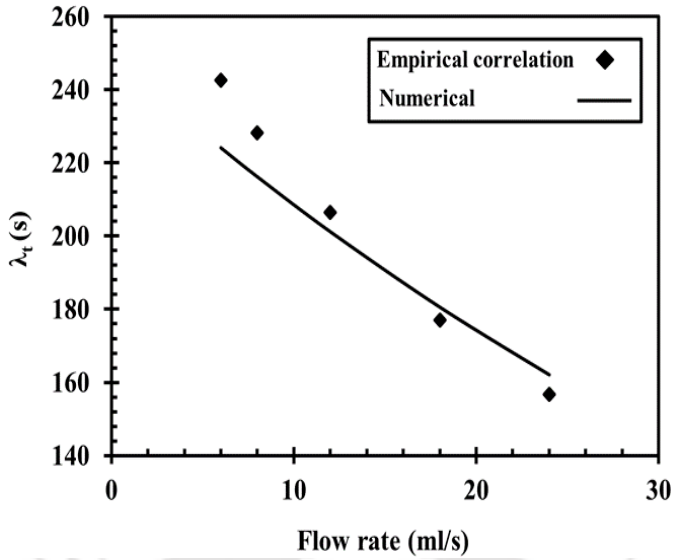

(c) Variation of working fluid transition time with flow rate.

Fig. 4.16, Validation of numerical model with the developed empirical correlation for working fluid transition time and influences of operating parameters on the variation of working fluid transition time.

In Fig. 4.16b, it is noticed that the working fluid transition time decreases with increase in working fluid inlet temperature. This is due to decrease in temperature difference between the U – tube surface and the incoming working fluid. From Fig. 4.16b, it is also noticed that with increase in working fluid inlet temperature from 23 ^{o}C to 38 ^{o}C, the percentage decrement in working fluid transition time is about 31%. The working fluid transition time decreases with increase in fluid flow rate as observed in Fig. 4.16c. This indicates that at lower flow rate, the time taken for heat exchange from inner U – tube surface to the incoming working fluid is high whereas with increase in flow rate, the time taken for an incoming working fluid to absorb heat from the U – tube inner surface decreases. Thus, the working fluid transition time decreases with increase in flow rate. From Fig. 4.16c, it is also observed that with increase in flow rate from 6 ml/s to 24 ml/s, the percentage of decrement in working fluid transition time is 49%.

Form Fig. 4.16, it is concluded that the sudden change in solar intensity will have a more significant effect on working fluid transition time than the fluctuation in working fluid flow rate and inlet temperature.

4.3 Summary

4.3.1 Liquid desiccant dehumidification/regeneration system

An experimental setup of the liquid desiccant dehumidification/regeneration system has been designed, fabricated and performance-tested using LiCl as a liquid desiccant. The influence of relative humidity on overall energy exchange, air and desiccant enthalpy differences, air specific humidity difference and desiccant concentration difference has been analysed for the liquid desiccant dehumidification/regeneration system. For a given range of operating and ambient parameters, an experimental correlation for specific humidity difference has been developed in terms of known inlet parameters for the liquid desiccant dehumidification and regeneration systems. The developed correlation is compared with the experimental data and good agreement between them is observed with a maximum error of $\pm 8\%$. Further, based on experimental data and developed correlations, the influence of L/G ratio on condensation and evaporation rates of the liquid desiccant dehumidification and regeneration systems, respectively, has been studied.

4.3.2 Evacuated U – tube solar collector system

An experimental setup of an evacuated U – tube solar collector system has been designed, fabricated and performance-tested. A simplified numerical model has been proposed for predicting the performance of the evacuated U – tube solar collector system. Within the range of operating parameters, the numerically predicted performance parameters of the solar collector and solar collector system are in (good) agreement with the experimental data. The working fluid transition time for an evacuated U – tube solar collector is defined and the variation of transition time for various operating conditions is analysed experimentally. Instantaneous heat gain variation along the length of the evacuated U – tube is also investigated numerically. Based on experimental data, an empirical correlation for working fluid transition time as a function of ambient temperature, solar intensity, working fluid inlet temperature and working fluid flow rate is formulated.

CHAPTER – 5

ENERGY AND EXERGY ANALYSES

Energy and exergy analyses plays a vital role in improving the performance of the liquid desiccant ACS components such as dehumidifier, regenerator and evacuated U – tube solar collector. Many researchers have investigated the energy and exergy analyses of the liquid desiccant dehumidifier (Wang et al. 2010; Xiang et al. 2010; Zhang et al. 2012; Zhang et al. 2014; Zhang et al. 2017; L. Zhang et al. 2017). But very few have investigated the energy and exergy performance of the liquid desiccant regenerator and evacuated U – tube solar collector. From the literature, it is observed that there is a lack of profound exergy analysis which account for the irreversibility of heat and mass transfer processes in the liquid desiccant regenerator and irreversibility of heat transfer process in the evacuated U – tube solar collector. Therefore, this chapter focuses on deriving the expressions for quantifying the energy exchange and exergy destruction along the liquid desiccant regenerator and evacuated U – tube solar collector. The major objectives of the present study are,

- To develop energy and exergy analyses for the liquid desiccant regenerator.
- To develop empirical correlations for exergy and energy efficiencies of the solar collector.
- To quantify the energy and exergy efficiencies of the regenerator and the solar collector.
- To propose a simplified approach for exergy analysis of the liquid desiccant.
- To investigate exergy performance of the evacuated U – tube bundle connected in series.

5.1 Energy and exergy analysis of liquid desiccant regenerator

5.1.1 Energy analysis model

Schematic of energy exchange that occurs between the ambient air and the desiccant solution is shown in Fig. 5.1. Following assumptions are made for analysing the transfer processes.

- Flow is steady.
- Regeneration process is adiabatic.
- Thermo – physical properties of the fluids are constant irrespective of temperature.

The overall energy exchange from desiccant solution to the ambient air can be written as

$$dQ_e = \dot{m}_s h_s - \dot{m}_s (h_s - dh_s) = \dot{m}_a h_a - \dot{m}_a (h_a + dh_a) \tag{5.1}$$

$$\text{or : } dQ_e = -\dot{m}_s dh_s = \dot{m}_a dh_a \tag{5.1a}$$

a) Air side

The enthalpy on the air side is given by

$$h_a(T_a, \omega_a) = C_{p,m} T_a + \varphi \omega_a \tag{5.2}$$

where φ is latent heat of vaporization (kJ/kg).

By differentiating Eq. 5.2, the change in air enthalpy is obtained as

$$dh_a = C_{p,m} dT_a + \varphi d\omega_a \tag{5.3}$$

b) Liquid desiccant side

The enthalpy on the solution side is given by

$$h_s(T_s, \omega_s) = C_{p,s} T_s + \varphi \omega_s \tag{5.4}$$

where ω_s is the specific humidity of saturated air which is in thermal equilibrium with the desiccant solution at the local desiccant temperature and concentration i.e. $\omega_s (T_s, \beta)$.

'ω_s' is calculated using following equation

$$\omega_s(T_s, \beta) = 0.622 \frac{P_s^{sat}(T_s, \beta)}{P_{atm} - P_s^{sat}(T_s, \beta)} \tag{5.4a}$$

where 'P_s^{sat}' denotes the statured vapour pressure at air – desiccant interface and it is the function of solution temperature and concentration. The specific heat, vapour pressure and other thermo-physical properties of the liquid desiccant (LiCl–H_2O) are obtained from the literature (M. R. Conde, 2004; Fumo and Goswami, 2002).

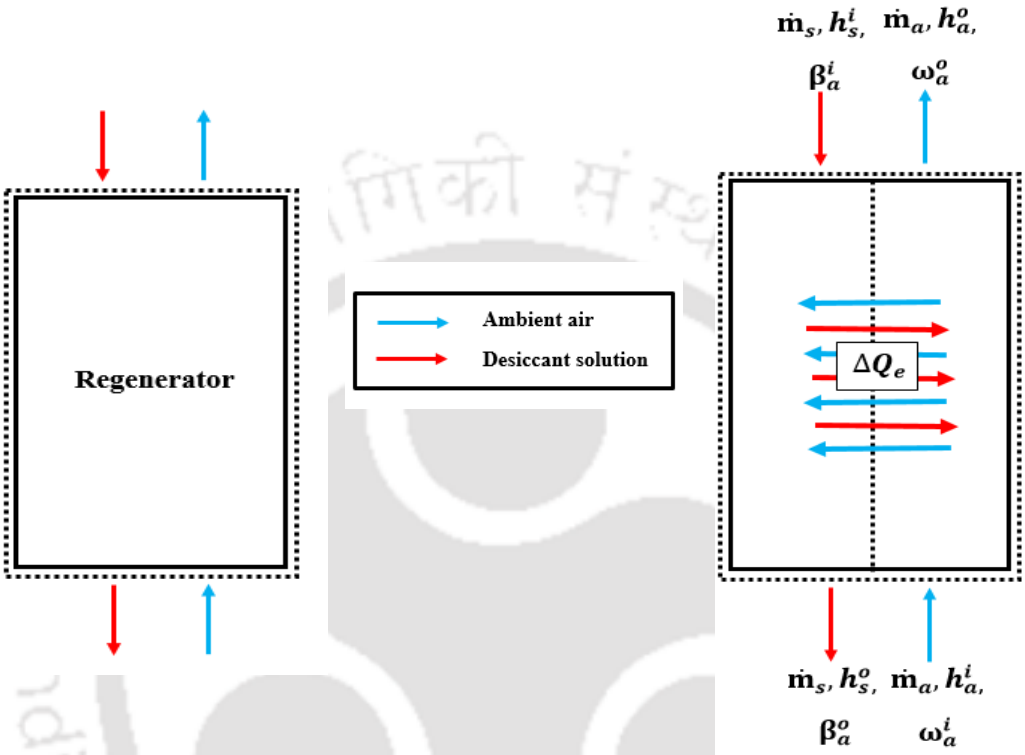

(a) Schematic (b) Energy balance

Fig. 5.1, Energy balance along the liquid desiccant regenerator

Differentiating Eq. 5.4;

$$dh_s = C_{p,s}dT_s + \varphi d\omega_s \tag{5.5}$$

Substituting Eq. 5.3 and Eq. 5.5 in Eq. 1a, the final equation is obtained as

$$dQ_e = \dot{m}_a\left(C_{p,m}dT_a + \varphi d\omega_a\right) = -\dot{m}_s\left(C_{p,s}dT_s + \varphi d\omega_s\right) \tag{5.6}$$

Eq. 6 can be integrated as

$$\int_{Q_e^i}^{Q_e^o} dQ_e = \int_{T_{a,i}}^{T_{a,o}} \dot{m}_a C_{p,m}dT_a + \int_{\omega_{a,i}}^{\omega_{a,o}} \dot{m}_a\varphi d\omega_a = -\int_{T_{s,i}}^{T_{s,o}} \dot{m}_s C_{p,s}dT_s - \int_{\omega_{s,i}}^{\omega_{s,o}} \dot{m}_s\varphi d\omega_s \tag{5.7}$$

After integrating Eq. 5.7, the energy exchange between the air and the desiccant solution along the regenerator is formulated as (Fig. 5.1b)

$$\Delta Q_e = \dot{m}_a C_{p,m}(T_a^o - T_a^i) + \dot{m}_a \varphi(\omega_a^o - \omega_a^i) = \dot{m}_s C_{p,s}(T_s^i - T_s^o) + \dot{m}_s \varphi(\omega_s^i - \omega_s^o) \quad (5.8)$$

where $\Delta Q_e = Q_e^o - Q_e^i$

c) Desorption efficiency

Desorption/energy efficiency of the liquid desiccant regenerator is defined as the ratio of energy exchanged between the desiccant solution and the air to the energy input and is given by

$$\eta_e = \frac{\Delta Q_e}{Q_e^i} \quad (5.9)$$

where $Q_e^i = Q_{es,a}^i + Q_{el,a}^i = \dot{m}_a C_{p,m} T_a^i + \dot{m}_a \varphi \omega_a^i$

5.1.2 Exergy analysis model

The exergy analysis plays a vital role in the design and development of efficient system as well as improving the performance of the existing system (Dincer and Rosen, 2007). Therefore, in the present study, the exergy destruction encountered in the liquid desiccant regenerator is analyzed for improving the system performance. In this system, there are two fluids i.e., desiccant solution and ambient air interacting with each other for regeneration of liquid desiccant. During this regeneration process, irreversible latent and sensible heats are released from the liquid desiccant to the ambient air due to water vapour transfer and temperature difference (Fig. 5.2a). Thus, the irreversible latent and sensible heats with respect to the reference state is quantified as exergy destruction. For analyzing the exergy destruction, reference state is chosen based on thermal (temperature) and chemical (specific humidity or desiccant concentration) equilibriums of the flow streams pertained to the reference environment.

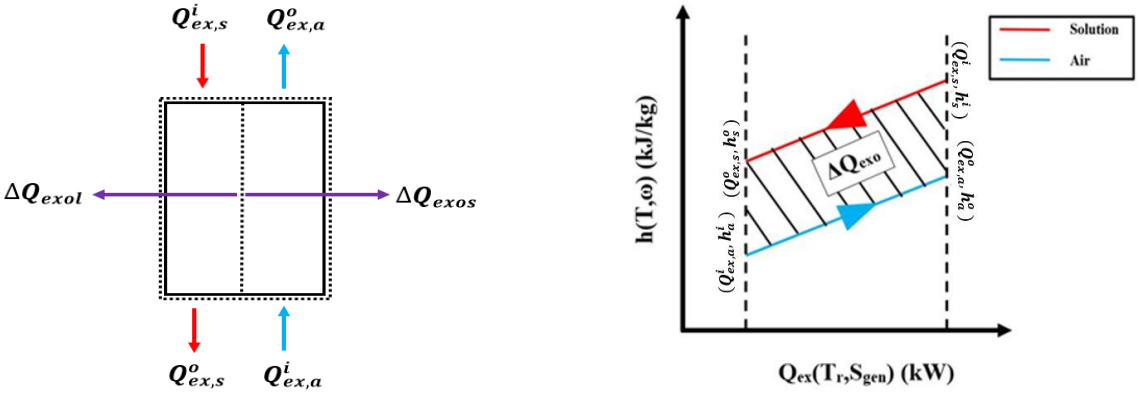

(a) Exergy destruction process (See Eq. 5.19)

(b) Q_{ex} – h chart

Fig. 5.2, Exergy destruction along the liquid desiccant regenerator.

Fig. 5.2b shows the variations of air and solution exergy flows for a given air and solution enthalpies along the counter – flow liquid desiccant regenerator. Q_{ex} – h chart indicates the variation of air and desiccant solution exergy destructions with respect to reference environment and signifies the inflow and outflow of the liquid desiccant and air. Using, Q_{ex} – h chart, the overall exergy destruction in the liquid desiccant regenerator can be obtained.

For analyzing the system (liquid desiccant regenerator) deviation from equilibrium with its reference environment, exergy destroyed is measured. It is formulated as (Dincer and Rosen, 2007)

$$Q_{ex}(T_r, S_{gen}) = T_r S_{gen} \tag{5.10}$$

In a liquid desiccant regenerator, exergy of coupled heat and mass transfer processes between air and desiccant solution is the sum of sensible and latent exergy (i.e. exergy destroyed due to heat transfer represent the physical/sensible exergy and exergy destroyed due to mass transfer represent the humid/latent exergy). Thus, Eq. 5.10 can be re-written as

$$Q_{ex} = T_r \int \frac{dQ_{es}}{T} + T_r \int \frac{dQ_{el}}{T} \tag{5.11}$$

where $S_{gen} = S_{gens} + S_{genl} = \int \frac{dQ_{es}}{T} + \int \frac{dQ_{el}}{T}$ for coupled heat and mass transfer process of the liquid desiccant regenerator.

As $dQ_{es} = \dot{m} d\phi_s = \dot{m} C_p dT$ and $dQ_{el} = \dot{m} d\phi_l = \dot{m} \varphi d\omega$, the exergy destroyed due to sensible exergy and humid exergy can be formulated as

$$Q_{ex} = T_r \dot{m} \left(C_p \int \frac{dT}{T} + \varphi \int \frac{d\omega}{T} \right) \tag{5.12}$$

a) Exergy analysis of moist air

The exergy inflow along the air side can be written as

$$Q_{ex,a}^{i} = T_r \dot{m}_a \left(C_{p,m} \int_{T_r}^{T_a^i} \frac{dT}{T} + \varphi \int_{\omega_r}^{\omega_a^i} \frac{d\omega}{T} \right) \tag{5.13}$$

After integrating Eq. 5.13, the exergy inflow along the air side is obtained as

$$Q_{ex,a}^{i} = T_r \dot{m}_a \left(C_{p,m} \ln \left(\frac{T_a^i}{T_r} \right) + \varphi \left(\frac{\omega_a^i - \omega_r}{T_a^*} \right) \right) \tag{5.14}$$

where T_a^* is the average of air temperature along the height of the regenerator

Similarly, the exergy outflow along the air side is derived as

$$Q_{ex,a}^{o} = T_r \dot{m}_a \left(C_{p,m} \ln \left(\frac{T_a^o}{T_r} \right) + \varphi \left(\frac{\omega_a^o - \omega_r}{T_a^*} \right) \right) \tag{5.15}$$

b) Exergy analysis of desiccant solution

The exergy inflow along the solution side can be written as

$$Q_{ex,s}^{i} = T_r \dot{m}_s \left(C_{p,s} \int_{T_r}^{T_s^i} \frac{dT}{T} + \varphi \int_{\omega_r}^{\omega_s^i} \frac{d\omega}{T} \right) \tag{5.16}$$

After integrating Eq. 5.16, the exergy inflow along the solution side is obtained as

$$Q_{ex,s}^{i} = T_r \dot{m}_s \left(C_{p,s} \ln\left(\frac{T_s^i}{T_r}\right) + \varphi\left(\frac{\omega_s^i - \omega_r}{T_s^*}\right)\right) \tag{5.17}$$

where T_s^* is the average of solution temperature along the height of the regenerator

Similarly, the exergy outflow along the solution side is derived as

$$Q_{ex,s}^{o} = T_r \dot{m}_s \left(C_{p,s} \ln\left(\frac{T_s^o}{T_r}\right) + \varphi\left(\frac{\omega_s^o - \omega_r}{T_s^*}\right)\right) \tag{5.18}$$

Overall exergy destruction in the liquid desiccant regenerator can be obtained by (see Fig. 5.2b)

$$\Delta Q_{exo} = Q_{ex}^{i} - Q_{ex}^{o} \tag{5.19}$$

or: $\Delta Q_{exo} = \left(Q_{ex,a}^{i} + Q_{ex,s}^{i}\right) - \left(Q_{ex,a}^{o} + Q_{ex,s}^{o}\right)$ (5.19a)

c) Exergy efficiency

Exergy efficiency is the ratio of overall exergy destruction to the inflow exergy. For the liquid desiccant regenerator, it is defined as

$$\eta_{ex} = 1 - \frac{\Delta Q_{exo}}{Q_{ex}^{i}} \tag{5.20}$$

where $Q_{ex}^{i} = Q_{ex,a}^{i} + Q_{ex,s}^{i}$

5.1.3 Validation of developed energy and exergy analyses model

Energy exchange occurred between air and the desiccant solution during desorption of water vapour from solution to air, i.e. amount of energy transferred to the air side, is equal to the latent and sensible heat transfers from solution to air. Therefore, a comparison is made between the energy generated at air side and the energy transferred from solution side for validating the developed energy and exergy analyses model. From Fig. 5.3, it is found that the energy variance at solution side (theoretical) holds reasonable agreement with the energy variance at air side

(experimental) for all the inlet conditions listed in Table 5.1a. The mean and maximum deviations between the experimental and theoretical energy variance of the adiabatic liquid desiccant regenerator are observed to be ±4.7 % and ±12.3 %, respectively. This deviation is mainly due to the assumptions made in the developed energy and exergy analyses model and experimental heat loss and uncertainty.

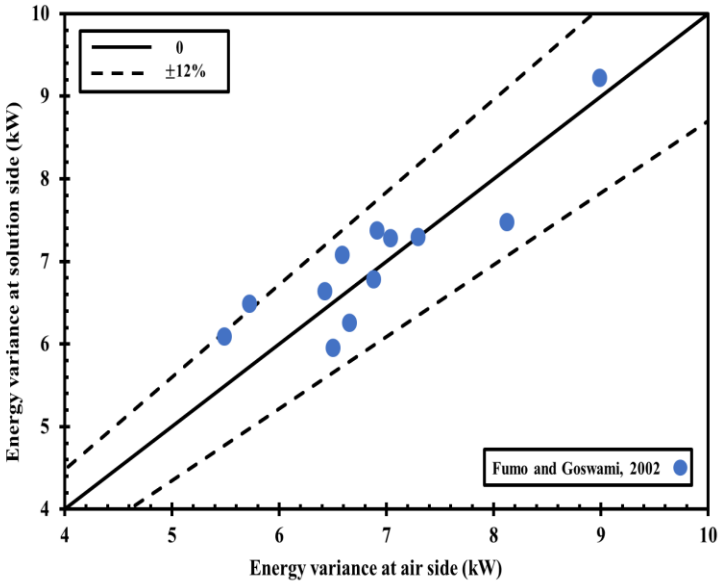

Fig. 5.3, Energy balance between air and desiccant solution for the experimental data reported in the literature (Fumo and Goswami, 2002).

Table 5.1a, Desorption and exergy efficiencies of the liquid desiccant regenerator (Fumo and Goswami, 2002).

Exp. no.	$\dot{m}_a$ (kg/s)	T_a^i (°C)	ω^i (g_{wv}/kg_{da})	$\dot{m}_s$ (kg/s)	T_s^i (°C)	β^i ($kg_{LiCl}/kg_{sol.}$)	$\Delta Q_{e,o}$ (kW)	$\Delta Q_{ex,o}$ (kW)	η_e (%)	η_{ex} (%)
1	0.039	30.4	18.3	0.30	65	34	5.72	10.84	53.4	76.2
2	0.052	30.1	18	0.29	65.1	34.1	6.91	11.61	37.6	75.6
3	0.068	29.8	17.7	0.30	65.1	34.5	8.13	13.81	33.8	71.8
4	0.052	35.1	18	0.30	65.1	33.4	6.88	11.59	36.9	72.6
5	0.052	40	17.8	0.30	65	33.6	6.66	10.99	35.1	72.8
6	0.053	30.2	14.3	0.30	65.2	34	7.30	12.55	39.6	71.9
7	0.052	29.4	21	0.30	65.5	33.6	6.59	12.25	35.1	74.9
8	0.052	30.3	18.2	0.24	65.4	34.4	6.50	11.13	34.7	71.6
9	0.052	29.9	18	0.35	65.2	34.3	7.29	14.62	39.5	73.1
10	0.052	30	18.7	0.29	60.3	34.4	5.39	7.88	28.8	79.1

11	0.051	29.7	18.4	0.30	70	34.5	8.99	21.61	49.4	64.7
12	0.052	29.7	17.7	0.30	64.8	32.8	7.04	11.97	38.4	72.0
13	0.052	30.3	18.2	0.30	65	34.9	6.43	12.94	34.3	72.6

5.1.4 Results and discussions

Energy and exergy analyses model developed in the above section is adopted for analyzing the energy exchange between the desiccant solution and the ambient air and exergy destruction encountered with respect to the reference environment. The experimental data reported by Fumo and Goswami (2002) is chosen for energy and exergy analyses of the liquid desiccant regenerator. In these analyses, the saturated air state of ambient temperature is selected as the reference state i.e., T_r = 25 °C and ω_r = 19.7 g_{wv}/kg_{da} (R.H. =100%). The latent heat of vaporization (φ) is assumed to be constant at 2346 kJ/kg for a given desiccant temperature and concentration encountered in the system (Gandhidasan, 2005).

Overall energy and exergy analyses results of the liquid desiccant regenerator are presented in Table 5.1a. It is observed that overall energy exchanged and exergy destroyed are in the range of 5 – 9 kW and 8 – 22 kW, respectively. Also, desorption/energy and exergy efficiencies of the liquid desiccant regenerator are in the range of 28 – 54 % and 64 – 80 %, respectively.

a) Energy and exergy analyses along the height of the liquid desiccant regenerator

For effective heat and mass transfer processes between the ambient air and the desiccant solution, the vapour pressure difference and temperature difference should be high. This can be achieved by increasing the desiccant temperature and decreasing the air specific humidity. Therefore, the desiccant temperature and air specific humidity are varied simultaneously by keeping the rest of the operating parameters as constant (air and desiccant flow rates, air temperature and desiccant concentration are kept constant) and analyzed the energy exchange and exergy destruction along the height of the counter – flow liquid desiccant regenerator.

Based on the aforementioned variation of operating parameters, experimental no. 10 and 6 from Table 5.1a are taken as inlet condition – I and inlet condition – II for energy and exergy analyses along the height of the liquid desiccant regenerator. During these analyses, the desiccant temperature is increased from 60.3 °C (experimental no. 10) to 65.2 °C (experimental no. 6) and the specific humidity is decreased from 18.7 g_{wv}/kg_{da} (experimental no. 10) to 14.3 g_{wv}/kg_{da} (experimental no. 6) simultaneously by keeping rest of operating parameters as constant. The height of the liquid desiccant regenerator is taken as 0.6 m (Fumo and Goswami 2002).

The energy exchange along the height of the counter – flow liquid desiccant regenerator is estimated by investigating the variation of air and desiccant temperatures, air humidity ratio and saturated humidity ratio (attained at local desiccant temperature and concentration). From Fig. 5.4, it is observed that with increase in tower height, the air temperature and the humidity ratio increase whereas the solution temperature and the saturated humidity ratio decrease in both the conditions (Inlet condition – I and II). This is due to simultaneous heat and mass exchange between the air and the desiccant solution along the tower height. It is also observed from Fig. 5.4 that with increase in height, the solution and air temperature difference and the difference between the air humidity ratio and saturated humidity ratio decrease. This happens because of reduction in evaporation process from desiccant solution to the ambient air with increase in tower height. By comparing inlet condition – I and II (Fig. 5.4a, 5.4b 5.4c, and 5.4d), it is found that the evaporation process in case of inlet condition – II is high compared to inlet condition – I. From Fig. 5.4, it is noticed that, with further increase in tower height, energy exchange along the liquid desiccant regenerator will be higher in case of condition – II compared to condition – I.

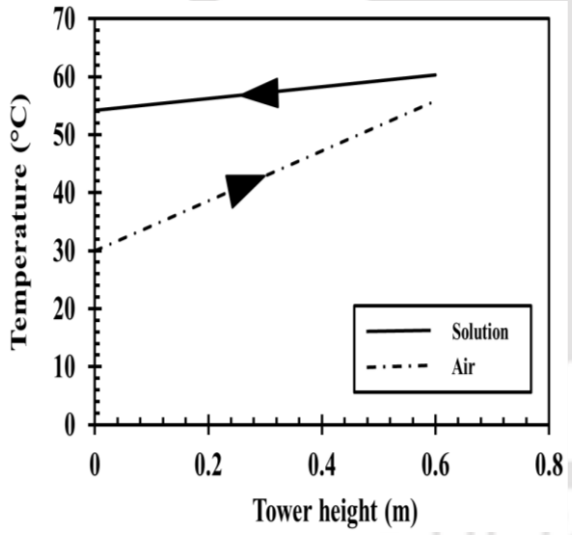

(a) Inlet condition – I

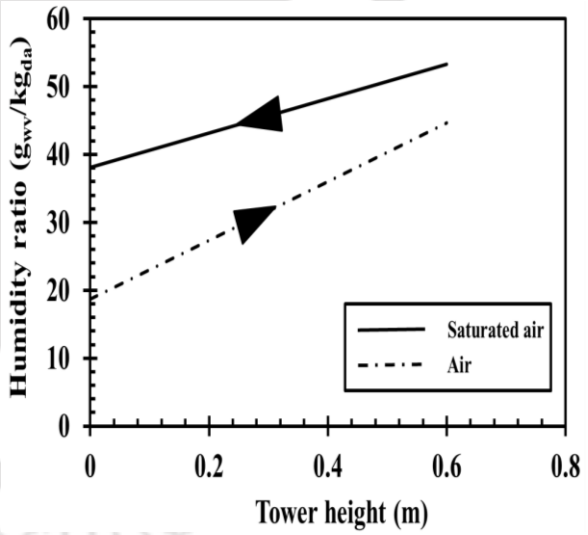

(b) Inlet condition – I

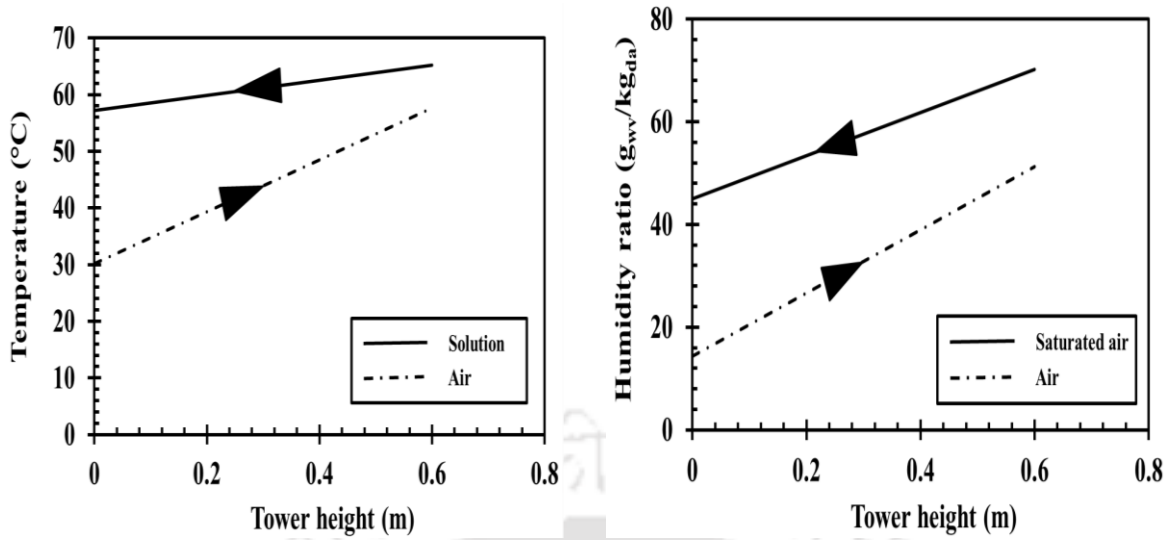

(c) Inlet condition – II (d) Inlet condition – II

Fig. 5.4, Variation of air and solution temperatures and specific humidity of the air along the tower height.

It is observed from Fig. 5.4a and 5.4c that with increase in distance along the height of the packed tower, the variation in air and solution temperature is about 25.8 °C and 6.1 °C for inlet condition – I whereas for inlet condition – II this difference is observed to be 27.4 °C and 8 °C, respectively. It is found from Fig. 5.4b and 5.4d that for inlet condition – I and II, with increase in tower distance along the height of the packed tower, the percentage increment in air specific humidity is about 58 % and 72 % whereas for saturated humidity ratio, the percentage decrement is found to be 29% and 36%, respectively.

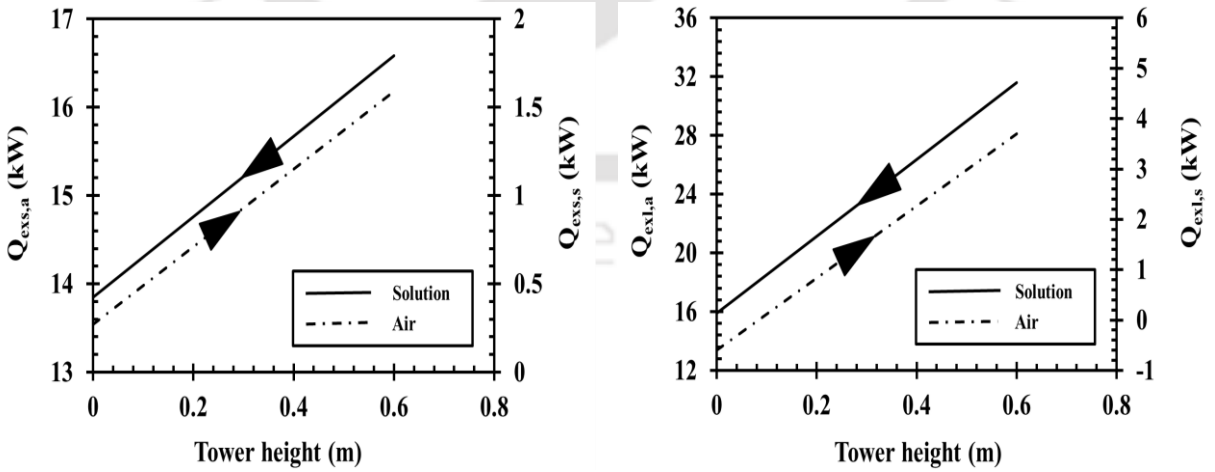

(a) Inlet condition – I (b) Inlet condition – I

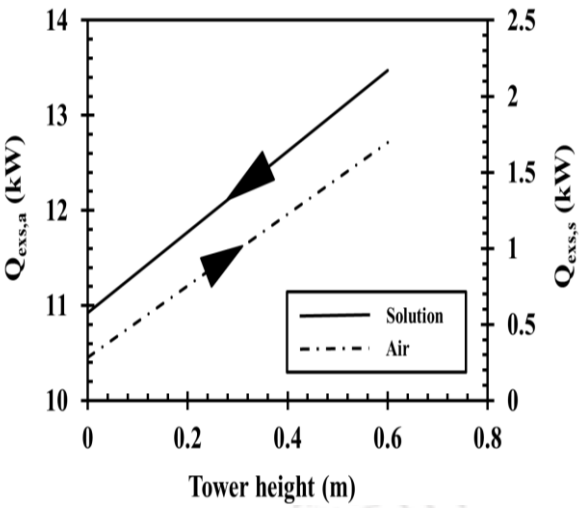

(c) Inlet condition – II

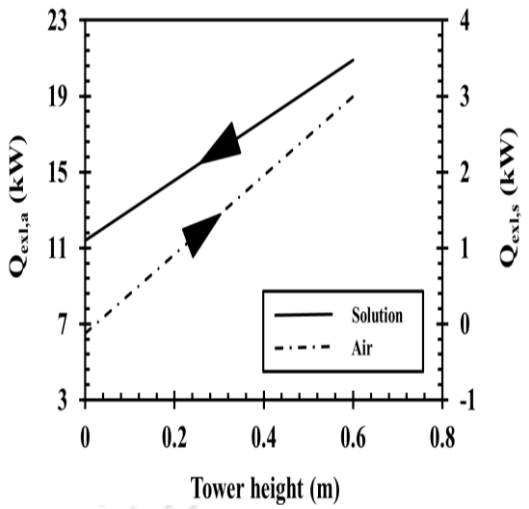

(d) Inlet condition – II

Fig. 5.5, Exergy losses along the tower height: (a) and (c) exergy losses due to sensible heat transfer for inlet condition – I and II and (b) and (d) exergy losses due to latent heat transfer for inlet condition – I and II, respectively.

Exergy destruction due to sensible and latent heat transfer processes along the tower height for the ambient air and the desiccant solution of both the inlet conditions are shown in Fig. 5.5. It is observed from Fig. 5.5 that with increase in tower height, the exergy losses associated with sensible and latent heat transfer processes for air side increases whereas for solution side, it decreases. This happens because with increase in tower height, the air vapour pressure and temperature increase and the desiccant vapour pressure and temperature decrease which in turn increases the exergy destruction along the air side and decreases the exergy destruction along the solution side with respect to the reference state. It is observed from Fig. 5.5a and 5.5c that, for inlet condition – I and inlet condition – II, with increase in tower distance along the height of the packed tower, the percentage of increment in exergy destruction associated with sensible heat transfer for air side is observed to be 16% and 19% whereas the percentage of decrement in exergy destruction along the solution side is observed to be 71% and 69%, respectively. With increase in distance along the height of the packed tower, the exergy destruction due to latent heat is observed to increase by 57 % and 63 % along the air side and it is observed to decrease by 116% and 104% along the solution side for inlet conditions – I and II, respectively (Fig. 5.5b and 5.5d). From these analyses, it is found that the exergy destruction due to latent and sensible heat transfer is higher along the solution side compared to air side for both the conditions.

Table 5.1b, Performance comparison between inlet condition – I (Exp. no. – 10 in Table 5.1a) and inlet condition – II (Exp. no. – 6 in Table 5.1a)

	Inlet condition – I	Inlet condition – II	%increment	%decrement
ΔQ_e (kW)	5.39	7.30	26	–
$\Delta Q_{ex,o}$ (kW)	7.88	12.55	37	–
η_e (%)	28.8	39.6	27	–
η_{ex} (%)	79.1	71.9	–	10

From Table 5.1b and Figs. 5.4 – 5.5, it is concluded that by increasing the desiccant temperature and decreasing the specific humidity of the regenerator, the energy exchange between the air and the desiccant solution and exergy losses with respect to the reference state increase.

b) Influence of operating parameters on energy and exergy efficiencies of the regenerator

On the basis of results presented in Table 5.1(a), the influence of operating parameters on desorption and exergy efficiencies of the regenerator are studied in detail (Fig. 5.6 & Table 5.2). It is found from Fig. 5.6a and Table 5.2 that with decrease in air flow rate, desorption efficiency increases. This is because of increase in contact time between the moist air and the desiccant solution with decrease in air flow rate. From Fig. 5.6b, 5.6c, 5.6e and 5.6f and Table 5.2, it is observed that the desorption efficiency of the regenerator increases with increase in desiccant temperature and decreases with increase in air temperature, specific humidity and desiccant concentration. This can be explained by the fact that, with increase in desiccant temperature and decrease in air temperature, air specific humidity and desiccant concentration, the partial pressure between the air and the desiccant solution increases and hence, there is a high potential for energy exchange (heat and mass exchange) between the air and the desiccant solution. With increase in desiccant flow rate, energy efficiency increases (Fig. 5.6d). This happens due to less reduction in desiccant temperature with increase in desiccant flow rate. Therefore, desiccant solution has a higher tendency to transfer water vapor to the moist air with increase in desiccant flow rate.

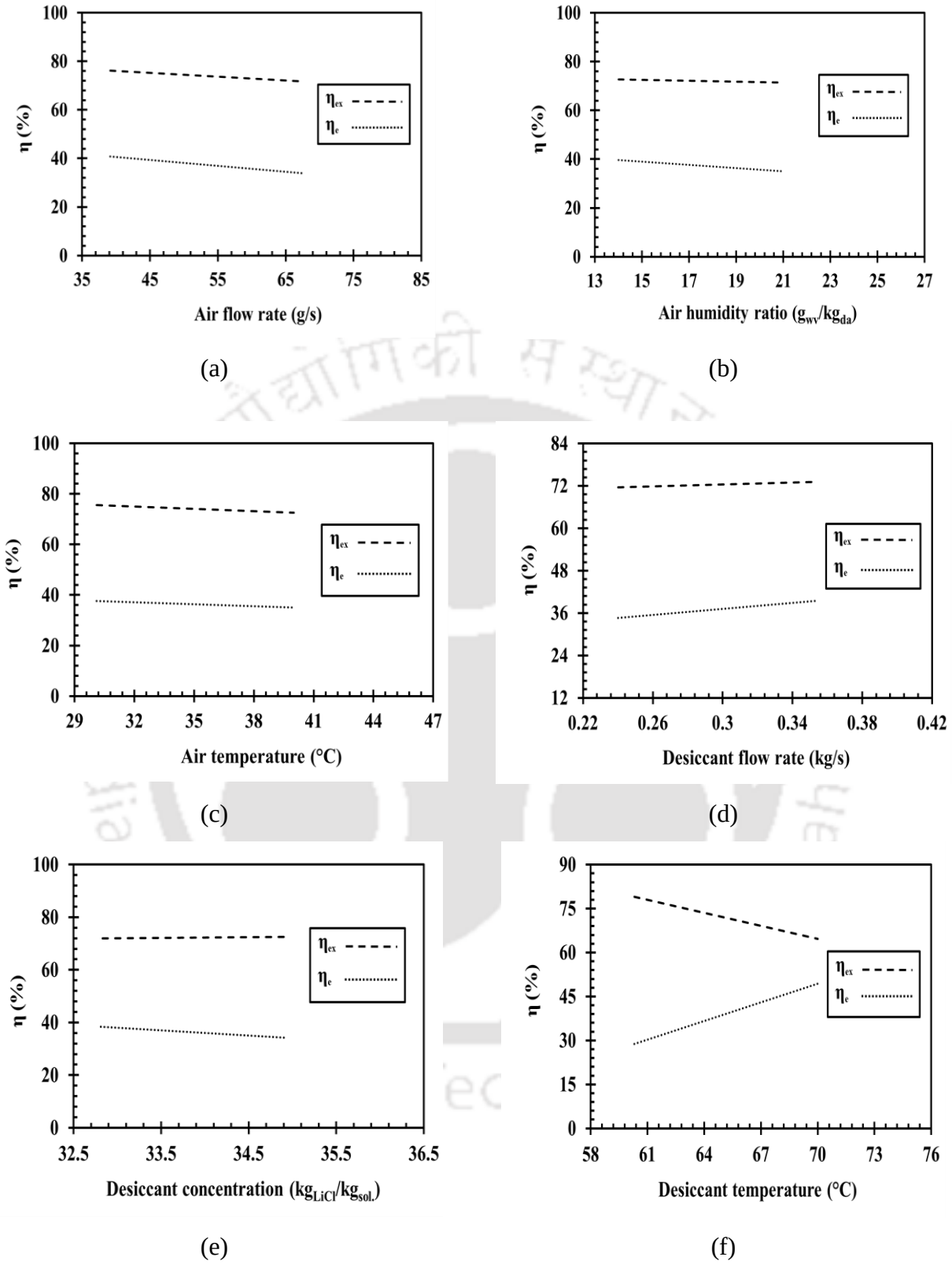

Fig. 5.6, Influence of air and desiccant parameters on energy and exergy efficiencies of the liquid desiccant regenerator: (a) Air flow rate, (b) air humidity ratio, (c) Air temperature, (d) desiccant flow rate, (e) desiccant concentration and (f) desiccant temperature.

Exergy efficiency of the liquid desiccant regenerator decreases with increase in air flow rate and decrease in desiccant flow rate, (Fig. 5.6a, 5.6d and Table 5.2). This is due to the exergy losses incurred during the evaporation of water vapour from desiccant solution to the ambient air. With decrease in air temperature, humidity ratio and desiccant temperature, the exergy efficiency increases (Fig. 5.6b, 5.6c and 5.6f and Table 5.2). This happens because with decrease in air temperature, humidity ratio and desiccant temperature, energy exchange associated with the irreversible heat and mass transfer processes decreases. Therefore, exergy losses within the regenerator decreases and exergy efficiency increases. From Fig. 5.6e and Table 5.2, it is observed that there is no phenomenal change in regenerator exergy efficiency by varying the desiccant concentration.

From Fig. 5.6, it has been concluded that except desiccant concentration, rest of the operating parameters such as desiccant and air temperatures, desiccant and air flow rates and air humidity ratio play a prominent role in improving the liquid desiccant regeneration system performance of the liquid desiccant regenerator.

Table 5.2, Influence of operating parameters on energy and exergy efficiencies of the regenerator (Fig. 5.6).

	Range	η_e		η_{ex}	
		% increment/ decrement		% increment/ decrement	
Air flow rate (kg/s) (↑)	39.2 – 67.6	↓	17	↓	6
Desiccant flow rate (kg/s) (↑)	0.24 – 0.35	↑	14	↑	2
Air humidity ratio (g_{wv}/kg_{da}) (↑)	14 – 21	↓	13	↓	2
Desiccant concentration ($kg_{LiCl}/kg_{sol.}$) (↑)	32.8 – 34.9	↓	7	↔	–
Air temperature (°C) (↑)	30.1 – 40	↓	12	↓	4
Desiccant temperature (°C) (↑)	60.3 – 70	↑	72	↓	18

*(↑) – Increment; (↓) – Decrement; (↔) – Intermediate (no change);

5.2 Energy and exergy analysis of evacuated U – tube solar collector

5.2.1 Energy efficiency analysis of an evacuated U – tube solar collector

a) Energy efficiency

The performance of an evacuated U – tube solar collector is analysed by means of energy efficiency (η_u). It is defined as the ratio of useful energy gained by the working fluid (Q_u) to the effective solar radiation incident onto the collector aperture area (A_c) and is formulated as

$$\eta_u = \frac{Q_u}{\zeta A_c} = \frac{\dot{m}_{wf} c_{p,wf} (T_{wf,o} - T_{wf,i})}{2\pi\zeta D_c L_c} \tag{5.21}$$

where 'ζ' is the effective heat absorbed from the evacuated tube (kW/m^2) ($\zeta = \tau_{g,o}\tau_{g,i}\alpha_c I$), D_c is the absorber tube diameter (m) and L_c is the length of the absorber tube (m).

b) Energy efficiency empirical correlation

In order to develop a correlation for energy efficiency, the operating parameters, such as working fluid inlet temperature, solar intensity, working fluid flow rate and ambient temperature are identified as the influencing parameters. Based on experimental data, a correlation is developed for theoretically analysing the energy efficiency of the evacuated U – tube solar collector within a given range of operating parameters and specifications (Table 4.5). The correlation for the energy efficiency of the evacuated U – tube solar collector is expressed as

$$\eta_u = f\left(T_{amb}, I, T_{wf,i}, \dot{m}_{wf}\right) \tag{5.22}$$

The general expression for aforementioned equation is as follows

$$\eta_u = \phi_1 T_{amb} + \phi_2 I + \phi_3 T_{wf,i} + \phi_4 \dot{m}_{wf} + \phi_5 \tag{5.23}$$

where $\phi_1 - \phi_4$ and ϕ_5 are coefficients and constants of individual model terms, respectively.

The statistical information about the developed correlation is presented in Table 5.3. The constant and coefficients 'ϕ_1' – 'ϕ_5' listed in Table 5.3 are obtained using linear regression technique. The R^2 and the adjusted R^2 values are 98 % and 95 %, respectively. From these values, it is well understood that the developed correlation provides the best fit within the range of operating parameters (Table 4.5c).

Table 5.3, Coefficients of the energy efficiency correlation.

Correlation					
η_u (%)	$\phi_1 T_{amb} + \phi_2 I + \phi_3 T_{wf,i} + \phi_4 \dot{m}_{wf} + \phi_5$				
Coefficients	ϕ_1	ϕ_2	ϕ_3	ϕ_4	ϕ_5
	0.65	-26.1	-0.18	5.73	14.8
Statistical information					
Regression Statistics					
R^2	0.98				
Adjusted R^2	0.95				
F – value	116.48				
F significance	2.4×10^{-15}				
P – value	ϕ_1	ϕ_2	ϕ_3	ϕ_4	ϕ_5
	5.2×10^{-4}	3.95×10^{-11}	5.2×10^{-4}	2.48×10^{-15}	0.028

Fig. 5.7a and 5.7b presents the comparison of predicted energy efficiency from the developed empirical correlation with the experimental data obtained from the evacuated U – tube solar collector. It is found that the energy efficiency obtained from the developed correlation and from the experimental data matches well with a maximum error of $\pm$6.9 %. Also, for a given range of operating conditions, the maximum and average energy efficiencies are observed to be 72 % and 51 %. The maximum energy efficiency of the evacuated U – tube solar collector is obtained at high solar intensity of 1.08 kW/m^2 and at lower working fluid inlet temperature and flow rate of 28.8 °C and 15 ml/s, respectively.

Fig. 5.7b presents the variation of energy efficiency as a function of normalized heat gain ((T_m – T_{amb})/I). From Fig. 5.7b, it is observed that as the normalized heat gain increases, the energy efficiency decreases. This is due to the fact that, with increase in working fluid temperature, the thermal losses across the evacuated U – tube solar collector increases and hence, the energy efficiency decreases. It is also observed from Fig. 5.7b that for a given range of operating parameters, with decrease in normalized heat gain from 15.3 (m^2 – K/kW) to 0.8 (m^2 – K/kW), the energy efficiency of the evacuated U – tube solar collector increases by 89%.

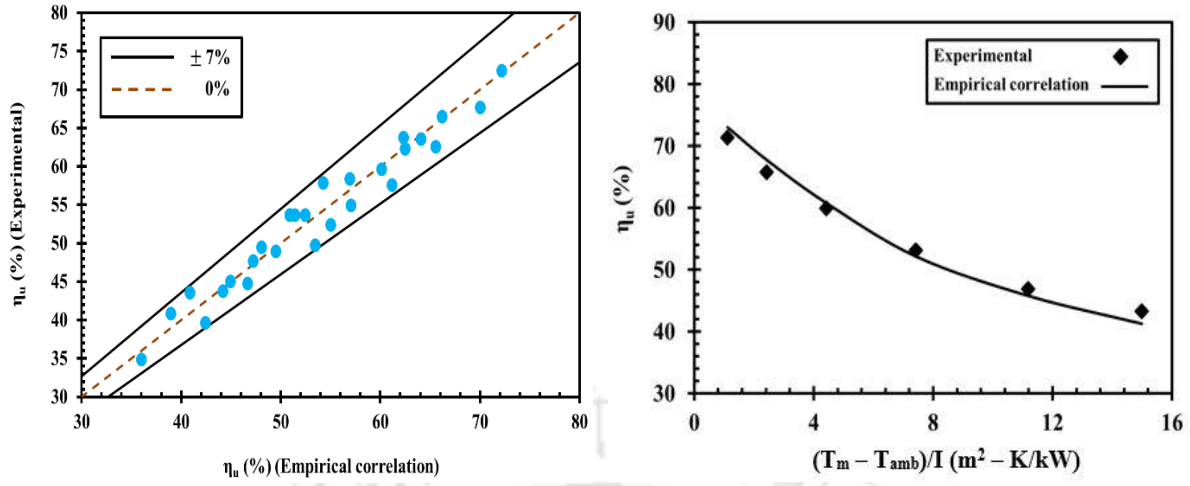

(a) Empirical correlation validation plot (b) Variation of energy efficiency with the normalized heat gain ($(T_m - T_{amb})/I$).

Fig. 5.7, Comparison of empirical correlation with the experimental data for energy efficiency of the evacuated U – tube solar collector.

5.2.2 Exergy efficiency analysis of an evacuated U – tube solar collector

a) Exergy efficiency

For minimizing the energy loss from evacuated tube heat pipe solar collector to the surroundings and to improve the performance of the solar collector, the exergy efficiency is chosen as a performance index. The exergy efficiency is defined as the ratio of useful exergy delivered (Lamnatau, 2012) to the exergy absorbed by the evacuated tube solar collector (Daghigh and Shafieian, 2016; Shah and Furbo, 2004).

$$\eta_{ex} = \frac{Ex_{ud}}{Ex_{ab}} = \frac{\dot{m}_{wf} c_{p,wf} \left[(T_{wf,o} - T_{wf,i}) - T_r \left(\ln \frac{T_{wf,o}}{T_{wf,i}} \right) \right]}{A_c I \left[1 + \frac{1}{3} \left(\frac{T_r}{T_{sr}} \right)^4 - \frac{4}{3} \left(\frac{T_r}{T_{sr}} \right) \right]} \tag{5.24}$$

where T_r is the reference temperature (K) (T_r = 298 K), I is the solar intensity (kW/m^2) and T_{sr} is the solar radiation temperature (T_{sr} = 6000 K) (Daghigh and Shafieian, 2016).

The overall solar intensity incident on the evacuated tube is not fully absorbed by the U – tube due to variation in transmissivity (τ_g) of the inner and outer glass surface and absorptivity (α_c) of the inner glass coating surface. Therefore, the exergy efficiency of the evacuated U – tube solar collector is modified as

$$\eta_{ex} = \frac{\dot{m}_{wf} c_{p,wf} \left[(T_{wf,o} - T_{wf,i}) - T_r \left(\ln \frac{T_{wf,o}}{T_{wf,i}} \right) \right]}{A_c \zeta \left[1 + \frac{1}{3} \left(\frac{T_r}{T_{sr}} \right)^4 - \frac{4}{3} \left(\frac{T_r}{T_{sr}} \right) \right]} \tag{5.25}$$

where 'ζ' is the effective heat absorbed from the evacuated tube and is written as $\zeta = \tau_{g,o}\tau_{g,i}\alpha_c I$.

b) Exergy efficiency empirical correlation

In order to predict the exergy efficiency of the evacuated U – tube solar collector in terms of known inlet parameters, an empirical correlation is developed based on data obtained from the experimental analysis. In this correlation, the ambient temperature, working fluid inlet temperature, solar intensity and working fluid flow rate are taken as inlet parameters. It should be noted that this correlation is valid for a given range of operating parameters and dimensions (Table 4.5), at the reference temperature and solar radiation temperature of 298 K and 6000 K, respectively. The correlation for the exergy efficiency of the evacuated U – tube solar collector can be expressed as

$$\eta_{ex} = f\left(T_{amb}, I, T_{wf,i}, \dot{m}_{wf}\right) \tag{5.26}$$

The empirical correlation is developed using linear regression analysis and the equation is formulated as follows

$$\eta_{ex} = \phi_1 T_{amb} + \phi_2 I + \phi_3 T_{wf,i} + \phi_4 \dot{m}_{wf} + \phi_5 \tag{5.27}$$

where $\phi_1 - \phi_4$ and ϕ_5 are coefficients and constants of individual model terms, respectively.

The statistical indices presented in Table 5.4 reveal that the developed correlation is suited for analysing the exergy efficiency of the evacuated U – tube solar collector. Also, from Fig. 5.8a and 5.8b, it is confirmed that the exergy efficiency obtained from the developed correlation holds good agreement with the experimental data with a maximum error of $\pm$7.8 %. It is seen from Fig. 5.8b that the exergy efficiency gradually increases as time progresses. At the end of

the day, the exergy efficiency reaches to a maximum value of 74 %. Due to high drop in ambient temperature from 3:00 pm, the exergy efficiency of the evacuated U – tube increases to such a high value. It is found that the maximum exergy destruction (irreversibility) is happening during the beginning of the day.

Table 5.4, Coefficients of the exergy efficiency correlation.

Correlation					
η_{ex} (%)	$\phi_1 T_{amb} + \phi_2 I + \phi_3 T_{wf,i} + \phi_4 \dot{m}_{wf} + \phi_5$				
Coefficients	ϕ_1	ϕ_2	ϕ_3	ϕ_4	ϕ_5
	0.68	-29.66	-0.56	1.38	57.82
Statistical information					
Regression Statistics					
R^2	0.95				
Adjusted R^2	0.93				
F – value	130.12				
F significance	6.7×10^{-16}				
P – value	ϕ_1	ϕ_2	ϕ_3	ϕ_4	ϕ_5
	6.7×10^{-5}	1.2×10^{-11}	2.8×10^{-6}	1.9×10^{-15}	2.92×10^{-9}

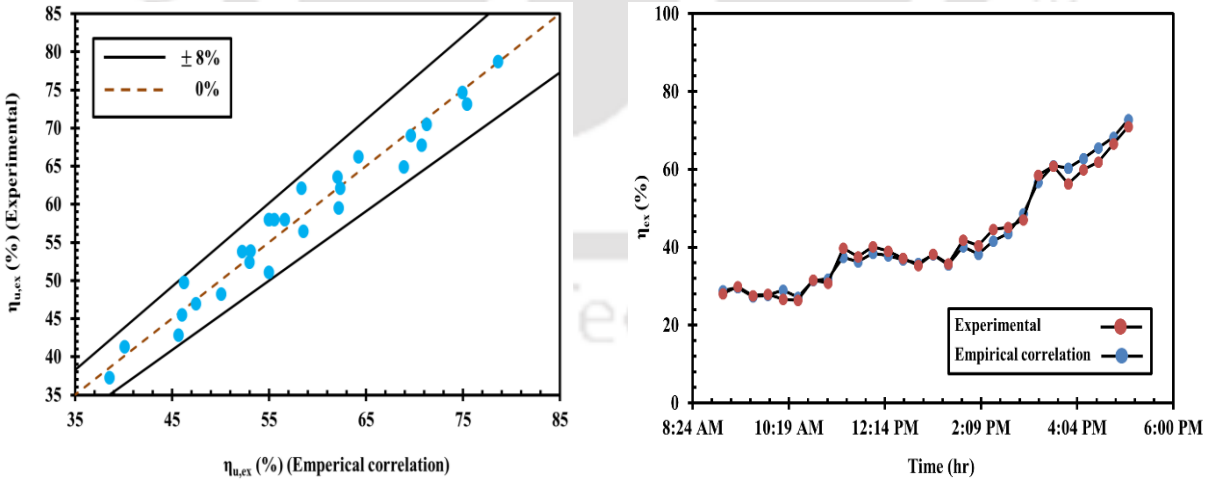

(a) Empirical correlation validation plot. (b) Exergy efficiency variation during a day.

Fig. 5.8, Comparison of empirical correlation with the experimental data for exergy efficiency of the evacuated U – tube solar collector.

5.3 Energy and exergy analysis of evacuated U – tube solar collector system

5.3.1 Efficiencies of the evacuated U – tube solar collector system

a) Energy efficiency of the system

The energy efficiency for the solar collector system (evacuated U – tube solar collector bundle connected in series) (Fig. 4.6) is reformulated based on Eq. 5.21 as

$$\eta_{u,sc} = \frac{Q_u}{N\zeta A_c} = \frac{\dot{m}_{wf} c_{p,wf} (T_{wM_3,o} - T_{wM_1,i})}{2\pi\zeta D_c L_c N} \tag{5.28}$$

where 'N' is number of manifolds (M_1, M_2 and M_3), $T_{wM1,i}$ is the working fluid inlet temperature at manifold – M_1 and $T_{wM3,o}$ is the working fluid outlet temperature at the outlet of the manifold – M_3.

b) Exergy efficiency of the system

The exergy efficiency for the evacuated U – tube solar collector system (Fig. 4.6a) is reformulated based on Eq. 5.25 as

$$\eta_{ex,sc} = \frac{\dot{m}_{wf} c_{p,wf} \left[(T_{wM_3,o} - T_{wM_1,i}) - T_r \left(\ln \frac{T_{wM_3,o}}{T_{wM_1,i}} \right) \right]}{NA_c\zeta \left[1 + \frac{1}{3}\left(\frac{T_r}{T_{sr}} \right)^4 - \frac{4}{3}\left(\frac{T_r}{T_{sr}} \right) \right]} \tag{5.29}$$

b) Variation of energy and exergy efficiencies of the system during a sunny day

For a humid subtropical climate, the variations in energy and exergy efficiencies of the evacuated U – tube solar collector system (three manifolds connected in series and each manifold is integrated with ten evacuated U – tubes in parallel) are analysed experimentally during a sunny day and their results are presented in Fig. 5.9a and 5.9b. From Fig. 5.9a, it is found that the energy efficiency varies from 31 % – 52 % with an average value of 43 %. In Fig. 5.9a, the peak energy efficiency is observed at 2: 00 PM. The fluctuation in energy efficiency is due to the variation in solar intensity. It is observed from Fig. 5.9b that the exergy efficiency varies from 27 % – 63 % with an average exergy efficiency of 41 % and increases with time during a day. With this phenomenon, it is understood that the useful heat gained by

the working fluid from surroundings increases with increase in duration of time during a sunny day. Exergy efficiency increases towards evening, but this is accompanied by a decrease of energy efficiency. This happens because at the end of the day, high drop in ambient temperature takes place, while the inlet and outlet temperatures of the collector will be still moderate. Therefore, lower thermal efficiency and higher exergy efficiency is observed during evening time.

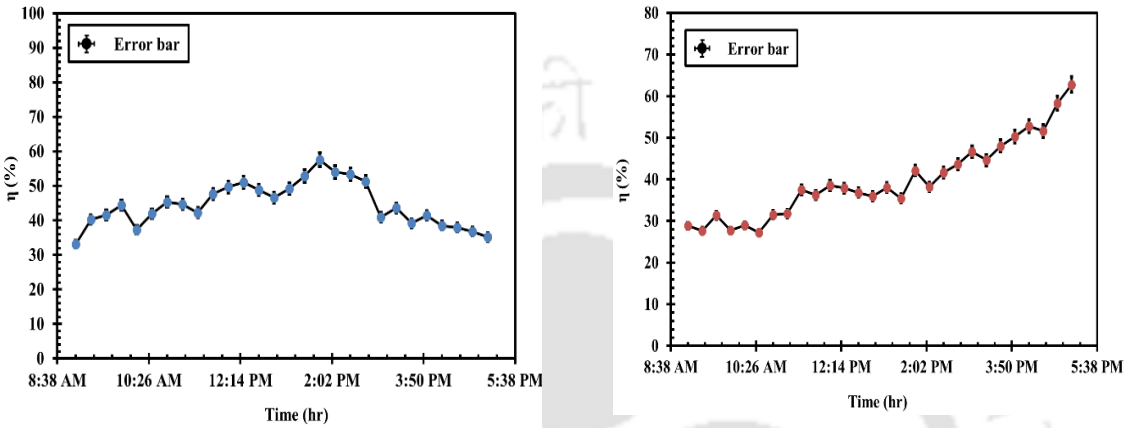

(a) Energy efficiency (b) Exergy efficiency

Fig. 5.9, Energy and exergy efficiencies variations of the evacuated U – tube solar collector system during a sunny day.

5. 4 Summary

5.4.1 Liquid desiccant regenerator

Energy and exergy analyses have been carried out for analysing the performance of the liquid desiccant regeneration system. With the simplified expressions formulated in the present work, energy required for regeneration of the liquid desiccant and exergy destroyed with respect to reference state are quantified. Energy exchange and exergy loss along the height of the liquid desiccant regenerator are quantified during coupled heat and mass transfer processes. The influence of air and desiccant temperatures, air and desiccant flow rates, air humidity ratio and desiccant concentration on desorption and exergy efficiencies of the liquid desiccant regenerator are also investigated.

5.4.2 Evacuated U – tube solar collector

Based on experimental data, two empirical correlations for energy efficiency and exergy efficiency as a function of ambient temperature, solar intensity, working fluid inlet temperature

and working fluid flow rate were formulated. The energy and exergy efficiency analyses were performed for the individual evacuated U – tube solar collector and for the whole solar collector system.

CHAPTER – 6

CROSS-FLOW DEHUMIDIFIER/REGENERATOR

6.1 Preface

Several researchers have investigated the performance of the liquid desiccant dehumidifier/regenerator employing numerical models and performing experimental studies. The estimation of air and desiccant property variations along the length and height of the dehumidifier and the regenerator are complicated. Thus, a numerical tool, is generally used to predict these variations. Very few models were developed for predicting the variations of air and desiccant properties and also for predicting the heat and mass transfer characteristics along the cross – flow liquid desiccant dehumidifier and regenerator. Only Li et al. (2005) reported the variations of air and desiccant properties along the liquid desiccant regenerator. Further, the models reported in the literature, generally require complicated simulation procedure for solving the governing equations. Moreover, the major challenges faced by several researchers are the estimation of heat and mass transfer coefficients or Lewis number. In addition, the reported models were used for predicting either the performance of the liquid desiccant dehumidifier or the performance of the liquid desiccant regenerator.

Therefore, this chapter focuses on proposing a simplified thermodynamic approach for analysing the performance of the cross – flow liquid desiccant dehumidifier as well as liquid desiccant regenerator using two developed correlations for predicting the heat and mass transfer coefficients in terms of thermal effectiveness and moisture effectiveness. A finite difference method is implemented for solving the developed thermodynamic model using a recursive algorithm. Using the developed model, the variations of air and desiccant enthalpies,

concentration of desiccant and air specific humidity along the packed tower (dehumidifier/regenerator) are presented. In addition, Lewis number is formulated in terms of thermal and moisture effectiveness and the influence of Lewis number on operating and performance parameters of the packed tower is studied.

6.2 Thermodynamic model

Fig. 6.1 shows the schematic of adiabatic cross-flow packed tower (dehumidifier/regenerator). In both the dehumidifier and the regenerator, the air and the desiccant solution flow in longitudinal and transverse directions, respectively. As shown in Fig. 6.1, the length, height and width of the packed tower are taken along x, y and z directions, respectively. The heat and mass transfer processes are uniform along the z direction of the packed tower. So, the transfer processes between the air and the desiccant remains same in any x – y plane along the z – direction. Therefore, in the present study, transfer processes in x – y plane at particular z – coordinate is chosen for deriving the governing equations (Fig. 6.2).

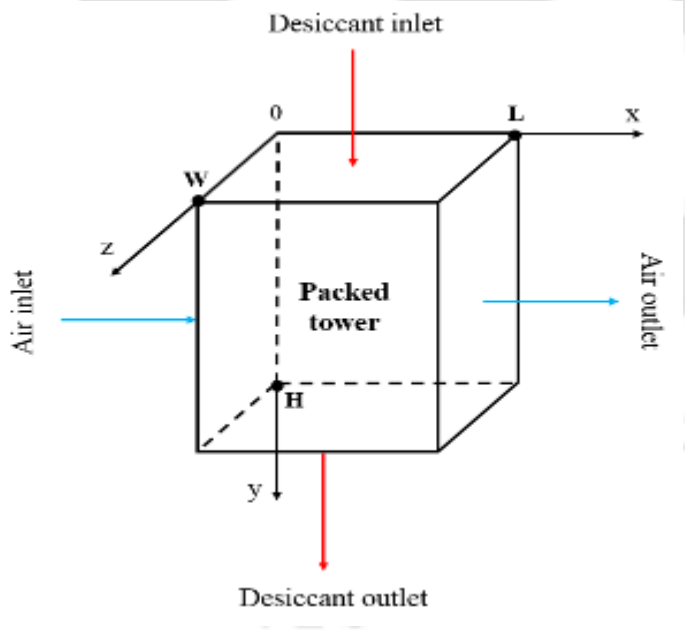

Fig. 6.1, Schematic of the cross-flow packed tower.

The assumptions considered for deriving the governing equations are,

- Working fluids are Newtonian.
- Velocities of working fluids are uniform along the longitudinal and transverse direction.
- No heat dissipation to the surroundings.
- Local heat and mass transfer coefficients do not vary during the transfer processes.

- Heat conduction and molecular diffusion among the liquid desiccant and air is negligible along the flow direction (Rajat and Jain, 2015; Shifang et al. 2017).
- Pressure drop across the tower height is neglected (Elsarrag et al., 2005).

6.2.1 Governing equations

The energy balance for the air side flow is given by

$$G_a \frac{\partial h_a}{\partial x} - G_a \delta \frac{\partial \omega_a}{\partial x} + \alpha_h a_s \left(T_a - T_s\right) = 0 \tag{6.1}$$

where $\delta \frac{\partial \omega_a}{\partial x}$ and $\alpha_h a_s \left(T_a - T_s\right)$ are the latent heat generated during dehumidification or humidification process and chemical heat liberated during exothermic reaction.

The energy balance for the desiccant side flow is given by

$$G_s \frac{\partial h_s}{\partial y} + G_s \delta \frac{\partial X_s}{\partial y} + \alpha_h a_s \left(T_s - T_a\right) = 0 \tag{6.2}$$

where $\delta \frac{\partial X_s}{\partial y}$ and $\alpha_h a_s \left(T_s - T_a\right)$ are the latent heat generated during vapour absorption/desorption process and chemical heat liberated during exothermic reaction.

The mass balance at the air – desiccant interface is given by,

$$G_s \frac{\partial X_s}{\partial y} + G_a \frac{\partial \omega_a}{\partial x} = 0 \tag{6.3}$$

The change in air humidity ratio along the length of the packed tower is given by (Yimo et al. 2014),

$$\frac{\partial \omega_a}{\partial x} + \frac{\alpha_m a_s}{G_a}\left(\omega_a - \omega_e\right) = 0 \tag{6.4}$$

where $\frac{\alpha_m a_s}{G_a}\left(\omega_a - \omega_e\right)$ is the mass transfer due to vapour pressure difference between liquid desiccant and air.

6.2.2 Heat and mass transfer coefficients

Overall heat and mass transfer coefficients (α_h & α_m) can be derived as follows:

a) Heat transfer coefficient at the interface

Variation of air temperature along the length of the packed tower is given by (Yimo et al. 2014),

$$\frac{\partial T_a}{\partial x} = \psi_h \left(T_s - T_a\right) \tag{6.5}$$

where $\psi_h = \dfrac{\alpha_h a_s}{G_a c_{p,m}}$

Also, the air temperature varies along the height of the packed tower. So, the change in air temperature along the height can be written as,

$$\frac{\partial T_a}{\partial y} = \psi_h b\left(T_s - T_a\right) \tag{6.6}$$

where b is a constant.

Thus, by combining Eqs. (5) & (6), the change in air temperature across the packed tower is written as,

$$dT_a = \frac{\partial T_a}{\partial x}dx + \frac{\partial T_a}{\partial y}dy = \psi_h \left(T_s - T_a\right)dx + \psi_h b\left(T_s - T_a\right)dy \tag{6.7}$$

On integration, Eq. (6.7) can be represented as

$$\int_{T_a^i}^{T_a^o} \frac{dT_a}{(T_a - T_s)} = -\psi_h \left(\int_0^L dx + \int_0^H b dy \right) \tag{6.8}$$

After integrating Eq. (6.8);

$$\frac{T_a^o - T_a^i}{T_s^{avg} - T_a^i} = 1 - e^{-\psi_h L^*} \tag{6.9}$$

where $L^* = L + bH$.

The thermal effectiveness (ξ_T) for the packed tower is given as (Gandhidasan, 2005, 2006)

$$\xi_T = \frac{(T_a^o - T_a^i)}{(T_s^i - T_a^i)} = \frac{(T_a^i - T_a^o)}{(T_a^i - T_s^i)} \tag{6.10}$$

From Eqs. (6.9) & (6.10), the thermal effectiveness can be reformulated as,

$$\xi_T = 1 - e^{-\psi_h L^*}\left(\frac{T_s^{avg} - T_a^i}{T_s^i - T_a^i}\right) \tag{6.11}$$

As $\left(\frac{T_s^{avg} - T_a^i}{T_s^i - T_a^i}\right) \approx 1$, Eq. (6.11) can be represented as,

$$\xi_T = 1 - e^{-\psi_h L^*} \tag{6.12}$$

Since $\psi_h = \frac{\alpha_h a_s}{G_a c_{p,m}}$, the heat transfer coefficient (α_h) is represented from Eq. (6.12) as,

$$\alpha_h = \frac{G_a c_{p,m}}{a L^*} \ln\left(\frac{1}{1-\xi_T}\right) \tag{6.13}$$

b) Mass transfer coefficient at the interface

As the air specific humidity varies in both longitudinal and transverse directions of the packed tower, the overall change in specific humidity for the packed tower can be written as,

$$d\omega_a = \frac{\partial \omega_a}{\partial x} dx + \frac{\partial \omega_a}{\partial y} dy = \psi_m (\omega_e - \omega_a) dx + \psi_m b (\omega_e - \omega_a) dy \tag{6.14}$$

where b is a constant and $\psi_m = \frac{\alpha_m a_s}{G_a}$.

On integration, Eq. (6.14) is represented as,

$$\int_{\omega_a^i}^{\omega_a^o} \frac{d\omega_a}{(\omega_e - \omega_a)} = -\psi_m \left(\int_0^L dx + \int_0^H b dy\right) \tag{6.15}$$

After integrating Eq. (6.15), the air outlet specific humidity is expressed as,

$$\frac{\omega_a^o - \omega_a^i}{\omega_e - \omega_a^i} = 1 - e^{-\psi_m L^*} \tag{6.15a}$$

where $L^* = L + bH$.

The moisture effectiveness (ξ_m) is given as (Gandhidasan, 2005, 2006)

$$\xi_m = \frac{\omega_a^o - \omega_a^i}{\omega_e - \omega_a^i} \tag{6.16}$$

Using Eqs. (15a) & (16) the moisture effectiveness is formulated as,

$$\xi_m = 1 - e^{-\psi_m L^*} \tag{6.17}$$

Since $\psi_m = \frac{\alpha_m a_s}{G_a}$, the mass transfer coefficient is represented from Eq. (6.17) as,

$$\alpha_m = \frac{G_a}{aL^*} \ln\left(\frac{1}{1-\xi_m}\right) \tag{6.18}$$

Here, assuming $a_s L^* \approx 1$ for a cross-flow packed tower (Yimo et al. 2014), the Eqs. (6.13) & (6.18) can be written as

$$\alpha_m = G_a \ln\left(\frac{1}{1-\xi_m}\right) \tag{6.19}$$

$$\alpha_h = G_a c_{p,m} \ln\left(\frac{1}{1-\xi_T}\right) \tag{6.20}$$

With known inlet parameters, overall heat and mass transfer coefficients for the packed tower (α_h & α_m) can be calculated using Eqs. (19) & (20).

The boundary conditions along the packed tower are

$h_s = h_s^i$; $X_s = X_s^i$, at y = 0 (6.21)

$h_a = h_a^i$, $\omega_a = \omega_a^i$, at x = 0 (6.22)

6.3 Finite difference model

In order to analyze the heat and mass transfer contours along the packed tower and to predict the outlet parameters of the air and desiccant solution, governing equations (Eq. (6.1) – (6.4)) derived in the thermodynamic model needs be solved numerically by applying boundary

conditions (Eq. (6.21) & Eq. (6.22)). A two dimensional x – y plane is considered as the computational domain and discretized into L × H equally spaced grids (Fig. 6.2). By applying boundary conditions, the governing equations are solved for each grid (i, j).

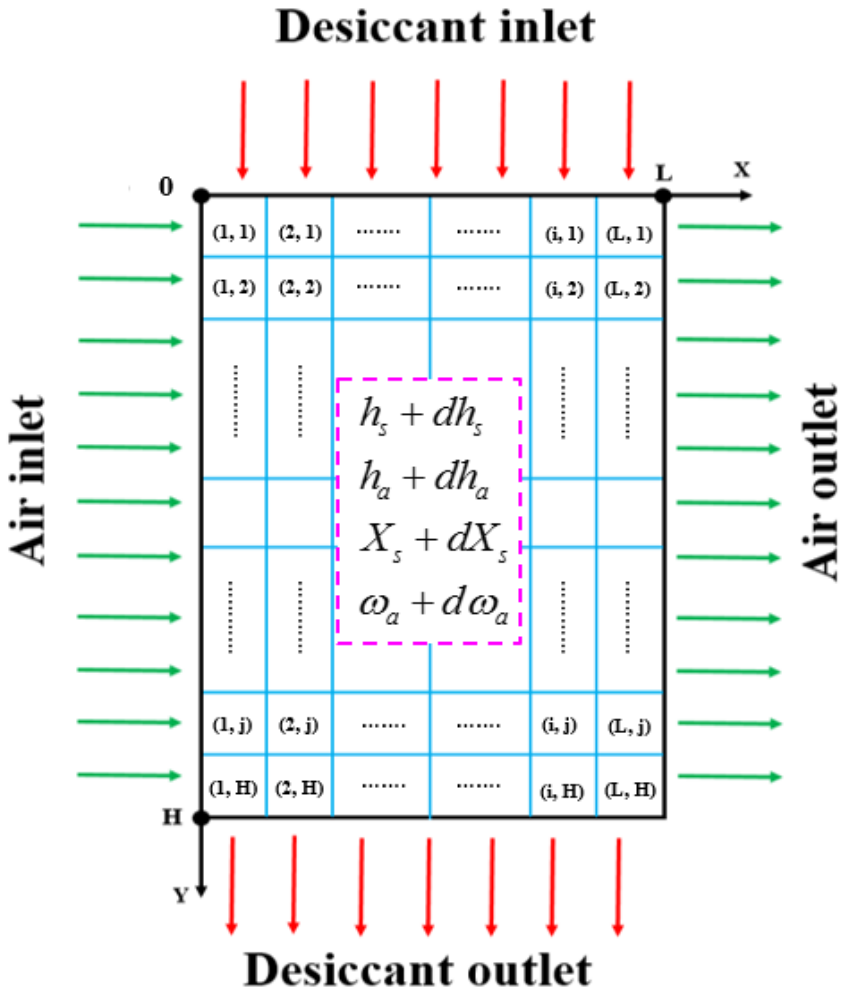

Fig. 6.2, Heat and mass transfer processes along the packed tower.

The discretized form of the governing equations for grid (i, j) are written as follows:

$$G_a(h_{a,i+1,j} - h_{a,i,j}) - G_a\delta(\omega_{a,i+1,j} - \omega_{a,i,j}) + \alpha_h a_s(T_{a,i,j} - T_{s,i,j}) = 0 \tag{6.23}$$

$$G_s(h_{s,i,j+1} - h_{s,i,j}) + G_s\delta(X_{s,i,j+1} - X_{s,i,j}) + \alpha_h a_s(T_{s,i,j} - T_{a,i,j}) = 0 \tag{6.24}$$

$$(\omega_{a,i+1,j} - \omega_{a,i,j}) - \frac{\alpha_m a_s}{G_a}(\omega_{e,i,j} - \omega_{a,i,j}) = 0 \tag{6.25}$$

$$G_s\left(X_{s,i,j+1} - X_{s,i,j}\right) + G_a\left(\omega_{a,i+1,j} - \omega_{a,i,j}\right) = 0 \tag{6.26}$$

6.3.1 Recursive Algorithm

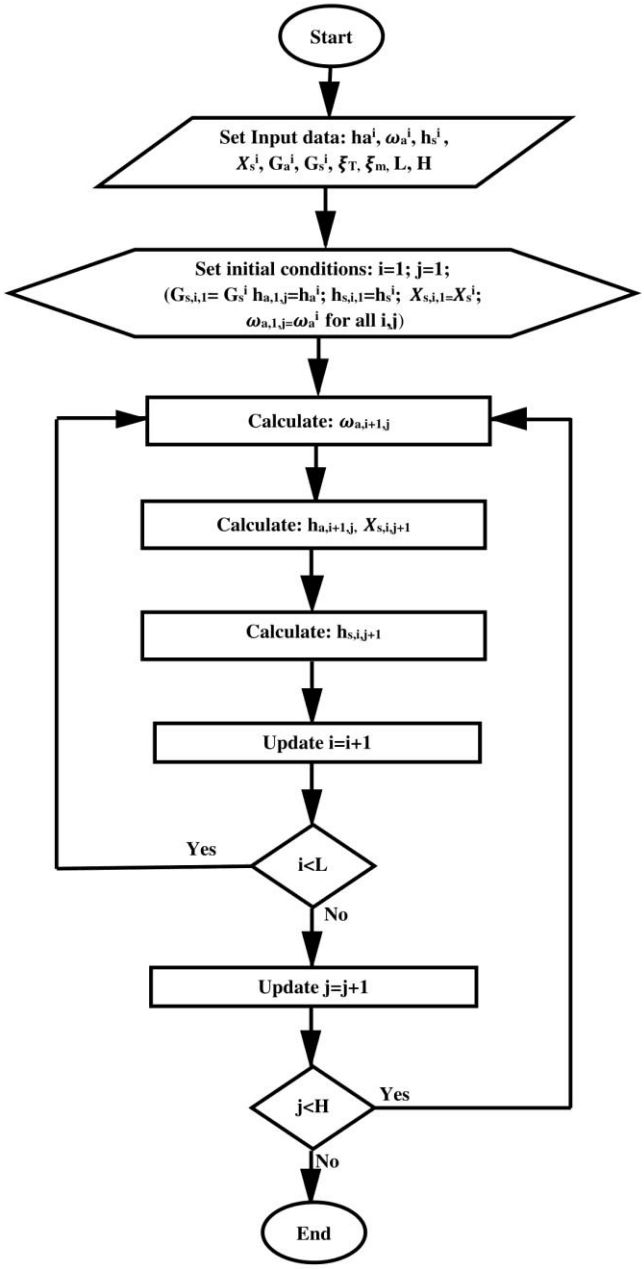

Fig. 6.3, Recursive algorithm for solving the developed model.

Recursive algorithm utilizes the output obtained in the current iteration as an input for solving the next iteration (Donggen et al. 2017). In the present study, recursive algorithm serves as a tool for solving the governing equations in each grid by iterating over the computational domain. The recursive algorithm for the computational domain is shown in Fig. 6.3. The simulation procedure contains nested spatial loop which iterates over the computational domain

and solves the discretized form of governing equations (Eq. (6.23) – Eq. (6.26)) in each grid by applying boundary conditions. The input parameters chosen for simulation procedure are the air and desiccant enthalpies (h_a^i & h_s^i), air specific humidity (ω_a^i), desiccant concentration (X_s^i), moisture effectiveness (ξ_m), thermal effectiveness (ξ_T), mass flux of air and desiccant solution (G_a & G_s) and the specifications of the packed tower. The initial conditions of air and desiccant solution for the grid (i, j) are fixed as $h_{a,i,j}=h_a^i$, $h_{s,i,j}=h_s^i$, $\omega_{a,i,j}=\omega_a^i$, $X_{s,i,j}=X_s^i$ and $G_{s,i,j}=G_s^i$. These initial conditions are implemented for obtaining the outlet parameters of the grid (i, j).

The obtained outlet parameters of grid (i, j) are equal to the air inlet parameters of grid (i+1, j) and desiccant inlet parameters of the grid (i, j+1), respectively. There are too loops in the algorithm i.e., external loop and internal loop. In the internal loop, the 'i' value is incremented every time keeping the 'j' value constant till 'i' value reaches L (length of the packed tower). After that, the control goes to the external loop where 'j' value varies from 0 to H (height of the packed tower). This process goes on till the loops reach to the last grid (L, H). The complete procedure for predicting the outlet parameters over the entire computational domain can be explained as follows,

(a) First set the inlet parameters of the air and desiccant solution, ξ_m, ξ_T, L and H as input data.
(b) Set the initial conditions as $h_{a,i,j}=h_a^i$, $h_{s,i,j}=h_s^i$, $\omega_{a,i,j}=\omega_a^i$, $X_{s,i,j}=X_s^i$ and $G_{s,i,j}=G_s^i$, set i =1 and j =1.
(c) Calculate specific humidity ($\omega_{a,i+1,j}$) using Eq. (6.25).
(d) Calculate air outlet enthalpy and desiccant concentration ($h_{a,i+1,j}$ & $X_{s,i,j+1}$) using Eqs. (23 & 26).
(e) Calculate the desiccant outlet enthalpy ($h_{s,i,j+1}$) using Eq. (6.24).
(f) Increase 'i' value by one unit and calculate the outlet parameters of (i+1, j) grid using outlet parameters of the previous grid (i, j).
(g) Repeat the steps (c) to (f) till i reaches the value L.
(h) If i = L, then go for the j+1 row by incrementing the value of j by one unit and calculate the outlet parameters for each grid of j+1 row by repeating the steps (c) to (f).
(i) Continue the whole process till i = L & j = H.
(j) Terminate the process.

The predicted outlet parameters of the packed tower can be taken as the average of their respective values along the outlet of the computational domain i.e., the average values of desiccant parameters at x =1 to L & y = H and the average values of air parameters at x = L & y = 1 to H (Fig. 6.2).

6.4 Validation of the developed model

To use the developed model for studying the heat and mass transfer processes across the packed tower (dehumidifier/regenerator), proper validation is required. For the validation of the developed model, experimental results presented by Li et al. (2005) (dehumidifier and regenerator), Rajat SD and Jain S (2015) (dehumidifier) are considered. The dimensions and specifications of the packed tower used for validation purpose are listed in Table 6.1. Table 6.2 shows the comparison of the predicted values with the experimental data (Li et al. (2005); Rajat and Jain (2015)). Using the inlet parameters given in Table 6.2, distribution of air and desiccant parameters (contour plots) across the dehumidifier and the regenerator are presented in Figs. 6.4 and 6.5. Also, a comparison of these results is shown in Figs. 6.6 and 6.7.

Table 6.1, Dimensions and specifications of the packed tower reported by Li et al. (2005) and Rajat and Jain (2015).

Experimental data	Li et al. (2005)	Rajat and Jain (2015)
Liquid desiccant	LiBr-H_2O	LiCl-H_2O
Height (m)	0.55	0.21
Length (m)	0.4	0.49
Width (m)	0.35	0.18
Specific surface area (m^2/m^3)	396	178
Type of component	Dehumidifier and regenerator	Dehumidifier

Table 6.2, Comparison of predicted results with experimental data.

Liu et al. (2005) – Regenerator						
	G_a (kg/m^2s)	T_a (^oC)	ω_a(kg_v/kg_{da})	G_s (kg/m^2s)	T_s(^oC)	X_s (%)
Inlet parameters	1.41	35.4	0.021	2.77	57.3	47.1
Outlet parameters obtained by experiments	-	46.6	0.031	-	46.1	47.6

Outlet parameters (Liu et al. (2005))	-	46.2	0.031	-	46.3	47.4
Percentage difference (Liu et al. (2005))	-	0.85	0.0	-	-0.43	0.42
Outlet parameters using present model	-	46.5	0.031	-	46	47.4
Percentage difference using present model (%)	-	0.21	0.0	-	0.21	0.42
Liu et al. (2005) – Dehumidifier						
Inlet parameters	1.97	31.7	0.013	3.08	22.9	45.7
Outlet parameters obtained by experiments	-	26.9	0.0099	-	27.8	45.7
Outlet parameters (Liu et al. (2005))	-	27.6	0.010	-	27.5	45.6
Percentage difference (Liu et al. (2005))		-2.60	-1.01	-	1.07	0.21
Outlet parameters using present model		27.3	0.010	-	27.4	45.62
Percentage difference using present model (%)		-1.48	-1.01	-	1.43	0.175
Rajat SD and Jain S (2015) – Dehumidifier						
Inlet parameters	0.34	40.8	0.02263	0.79	54.6	38
Outlet parameters obtained by experiments	-	37.2	0.0123	-	37.9	37.7
Outlet parameters (Rajat SD and Jain S (2015))	-	37.1	0.0124	-	37.2	37.76
Percentage difference (Rajat SD and Jain S (2015))	-	0.26	-0.404	-	1.84	-0.159
Outlet parameters using present model	-	37.1	0.0124	-	37.6	37.6
Percentage difference using present model (%)	-	0.26	-0.404	-	0.79	0.26

It is observed that the predicted values of outlet parameters from the current model are in good agreement with the experimental data (given in Table 6.2). The deviation of the predicted values with the experimental data is less than $\pm 2\%$.

6.4.1 Distribution profiles

Figs. 6.4 and 6.5 represent the variation of air and desiccant properties along the dehumidifier and the regenerator. The inlet parameters for analyzing the heat and mass transfer processes across the packed tower are taken from the experimental results reported by Liu et al. (2005) (Table 6.2). From Fig. 6.4, it is seen that as the air flows along the longitudinal direction, it cools and dehumidifies whereas the desiccant solution that flows along transverse direction is heated and diluted. The air enthalpy and humidity ratio is minimum at the top corner of the air outlet (x = 0.4 m & y = 0 m; Fig. 6.4b and 6.4d). This is because the driving force for the heat and mass transfer processes is maximum at that location due to the contact of cold and strong solution. The desiccant enthalpy is maximum and desiccant concentration is minimum at the left corner of the desiccant outlet (x = 0 m & y = 0.55 m; Fig. 6.4a & 6.4c). It happens because the desiccant solution at this point contacts colder and more humid air compared to other locations.

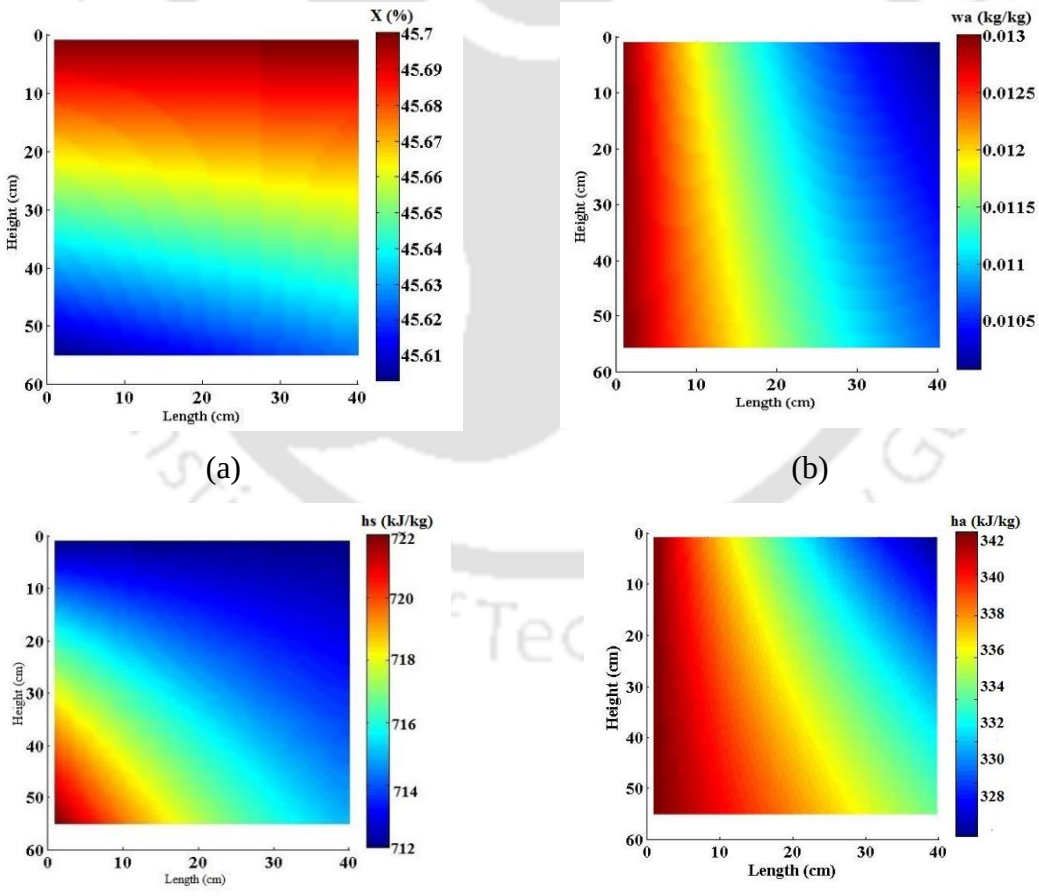

Fig. 6.4, Contour plots for air and desiccant parameters of the dehumidifier (a) desiccant concentration (b) air specific humidity, (c) desiccant enthalpy and (d) air enthalpy.

Along the longitudinal direction (x = 0 m to 0.4 m & y = 0.55 m), the difference in air enthalpy and specific humidity are about 9 kJ/kg and 3 $g_v/kg_{da,}$ respectively. Similarly, along the transverse direction (x = 0.4 m & y = 0 m to 0.55 m), the differences in desiccant enthalpy and concentration are 6 kJ/kg and 0.08%.

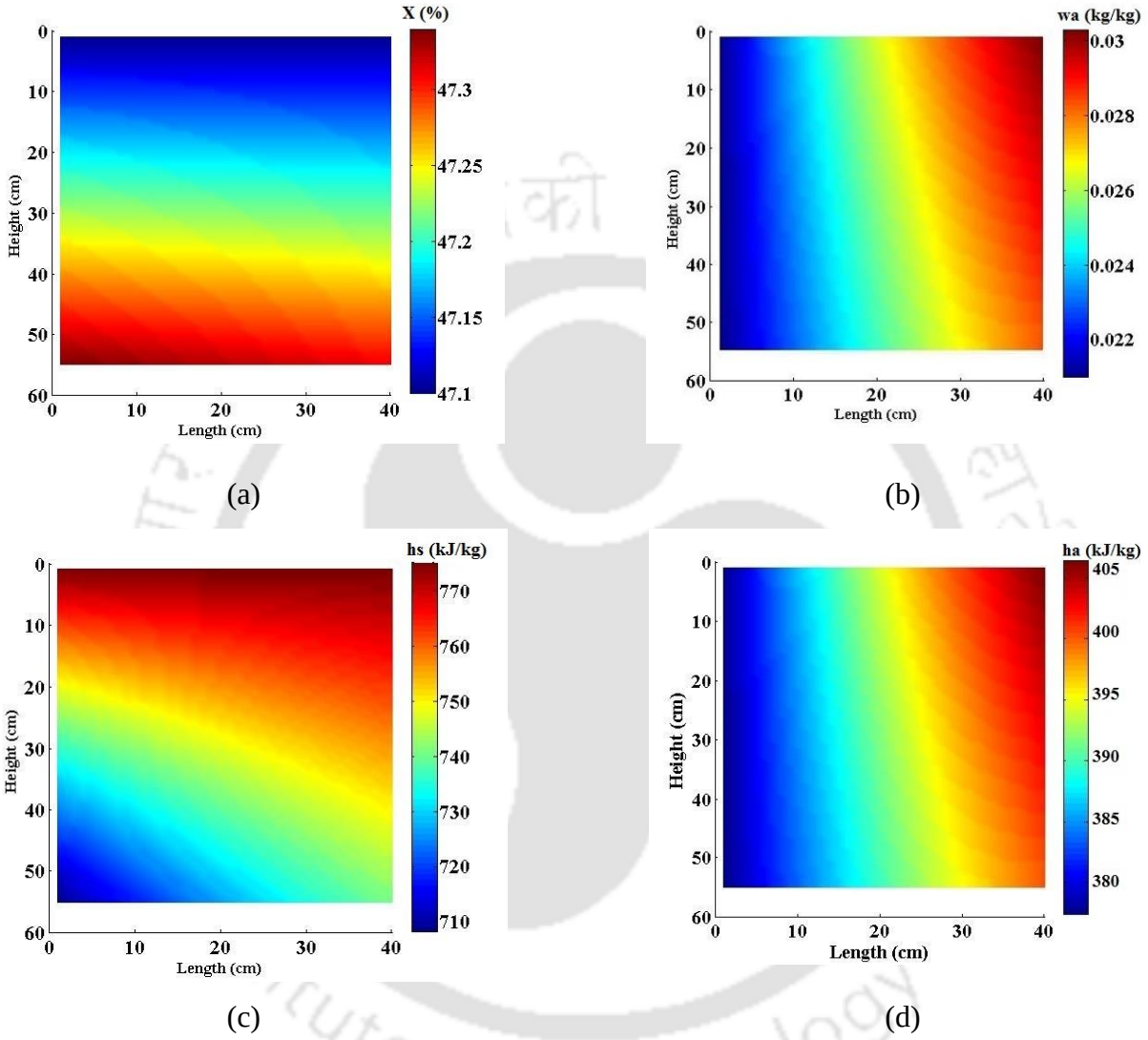

Fig. 6.5, Contour plots for air and desiccant parameters of the regenerator (a) desiccant concentration (b) air specific humidity, (c) desiccant enthalpy and (d) air enthalpy.

The air in the regenerator is heated and humidified as it flows along the longitudinal direction, while the solution cools and gets concentrated as it flows along the transverse direction (shown in Fig. 6.5). At the air outlet (x = 0.4 m), the air at the top of the regenerator has the highest enthalpy and specific humidity because it contacts the hotter and weaker solution (Fig. 6.5b and 6.5d). Similarly, at the left corner of the desiccant outlet (y = 0.55 m), the solution has the highest concentration and the lowest enthalpy because it contacts colder and drier air compared

with other locations (Fig. 6.5a and 6.5c). Along the longitudinal direction (x = 0 m to 0.4 m & y = 0.55 m), the differences in air enthalpy and specific humidity are 25 kJ/kg and 10 g_v/kg_{da}, respectively. Similarly, along the transverse direction (x = 0.4m & y = 0 m to 0.55 m), the differences in desiccant enthalpy and concentration are 40 kJ/kg and 0.3%.

6.4.2 Validation of operating parameters

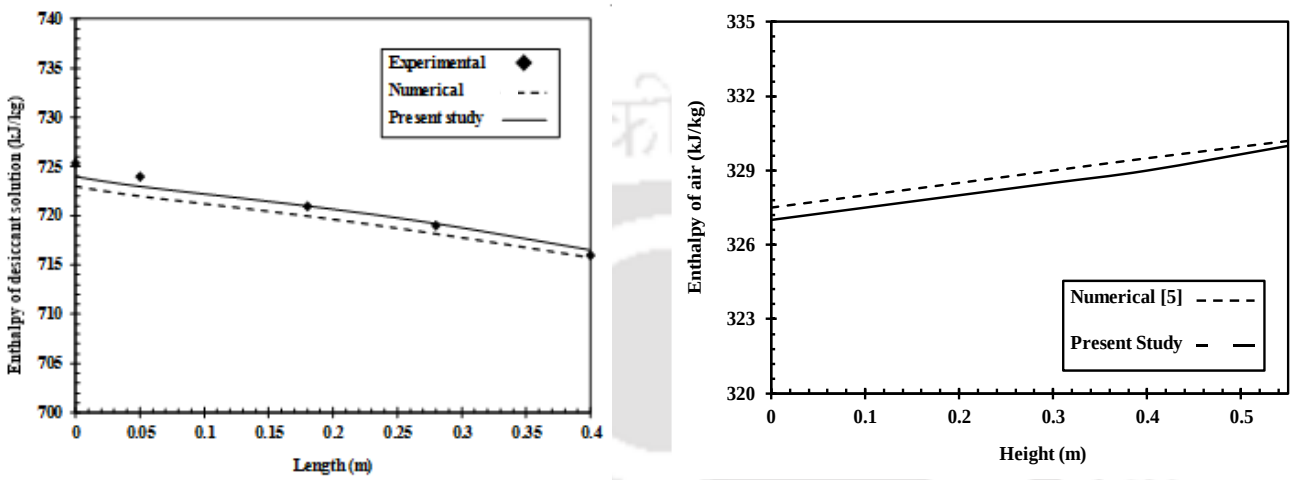

(a) **(b)**

Fig. 6.6, Comparison of simulation results with the numerical and experimental data of (a) desiccant solution enthalpy in dehumidifier and (b) air enthalpy in dehumidifier.

Figs. 6.6 and 6.7 present the comparison of simulated results with the experimental and numerical results presented by Liu et al. (2005). Since, Liu et al. (2005) presented only the experimental results for solution enthalpy, numerically predicted solution enthalpy has been validated with experimental data of solution enthalpy of the dehumidifier and the regenerator (Fig. 6.6a and 6.7a). As shown in Fig. 6.6a and 6.7a, the predicted outlet solution enthalpy variation along the length of the packed tower (dehumidifier – 6.6a and regenerator – 6.7a) matches well with the experimental and numerical data reported by Liu et al. (2005). From Fig. 6.6a, it is found that with increase in length of the dehumidifier from 0 m to 0.4 m, the desiccant enthalpy decreases only by 0.4 %. This small decrease is due to the fact that at the left corner of the dehumidifier (L = 0 m), the air temperature and moisture content are high compared with the right corner (L = 0.4 m). Therefore, there is more heat transfer from air to the desiccant solution at the left side compared to the right side of the dehumidifier. From Fig. 6.7a, it is observed that with increase in length of the regenerator from 0 m to 0.4 m, the solution enthalpy increases by 1.8 %. This happens because at the left corner of the regenerator (L = 0 m), air temperature and moisture are low compared with the right corner (L = 0.4 m). Thus, there is

high sensible and latent heat transfer from the desiccant solution to the air side at the left corner compared to the right corner of the regenerator.

As illustrated in Fig. 6.6b and 6.7b, the predicted outlet air enthalpy variation along the height of the packed tower (dehumidifier – Fig. 6.6b and regenerator – Fig. 6.7b) has a good agreement with the numerical values reported by Liu et al. (2005). It is observed from Fig. 6.6b that with increase in height of the dehumidifier from 0 m to 0.55 m, the air enthalpy increases by 0.6 %. This is because, the air at the top of the dehumidifier (H=0) is in contact with the cold and concentrated solution. So, the potential for heat and moisture transfer from the air to the desiccant is high at the top in comparison with the bottom of the dehumidifier (H = 0.55 m).

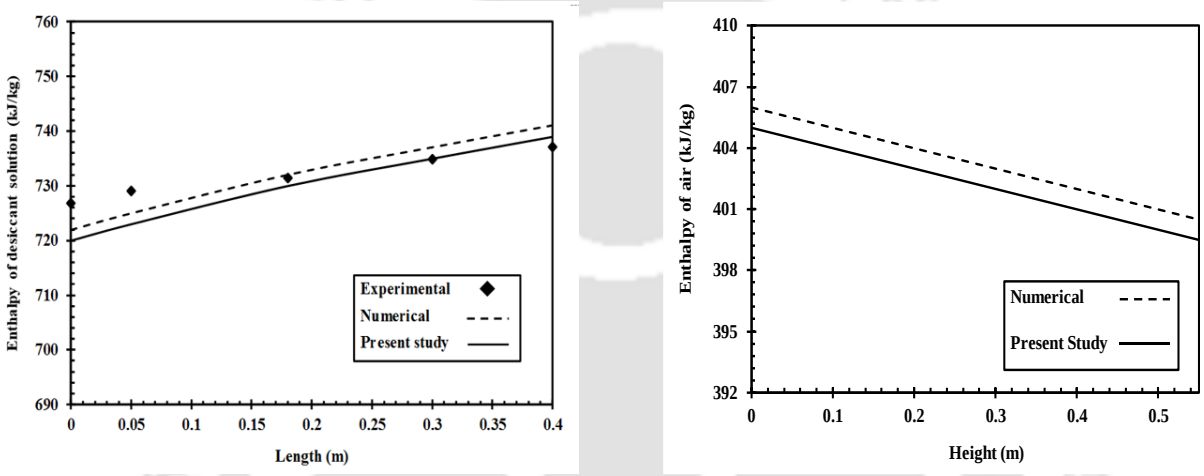

(a) (b)

Fig. 6.7, Comparison of simulated results with the numerical and experimental data of (a) desiccant enthalpy in regenerator and (b) air enthalpy in regenerator.

It is also observed from Fig. 6.7b that with increase in height from 0 m to 0.55 m, the air enthalpy decreases merely by 0.7 %. This marginal decrease happens because, the air at the top (H = 0 m) contacts with the hot and diluted solution. So, the potential for heat and mass transfer is higher at the top from the desiccant to the air than at the bottom (H = 0.55 m) of the regenerator.

6.5 Influence of Lewis number on dehumidification and regeneration processes

6.5.1 Lewis Number

Lewis number is a dimensionless number for determining the relationship between the heat and mass transfer coefficients and is expressed as

$$Le = \frac{\alpha_h}{\alpha_m c_{p,m}} \tag{6.27}$$

By substituting, Eqs. (6.19) & (20) in Eq. (6.27), Le is defined in terms of moisture and thermal effectiveness's as

$$Le = \frac{\ln\left(\frac{1}{1-\xi_T}\right)}{\ln\left(\frac{1}{1-\xi_m}\right)} \tag{6.28}$$

In section 6.5.2 and 6.5.3, by using the developed model, the influence of Lewis number on the performance characteristics of the dehumidifier and the regenerator is studied. The operating parameters and the packed tower specifications considered for analyzing the heat and mass transfer processes across the packed tower are listed in Table 6.3.

Table 6.3, Constant operating parameters for the dehumidification and regeneration processes.

Liquid desiccant	LiBr-H_2O
Air inlet temperature(^oC)	32
Relative humidity (%)	60
Air flow rate ($kg/m^2 - s$)	2
Desiccant flow rate($kg/m^2 - s$)	3.1
Desiccant inlet temperature for dehumidifier (^oC)	23
Desiccant inlet temperature for Regenerator (^oC)	57
Concentration of desiccant solution (% by mass)	46
Thermal Effectiveness	0.6
Height (m)	0.55
Length (m)	0.4
Specific surface area (m^2/m^3)	396

6.5.2 Influence of Lewis number on operating parameters

Figs. 6.8 – 6.10 describe the effect of Le on the desiccant concentration of the dehumidifier and the regenerator. For a given height, as Le increases, the desiccant concentration increases

in the dehumidifier and decreases in the regenerator. At a specified height (H = 27.5m), the increase in the solution concentration is only 0.18% in the dehumidifier and the decrease in the regenerator is about 0.43% as the Lewis number varies from 0.5 to 1.5. With increase in height, desiccant concentration decreases in the dehumidifier and increases in the regenerator (Figs. 6.8 – 6.10). For a specified Le (Le = 1), the decrease is in the solution concentration is about 0.32% in the dehumidifier and the increase is about 1.58 % in the liquid desiccant regenerator.

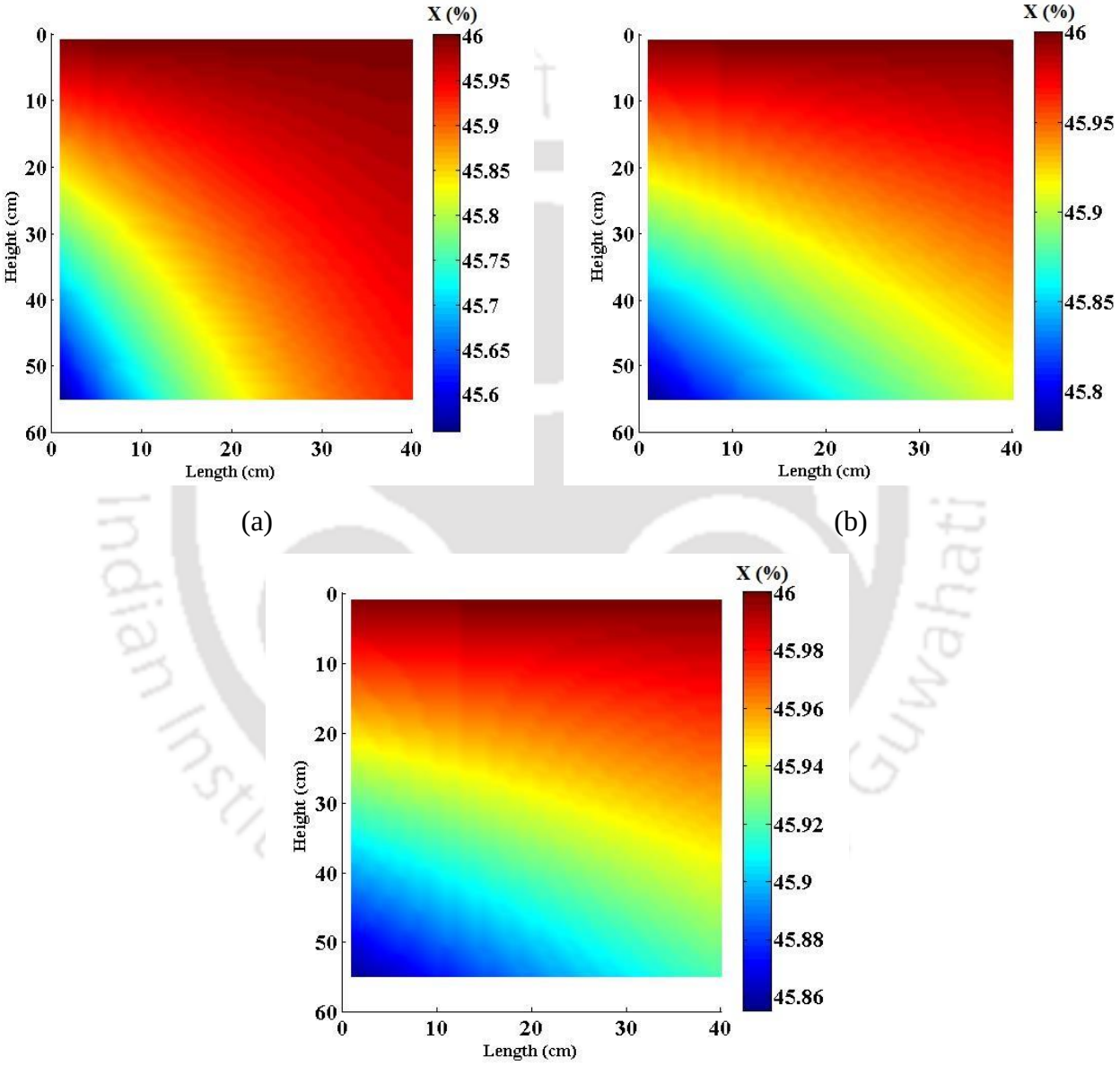

Fig. 6.8, Concentration profile for different Lewis numbers during the dehumidification process: (a) Le=0.5, (b) Le=1 and (c) Le=1.5.

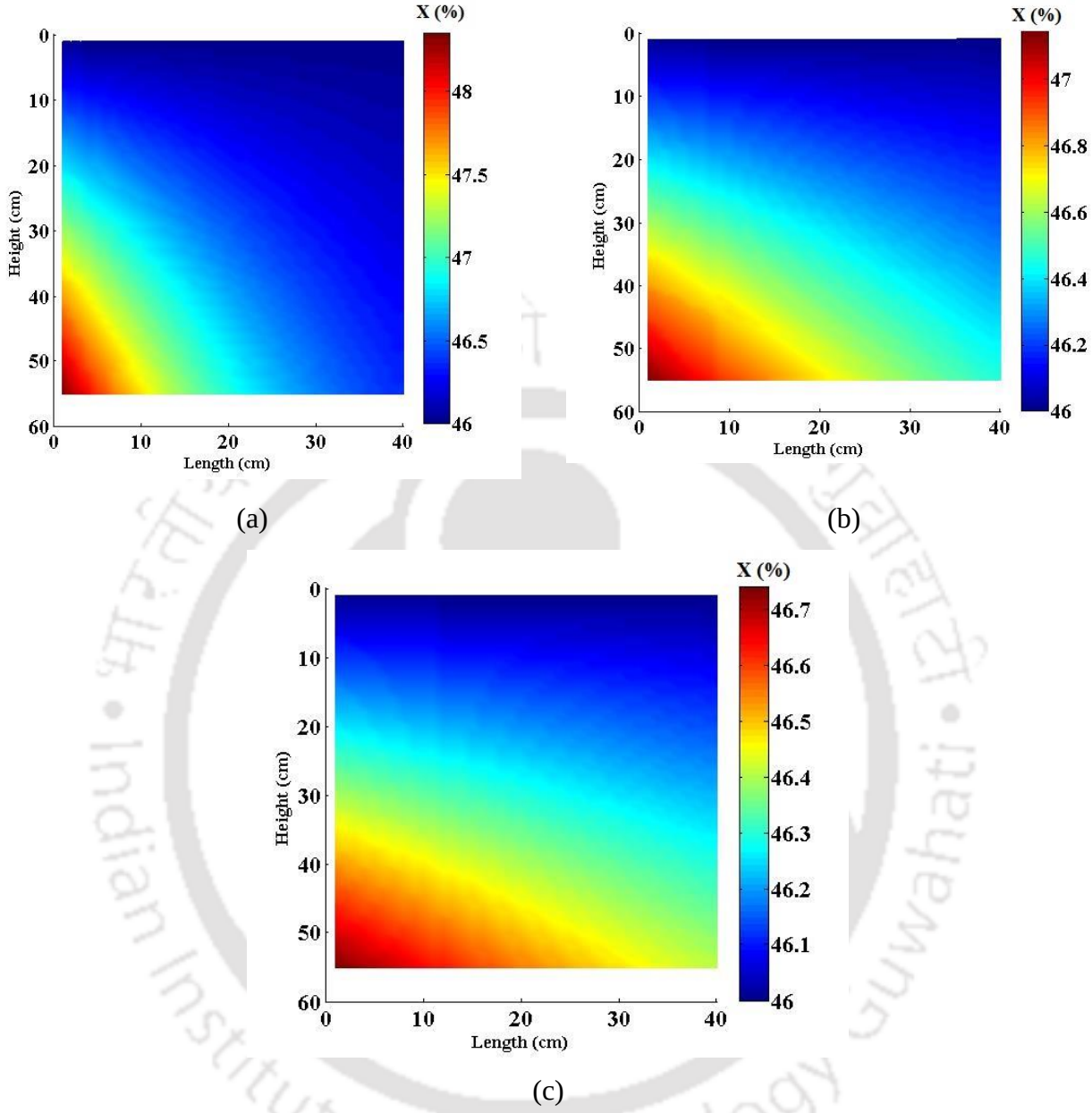

Fig. 6.9, Concentration profile for different Lewis numbers during the regeneration process: (a) Le=0.5, (b) Le=1 and (c) Le=1.5.

It is also observed from Figs. 6.8 and 6.9, that with increase in length from 0 m to 0.4 m, the desiccant concentration increases by 0.65 %, 0.26% and 0.13% for the dehumidifier and decreases by 4.12%, 1.69% and 0.85% for the regenerator, respectively for the Le of 0.5, 1 and 1.5. As evident from the results presented in Figs. 6.8 – 6.10 that Lewis number (Le) does not have a significant effect on solution concentration of both the dehumidifier and the regenerator.

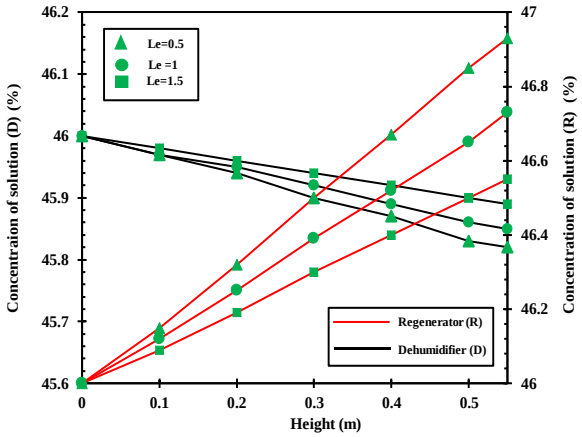

Fig. 6.10, Variation of the solution concentration along the height of the packed tower.

Fig. 6.11a shows the variation of air enthalpy along the length of the packed tower (dehumidifier and regenerator) for different Lewis numbers (Le = 0.5 to 1.5). From Fig. 6.11a, it is observed that for a given length, with increase in Le, the air enthalpy increases in the dehumidifier and decreases in the regenerator. This happens because with increase in Le, mass transfer rate decreases. Thus, the latent heat transfer between the desiccant solution and the process air decreases. For a given length (L = 0.2 m), with increase in Le from 0.5 to 1.5, the air enthalpy increases by 21% in the dehumidifier and decreases by 31% in the regenerator. From Fig. 6.11a, it is also observed that for a given Le, with increase in length of the packed tower, the enthalpy of the process air decreases in the dehumidifier and increases in the regenerator. This is due to the fact that as the length increases, release in latent heat of condensation/evaporation between the air and the desiccant solution increases.

Therefore, the air enthalpy decreases in the dehumidifier and increases in the regenerator. For a particular Le (Le =1), with increase in length of the packed tower from 0 to 0.4 m, the enthalpy of the air decreases by 36% in the dehumidifier and increases by 168% in the regenerator. The variation of specific humidity of the process air along the length of the dehumidifier and regenerator for different Lewis numbers is shown in Fig. 6.11b. It is seen from Fig. 6.11b that at a particular length with increase in Le, the specific humidity of air increases in the dehumidifier and decreases in the regenerator. This is because as the Le increases, moisture transfer rate at the air – desiccant interface decreases and subsequently, change in air specific humidity takes place. At a particular length (L = 0.2 m), with increase in Le from 0.5 to 1.5, air specific humidity in the dehumidifier increases by 51.6% and decreases in the regenerator by 46.1%.

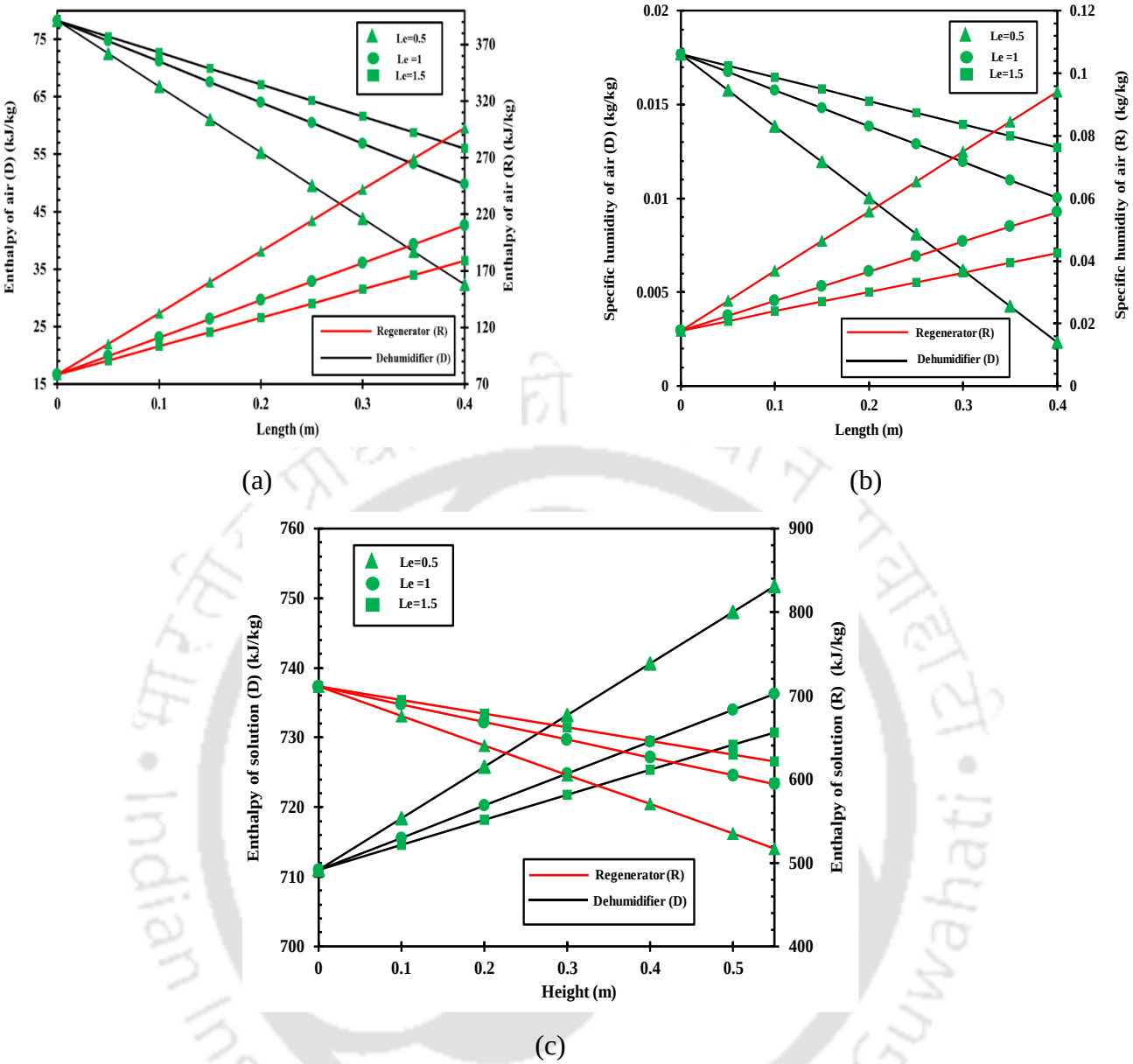

Fig. 6.11, Influence of Le on the enthalpies of working fluid and specific humidity of air (a) variation of air enthalpy along the length of the packed tower, (b) variation of air specific humidity along the length of the packed tower and (c) variation of the desiccant enthalpy along the height of the packed tower.

It is also found from Fig. 6.11b that for a particular Le, as the length increases, the air specific humidity decreases in the dehumidifier and increases in the regenerator. It happens because with increase in length, amount of moisture desorbed/absorbed from the air/desiccant in the dehumidifier/regenerator increases. At Le = 1, as the length varies from 0 m to 0.4 m, the decrease in air specific humidity in the dehumidifier is 44% whereas in the regenerator it increases by 218%.

Fig. 6.11c illustrates, the influence of Le and height of the packed tower on the enthalpy of the desiccant solution in the dehumidifier and regenerator. As observed from Fig. 6.11c, as Le increases, the enthalpy of the desiccant solution decreases in the dehumidifier and increases in the regenerator. This can be explained by the fact that as the Le increases, mass transfer rate decreases and thereby, the heat absorbed/desorbed by the desiccant solution in the dehumidifier/regenerator decreases. At a height of 0.275 m, the variation of Le from 0.5 to 1.5 leads to decrease in desiccant solution enthalpy by 1.6% in the dehumidifier and leads to increase in the regenerator by 9.4%. It is also observed from Fig. 6.11c that for a given Le, as the height increases, the enthalpy of the desiccant solution increases in the dehumidifier and decreases in the regenerator. This variation is due to the increase in amount of heat transferred between the desiccant and the air. At Le = 1, with increase in height from 0 m to 0.55 m, the solution enthalpy increases by 3.15% in the dehumidifier and decreases by 16.4% in the regenerator.

It is concluded from Fig. 6.11 that the variation of the outlet parameters is more prominent in the regenerator as compared to the dehumidifier. This is due to higher heat and mass transfer potentials of the regenerator. Further, it is also observed that Le is having dominant effect on both air enthalpy and desiccant solution enthalpy.

6.5.3 Influence of Lewis number on condensation and evaporation rates

From Figs. 6.12a – 6.12d, it is observed that for a given inlet parameter, as the Le increases from 0.5 to 1.5, both the condensation rate of the dehumidifier and the evaporation rate of the regenerator decreases. This happens because with increase in the Le, potential for moisture transfer decreases. This is due to decrease in vapor pressure difference between the air and working fluid. It is also found from Fig. 6.12a – 6.12c that for a given air temperature of 28 ^{o}C, air humidity ratio of 21 g_v/kg_{da} and desiccant concentration of 45%, increases in Le from 0.5 to 1.5, the condensation rate of the dehumidifier decreases by 45% and also the evaporation rate of the regenerator decreases by 45%. From Fig. 6.12d, it is found that with increase in Le from 0.5 to 1.5, the decrease in the condensation rate of the dehumidifier is about 47 % at a desiccant temperature of 28 ^{o}C and the decrease in evaporation rate of the regenerator is about 37% at a desiccant temperature of 60 ^{o}C. It is observed from Fig. 6.12a – 6.12d that for a given Le, with increase in the air humidity ratio, desiccant concentration and air temperature, the condensation rate of the dehumidifier increases and it decreases with increase in the desiccant

temperature. This is because of decrease in simultaneous heat and mass transfer potentials across the air – desiccant interface.

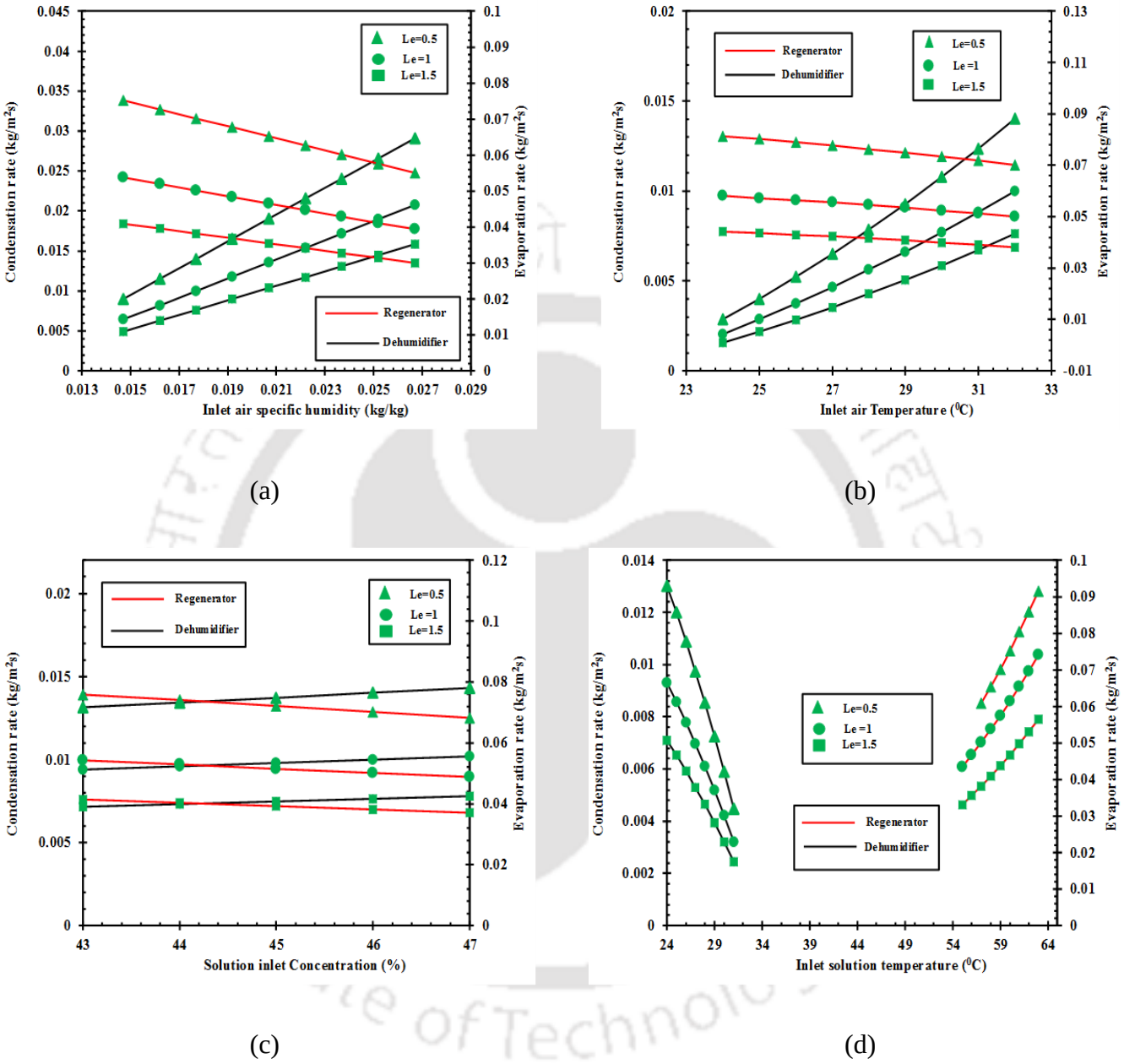

Fig. 6.12, Influence of Le on the performances of dehumidifier and regenerator (a) variations of evaporation and condensation rates with the inlet air specific humidity, (b) Variation of evaporation and condensation rate with the air inlet temperature, (c) variation of evaporation and condensation rates with the concentration of the solution and (d) variation of evaporation and condensation rates with desiccant inlet temperature.

From Fig. 6.12a – 6.12d, it is also found that for a specified Le, with increase in the air humidity ratio, desiccant concentration and air temperature, the evaporation rate of the regenerator decreases and it increases with increase in the desiccant temperature. At Le = 1, for a given air and desiccant inlet parameters, with increase in air temperature from 24 ^{o}C to 32 ^{o}C, desiccant concentration from 43% to 47% and air humidity ratio from 14.72 g_v/kg_{da} to 26.69 g_v/kg_{da}, the condensation rate of the dehumidifier increases by 75%, 12.5% and 22.3 %, respectively whereas the evaporation rate of the regenerator decreases by 28%, 10.1% and 26.14%, respectively (Fig. 6.12a – 6.12c). It is found from Fig. 6.12d that for a given Le = 1, the increase in the dehumidifier desiccant temperature from 23 ^{o}C to 31 ^{o}C, the condensation rate decreases by 68% whereas with increase in the regenerator desiccant temperature from 55 ^{o}C to 63 ^{o}C, the evaporation rate increases by 75%.

It should be noted that most of the researchers simulated the performances of the dehumidifier and the regenerator, assuming Le as unity (Le = 1) (Jain et al. 2000; Liu et al. 2007; Donggen et al. 2017). However, in the real situation it may vary from 0.5 to 1.5. First time, in this thesis, Le has been varied from 0.5 to 1.5 for investigating the heat and mass transfer characteristics of the liquid desiccant dehumidifier and regenerator. It is found that Le has significant effect on condensation and evaporation of water vapour occurring in the dehumidifier and the regenerator, respectively.

6.6 Summary

A two dimensional finite difference model has been developed for analyzing the variations of air and desiccant properties and the rates of water evaporation and condensation in the packed tower. In order to solve the developed model numerically, a recursive algorithm has been proposed. The simulated results are in good agreement with the experimental results and as well as the numerical prediction reported in the literature. The variation of air and desiccant properties along the length and height of the packed tower (dehumidifier/regenerator) are visualized through contour plots and it is found that these parameters will vary in both transverse and longitudinal flow directions. The desiccant concentration variation along the transverse direction is negligible whereas the air enthalpy, air specific humidity and desiccant enthalpy have significant variation along their transverse directions. The influence of Le on operating and performance parameters of the dehumidifier and regenerator and the influence of inlet parameters on the performance of the packed tower are also investigated.

CHAPTER – 7

ENTRANSY ANALYSIS

In this chapter, entransy dissipation theory of the liquid desiccant regenerator is introduced. Expressions are derived for entransy dissipation along the liquid desiccant regenerator. A concept of entransy efficiency of the regenerator is presented. Further, the present study highlights the importance of entransy dissipation occurring in an adiabatic regenerator.

7.1 Entransy analysis model

Entransy is a newly defined parameter which evaluates the transport ability of heat and also, it is used for optimizing the heat transfer process (Guo et al. 2007; Xia et al. 2009). The relationship between the latent entransy dissipation due to irreversible mass transfer process and sensible entransy dissipation due to irreversible heat transfer process is shown in Fig. 7.1a. During the coupled heat and mass transfer processes in the liquid desiccant regenerator, there will always be a vapour pressure difference and temperature difference between the ambient air and the liquid desiccant due to latent and sensible heat dissipations existing in the system. Thus, in order to evaluate the latent and sensible heat dissipation capabilities due to irreversible heat and mass transfer processes, entransy is chosen as a performance tool.

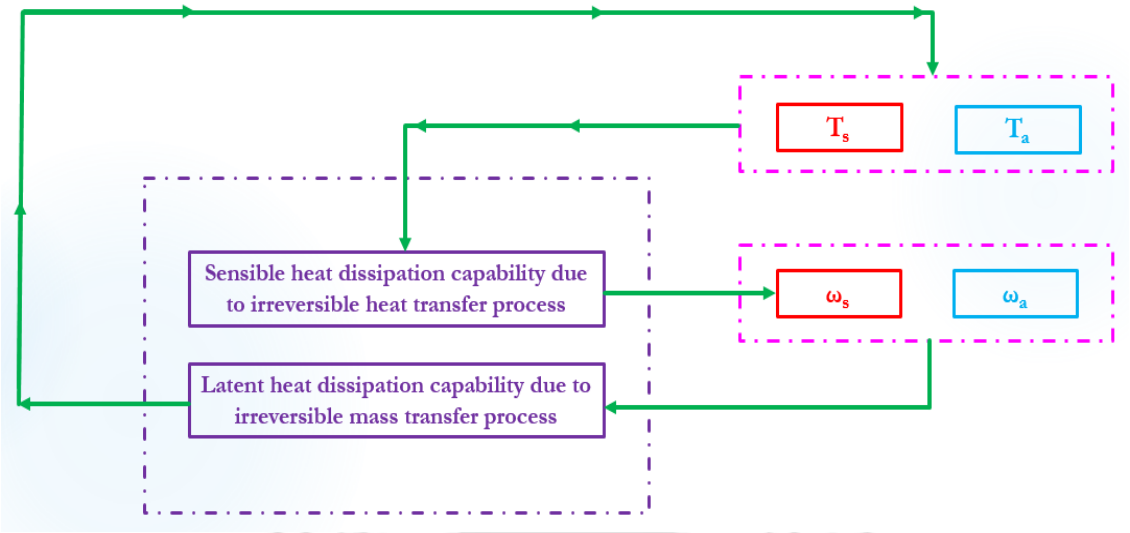

(a) Entransy dissipiation due to sensible and latent heats

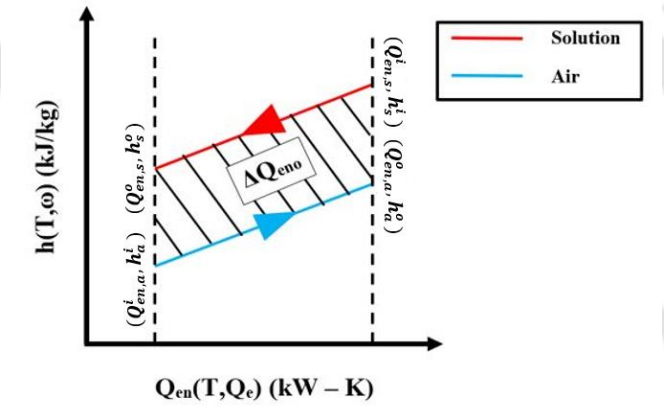

(b) Q_{en} – h chart

Fig. 7.1, Entransy dissipation process along the liquid desiccant regenerator.

Fig. 7.1b shows the overall entransy dissipation capability (ΔQ_{en}) of counter – flow liquid desiccant regenerator using Q_{en} – h chart. Assuming thermo – physical properties of the air and desiccant solution as constant, the air and desiccant solution entransy dissipation for a given air and solution enthalpy is plotted. In order to evaluate the overall entransy dissipation during coupled heat and mass transfer processes between the liquid desiccant and the ambient air, this Q_{en} – h chart is used.

The entransy dissipation for analyzing the heat transfer potential of the given system is expressed as (Guo et al. 2007; Xia et al. 2009; Zhang et al. 2016)

$$Q_{en}(T,Q_e)=\int_0^T Q_e dT \tag{7.1}$$

As $Q_e = Q_{es} + Q_{el} = \dot{m}\phi_s + \dot{m}\phi_l$; for sensible and latent heat generation processes, Eq. 7.1 can be formulated as

$$Q_{en}(T,Q_e)=\dot{m}\left(\int_0^T \phi_s dT+\int_0^T \phi_l dT\right) \tag{7.2}$$

where ϕ_s and ϕ_l denotes the sensible and latent enthalpies (kJ/kg).

For analyzing the entransy dissipation of moist air and desiccant solution flowing along the liquid desiccant regenerator, Eq. 7.2 can be reformulated as

Moist air:

$$Q_{en,a}(T_a,Q_{e,a})=\dot{m}_a\left(C_{p,a}\int_0^{T_a} T_a dT_a+\varphi\omega_a\int_0^{T_a} dT_a\right)\ \left(\because \phi_{s,a}=C_{p,a}\,\mathrm{T}_a \,\&\, \phi_{l,a}=\varphi\omega_a\right) \tag{7.3}$$

$$\text{or: } Q_{en,a}(T_a,Q_{e,a})=\tfrac{1}{2}\dot{m}_a C_{p,a}T_a^{\,2}+\dot{m}_a\varphi\omega_a T_a \tag{7.3a}$$

Desiccant solution:

$$Q_{en,s}(T_s,Q_{e,s})=\dot{m}_s\left(C_{p,s}\int_0^{T_s} T_s dT_s+\varphi\omega_s\int_0^{T_s} dT_s\right)\left(\because \phi_{s,s}=C_{p,s}\,\mathrm{T}_s \,\&\, \phi_{l,s}=\varphi\omega_s\right) \tag{7.4}$$

$$\text{or: } Q_{en,s}(T_s,Q_{e,s})=\tfrac{1}{2}\dot{m}_s C_{p,s}T_s^{\,2}+\dot{m}_s\varphi\omega_s T_s \tag{7.4a}$$

7.1.1 Entransy dissipation in the liquid desiccant regenerator

The overall entransy dissipation during coupled heat and mass transfer processes between the liquid desiccant and the ambient air is defined as (see Fig. 7.1b),

$$\Delta Q_{eno}=Q^i_{en,s}+Q^i_{en,a}-Q^o_{en,a}-Q^o_{en,s} \tag{7.5}$$

where,

$$Q_{en,a}^{i} = \tfrac{1}{2}\dot{m}_a C_{p,a} T_a^{i2} + \dot{m}_a \varphi \omega_a^{i} T_a^{i} \tag{7.5a}$$

$$Q_{en,a}^{o} = \tfrac{1}{2}\dot{m}_a C_{p,a} T_a^{o2} + \dot{m}_a \varphi \omega_a^{o} T_a^{o} \tag{7.5b}$$

$$Q_{en,s}^{i} = \tfrac{1}{2}\dot{m}_s C_{p,s} T_s^{i2} + \dot{m}_s \varphi \omega_s^{i} T_s^{i} \tag{7.5c}$$

$$Q_{en,s}^{o} = \tfrac{1}{2}\dot{m}_s C_{p,s} T_s^{o2} + \dot{m}_s \varphi \omega_s^{o} T_s^{o} \tag{7.5d}$$

7.1.2 Entransy efficiency

The ratio of overall entransy dissipation to the inlet entransy dissipation of the hot fluid within a system is termed as entransy efficiency (Gu and Gan, 2014). For the liquid desiccant regenerator, it is introduced as

$$\eta_{en} = 1 - \frac{Q_{en,s}^{o}}{Q_{en,s}^{i}} \tag{7.6}$$

7.2 Entransy analysis of the liquid desiccant regenerator

Entransy analysis model developed in the above section is adopted for analyzing the entransy dissipation along the liquid desiccant regenerator. The experimental data reported by Fumo and Goswami (2002) is chosen for entransy analysis of the liquid desiccant regenerator. The latent heat of vaporization (φ) is assumed to be constant at 2346 kJ/kg for a given desiccant temperature and concentration encountered in the system (Gandhidasan, 2005). Overall entransy analysis results of the liquid desiccant regenerator are presented in Table 7.1a. It is observed that overall entransy dissipated is in the range of $4 \times 10^3 - 10 \times 10^3$ kW–K. Also, entransy efficiency of the liquid desiccant regenerator is in the range of 16 – 27 %.

7.2.1 Entransy analysis along the height of the liquid desiccant regenerator

As discussed in Section 5.1.4, for analysing the entransy dissipation along the height of the counter – flow liquid desiccant regenerator, the desiccant temperature and specific humidity are varied simultaneously by keeping the rest of the operating parameters as constant (air and

desiccant flow rates, air temperature and desiccant concentration are kept constant). Based on the aforementioned variation of operating parameters, the experiment no. 10 and 6 from Table – 7.1a are taken as inlet condition – I and inlet condition – II for entransy analysis along the height of the liquid desiccant regenerator. During this analysis, the desiccant temperature is increased from 60.3 °C to 65 .2 °C and the specific humidity is decreased from 18.7 g_{wv}/kg_{da} to 14.3 g_{wv}/kg_{da} simultaneously by keeping rest of operating parameters as constant. The height of the liquid desiccant regenerator is taken as 0.6 m (Fumo and Goswami 2002).

Table 7.1a, Entransy analysis of liquid desiccant regenerator (Fumo and Goswami, 2002).

Exp. no.	$\dot{m}_a$ (kg/s)	T_a^i (°C)	ω^i (g_{wv}/kg_{da})	$\dot{m}_s$ (kg/s)	T_s^i (°C)	β^i ($kg_{LiCl}/kg_{sol.}$)	$\Delta Q_{en,o}$ ($kW - K \times 10^3$)	η_{en} (%)
1	0.039	30.4	18.3	0.30	65	34	4.89	16.0
2	0.052	30.1	18	0.29	65.1	34.1	5.28	16.1
3	0.068	29.8	17.7	0.30	65.1	34.5	6.26	19.0
4	0.052	35.1	18	0.30	65.1	33.4	5.30	19.8
5	0.052	40	17.8	0.30	65	33.6	5.04	20.8
6	0.053	30.2	14.3	0.30	65.2	34	5.73	19.4
7	0.052	29.4	21	0.30	65.5	33.6	5.52	16.6
8	0.052	30.3	18.2	0.24	65.4	34.4	5.05	19.4
9	0.052	29.9	18	0.35	65.2	34.3	6.53	17.8
10	0.052	30	18.7	0.29	60.3	34.4	3.53	11.7
11	0.051	29.7	18.4	0.30	70	34.5	9.68	26.5
12	0.052	29.7	17.7	0.30	64.8	32.8	5.44	18.9
13	0.052	30.3	18.2	0.30	65	34.9	5.76	18.1

The overall sensible and latent entransy dissipations along the height of the liquid desiccant regenerator for inlet conditions I & II are shown in Fig. 7.2. As the regenerator height increases, overall latent and sensible entransy dissipations also increase for both the inlet conditions. This is due to the fact that as the tower height increases, the temperature difference between the desiccant solution and the ambient air decreases and the specific humidity difference between the ambient air and saturated air also decreases, thereby decreasing the irreversible latent and sensible heat transfers and increasing the sensible and latent entransy dissipation capabilities.

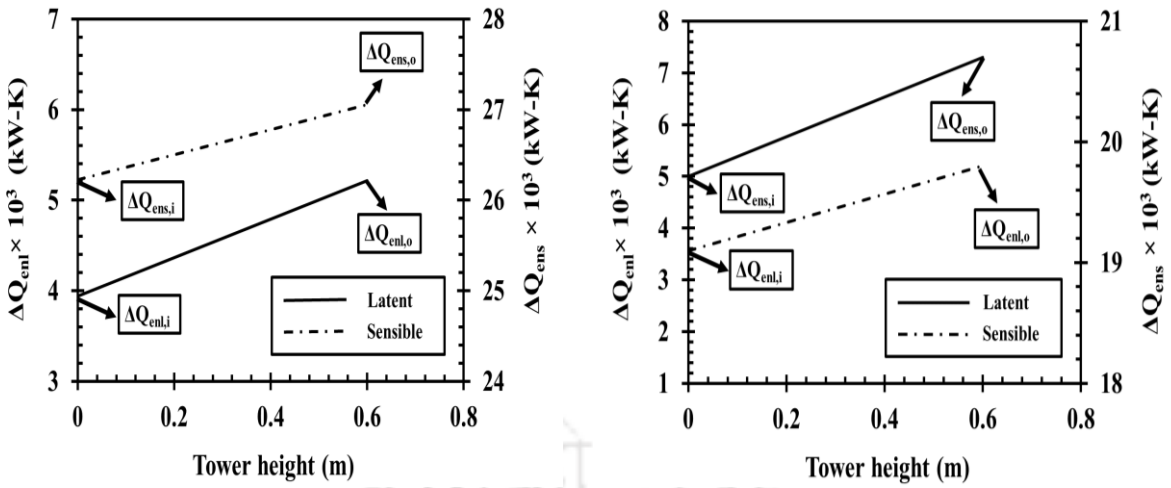

(a) Inlet condition – I (b) Inlet condition – II

Fig. 7.2, Overall latent and sensible entransy dissipations along the height of the regenerator.

By comparing the inlet conditions – I and II (Fig. 7.2a and 7.2b), it is found that the overall latent and sensible entransy dissipations are high in case of inlet condition – II compared with inlet condition – I. This is due to high potential for energy exchange in condition – II compared to condition – I. From Fig. 7.2, it is found that, for inlet condition – I and II, with increase in tower distance along the height of the packed tower, the increment in overall sensible entransy dissipations are observed to be 3% and 4 % whereas an increment in overall latent entransy dissipations are observed to be 24% and 32%, respectively. From this analysis, it is observed that with increase in height, the percentage increment in overall latent entarnsy dissipation is high compared to sensible entransy dissipation. This is due to decrease in evaporation process with increase in tower height.

Table 7.1b, Performance comparison between inlet condition – I (Exp. no. – 10 in Table 7.1a) and inlet condition – II (Exp. no. – 6 in Table 7.1a)

	Inlet condition – I	Inlet condition – II	%increment	%decrement
$\Delta Q_{en,o}$ (kW – K × 10^3)	3.53	5.73	38	–
η_{en} (%)	11.7	19.4	40	–

From Table 7.1b and Fig. 7.2, it is concluded that by increasing the desiccant temperature and decreasing the specific humidity of the regenerator, entransy dissipation along the liquid desiccant regenerator will increase.

7.2.2 Influence of operating parameters on entransy efficiency of the regenerator

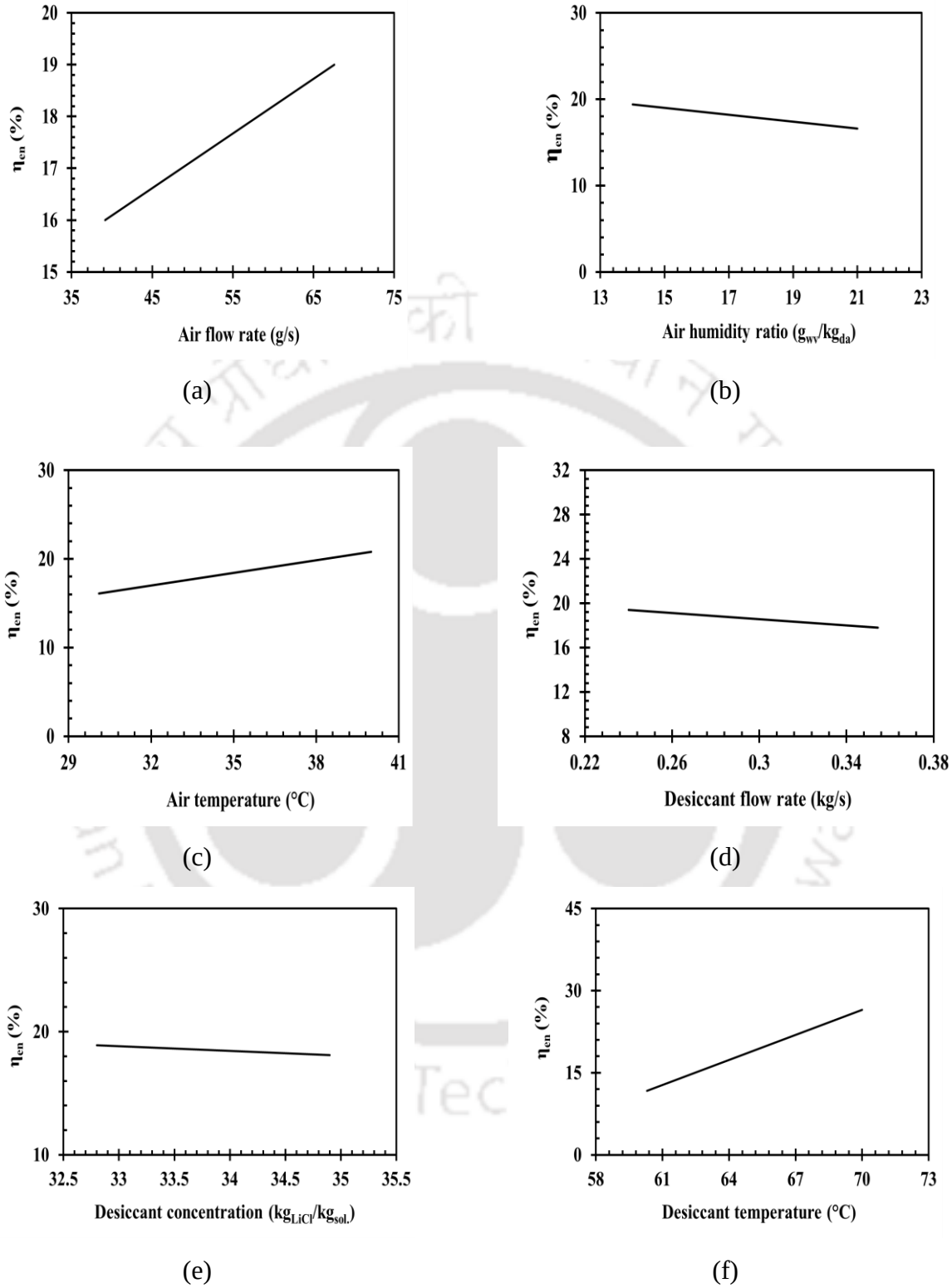

Fig. 7.3 – Influence of air and desiccant parameters on entransy efficiency of the liquid desiccant regenerator: (a) Air flow rate, (b) air humidity ratio, (c) Air temperature, (d) desiccant flow rate, (e) desiccant concentration and (f) desiccant temperature.

It is found from Fig. 7.3a and Table 7.2 that the regenerator entransy efficiency increases with increase in air flow rate. This happens because, as the air flow rate increases, less vapour transfer from the desiccant solution to the ambient air takes place. Therefore, the sensible and latent heat transfer capabilities between the ambient air and desiccant solution increases and this results in increase of entarnsy efficiency. With decrease in air humidity ratio and increase in air and desiccant temperatures, the entransy efficiency increases (Fig. 7.3a – 7.3c, 7.3f) and Table 7.2). It can be explained by the fact that when the humidity ratio decreases and air and desiccant temperatures increase, the sensible and latent heat dissipation capabilities existing in the regeneration system increase, thereby increasing the regenerator entarnsy efficiency. As the desiccant flow rate increases, the entarnsy efficiency decreases (Fig. 7.3d and Table 7.2). This happens because as the desiccant flow rate increases, the desiccant solution will be in contact with the ambient air for shorter duration, maintaining higher potential for latent and sensible heat transfer processes. As a consequence, latent and sensible entransy dissipations decrease. With increase in desiccant concentration, the change in entransy efficiency is negligible (Fig. 7.3e and Table 7.2).

Table 7.2, Influence of operating parameters on entransy efficiency of the regenerator (Fig. 7.3).

	Range	η_{en}	
		% increment/ decrement	
Air flow rate (kg/s) (↑)	39.2 – 67.6	↑	19
Desiccant flow rate (kg/s) (↑)	0.24 – 0.35	↓	9
Air humidity ratio (g_{wv}/kg_{da}) (↑)	14 – 21	↓	17
Desiccant concentration ($kg_{LiCl}/kg_{sol.}$) (↑)	32.8 – 34.9	↔	–
Air temperature (°C) (↑)	30.1 – 40	↑	29
Desiccant temperature (°C) (↑)	60.3 – 70	↑	126

*(↑) – Increment; (↓) – Decrement; (↔) – Intermediate (no change);

7.3 Summary

Entransy analysis model has been developed for analysing the performance of the liquid desiccant regeneration system. With the simplified expressions formulated in the present work, entransy dissipation due to irreversible sensible and latent loads is quantified. A new concept of entransy efficiency of the regenerator has been introduced. Entransy dissipation along the

height of the liquid desiccant regenerator is quantified during coupled heat and mass transfer processes. The influence of air and desiccant temperatures, air and desiccant flow rates, air humidity ratio and desiccant concentration on entransy efficiency of the liquid desiccant regenerator is also investigated.

CHAPTER – 8

CONCLUSIONS AND FUTURE SCOPE

This chapter outlines the major conclusions drawn from the numerical, experimental, energy and exergy analyses of the liquid desiccant dehumidification/regeneration system and evacuated U – tube solar collector system. Further, key observations made from the entransy dissipation theory of the liquid desiccant regenerator are also summarized.

8.1 Liquid desiccant dehumidification/regeneration system

8.1.1 Numerical studies

Developed the thermal models for counter and cross-flow liquid desiccant dehumidifier/regenerator for analysing the heat and mass transfer aspects at the air – desiccant interface. Introduced backtracking and recursive algorithms for solving the developed thermal models of the counter and cross-flow liquid desiccant dehumidifier/regenerator, respectively. Derived expressions for heat and mass transfer coefficients in terms of thermal and moisture effectiveness. Plotted distribution contours for analysing the heat and mass transfer characteristics along the height of the liquid desiccant dehumidifier/regenerator and observed that condensation/evaporation rate decreases along the ambient air flow direction. Further, theoretically analysed the effect of Lewis number and inlet parameters on the performance of the liquid desiccant dehumidifier/regenerator. The key observations from the performance analysis are as follows:

- With increase in Le, the variation in air and desiccant properties is more prominent in the regenerator compared to the dehumidifier. This is because of high temperature difference and vapour pressure difference at the air – desiccant interface of the dehumidifier.
- With increase in Le from 0.5 to 1.5, condensation rate in the dehumidifier and the evaporation rate in the regenerator decreases. It is due to decrease in mass transfer between the air and the desiccant solution.
- In order to improve the performance of the liquid desiccant dehumidifier and regenerator, the Le should be maintained less than one (Le < 1).
- It is found that the variation of Le has a significant effect on the air enthalpy and humidity ratio and desiccant enthalpy in the packed tower and has an insignificant effect on the desiccant concentration in the packed tower.
- At Le = 1, with decrease in air specific humidity from 26.7 g_v/kg_{da} to 14.7 g_v/kg_{da} and air temperature from 32 ^oC to 24 ^oC, condensation rate in the dehumidifier decreases by 22.3 % and 75 %, respectively whereas with decrease in desiccant temperature from 31 ^oC to 23 ^oC, it increases by 68 %.
- At Le = 1, with decrease in air specific humidity from 26.7 g_v/kg_{da} to 14.7 g_v/kg_{da} and air temperature from 32 ^oC to 24 ^oC, evaporation rate in the regenerator increases by 28% (for both the cases) whereas with decrease in desiccant temperature from 63 ^oC to 55 ^oC, it decreases by 75%.

8.1.2 Experimental studies

In accordance with humid subtropical climate, an experimental investigation is carried out with the fabricated liquid desiccant dehumidification/regeneration system using LiCl as liquid desiccant. Further, developed an experimental correlation for specific humidity ratio difference in terms of inlet parameters. From the experimental analysis, following important observations are made;

- With increase in relative humidity, solution enthalpy and air specific humidity has significant impact on performance of the dehumidification system whereas in the regeneration system, solution enthalpy, air specific humidity and air enthalpy has a significant impact.
- From the developed correlations for specific humidity difference of dehumidification and regeneration systems, it is observed that with increase in L/G ratio, from 0.8 to 3.9, the

vapour transfer between the desiccant solution and the ambient air decreases by 51% and 58% during dehumidification and regeneration processes, respectively.

- In order to increase the latent heat of condensation in the dehumidification system and latent heat of evaporation in the regeneration system, the Lewis number (Le) needs to be less than one and L/G ratio should be maintained as low as possible.
- For a given operating conditions, it is found that as the relative humidity increases from 63% to 87%, and decreases by 39% in the dehumidification and regeneration systems, respectively.
- During maximum vapour transfer process in the dehumidification and regeneration systems, the latent energy exchange between the desiccant solution and ambient air is predominant than sensible energy exchange.

8.1.3 EEE analyses of liquid desiccant regenerator

Energy, exergy and entransy (EEE) models have been developed for analysing the performance of the liquid desiccant regeneration system. With the simplified expressions formulated in the present work, energy required for regeneration of the liquid desiccant, exergy destroyed with respect to reference state and entransy dissipation due to irreversible sensible and latent loads are quantified. A new concept of entransy efficiency of the regenerator has been introduced. Energy exchange, exergy loss and entransy dissipation along the height of the liquid desiccant regenerator are quantified during coupled heat and mass transfer processes. The influence of air and desiccant temperatures, air and desiccant flow rates, air humidity ratio and desiccant concentration on desorption, entransy and exergy efficiencies of the liquid desiccant regenerator are also investigated. The major conclusions from EEE analyses of the regeneration system are as follows:

- With increase in regenerator height, the air temperature, humidity ratio and exergy destruction of the air increase whereas the desiccant temperature, water content in the desiccant solution and exergy destruction of the solution decrease. Also, the latent and sensible entransy dissipation capabilities due to irreversible heat and mass transfer process are also found to increase.
- It is observed that by increasing the desiccant inlet temperature from 60.3 °C to 65.2 °C and decreasing the air inlet humidity ratio from 18.7 g_{wv}/kg_{da} to 14.3 g_{wv}/kg_{da} simultaneously, potential for energy exchange between the desiccant solution and air increases by 26% and overall entransy dissipation and exergy destruction in the liquid

desiccant regenerator increase by 39% and 37%, respectively. Also, the exergy efficiency of the regenerator decreases by 10% whereas the entransy and desorption efficiencies of the regenerator increase by 27% and 40%, respectively.

- By investigating the influence of operating parameters on desorption, exergy and entransy efficiencies of the regenerator, it has been concluded that the desiccant temperature has a more significant influence on the performance of the regeneration system compared to other operating parameters.

8.2 Evacuated U – tube solar collector system

8.2.1 Numerical studies

Developed three dimensional thermal model for analysing the heat transfer process occurring across the evacuated U – tube solar collector and introduced a time dependent three dimensional model for analysing the thermal process occurring along the evacuated U – solar collector system. Numerically predicted the performance of the individual evacuated U – tube solar collector and whole evacuated U – tube collector bundle connected in series. By employing filler material theoretically investigated the heat transfer enhancement along the evacuated U – tube solar collector. From the numerical studies following conclusions are drawn.

- Copper is the best material compared to brass and aluminium as a fin material and water is better than air as working fluid.
- For a given U–tube material, with increase in flow rate, the useful heat absorption capacity increases. It is observed that by increasing the flow rate from 0.01 to 0.05 kg/s, the net heat absorption rate of copper increases by 84 % for water as working fluid and 82.5 % for air as working fluid.
- The performance of low thermal conductive U–tube material can be improved by increasing the flow rate of the working fluid.
- For a given flow rate, a high collector efficiency is achieved for water and copper as working fluid and U–tube material combination and a low collector efficiency is achieved for air and brass as working fluid and U–tube material combination. For the aforementioned working fluid and U–tube material combination, the higher/lower collector efficiency is attained to be 76%/24%.
- Compared to magnesium oxide and aluminium oxide filler material, graphite filler yields higher efficiency. Employing graphite as filler material in between the evacuated tube

absorber surface (fin) and the U–tube, the thermal efficiency of the existing evacuated tube solar collector is increased by 15.3%.

8.2.2 Experimental studies

Designed and fabricated an evacuated U – tube solar collector system and experimentally investigated the performance of this system in accordance with humid subtropical climate. Developed an experimental correlation for working fluid transition time as a function of process parameters. By investigating the performance of the evacuated U – tube solar collector system experimentally, following important observations are made;

- Solar intensity, working fluid flow rate and working fluid inlet temperature have significant influence on useful heat gained by the working fluid flowing inside an evacuated U – tube solar collector. Whereas, the ambient temperature does not have any significant effect on useful heat flux.
- For a given range of operating parameters, increasing the number of manifolds (integrated with ten evacuated U – tubes) connected in series will provide higher temperature raise at high solar intensity, lower working fluid inlet temperature and higher flow rate of working fluid.
- In accordance with humid subtropical climate, the maximum working fluid (water) temperature difference between the inlet and exit of each manifold was observed as 6.1 ^{o}C. Within the range of operating parameters investigated, the maximum working fluid transition time in an evacuated U – tube was recorded as 327 s.
- From the developed correlation for working fluid transition time, it is observed that the ambient temperature has an insignificant effect on the variation of transition time compared to other operating parameters such as solar intensity and working fluid inlet temperature and flow rate.

8.2.3 Energy and exergy analyses

Developed two experimental correlations for energy efficiency and exergy efficiency as a function of process parameters. Energy and exergy analyses of the individual evacuated U – tube solar collector and whole solar collector system are analysed and following conclusions are drawn;

- Within the range of parameters varied, the maximum energy efficiency of the evacuated U – tube solar collector was found to be 72 % at a lower normalized heat gain of 0.8 (m^2 – K/kW). The average energy efficiency of the solar collector was observed as 51%.
- Influences of solar intensity and working fluid flow rate on energy efficiency of the evacuated U – tube solar collector is prominent compared to ambient and working fluid temperatures.
- During a sunny day, the peak energy efficiency of 52 % was observed in between 1: 00 PM – 3: 00 PM whereas low energy efficiency of 31 % was observed at 8:30 AM and 5: 30 PM for the evacuated U – tube solar collector system.
- The exergy efficiency of the evacuated U – tube solar collector and the solar collector system increase as the time progress. The exergy destruction of the evacuated U – tube solar collector and the solar collector system is high at 8: 30 AM.
- In a humid subtropical climatic conditions, the average estimated energy and exergy efficiencies of the evacuated U – tube solar collector system during a sunny day are 43 % and 41 %, respectively.

8.3 Future scope

The work presented in the thesis opens up several opportunities to broaden the research work on solar driven liquid desiccant ACS components (Liquid desiccant dehumidifier, liquid desiccant regenerator and evacuated U – tube solar collector). The scope of future work is outlined is as follows:

8.3.1 Liquid desiccant dehumidification system

- This system can be alternatively used in solar dryer applications.
- Hybrid systems can be formed by integrating with solid desiccant based dehumidification system or with another liquid desiccant based dehumidification system for deep drying applications.
- Thermal model can be extended considering the pressure drop across the packed tower.

8.3.2 Liquid desiccant regeneration system

- Liquid desiccant regeneration system can be integrated with the waste heat recovery heat exchanger for air preheating purposes.

- This system can be integrated with heat storage system (using low/medium scale heat storage materials) for waste heat recovery.
- Hybrid systems can be formed by integrating with solid desiccant based dehumidification system or with another liquid desiccant based dehumidification system for solar dryer applications.
- Thermal model can be extended considering the pressure drop across the packed tower.

8.3.3 Evacuated U – tube solar collector system

- Performance of these systems can be improved by integrating with parabolic reflector as well as by using novel U – tube designs.
- For increasing the instantaneous working fluid heat gain, no. of manifolds can be connected in series.
- Instead of evacuated U – tubes connected in parallel to the manifold, they can also be integrated in series for maximizing the instantaneous working fluid heat gain.
- For heating more amount of working fluid at less time, the manifolds can be connected in parallel.

8.3.4 Liquid desiccant materials

- The liquid desiccant materials such as potassium formate, potassium acetate, lithium nitrate, magnesium chloride, sodium formate and sodium sulphate can be used for dehumidification purpose.
- Composite materials (mixing of two or three desiccants) may be also explored for improving vapour absorption capability.
- There are many natural liquid desiccant materials; research needs to be carried out to utilise these desiccant materials.

REFERENCES

Ameel TA, Gee KG, Wood BD (1995) Performance predictions of alternative, low cost absorbents for open-cycle absorption solar cooling, Solar Energy, vol. 54, pp. 65–73.

Ataee S, Ameri M (2015) Energy and exergy analysis of all-glass evacuated solar collector tubes with coaxial fluid conduit, Solar Energy, vol. 118, pp. 575 – 591.

Al-Farayedhi AA, Gandhidasan P, Al-Mutairi MA (2002) Evaluation of heat and mass transfer coefficients in a gauze-type structured packing air dehumidifier operating with liquid desiccant, International Journal of Refrigeration, vol.25, pp. 330–339.

ASHRAE fundamentals (1989) Atlanta, Georgia: American Society of Heating, Refrigerating and Air-Conditioning Engineers.

Ayala JAA, Rodriguez GM, Nunez MP, Ramirez ARU, Munoz AG (2015) Numerical study of a low temperature water-in-glass evacuated tube solar collector, Int. J. Energy Convers Manage., vol. 94, pp. 472–481.

Amir R, Davoud B (2013) Mathematical modeling of a packed-bed air dehumidifier: The impact of empirical correlations. Journal of Petroleum Science and Engineering, vol. 108, pp. 222 – 229.

Bravo JL, Rocha JA, Fair JR (1985) Mass transfer in gauze packing's, Hydrocarbon Processing, vol.64, pp. 91-105.

Babakhani D, Soleymani M (2010) Simplified analysis of heat and mass transfer model in liquid desiccant regeneration process. Journal of the Taiwan Institute of Chemical Engineers, vol. 41, pp. 259–267.

Badar AW, Buchholz B, Ziegler F (2011) Experimental and theoretical evaluation of the overall heat loss coefficient of vacuum tubes of a solar collector, Int. J. Solar Energy, vol. 85, pp. 1447–1456.

Chen LC, Kuo CL, Shyu RJ (1989) The performance of a packed bed dehumidifier for solar liquid desiccant systems, Annual Solar Energy Conference, California, pp. 371-377.

Chen XY, Jiang Y, Li Z, Qu KY (2005) Field study on independent dehumidification air-conditioning system – I: performance of liquid desiccant dehumidification system. ASHRAE Transactions vol.111, pp. 271–76.

Chen G, Liu C, N. Li, F. Li (2017) A study on heat absorbing and vapour generating characteristics of H2O/LiBr mixture in an evacuated tube, Applied Energy ,vol.185,pp. 294 – 299.

Chung TW, Lai CH, and Wu H (1999) Analysis of Mass Transfer Performance in an Air Stripping Tower, Separation Science and Technology, vol.34, pp.2837-2851.

Conde MR (2004) Properties of aqueous solutions of lithium and calcium chlorides: formulations for use in AC equipment design, Int. J. Thermal Sciences vol. 43,pp. 367–382.

Coellner J (1986) Energymaster—Desiccant Cooling in the Marketplace, Desiccant Cooling and Dehumidification Opportunities for Buildings Workshop, Chattanooga, TN.

Dai YJ, Zhang HF (2004) Numerical simulation and theoretical analysis of heat and mass transfer in a cross-flow liquid desiccant air dehumidifier packed with honeycomb paper, Energy Conversion and Management, vol.45, pp.1343-1356.

Daghigh R, Shafieian A (2016) Energy – exergy analysis of a multipurpose evacuated tube heat pipe solar water heating – drying system, Experimental Thermal and Fluid Science vol. 78, pp. 266 – 277.

Daou K, Wang RZ, Xia ZZ (2006) Desiccant cooling AC: a review, Renewable and Sustainable Energy Reviews, vol.85, pp. 55–77.

Davoud B, Meysam S (2009) An analytical solution for air dehumidification by liquid desiccant in a packed column, International Common Heat Mass, vol.36, pp. 969–77.

Datta N, Chakraborty A, Ali SM, Choo FH (2017) Experimental investigation of multi-effect regenerator for desiccant dehumidifier: Effects of various regeneration temperatures and solution flow rates on system performances. Int. J. Refrigeration, vol.76, pp. 7 – 18.

Donggen P, Junming Z, Danting L (2017) Exergy analysis of a liquid desiccant evaporative cooling system. Int. J. Refrigeration,vol. 82,pp. 495 – 508.

Derringer G, Suich R (1980) Simultaneous Optimization of Several Response Variables, Journal of Quality Technology, vol.12, pp.214–219.

Dincer I, Rosen MA, (2007) Exergy, Energy, Environment and Sustainable Development, 1st ed., Elsevier, UK.

Diaz G (2010), Numerical investigation of transient heat and mass transfer in a parallel-flow liquid-desiccant absorber, Heat and Mass Transfer, vol. 46, pp. 1335 – 1344.

Deng J, Wang RZ, Han GY (2011) A review of thermally activated cooling technologies for combined cooling, heating and power systems, Progress in Energy and Combustion Science vol.37 pp. 172-203.

Ducool, <www.ducool.com> (retrieved April 2015).

Eberlein MB (1976) Analysis and Performance Predictions of Evacuated Tubular Solar Collectors using Air as the Working Fluid, University of Wisconsin.

Elsarrag E, Ali EEM, Jain S (2005) Design Guidelines and Performance Study on a Structured Packed Liquid Desiccant ACS, HVAC & R Research, 11 319–337.

Factor HM, Grossman G (1980) A packed bed dehumidifier/ regenerator for solar AC with liquid desiccants Solar Energy, vol.24, pp. 541–550.

Fang Y, Guo J, Li D, Gao X (2011) Chacterisation of rare earth modified zeolites for dehumidification, Chemcial Engineering Journal (Chinese), vol.6, pp. 25–29.

Fumo N, Goswami DY, (2002) Study of an aqueous lithium chloride desiccant system: Air dehumidification and desiccant regeneration,Solar Energyvol.72, pp. 351–361.

Factor HM, Grossman G (1980) A packed bed dehumidifier/regenerator for solar AC with liquid desiccants, Solar Energy, vol. 24, pp. 541–550.

Farjallah R ,Chaabane M ,Mhiri H, Bournot P, Dhaouadi H (2016) Thermal performance of the U – tube solar collector using computational fluid dynamics simulation, Journal of Solar Energy Engineering, ASME Transactions, vol. 138, pp. 1– 8.

Farayedhi AA, Gandhidasan P, Al-Mutairi MA (2002) Evaluation of heat and mass transfer coefficients in a gauze-type structured packing air dehumidifier operating with liquid desiccant. Int. J. Refrigeration, vol.25, pp. 330 – 339.

Gandhidasan P (2004) A simplified model for air dehumidification with liquid desiccant, Solar Energy vol.76, pp. 409-416.

Gandhidasan P, (2005) Quick performance prediction of liquid desiccant regeneration in a packed bed, Solar Energyvol.76, pp. 409–416.

Gao WZ, Liu JH, Cheng YP (2012) Experimental investigation on the heat and mass transfer between air and liquid desiccant in a cross-flow dehumidifier, Renew. Energy, vol.37, pp.117–123.

Gao Y, Fan R, Zhang XY, An YJ, Wang MX, Gao YK, Yu Y (2014) Thermal performance and parameter analysis of a U-pipe evacuated solar tube collector, Int. J. Solar energy, vol. 107, pp. 714-727.

Gautam A, Chamoli S, Kumar A, Singh S (2017) A review on technical improvements, economic feasibility and world scenario of solar water heating system, Renewable and Sustainable Energy Reviews , vol. 68, pp. 541 – 562.

Genius, <www.geniusac.com> (retrieved April 2015).

Gershon G, Alex J (1981) Solar cooling and AC, Energy Combustion Science journal, vol.7, pp. 185-228.

Ghafoor A, Munir A (2015) Worldwide overview of solar thermal cooling technologies Renewable and Sustainable Energy Reviews vol.43 pp.763-774.

Gommed K, Grossman G (2004) A Liquid Desiccant System for Solar Cooling and Dehumidification, Journal of Solar Energy Engineering vol.126 pp. 879-885.

Guo ZY, Zhu HY, and Liang XG (2007) Entransy—A physical quantity describing heat transfer ability, Int. J. Heat Mass Transfervol.50, pp. 2545–2556.

Gu J, Gan Z (2014) Entransy in phase – change systems, Springer Briefs in Thermal Engineering and Applied Science, pp. 11 – 19.

Gurubalan A, Maiya MP, Tiwari S (2017) Performance characterization of membrane dehumidifier with desiccants in flat-plate arrangement. Energy and Buildings, vol. 156, pp. 151 – 162.

Ha CX, Dai YJ, Wu JY, Wang RZ (2006) Experimental comparison of two honeycombed desiccant wheels fabricated with silica gel and composite desiccant material, Energy Conversion and Management, vol.47, pp. 2523–2534.

Hamed AM (2003) Desorption characteristics of desiccant bed for solar dehumidification/humidification ACSs, Renewable Energy, vol.28, pp. 2099-2111.

Huang S, Lv Z, Liang C, Zhang X (2017) Experimental study of heat and mass transfer characteristics in a cross-flow heating tower, Int. J. Ref., vol. 77, pp. 116 – 127.

Harding G, Zhiqiang Y, Mackey DW (1985) Heat extraction efficiency of a concentric glass tubular evacuated collector, Int. J. Solar Energy, vol. 35, pp. 71–79.

Hazami M, Naili N, Attar I, Farhat A (2013) Solar water heating systems feasibility for domestic requests in Tunisia: thermal potential and economic analysis, Int. J. Energy Convers Manage., vol. 76, pp. 599–608.

Islam MR,Alan SWL, Chua KJ (2018) Studying the heat and mass transfer process of liquid desiccant for dehumidification and cooling, Applied Energy, vol. 221, pp. 334 – 347.

Jain S, Dhar PL, Kaushik SC (1994) Evaluation of liquid desiccant based evaporative cooling cycles for typical hot and humid climates, Heat Recovery System and CHP vol.14, pp. 621-632.

Jain S, Dhar PL, Kaushik SC (2000) Experimental studies on the dehumidifier and regenerator of a liquid desiccant cooling system, Applied Thermal Engineering, vol.20, pp. 253-267.

Jain S, Bansal PK (2007) Performance analysis of liquid desiccant dehumidification systems, Int. J. Refrigeration, vol.30, pp. 861-872.

Jilier, Jilier Science and Technology Co. Ltd., China, <www.jilier.com/eng2.asp> (retrieved April 2015).

Kathabar, <www.kathabar.com> (retrieved April 2015).

Kaya H, Arslan K, Elturgal N (2018) Experimental investigation of thermal performance of an evacuated U-Tube solar collector with ZnO/Ethylene glycol-pure water Nano fluids, Renewable Energy, vol.122, pp. 329 – 338.

Koronaki IP, Christodoulaki RI, Papaefthimiou VD, Rogdakis ED (2013) Thermodynamic analysis of a counter-flow adiabatic dehumidifier with different liquid desiccant materials, Applied Thermal Engineering, vol. 50, pp. 361 – 373.

Killion JD, Garimella S (2001) A critical review of models of coupled heat and mass transfer in falling-film absorption, Int. J. Refrigeration, vol. 24, pp. 755–797.

Kim H, Ham J, Park C, Cho H (2016) Theoretical investigation of the efficiency of a U-tube solar collector using various nanofluids, Energy ,vol.94,pp. 497 – 507.

Kim H, Kim J, Cho H (2017) Experimental study on performance improvement of U-tube solar collector depending on nanoparticle size and concentration of Al_2O_3 nanofluid, Energy, vol. 118, pp. 1304 – 1312.

Kline S J, Clintock MC (1953) Describing uncertainties in single – sample experiments, Journal of Mechanical Engineering pp. 3 – 12.

Khan AY, Sulsona FJ (1998) Modelling and parametric analysis of heat and mass transfer performance of refrigerant cooled liquid desiccant absorbers, International Journal Energy, vol.22, pp.813–832.

Khan AY, Ball HD (1992) Development of a generalized model for performance evaluation of packed-type liquid sorbent dehumidifiers and regenerators. ASHRAE Trans. Vol.98, pp. 525 – 533.

Khan AY (1994) Sensitivity analysis and component modelling of a packed type liquid desiccant system at partial load operating conditions. Int. J. Energy Re, vol.18, pp. 643 – 655.

Khan AY, Martinez JL (1998) Modelling and parametric analysis of heat and mass transfer performance of a hybrid liquid desiccant absorber. Energy Conversion Management, vol. 39, pp. 1095 – 1112.

Khin Z, Reza SM, Joachim L, Kim CN (2013) Analysis of a membrane based air-dehumidification unit for AC in tropical climates. Applied Thermal Engineering, vol. 59, pp. 370 – 379.

Lazzarin, RM, Gasparella A, Longo GA (1999) Chemical dehumidification by liquid desiccants theory and experiments, International Journal of Refrigeration, vol. 22, pp. 334-347.

Lamnatau C, Papanicolaou E, Belessiotis V, Kyriakis N (2012) Experimental investigation and thermodynamic performance analysis of a solar dryer using an evacuated-tube air collector, Applied Energy, vol. 94, pp. 232 – 243.

L-DCS Technology <www.l-dcs.de> (retrieved April 2015).

Liangdong M Zhen L, Jili Z, Ruobing L (2010) Thermal performance analysis of the glass evacuated tube solar collector with U-tube, Building and Environment, vol. 45, pp. 1959 – 1967.

Laingdong M, Tianyi H, Zhang J, Zhao D (2016) Numerical study on the heat transfer characteristics of filled-type solar collector with U-tube, Applied Thermal Engineering, vol. 107, pp. 642 – 652.

Liang R, Liangdong M, Zhang J, Zhao D (2011) Theoretical and experimental investigation of the filled-type evacuated tube solar collector with U tube, Solar Energy pp. 1735 – 1744.

Liu XH, Jiang Y, Qu KY (2006) Analytical solution of combined heat and mass transfer processes of cross-flow dehumidifier using liquid desiccant, TaiyangnengXuebao/Acta Energy Solar Singapore vol.27, pp.774–781.

Liu XH, Jiang Y, Xia J, Chang X (2007) Analytical solutions of coupled heat and mass transfer processes in liquid desiccant air dehumidifier/ regenerator, Energy Conversion Management vol.48, pp.2221–2232.

Liu XH, Jiang Y, Qu (2007) Heat and mass transfer model of cross-flow liquid desiccant air dehumidifier/regenerator, Energy Conversion Management, vol.48, pp. 46–54.

Liu XH, Qy KY, Jiang Y (2006) Experimental study on mass transfer performances of cross-flow dehumidifier using liquid desiccant, Energy Conversion and Management, vol.47, pp. 2682-2692.

Liu X, Jiang Y, Xia J, Chang X., (2010) Analytical solutions of coupled heat and mass transfer processes in liquid desiccant air dehumidifier/regenerator,Energy Conversion and Managementvol.48, pp. 2221–2232.

Luo Y, Yang H, Lu L (2014) Liquid desiccant dehumidifier: Development of a new performance predication model based on CFD, Int. J. Heat Mass Transf., vol.69, pp.408 – 416.

Luo Y, Yang H, Lu L (2014) Dynamic and microscopic simulation of the counter-current flow in a liquid desiccant dehumidifier, Applied Energy, vol.136, pp.1018 – 1025.

Luo Y, Yang H, Lu Land Qi R (2014) A review of the mathematical models for predicting the heat and mass transfer process in the liquid desiccant dehumidifier, Renewable and Sustainable Energy Reviews, vol. 31, pp. 587–599.

Longo GA, Gasparella G (2005) Experimental and Theoretical Analysis of heat and mass transfer in a packed column dehumidifier/regenerator with liquid desiccant,Int. J. Heat Mass Transfer vol.48, pp. 40 – 52.

Longo GA, Gasparella A (2016) Experimental measurement of thermophysical properties of H2O/KCOOH (potassium formate) desiccant, Int. J. Ref., vol. 62, pp. 106 – 113.

Lowenstein A, Slayzak S, Kozubal E (2007) A zero carryover liquid desiccant air conditioner for solar applications, Proceedings of International Solar Energy Conference, pp.397 – 407.

Lucio CD, Mesquita S (2007) Analysis of a Flat-Plate, Liquid-Desiccant, Dehumidifier and Regenerator, PhD thesis, Queen's University.

Lu ZF, Chen PL, Zhang X (2001) Approximate analytical solution of heat and mass transfer processes in packed-type cross-flow liquid desiccant system and its experimental verification, J Tongji University vol.29, pp.149–53.

Martin V, Goswami DY (2000) Effectiveness of Heat and Mass Transfer Processes in a Packed Bed Liquid Desiccant Dehumidifier/Regenerator, HVAC&R Res. vol.6, pp. 21 – 39.

Mei VC, Chen FC, Lanan Z, Collier RK, Meckler G (1992) An assessment of desiccant cooling and dehumidification technology, Oak Ridge National Laboratory.

Mehrorang G, Syamak NK (2015) Removal of methylene blue from aqueous solution by wood millet carbon optimization using response surface methodology, Spectrochimica Acta Part A: Molecular and Biomolecular spectroscopy, vol.136, pp.141 – 148.

Mesquita LCS, Harrison SJ (2005) Non-isothermal, flat-plate liquid-desiccant regenerators: A numerical study, International Solar Energy Conference, pp.325 – 331.

Morrison G, Budihardjo I, Behnia M (2005) Measurement and simulation of flow rate in a water-in-glass evacuated tube solar water heater, Int. J. Solar Energy, vol. 78, pp. 257–267.

Miller J, Lowenstein A (2008) The field operation of a thermally driven Liquid-desiccant air conditioner, International Solar Energy Conference.

Miao RS (1997) Study of alternative liquid absorbents using a thermodynamic model and a combined physico-optical method, PhD thesis, Department of Mechanical Engineering, University of Illinois at Chicago, Chicago.

McDonald B, Waugman DG, Kettleborough CF (1992) A statistical analysis of a packed tower dehumidifier, Drying Technology, vol.10, pp.223–237.

Muthukumar P, Naik BK, Goswami A (2018) Performance Evaluation of a Mechanical Draft Cross-flow Cooling Towers Employed in a Subtropical Region, Journal of The Institution of Engineers (India): Series C, pp. 1–9.

Naik BK, Muthukumar P (2017) A novel approach for performance assessment of mechanical draft wet cooling towers, Applied Thermal Engineering, vol. 121, pp. 14–26.

Naik BK, Choudhary V, Muthukumar P, Somayaji C (2017) Performance Assessment of a Counter-flow Cooling Tower–Unique Approach, Energy Procedia, vol. 109, pp. 243–252.

Naik BK, Muthukumar P (2017) Empirical Correlation Based Models for Estimation of Air Cooled and Water Cooled Condenser's Performance, Energy Procedia, vol. 109, pp. 293–305.

Niagara Blower, <www.niagarablower.com> (retrieved April 2015).

Nkwetta DN, Smyth M, Zacharopoulos A, Hyde T (2013), Experimental performance evaluation and comparative analyses of heat pipe and direct flow augmented solar collector, Applied Thermal Engineering, vol. 60, pp. 225–33.

Neeraj M, Avadhesh Y (2015) Experimental analysis of thermal performance of evacuated tube solar air collector with phase change material for sunshine and off sunshine hours, Int. J. Amb. Energy, pp. 2162-8246.

Oberg V, Goswami DY (1998a) A Review of Liquid Desiccant Cooling, Advances in Solar Energy vol.12, pp.413-470.

Oberg V, Goswami DY (1998b) Experimental study of the heat and mass transfer in a packed bed liquid desiccant air dehumidifier, Journal of Solar Energy Engineering, ASME, vol.120, pp. 289–297.

Onda K, Takeuchi H, Okumoto Y (1968) Mass transfer coefficients between gas and liquid phases in packed columns, Journal of Chemical Engineering of Japan, vol. 1, pp. 56 – 62.

Peng CSP, Howell JR (1981) Analysis and design of efficient absorbers for low temperature desiccant air conditioners, ASME Journal of Solar Energy Engineering, vol. 103, pp. 67-74.

Peng D, Zhang X (2011) An analytical model for coupled heat and mass transfer processes in solar collector/regenerator using liquid desiccant, Applied Energy, vol. 80, pp. 2436 – 2444.

Patnaik S, Lenz TG, Lof GOG (1990) Performance studies for an experimental solar open cycle liquid desiccant air dehumidification system, Solar Energy, vol.44, pp. 123-135.

Patek J, Klomfar J (2006) A computationally effective formulation of the thermodynamic properties of LiBr-H2O solutions from 273 to 500 K over full composition range, Int. J. Refrig., vol.29, pp.566–578.

Ren CQ, Jiang Y, Zhang YP (2006) Simplified analysis of coupled heat and mass transfer processes in packed bed liquid desiccant-air contact system, Solar Energy vol.80, pp. 121–131.

Robison H (1983) Operational Experience with a Liquid Desiccant Heating and Cooling System, 18th IECEC, Orlando, FL.

Rodriguez GM, Silva ALF, Nunez MP (2018) Solar thermal networks operating with evacuated-tube collectors, Energy, vol. 146, pp. 26 – 33.

Ren C, Jiang Y, Zhang Y (2006) Simplified analysis of coupled heat and mass transfer processes in packed bed liquid desiccant-air contact system, Solar Energy, vol. 80, pp. 121–131.

Rajat SD, Jain S (2015) Performance characteristics of cross-flow membrane contactors for liquid desiccant systems. Applied Energy, vol. 141, pp. 1–11.

Sarbu I, Sebarchievici C (2013) Review of solar refrigeration and cooling systems, Energy and Buildings, vol.67, pp. 286–297.

Sabhia MA, Saidur R, Mekhilef S, Mahian O (2015) Progress and latest developments of evacuated tube solar collectors, Renewable and Sustainable Energy Reviews, vol. 51, pp. 1038 – 1054.

Saman WY, Alizadeh S (2001) Modelling and performance analysis of a cross-flow type plate heat exchanger for dehumidification/cooling. Solar Energy, vol. 70, pp. 361– 372.

Shahl LJ, Furbo S (2004) Vertical evacuated tubular-collectors utilizing solar radiation from all directions, Applied Energy ,vol. 78, pp. 371 – 395.

Schlepp, Schultz (1984) High Performance Solar Desiccant Cooling System: Performance Evaluations and Research Recommendations, SERI/TR, pp. 252-2497.

Seo YK, Yoon JW, Lee JS, Hwang YK, Jun CH, Chang JS, Wuttke S, Bazin P, Vimont A, Daturi M, Bourrelly S, Llewellyn PL, Horcajada P, Serre C, Ferey G (2012) Energy-efficient humidification over hierarchically porous metal-organic frame works as advanced water adsorbents, Advanced Materials, vol. 24, pp. 806–810.

Stevens DI, Braun JE, Klein SA, (1989) An effectiveness model of liquid desiccant system heat/mass exchangers, Solar Energy, vol. 42, pp. 449–55.

Shajimohan B, Maiya MP, Shaligram T (2007) Performance characterisation of liquid desiccant columns for a hybrid air-conditioner, Applied thermal engineering, vol. 28, pp. 1342-1355.

Shajimohan B, Shaligram T, Maiya MP (2015) Experimental investigations on performance of liquid desiccant-vapour compression hybrid air conditioner, Applied thermal engineering, vol.77, pp. 16-162.

Sultan GI, Hamed AM, Sultan AA (2002) The effect of inlet parameters on the performance of packed tower regenerator, Renewable Energy vol. 26, pp. 271–283.

Shanghai Canmu, < www.cncanmu.com > (retrieved April 2015).

Shifang H, Zhenyu L, Caihua L, Xiaosong Z (2017) Experimental study of heat and mass transfer characteristics in a cross-flow heating tower. Int. J. Refrigeration vol. 77, pp. 116 – 127.

Talal K, Kassem A, Alosaimy S, Ahmed MH, Mohammad F (2013) Solar Powered Dehumidification Systems Using Desert Evaporative Coolers: Review, International Journal of Engineering and Advanced Technology (IJEAT),vol. 3.

Treybal RE (1969) Mass transfer operations, 3rd ed., New York: McGraw-Hill, pp.186–211.

Tokarev M, Gordeeva L, Romannikov V, Glaznev I, Aristov Y (2002) New composite sorbent CaCl2 in mesopores for sorption cooling/heating, International Journal of Thermal Sciences, vol.41, pp. 470–474.

Vafai AK (2004) An investigation of heat and mass transfer between air and desiccant film in parallel and counter-flow channels, Applied Thermal Engineering, vol. 47 pp. 1745–60.

Varela RJ, Yamamguchi S, Giannetti N, Saito K, Harada M, Miyauchi H (2018) General correlations for the heat and mass transfer coefficients in an air-solution contactor of a liquid desiccant system and an experimental case application, Int. J. Heat Mass Transf., vol. 120, pp. 851 – 860.

Varela RJ, Giannetti N, Yamaguchi S, Saito K, Wang X, Nakayama H (2018) Experimental investigation of the wetting characteristics of an aqueous ionic liquid solution on an aluminum fin-tube substrate, Int. J. Ref., vol. 88, pp. 472 – 482.

Vishal D, Avadesh Y (2017) Effect of Pressure Drop and Air Mass Flow Rate on the Performance of Concentric Coaxial Glass Tube Solar Air Collector: A Theoretical Approach, Arabian Journal for Science and Engineering, 1 – 11.

Wang L, Nianping L, Zhao B (2010) Exergy performance and thermodynamic properties of the ideal liquid desiccant dehumidification system, Energy and Buildings, vol. 42, pp. 2437 – 2444.

Wang L, Xiao F, Zhang X, Kumar R (2016) An experimental study on the dehumidification performance of a counter-flow liquid desiccant dehumidifier, Int. J. Ref., vol. 70, pp. 289 – 301.

Wirth (1976), Niklaus Algorithms + Data Structures = Programs. Prentice-Hall 126.

Wu Q, Cai W, Shen S, Wang X, Ren H (2017) A regulation strategy of working concentration in the dehumidifier of liquid desiccant air conditioner, vol. 202, pp. 648 – 661.

Waugaman DG, Kini A, Kettleborough CF (1993) A review of desiccant cooling systems. J. Energy Res. Technology – Transactions ASME, vol. 115, pp. 1 – 8.

Xiong ZQ, Dai YJ, Wang RZ (2010) Exergy analysis of liquid desiccant dehumidification system, International Journal of Green Energy vol. 7, pp. 241 – 262.

Xian Li, Liu S, Tan KK, Wang QG, Cai WJ, Xie L (2016) Dynamic modelling of a liquid desiccant dehumidifier, Applied Energy, pp. 435 – 445.

Xia SJ, Chen LG, Sun FR (2009) Optimization for entransy dissipation minimization in heat exchanger, Chinese Sci. Bull., vol. 54, pp. 3587–3595.

Xianhua N, Li Z, Shuai D, Xueyin L (2017) Experimental study on thermal performance of U-type evacuated glass tubular solar collector with low inlet temperature, Solar Energy, vol. 150, pp. 192 – 201.

Zhang T, Liu X, Zhang L, Jiang J (2012) Match properties of heat transfer and coupled heat and mass transfer processes in air-conditioning system, Energy Conversion and Management, vol. 59, pp. 103-113.

Zhang T, Liu X, Tang H, Liu J, Jiang Y (2016) Exergy and entransy analysis in air – conditioning system part 1 – Similarity and distinction, Energy and buildings, vol.128, pp. 876 – 885.

Zhang T, Liu X, Liu J, Tang H, Jiang Y (2017) Exergy and entransy analysis in air – conditioning system part 2 – Humid air handling process, Energy and buildings, vol. 139, pp. 10 – 21.

Zhang L, Xiaohua L, Jingjing J, Yi J (2014) Exergy calculation and analysis of a dehumidification system using liquid desiccant, Energy and Buildings, vol. 69, pp. 318 – 328.

Zhang L, HongyangW, Xiaosong Z (2014) Theoretical analysis of heat and mass transfer characteristics of a counter – flow packing tower and liquid desiccant dehumidification systems based on entransy theory, Energy, vol. 141, pp. 661 – 672.

Zhiqiang Y, Harding G, Window B (1985) Water-in-glass manifolds for heat extraction from evacuated solar collector tubes, Int. J. Solar Energy, vol. 32, pp. 223–230.

Zurigat, YH, Abu-Arabi MK, Abdul-Wahab SA (2003) Air dehumidification by triethylene glycol desiccant in a packed column, Energy Conversion & Management, vol.45, pp. 141-155.

Yimo L, HongxingY, Lin L, Ronghui Q (2014) A review of the mathematical models for predicting the heat and mass transfer process in the liquid desiccant dehumidifier, Renewable and Sustainable Energy Reviews, vol. 31, pp. 587–599.

Yin YG, Zhang XS, Peng DG, Li XW (2009) Model validation and case study on internally cooled/heated dehumidifier/regenerator of liquid desiccant systems. Int. J. Ther. Sci, vol. 48, pp. 1664 – 1671.

Yunho H, Reinhard R (2007) Review of Solar Cooling Technologies, HVAC & R Research, vol. 14, pp. 507- 528.

Yuan Z, Herold KE (2005) Thermodynamic properties of aqueous lithium bromide using a multi property free energy correlation, HVAC&R Res., vol. 11, pp. 377–393.

Young HD (1992), University Physics, 7th Ed., Addison Wesley.

APPENDIX A

SIMPLIFIED U – TUBE SOLAR COLLECTOR MODEL

A.1 Governing Equations Derivation

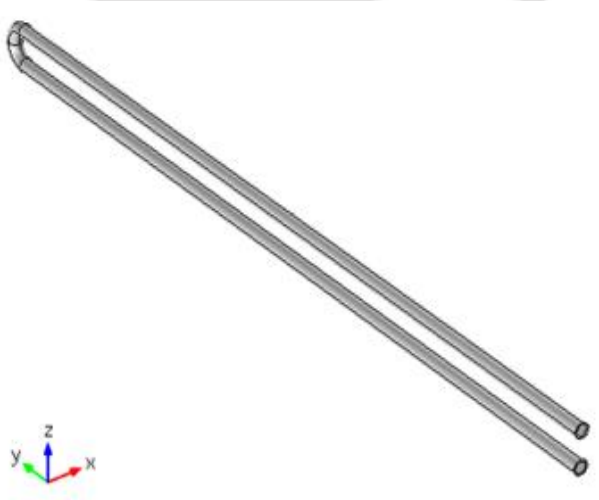

Fig. A.1, U – tube solar collector model.

The continuity and Naiver – Stokes momentum equations are solved simultaneously for simulating the behaviour of working fluid flowing inside the U – tube (Eqs. A.1 and A.2a – A.2c). The velocity field obtained from Eqs. A.1 and A.2a – A.2c are used for solving the convective heat transfer taking place from U – tube wall surface to the working fluid (Eq. A.3). In order to include the effect of buoyancy and to reduce the complexity in solving the Navier

– Stokes equations, Boussinesq approximation is added to the momentum equation along the Z – direction (Eq. A.2c) and is expressed as $-g_z\beta_T(T_\infty - T)$. The axial direction of simplified U – tube solar collector model is shown in Fig. A.1.

Continuity equation:

$$\rho\frac{\partial V_{wf,x}}{\partial x}+\rho\frac{\partial V_{wf,y}}{\partial y}+\rho\frac{\partial V_{wf,z}}{\partial z}=0 \tag{A.1}$$

Momentum equation:

Component x

$$\frac{\partial V_{wf}}{\partial t}+V_{wf,x}\frac{\partial V_{wf,x}}{\partial x}+V_{wf,y}\frac{\partial V_{wf,x}}{\partial y}+V_{wf,z}\frac{\partial V_{wf,x}}{\partial z}=-\frac{1}{\rho}\frac{\partial P}{\partial x}+\frac{\mu}{\rho}\left(\frac{\partial^2 V_{wf,x}}{\partial x^2}+\frac{\partial^2 V_{wf,x}}{\partial y^2}+\frac{\partial^2 V_{wf,x}}{\partial z^2}\right) \tag{A.2a}$$

Component y

$$\frac{\partial V_{wf}}{\partial t}+V_{wf,x}\frac{\partial V_{wf,y}}{\partial x}+V_{wf,y}\frac{\partial V_{wf,y}}{\partial y}+V_{wf,z}\frac{\partial V_{wf,y}}{\partial z}=-\frac{1}{\rho}\frac{\partial P}{\partial y}+\frac{\mu}{\rho}\left(\frac{\partial^2 V_{wf,y}}{\partial x^2}+\frac{\partial^2 V_{wf,y}}{\partial y^2}+\frac{\partial^2 V_{wf,y}}{\partial z^2}\right) \tag{A.2b}$$

Component z

$$\frac{\partial V_{wf}}{\partial t}+V_{wf,x}\frac{\partial V_{wf,z}}{\partial x}+V_{wf,y}\frac{\partial V_{wf,z}}{\partial y}+V_{wf,z}\frac{\partial V_{wf,z}}{\partial z}=-g_z\beta_T\left(T_\infty-T\right)+\frac{\mu}{\rho}\left(\frac{\partial^2 V_{wf,z}}{\partial x^2}+\frac{\partial^2 V_{wf,z}}{\partial y^2}+\frac{\partial^2 V_{wf,z}}{\partial z^2}\right) \tag{A.2c}$$

Energy equation:

$$\rho C_{p,wf}\left(\frac{\partial T}{\partial t}+V_{wf,x}\frac{\partial T}{\partial x}+V_{wf,y}\frac{\partial T}{\partial y}+V_{wf,z}\frac{\partial T}{\partial z}\right)=k\left(\frac{\partial^2 T}{\partial x^2}+\frac{\partial^2 T}{\partial y^2}+\frac{\partial^2 T}{\partial z^2}\right) \tag{A.3}$$

where ρ, V_{wf}, and $C_{p,wf}$ are the density (kg/m^3), velocity (m/s) and specific heat (kJ/kg – K) of the working fluid and k is the thermal conductivity (kW/m – K) of the U – tube material.

APPENDIX B

UNCERTAINTY ANALYSIS

Kline and McClintok (1953) proposed a method for estimating the uncertainty of dependent parameter, which depends on certain measured quantities of the experimental studies. If a parameter 'Ω' depends on the independent variables such as k_1, k_2, k_3, k_4……..k_n then 'Ω' can be expressed as a function of all the independent variables as given in Eq. B.1.

$$\Omega = \Omega (k_1, k_2, k_3, k_4\text{……..}k_n) \tag{B.1}$$

Then the total uncertainty of the parameter 'ΔΩ' is given as

$$\Delta\Omega = \sqrt{\left(\frac{\partial\Omega}{\partial k_1}\Delta k_1\right)^2 + \left(\frac{\partial\Omega}{\partial k_2}\Delta k_2\right)^2 + \left(\frac{\partial\Omega}{\partial k_3}\Delta k_3\right)^2 + \text{.....} + \left(\frac{\partial\Omega}{\partial k_n}\Delta k_n\right)^2} \tag{B.2}$$

Thus, using Eq. B.2 the uncertainties in the dependent parameters are calculated as follows,

The uncertainty in condensation/evaporation rate is calculated using Eq. B.2a

Condensation/evaporation rate (λ):

$$\Delta\lambda = \sqrt{2\left(\frac{\partial\lambda}{\partial(\Delta\omega)}\Delta(\Delta\omega)\right)^2 + \left(\frac{\partial\lambda}{\partial v}\Delta v\right)^2 + \left(\frac{\partial\lambda}{\partial d}\Delta d\right)^2} \tag{B.2a}$$

The uncertainty in air and solution enthalpy are calculated using Eq. B.2b and B.2c

Air enthalpy (h_a): $$\Delta h_a = \sqrt{2\left(\frac{\partial h_a}{\partial \omega}\Delta\omega\right)^2 + 2\left(\frac{\partial h_a}{\partial T_a}\Delta T_a\right)^2} \quad \text{(B.2b)}$$

Solution enthalpy (h_s): $$\Delta h_s = \sqrt{2\left(\frac{\partial h_a}{\partial \beta}\Delta\beta\right)^2 + 2\left(\frac{\partial h_s}{\partial T_s}\Delta T_s\right)^2} \quad \text{(B.2c)}$$

The uncertainty in overall energy exchange is calculated using Eq. B.2d

Overall energy exchange (Q_e):

$$\Delta Q_e = \sqrt{\left(\frac{\partial Q_e}{\partial \dot{m}}\Delta\dot{m}\right)^2 + 2\left(\frac{\partial Q_e}{\partial T_a}\Delta T_a\right)^2} \quad \text{(B.2d)}$$

The uncertainty in useful heat flux is calculated using Eq. B.2e

Useful heat flux (Q_{uh}):

$$\Delta Q_{uh} = \sqrt{\left(\frac{\partial Q_{uh}}{\partial v_{wf}}\Delta v_{wf}\right)^2 + 2\left(\frac{\partial Q_{uh}}{\partial T_{wf}}\Delta T_{wf}\right)^2} \quad \text{(B.2e)}$$

A.1 Sample calculation

a) Condensation/evaporation rate (λ)

As condensation/evaporation rate (λ) = ρAvΔω, Using Eq. B.1a, the uncertainty in condensation/evaporation rate ($\Delta\lambda/\lambda$) is calculated as follows

$$\Delta\lambda = \sqrt{2\left(\frac{\lambda}{\omega}\Delta\omega\right)^2 + \left(\frac{\lambda}{v}\Delta v\right)^2 + \left(\frac{\lambda}{d}\Delta d\right)^2} \quad \text{(B.3)}$$

where $\frac{\partial\lambda}{\partial\omega} = \frac{\lambda}{\omega}; \frac{\partial\lambda}{\partial v} = \frac{\lambda}{v}; \frac{\partial\lambda}{\partial A} = \frac{\lambda}{A}$

$$\frac{\Delta\lambda}{\lambda}=\sqrt{2\left(\frac{\Delta\omega}{\omega}\right)^2+\left(\frac{\Delta v}{v}\right)^2+\left(\frac{\Delta d}{d}\right)^2} \tag{B.4}$$

Here, uncertainty of change in specific humidity ($\Delta\omega$) tends to $2(\Delta\omega/\omega)^2$.

$$\frac{\Delta\lambda}{\lambda}=\sqrt{2(0.02)^2+(0.01)^2+(0.01)^2}=\pm 0.032 \tag{B.5}$$

where $\frac{\Delta\omega}{\omega}=\pm 2\%\,;\frac{\Delta v}{v}=\pm 1\%\,;\frac{\Delta d}{d}=\pm 1\%$

Thus, the uncertainty in condensation/evaporation rate is obtained as $\pm$3.2%. Similarly using Eq. 3.2b – 3.2e, uncertainty in the estimation of air enthalpy, solution enthalpy, overall energy exchange and useful heat flux are obtained as $\pm$4.3%, $\pm$4.3%, $\pm$4.3% and $\pm$3.2%, respectively.

List of Publications

Journals

1. **B. Kiran Naik** and P. Muthukumar, Experimental investigation and parametric studies on structured packing chamber based liquid desiccant dehumidification and regeneration systems, **Building and Environment** (2019).
   DOI: https://doi.org/10.1016/j.buildenv.2018.12.028
2. **B. Kiran Naik**, Mrinal Bhowmik and P. Muthukumar, Experimental investigation and numerical modelling on the performance assessments of evacuated u – tube solar collector systems, **Renewable Energy** (2019).
   DOI: https://doi.org/10.1016/j.renene.2018.09.066
3. **B. Kiran Naik** and P. Muthukumar, Energy, exergy and entransy analyses of a liquid desiccant regenerator, **International Journal of Refrigeration** (2018).
   DOI: https://doi.org/10.1016/j.ijrefrig.2018.08.016
4. **B. Kiran Naik**, P. Muthukumar and P. Sunil kumar, A novel finite difference model coupled with recursive algorithm for analyzing heat and mass transfer processes in a cross-flow dehumidifier/regenerator, **International Journal of Thermal Sciences** (2018).
   DOI: https://doi.org/10.1016/j.ijthermalsci.2018.05.029
5. **B. Kiran Naik**, P. Muthukumar and C. Bhattacharya, Thermal modelling and parametric investigation on coupled heat and mass transfer processes occured in a packed tower, **Heat and Mass Transfer** (2018).
   DOI: https://doi.org/10.1007/s00231-018-2440-1
6. **B. Kiran Naik** and P. Muthukumar, Performance assessment of evacuated U-tube solar collector: a numerical study, **Sadhana** (2019).
   DOI: https://doi.org/10.1007/s12046-018-0974-z
7. **B. Kiran Naik**, Ankit Varshney, P. Muthukumar and C. Somayaji, Modelling and performance analysis of u type evacuated tube solar collector using different working fluids, **Energy Procedia** (2016).
   DOI: https://doi.org/10.1016/j.egypro.2016.11.189
8. **B. Kiran Naik**, Ankit Soni, Amit kumar, P. Muthukumar and C. Somayaji, Coupled heat and mass transfer analysis of an adiabatic dehumidifier – unique approach, **Energy Procedia** (2016).
   DOI: https://doi.org/10.1016/j.egypro.2016.11.198

Conferences

1. B. Kiran Naik, and P. Muthukumar, Energy, Entransy and Exergy Analyses of a Liquid Desiccant Regenerator, **International Sorption Heat Pump Conference (ISHPC – 2017)**, Tokyo, Japan, Aug. 7-10, 2017.
2. B. Kiran Naik, P. Muthukumar and C. Somayaji, Thermodynamic Analysis of Liquid Desiccant Dehumidification System - A Novel Approach, **23rd National Heat and Mass Transfer Conference and 1st International ISHMT-ASTFE Heat and Mass Transfer Conference IHMTC**, ISRO Thiruvananthapuram, India, Dec. 17-20, 2015.
3. B. Kiran Naik, Ankit Soni, Amit kumar, P. Muthukumar and C. Somayaji, Coupled Heat and Mass Transfer Analysis of an Adiabatic Dehumidifier – Unique Approach, **5th International Conference on Advances in Energy Research (ICAER -2015)**, IIT Bombay, Mumbai, India, Dec. 15-17, 2015.
4. B. Kiran Naik, Ankit Varshney, P. Muthukumar and C. Somayaji, Modelling and Performance Analysis of U Type Evacuated Tube Solar Collector Using Different Working Fluids, **5th International Conference on Advances in Energy Research (ICAER -2015)**, IIT Bombay, Mumbai, India, Dec. 15-17, 2015.
5. B. Kiran Naik, Amit Kumar, Ankit Soni, P. Muthukumar and C. Somayaji, Coupled Heat and Mass Transfer Analysis of an Adiabatic Regenerator – Unique Approach, **International Conference on Aerospace and Mechanical Engineering (ICAME - 2015)**, Kerala, India, Dec. 14-16, 2015.